ISSN 0915-6364

NATIONAL INSTITUTE FOR FUSION SCIENCE

# Energy Dependence of Ion-Induced Sputtering Yields from Monoatomic Solids at Normal Incidence

Y. Yamamura and H. Tawara

(Received — Mar. 9, 1995)

NIFS-DATA-23 Mar. 1995

RESEARCH REPORT
NIFS-DATA Series



NAGOYA, JAPAN

# ENERGY DEPENDENCE OF ION-INDUCED SPUTTERING YIELDS FROM MONOATOMIC SOLIDS AT NORMAL INCIDENCE

Yasunori Yamamura[a)] and Hiro Tawara

National Institute for Fusion Science, Chigusa-ku

Nagoya 464-01, Japan

Abstract

The yields of the ion-induced sputtering from monoatomic solids at normal incidence for various ion-target combinations are presented graphically as a function of the incident ion energy. In order to fill the lack of the experimental data, the sputtering yields are also calculated by the Monte Carlo simulation code ACAT for some ion-target combinations. Each graph shows available experimental data points and the ACAT data, together with the sputtering yields calculated by the present empirical formula, whose parameters are determined by the best-fit to available data.

[Keywords : sputtering yields, monatomic solids, normal incidence,
ion impact, analytic expression]

Permanent address:

a) Department of Applied Physics, Okayama University of Science, Ridai-cho, Okayama 700, Japan

## 1. Introduction

Sputtering of surfaces is an important parameter in the understanding of fusion energy device operation. Sputtering ejects high atomic number materials into the plasma causing significant contamination, increases in the effective charge of the plasma and results in inefficient heating of the fuel. From the view point of the plasma-wall-interaction, sputtering is an undesired effect which contaminates the plasma and erodes the surrounding walls. On the other hand, sputtering is also widely used for many applications. Sputtering allows us a controlled removal of surface layers on a nearly atomic scale and the submicron spatial resolution if a well-focused ion beam is used. One of the largest applications of sputtering is the deposition of thin films on a large variety of substrates. Therefore, it is important to present the empirical, analytical formula which can easily provide the sputtering yield for any ion-target combination.

In 1984 the working group at Institute of Plasma Physics, Nagoya University, published the compiled sputtering yield data available to the early 1983 and proposed the empirical formula which could predict the energy dependence of sputtering yields for any ion-target combination [1]. Since then, a large number of new data have been published. Therefore, it seems to be time to collect new experimental sputtering data published during 1983 - 1994 and to revise the previous empirical formula.

Recently, Eckstein et al.[2] have reported their survey of the experimental sputtering yield data measured at Max-Plank Institüt für Plasmaphysik (Garching) where the data for normal incidence as a function of ion energy were fitted by a formula derived by Bohdansky [3]. Recently, Thomas et al.[4] also presented an evaluated data base for light ion sputtering, based on the Bohdansky's formula [3]. Basically, these two groups used the following Bohdansky's formula:

$$Y(E) = Q\, s_n(\varepsilon)\left[1 - \left(\frac{E_{th}}{E}\right)^{2/3}\right]\left[1 - \left(\frac{E_{th}}{E}\right)\right]^2 , \qquad (1)$$

where $E$ is the projectile energy, $s_n(\varepsilon)$ is the reduced nuclear stopping cross section, and $\varepsilon$ is the reduced energy

$$\varepsilon = E \frac{M_2}{M_1+M_2} \frac{a_L}{Z_1 Z_2 e^2} \quad . \qquad (2)$$

$Z_1$ and $Z_2$ are the atomic numbers, and $M_1$ and $M_2$ the masses of the projectile and the target atom, respectively. $e$ is the electron charge. The Lindhard screening length $a_L$ is given as [5]

$$a_L = 0.4685 \left\{ Z_1^{2/3} + Z_2^{2/3} \right\}^{-1/2} \ \text{Å} \qquad (3)$$

The values $Q$ and $E_{th}$ are used as parameters to fit to the data available.

For the reduced nuclear stopping power in eq. (1) the original Bohdansky formula used the following analytical expression based on the Thomas-Fermi potential [1]:

$$s_n^{TF}(\varepsilon) = \frac{3.441\sqrt{\varepsilon}\ln(\varepsilon + 2.718)}{1 + 6.355\sqrt{\varepsilon} + \varepsilon(6.882\sqrt{\varepsilon} - 1.708)} \quad . \qquad (4)$$

In a recently revised Bohdansky's formula, Eckstein et al. used the following reduced nuclear stopping power based on the Kr-C potential [2]:

$$s_n^{KrC}(\varepsilon) = \frac{0.5 \ln(1 + 1.2288\varepsilon)}{\varepsilon + 0.1728\sqrt{\varepsilon} + 0.008\varepsilon^{0.1504}} \quad . \qquad (5)$$

And the best-fit values of $Q$ and $E_{th}$ are listed for each ion-target combination in their data book [2].

From the theoretical point of view, the high-energy light-ion sputtering yield is not directly proportional to the reduced nuclear stopping cross section $s_n(\varepsilon)$ corresponding to the incident projectile energy, because it is affected strongly by the electronic energy loss. In this sense, it is difficult for the Bohdansky' s formula to predict the sputtering yield by high-energy light-ions. The Bohdansky's Q factor includes the effect of the electronic stopping, but the contribution of the electronic stopping to sputtering depends on the incident energy. From the viewpoint of plasma-wall-interaction, of which the main interest is the low-energy sputtering yield, it seems that the Bohdansky' s formula can predict the sputtering yield reasonably well.

The purpose of this report is to propose a new empirical formula which presents the relation

between the ion-induced sputtering yield and the energy of the incident ions for various ion-target combinations, based on sputtering yield data published before 1994. In this report, some calculated data by the ACAT code are added to the present data base. The compiled experimental data of sputtering yields at normal incidence are shown in graphs, which include the energy-yield curve calculated by our proposed empirical formula.

## 2. Theoretical background for the empirical formula

The sputtering mechanism can be classified into two categories [6]. When a relatively heavy ion is bombarded on the solid surface, the incoming ion deposits its energy near the surface and the collision cascade is developed. As a result target atoms are ejected from the surface (mechanism A). On the contrary, in the case of a light ion such as $H^+$ and $D^+$, the incoming light ion does not produce the collision cascade near the surface. Instead, when the reflected ion escapes from the surface layer, it hits the surface atoms. As a result, the recoil atoms is sputtered if their kinetic energies overcome the surface barrier (mechanism B). When the mass of the incident ion becomes lighter, the sputtering mechanism shifts the mechanism A to the mechanism B gradually. For intermediate ions such as an Ar ion, both mechanism A-sputtering and mechanism B-sputtering contribute to the total sputtering yield.

In 1969 Sigmund derived the formula of the sputtering yield [7]

$$Y(E) = \Lambda F_D(E) \quad , \tag{6}$$

solving the linearized Boltzmann equation based on the assumption that the collision cascade is well developed in the infinite medium, where $\Lambda$ is given as

$$\Lambda = \frac{3}{4\pi^2} \frac{1}{NC_0U_s} = \frac{0.0420}{NU_s} \quad , \tag{7}$$

and $F_D(E)$ is the deposited energy at the surface which is given as

$$F_D(E) = \alpha(M_2/M_1)NS_n(E) \quad . \tag{8}$$

$N$ and $U_s$ are the number density and the surface binding energy, respectively. $S_n(E)$ is the nuclear stopping cross section. As the surface binding energy we use the heat of sublimation in this report. $C_0$ is the coefficient of nuclear stopping cross section when the power approximation of $m = 0$ is used for the interatomic potential.

When the energy of the incident ion becomes smaller, the angular distribution of the recoil spectrum in the collision cascade becomes anisotropic, and so the sputtering has its threshold. Then, the original Sigmund formula should be modified as [8]

$$Y(E)= 0.042 \frac{F_D(E)}{NU_s} \left[1 - \sqrt{\frac{E_{th}}{E}}\right] = 0.042 \frac{\alpha(M_2/M_1)S_n(E)}{U_s} \left[1 - \sqrt{\frac{E_{th}}{E}}\right] \tag{9}$$

for the low-energy heavy-ion sputtering, where $E_{\rm th}$ is the sputtering threshold energy.

As another extreme, let us consider the high-energy light-ion sputtering, where the sputtering yield is proportional to particle reflection coefficient. A single collision approximation says that the particle reflection coefficient $R_N(E)$ is proportional to the ratio of nuclear stopping cross section $S_{\rm n}(E)$ to electronic stopping cross section $S_e(E)$ [9], i.e.,

$$R_N(E) \propto \frac{M_2}{M_1} \frac{S_n(E)}{S_e(E)} \quad . \tag{10}$$

Since the high-energy light-ion sputtering is due to the deposited energy $F_D(E^*)$ at the surface by the reflected particle, its yield can be represented by [10]

$$Y(E)= 0.042 \frac{F_D(E^*)R_N(E)}{NU_s} \left[1 - \sqrt{\frac{E_{th}^L}{E}}\right]^s \quad , \tag{11}$$

where $E^*$ is the average energy of reflected ions escaping from the surface layer, $E_{\rm th}{}^{\rm L}$ is the

threshold energy of the light-ion sputtering, and the power $s$ of eq.(11) is equal to $2.8$ if the power approximation of $m = 1$ is used.

Generally speaking, the real sputtering mechanisms are composed of both mechanisms A and B. Therefore, the sputtering formula can be expressed by the interpolation between eq. (9) and eq. (11), i.e.,

$$Y(E) = 0.042 \frac{\alpha(M_2/M_1)}{U_s} \frac{S_n(E) s_n(\varepsilon)}{s_n(\varepsilon) + \Gamma s_e(\varepsilon)} \left[1 - \sqrt{\frac{E_{th}}{E}}\right]^s$$
$$= 0.042 \frac{\alpha(M_2/M_1)}{U_s} \frac{S_n(E)}{1 + \Gamma s_e(\varepsilon)/s_n(\varepsilon)} \left[1 - \sqrt{\frac{E_{th}}{E}}\right]^s \quad , \qquad (12)$$

where $s_n(\varepsilon)$ and $s_e(\varepsilon)$ are the reduced nuclear stopping power and the reduced electronic stopping power, respectively. The parameter $\Gamma$ means the contribution of the mechanism B-sputtering to the total sputtering yield. For the low-energy heavy-ion sputtering where $s_e(\varepsilon)$ is very small, eq.(12) becomes equal to eq. (9), meanwhile for high-energy light-ion sputtering where $s_n(\varepsilon)$ is negligibly small, eq.(12) is reduced to eq. (11).

## 3. A new empirical formula

The important requests for empirical formulas are the following: The empirical formula should predict the energy dependence of the sputtering yield as precisely as possible, using as parameters as few as possible. For example, if we employ the ZBL formula for $s_e(\varepsilon)$ in eq.(12), we can estimate more precisely the electronic stopping power for any ion-target combination, but at the same time we have to prepare a lot of parameters for this purpose.

In order to propose as simple an empirical formula as possible, we use the power approximation for $s_n(\varepsilon)$ [5] and the Lindhard electronic stopping power for $s_e(\varepsilon)$ [12], i.e.,

$$s_n(\varepsilon) = \frac{2\lambda_m}{3\text{-}2m}\,\varepsilon^{0.5-m} \quad , \tag{13}$$

$$s_e(\varepsilon) = k_e\,\varepsilon^{0.5} \quad , \tag{14}$$

where $\lambda_m$ is the calculable constant if m is given, and $k_e$ is the Lindhard electronic stopping coefficient. In the previous empirical formula published in 1985 we used $m = 0.5$ for $s_n(\varepsilon)$. In the new empirical formula we use $m = 0.3$ for $s_n(\varepsilon)$.

Since $\alpha(M_2/M_1)$ of eq. (12) has the $Z_2$-dependence[1], we factorize it as $\alpha(M_2/M_1) = Q(Z_2)\alpha^*(M_2/M_1)$. Then, finally the new empirical formula is given in the form

$$Y(E) = 0.042\,\frac{Q(Z_2)\alpha^*(M_2/M_1)}{U_s}\,\frac{S_n(E)}{1 + \Gamma k_e \varepsilon^{0.3}}\left[1 - \sqrt{\frac{E_{th}}{E}}\right]^s \quad , \tag{15}$$

where the $\Gamma$ factor has the following expression:

$$\Gamma = \frac{W(Z_2)}{1 + (M_1/7)^3} \quad . \tag{16}$$

The factor $\Gamma$ corresponds to $0.35U_s$ in the previous empirical formula and the best-fit values of $W(Z_2)$ and $Q(Z_2)$ are listed in Table 1. The power $s$ of the previous empirical formula was fixed to be 2.8 for all target materials. On the contrary, the $s$ of the new empirical formula is slightly dependent on the target material, as is shown in Table 1. The best-fit values of $\alpha^*$ are described as a function of mass ratio $M_2/M_1$ in the following manner:

$$\begin{aligned} \alpha^* &= 0.249(M_2/M_1)^{0.56} + 0.0035(M_2/M_1)^{1.5} \qquad M_1 \geq M_2 \\ &= 0.088(M_2/M_1)^{-0.15} + 0.165(M_2/M_1) \qquad M_1 \leq M_2 \end{aligned} \tag{17}$$

Concerning the sputtering threshold in eq.(15), we use the following best-fit functional relation

$$\begin{aligned} \frac{E_{th}}{U_s} &= \frac{6.7}{\gamma} \qquad M_1 \geq M_2 \\ &= \frac{1 + 5.7(M_1/M_2)}{\gamma} \qquad M_1 \leq M_2 \end{aligned} \tag{18}$$

which is derived based on Yamamura and Bohdansky's theory [13], where $\gamma$ is the energy transfer factor at an elastic collision and is given as

$$\gamma = \frac{4M_1M_2}{(M_1+M_2)^2}. \tag{19}$$

The Lindhard electronic stopping coefficient $k_e$ is given as

$$k_e = 0.079\frac{(M_1+M_2)^{3/2}}{M_1^{3/2}M_2^{1/2}}\frac{Z_1^{2/3}Z_2^{1/2}}{(Z_1^{2/3}+Z_2^{2/3})^{3/4}} \tag{20}$$

The nuclear stopping cross section $S_n(E)$ in the present formula is calculated by

$$S_n(E) = 84.78\frac{Z_1Z_2}{\{Z_1^{2/3}+Z_2^{2/3}\}^{1/2}}\frac{M_1}{M_1+M_2}s_n^{TF}(\varepsilon), \tag{21}$$

where we use an analytic expression of $s_n^{TF}(\varepsilon)$ which is given in eq. (4). The explicit expression of the reduced energy $\varepsilon$ is

$$\varepsilon = \frac{0.03255}{Z_1Z_2(Z_1^{2/3}+Z_2^{2/3})^{1/2}}\frac{M_2}{M_1+M_2}E(\text{eV}) \tag{22}$$

The procedures of obtaining the best-fit values of parameters from available experimental data are the same as in the previous compilation work done in 1984. The physical meaning of the $Z_2$ dependence of $Q(Z_2)$ is that though Sigmund used the nuclear stopping power of $m = 0$ for all target materials in the calculation of $A$ in eq. (7), the stopping power of sputtering particles depends on the Z number of the target material and the energy of the escaping particles which are of the order of the surface binding energy. The best-fit values of $\alpha^*$ are shown in Fig. 1 as a function of mass ratio $M_2/M_1$, where the solid line represents eq. (17). The best-fit values of relative threshold energies $E_{th}/U_s$ are shown in Fig. 2 as a function of mass ratio $M_2/M_1$, where the solid line represents eq. (18). The $Z_2$ dependence of $W(Z_2)$ may reflect that of electronic stopping power. The most important

advantage of our new empirical formula over Bohdansky's empirical formula is that eq. (15) can be applied to all the possible ion-target combinations over any incident ion energy.

## 4. Simulations

For several ion-target combinations, especially for light-ion sputtering, sputtering yield data have been calculated with the ACAT program [14], in order to fill the lack of the experimental data. The ACAT program is based on the binary collision approximation, the target is assumed to be amorphous, and the surface is randomly rough in a depth of half a monolayer.

As an interatomic potential we used the Kr-C potential [15] with the Firsov screening length $a_F$ for heavy ion ($Z_1 > 3$) sputtering, where $a_F$ is given as

$$a_F = 0.4685 \left\{ Z_1^{1/2} + Z_2^{1/2} \right\}^{-2/3} \ \text{Å}$$

For light-ion sputtering such as $H^+$, $D^+$ and $He^+$ ions some efforts were undertaken to get good agreement with experimental data by adjusting the Firsov screening length, i.e., $a_F(1+q)$, because in principle the Thomas-Fermi statistical model cannot be applied to light ions. The adjusting values $q$ are listed in Table 2 for possible target materials. For heavier projectiles ($Z_1 > 2$) we used the original Firsov screening length for all ion-target combinations.

The electronic energy loss is simulated with the path-length-dependent non-local model, where we used the ZBL electronic stopping formula[11] for all the ion-target combinations. For light-ion sputtering, the electronic energy loss due to the violent collision is estimated by the Oen-Robinson (OS) model [16]. The bulk binding energy is set to be zero for all ion-target combinations.

It is well known that the calculated sputtering yields are dependent on which electronic stopping loss model is used, the non-local or the local model. For several targets such as C, Cu, Ag Tb, Tm and Au which have the star marks in Table 2, we have obtained better energy dependence of sputtering yields if we employ the OS local model for possible projectile-target combinations. For heavier projectile ($Z_1 > 2$) the electronic energy losses at low collision energies are estimated by the OS local model.

## 5. Presentation of data and discussions

Each graph shows experimental data, the ACAT data and the yield-energy curve calculated by the present empirical formula, eq.(15), for each ion-target combination. For plots of experimental data and ACAT data, different symbols are used for different references. The calculated yield-energy curves are shown with solid lines. The ion-target combinations shown in graphs are listed in Table 3, where the number in each column represents the number of references of experimental works. If one estimate the preliminary sputtering yield for unlisted target materials by the present formula, one should use $Q = 1.0$, $W = 0.35U_s$, $s = 2.5$, where $U_s$ is the heat of sublimation.

Agreement between the solid-curve and data points is much more improved as compared with the previous work [1], especially for light-ion sputtering. The sputtering data near the threshold energy region for some ion-target combinations cannot be described by the present empirical formula, and the deviation of measured data from the solid curve can not be systematically explained. This may be due to the fact that the sputtering yield is strongly dependent on the surface conditions and the vacuum conditions.

## 6. Explanation of graphs

The graphs are ordered first by increasing projectile atomic number, and then by increasing target atomic number.

| | |
|---|---|
| Ordinate | Sputtering yield (atoms/incident ion) at normal incidence. |
| Abscissa | Kinetic ion energy of incidence in eV. |
| Heading | Ion-target combination |
| | He → Cu means He ion on Cu target. |
| | $Sb_3$ → Pt (molecule) means a trimer of Sb on Pt target, but the yield is reduced to that per a monoatomic ion. |
| Symbols | Experimental data and ACAT simulation data. |
| | The first author and the year published for each reference are listed and the ACAT data are denoted by YAMAMURA (ACAT). |
| Solid line | Energy dependence of the sputtering yield calculated by the newly proposed empirical formula. |

## 7. A sample calculation of the sputtering yield

If one estimate preliminary sputtering yield for the unlisted target materials by the present formula, one should use $Q = 1.0$, $W = 0.35U_s$, $s = 2.5$, where $U_s$ is the heat of sublimation. As an example we calculate the sputtering yield of He on Au at an incident energy of 1 keV according to the present new formula (15). First calculate ε using eq. (22).

$$\varepsilon = \frac{0.03255}{2\times 79\times\left(2^{2/3}+79^{2/3}\right)^{1/2}}\frac{195.1}{4.002+195.1}\times 1000 = \frac{0.03255\times 195.1}{706.5\times 199.1}\times 1000 = 0.0451$$

Then we can obtain

$s_n^{TF}(\varepsilon)$ using eq. (4), i.e.,

$$s_n^{TF}(\varepsilon) = \frac{3.441\times\sqrt{0.0451}\ln 2.763}{1+6.355\times\sqrt{0.0451}+0.0451(6.882\times\sqrt{0.0451}-1.708)} = \frac{0.7427}{2.350-0.01112} = 0.318$$

Calculate $k_e(\varepsilon)$ using eq. (20).

$$k_e(\varepsilon) = 0.079\times\frac{(4.002+195.1)^{3/2}}{4.002^{3/2}195.1^{1/2}}\frac{2^{2/3}\times 79^{1/2}}{\left(2^{2/3}+79^{2/3}\right)^{3/4}} = \frac{221.9\times 14.11}{111.8\times 9.455} = 2.96$$

Then calculate the nuclear stopping cross section $S_n(E)$ from eq. (21):

$$S_n(E) = 84.78\frac{2\times 79}{\left(2^{2/3}+79^{2/3}\right)^{1/2}}\times\frac{4.002}{4.002+195.1}\times 0.318 = \frac{84.78\times 201.1}{4.471\times 199.1} = 19.15$$

Pick up the values of Q, $U_s$, W and s from Table 2, and we have $Q = 1.08$, $U_s = 3.81$, $W = 1.64$, and $s = 2.8$. Then, we have $\Gamma = 1.38$ from eq. (16). Next, calculate $\alpha^*$ using eq. (17), where $M_2/M_1 = 48.75$:

$$\alpha^* = 0.249\times(48.75)^{0.56}+0.0035\times(48.75)^{1.5} = 2.190+1.184 = 3.37$$

The threshold energy of this combination is calculated by eq. (18). Since the energy transfer factor $\gamma$ is calculated using eq. (19), i.e., $\gamma = 4\times 4.003\times 197/(4.003+197)^2 = 0.07878$, we have

$$E_{th} = \frac{1+5.7/48.75}{0.07878}\times 3.81 = 54.0$$

Now the sputtering yield of 1 keV He → Au is

$$Y = 0.042\frac{1.08\times 3.374\times 19.15}{3.81\times(1+1.38\times 2.96\times 0.0451^{0.3})}\left[1-\sqrt{\frac{54.0}{1000}}\right]^{2.8} = \frac{2.932}{9.952}\times 0.4769 = 0.140$$

which is found to be in good agreement with the yield shown in Fig. 307.

**Acknowledgement**

The present authors would like to express their sincere thanks to a number of students of

Okayama University of Science for their continuous supports of picking up experimental data from many published articles.

## References

[1] N.Matsunami,Y.Yamamura,Y.Itikawa,N.Itoh,Y.Kazumata,S.Miyagawa,K.Morita,R.Shimizu and H.Tawara, At. Data Nucl. Data Tables 31, 1 (1984).

[2] W. Eckstein, C. Garcia-Rosales, J. Roth and W. Ottenberger, IPP 9/82 (1993).

[3] J. Bohdansky, Nucl. Instr. Meth. B2, 587 (1984)

[4] E.W. Thomas, R.K. Janev, J. Botero, J.J. Smith and Yanghui Qiu, INDC(NDS)-287 (1993).

[5] J.Lindhard, V.Nielson and M.Scharff, Mat. Fys. Medd. Dan. Vid. Selsk., 36 no.10 (1968).

[6] R. Weissmann and R. Behrisch, Rad. Eff. 19, 69 (1973).

[7] P.Sigmund, Phys. Rev., 184 383 (1969).

[8] Y.Yamamura, Radiat.Eff., 55, 49 (1981).

[9] J. Vukanic and P. Sigmund, Appl. Phys. 11, 265 (1976).

[10] Y.Yamamura, N. Matsunami and N. Itoh, Rad. Eff. 71, 65 (1983).

[11] H.H.Andersen and J.F.Ziegler, Hydrogen Stopping and Ranges in All Elements (Pergamon, New York, 1985).

[12} J.Lindhard and M.Scharff, Phys. Rev., 124 128 (1961).

[13] Y.Yamamura and J.Bohdansky, Vacuum 35 561 (1985).

[14] Y.Yamamura and Y. Mizuno, IPPJ-AM-40. Inst. Plasma Physics. Nagoya University (1985).

[15] W.D. Wilson, L.G. Haggmark and J. Biersack, Phys. Rev. B15 (1977) 2458.

[16] O.S. Oen and M.T. Robinson, Nucl. Instr. Meth. 132 (1976) 647.

Table 1 The surface binding energies $U_s$ and best-fit values of $Q(Z_2)$, $W(Z_2)$ and $s(Z_2)$

| target | Z | $U_s$ (eV) | Q | W | s |
|---|---|---|---|---|---|
| Be | 4 | 3.32 | 1.66 | 2.32 | 2.5 |
| B | 5 | 5.77 | 2.62 | 4.39 | 2.5 |
| C | 6 | 7.37 | 1.70 | 1.84 | 2.5 |
| Al | 13 | 3.39 | 1.0 | 2.17 | 2.5 |
| Si | 14 | 4.63 | 0.66 | 2.32 | 2.5 |
| Ti | 22 | 4.85 | 0.54 | 2.57 | 2.5 |
| V | 23 | 5.31 | 0.72 | 2.39 | 2.5 |
| Cr | 24 | 4.10 | 0.93 | 1.44 | 2.5 |
| Mn | 25 | 2.92 | 0.95 | 0.88 | 2.5 |
| Fe | 26 | 4.28 | 0.75 | 1.20 | 2.5 |
| Co | 27 | 4.39 | 1.02 | 1.54 | 2.5 |
| Ni | 28 | 4.44 | 0.94 | 1.33 | 2.5 |
| Cu | 29 | 3.49 | 1.0 | 0.73 | 2.5 |
| Ge | 32 | 3.85 | 0.59 | 2.08 | 2.5 |
| Zr | 40 | 6.25 | 0.54 | 2.50 | 2.8 |
| Nb | 41 | 7.57 | 0.93 | 2.65 | 2.8 |
| Mo | 42 | 6.82 | 0.85 | 2.39 | 2.8 |
| Ru | 44 | 6.74 | 1.31 | 2.36 | 2.5 |
| Rh | 45 | 5.75 | 1.14 | 2.59 | 2.5 |
| Pd | 46 | 3.89 | 0.85 | 1.36 | 2.5 |
| Ag | 47 | 2.95 | 1.08 | 1.03 | 2.8 |
| Sn | 50 | 3.14 | 0.47 | 0.88 | 2.5 |
| Tb | 65 | 4.05 | 0.90 | 1.42 | 2.5 |
| Tm | 69 | 2.42 | 0.65 | 0.85 | 2.5 |
| Hf | 72 | 6.44 | 0.65 | 2.25 | 2.5 |
| Ta | 73 | 8.1 | 0.56 | 2.84 | 2.8 |
| W | 74 | 8.9 | 0.72 | 2.14 | 2.8 |
| Re | 75 | 8.03 | 1.03 | 2.81 | 2.5 |
| Os | 76 | 8.17 | 1.11 | 2.86 | 2.5 |
| Ir | 77 | 6.94 | 0.96 | 2.43 | 2.5 |
| Pt | 78 | 5.84 | 1.03 | 3.21 | 2.5 |
| Au | 79 | 3.81 | 1.08 | 1.64 | 2.8 |
| Th | 90 | 6.2 | 0.63 | 2.79 | 2.5 |
| U | 93 | 5.55 | 0.66 | 2.78 | 2.5 |

Table 2 Values of the adjusting parameter $q$

| target | Z | H | D | He |
|---|---|---|---|---|
| Be | 4 | -0.1 | -0.1 | 0.0 |
| B | 5 | -0.1 | -0.1 | 0.0 |
| C* | 6 | 0.0 | 0.0 | 0.1 |
| Al | 13 | -0.1 | -0.1 | -0.1 |
| Si | 14 | -0.25 | -0.25 | -0.4 |
| Ti | 22 | -0.35 | -0.35 | -0.35 |
| V | 23 | -0.3 | -0.3 | -0.25 |
| Cr | 24 | -0.1 | -0.1 | -0.1 |
| Mn | 25 | 0.0 | 0.0 | 0.0 |
| Fe | 26 | -0.25 | -0.25 | -0.2 |
| Co | 27 | -0.2 | -0.2 | -0.2 |
| Ni | 28 | -0.2 | -0.2 | -0.15 |
| Cu* | 29 | 0.0 | -0.1 | -0.1 |
| Ge | 32 | -0.2 | -0.2 | -0.2 |
| Zr | 40 | -0.25 | -0.25 | -0.25 |
| Mo | 42 | -0.2 | -0.2 | -0.2 |
| Ru | 44 | 0.0 | 0.0 | 0.0 |
| Rh | 45 | -0.1 | -0.1 | -0.2 |
| Pd | 46 | 0.0 | 0.0 | 0.0 |
| Ag* | 47 | -0.1 | 0.0 | 0.0 |
| Sn | 50 | 0.0 | 0.0 | 0.0 |
| Tb* | 65 | -0.1 | 0.0 | 0.0 |
| Tm* | 69 | 0.0 | 0.0 | 0.0 |
| Hf | 72 | -0.2 | -0.2 | -0.2 |
| Ta | 73 | -0.4 | -0.5 | -0.3 |
| W | 74 | -0.35 | -0.4 | -0.2 |
| Os | 76 | -0.2 | -0.2 | -0.2 |
| Ir | 77 | -0.2 | -0.2 | -0.2 |
| Pt | 78 | -0.2 | -0.2 | -0.2 |
| Au* | 79 | 0.0 | -0.1 | -0.2 |
| Th | 90 | -0.2 | -0.1 | -0.2 |
| U | 92 | -0.2 | -0.2 | -0.2 |

fn. The OR local model of the electronic energy loss is used for the target material with the star mark.

Table 3 Ion-target combinations of which was drawn by graphs

| Target \ Ion | | H | D | $^3$He | He | Li | C | N | O | F | Ne | Na | Si | P | S | Cl | Ar | K | Ni | Zn | As | Se | Br | Kr | Cd | Sb | Te | Xe | Cs | Hg | Tl | Pb | Bi | + |
|---|---|---|---|---|---|---|---|---|---|---|---|---|---|---|---|---|---|---|---|---|---|---|---|---|---|---|---|---|---|---|---|---|---|---|
| | | 1 | 1 | 2 | 2 | 3 | 6 | 7 | 8 | 9 | 10 | 11 | 14 | 15 | 16 | 17 | 18 | 19 | 28 | 30 | 33 | 34 | 35 | 36 | 48 | 51 | 52 | 54 | 55 | 80 | 81 | 82 | 83 | |
| Be | 4 | 4 | 4 | | 6 | | | | 1 | | 2 | | | | | | 2 | | | | | | | 2 | | | | 2 | | | | | | |
| B | 5 | 1 | 1 | | 2 | | | | | | | | | | | | | | | | | | | | | | | | | | | | | 1 |
| C | 6 | 8 | 5 | | 7 | | | | 2 | | 2 | | | | | | 4 | | | | | | | 4 | 1 | | | 3 | | 3 | | | | 2 |
| Al | 13 | 2 | 3 | | 4 | | | | | | 2 | | | | | | 8 | | | | | | | 2 | | | | 1 | | 4 | | | | 3 |
| Si | 14 | 1 | 1 | | 3 | | | | 1 | 1 | 3 | | | | | | 11 | | | | | | | 4 | | | | 3 | | 2 | | 1 | | |
| Ti | 22 | 2 | 4 | | 8 | | | | | | 1 | | | | | | 6 | | | | | | | 1 | 1 | | | 1 | | 6 | | | | |
| V | 23 | 1 | 1 | | 6 | | | | | | 2 | | | | | | 4 | | | | | | | 2 | | | | 2 | | 3 | | | | |
| Cr | 24 | | | | 1 | | | | | | 1 | | | | | | 4 | | | | | | | 2 | | | | 1 | | 5 | | | | 2 |
| Mn | 25 | | | | | | | | | | | | | | | | | | | | | | | 1 | | | | 1 | | | | | | |
| Fe | 26 | 3 | 3 | | 3 | | | 2 | | | 3 | | | | | | 5 | | | | | | | 4 | | | | 4 | 1 | 7 | | 1 | | |
| Co | 27 | | | | 1 | | | | | | 1 | | | | | | 4 | | | | | | | 3 | | | | 1 | 2 | 4 | | | | 2 |
| Ni | 28 | 5 | 1 | | 6 | | | 1 | 1 | | 5 | | | | | | 12 | | | | | | | 7 | | | | 6 | | 7 | | | | 5 |
| Cu | 29 | 4 | 4 | | 6 | | | 4 | | | 10 | 2 | 1 | 2 | 2 | 2 | 27 | 2 | 2 | 2 | | | | 12 | 3 | | | 13 | 3 | 7 | 2 | 3 | | 7 |
| Ge | 32 | | | | 1 | | | | | | 1 | | | | | | 5 | | | | | | | 3 | | | | 2 | | 1 | | | | 1 |
| Zr | 40 | 1 | 1 | | 3 | 1 | | | | | 1 | | | | | | 5 | | | | | | | 2 | 1 | | | 1 | | 3 | | | | |
| Nb | 41 | 2 | 3 | | 3 | 1 | | | | | 2 | | | | | | 7 | | | | | | 1 | 3 | | | | 2 | 1 | 3 | | | | 2 |
| Mo | 42 | 7 | 3 | 1 | 10 | | | 1 | 1 | | 4 | | | | | | 10 | | | | | | | 4 | 1 | | | 5 | 1 | 7 | | 1 | | 2 |
| Ru | 44 | | | | | | | | | | 1 | | | | | | 1 | | | | | | | 1 | | | | 1 | | | | | | |
| Rh | 45 | | | | 1 | | | | | | 1 | | | | | | 1 | | | | | | | 2 | | | | 1 | | 3 | | | | |
| Pd | 46 | | | | 1 | | | | | | 2 | | | | | | 3 | | | | | | | 2 | | | | 2 | | 3 | | | | |
| Ag | 47 | 4 | 3 | | 4 | | | 2 | | | 5 | | | 1 | | 1 | 15 | | | | 1 | 1 | | 7 | | 1 | 1 | 7 | | 6 | | | 3 | 4 |
| Sn | 50 | | | | | | | | | | 1 | | | | | | 4 | | | | | | | 1 | | | | 1 | | | | | | 2 |
| Tb | 65 | | | | | | | | | | | | | | | | 1 | | | | | | | | | | | | | | | | | |
| Tm | 69 | | | | | | | | | | | | | | | | 1 | | | | | | | | | | | | | | | | | |
| Hf | 72 | | | | 1 | | | | | | 1 | | | | | | 2 | | | | | | | 2 | | | | 1 | | 1 | | | | |
| Ta | 73 | 3 | 3 | | 5 | | | | | | 3 | | | | | | 8 | | | | | | | 4 | 1 | | | 3 | | 7 | | | | |
| W | 74 | 3 | 3 | | 5 | | 1 | 1 | 6 | | 6 | | | | | | 10 | 1 | | | | | | 7 | 1 | | | 8 | 1 | 6 | | 1 | | 3 |
| Re | 75 | | | | | | | | | | 1 | | | | | | 2 | | | | | | | 1 | | | | 1 | | 2 | | | | |
| Os | 76 | | | | 1 | | | | | | 1 | | | | | | 1 | | | | | | | 1 | | | | 1 | | | | | | |
| Ir | 77 | | | | 1 | | | | | | 1 | | | | | | 1 | | | | | | | 2 | | | | 1 | | 2 | | | | |
| Pt | 78 | | | | 1 | | | | | | 3 | | | | | | 5 | | | | | | | 3 | | 1 | | 3 | | 5 | | 1 | | |
| Au | 79 | 4 | 3 | 2 | 4 | | | 1 | | | 7 | | | | | | 27 | | | | | 1 | | 5 | | 1 | | 8 | | 4 | | 2 | | 5 |
| Th | 90 | | | | 1 | | | | | | 1 | | | | | | 3 | | | | | | | 1 | | | | 1 | | 1 | | | | |
| U | 92 | | | | 1 | | | | | | 1 | | | | | | 2 | | | | | | | 1 | | | | 1 | | 3 | | | | |

+ self-sputtering

The figures in the table indicates the number of references of experimental work.

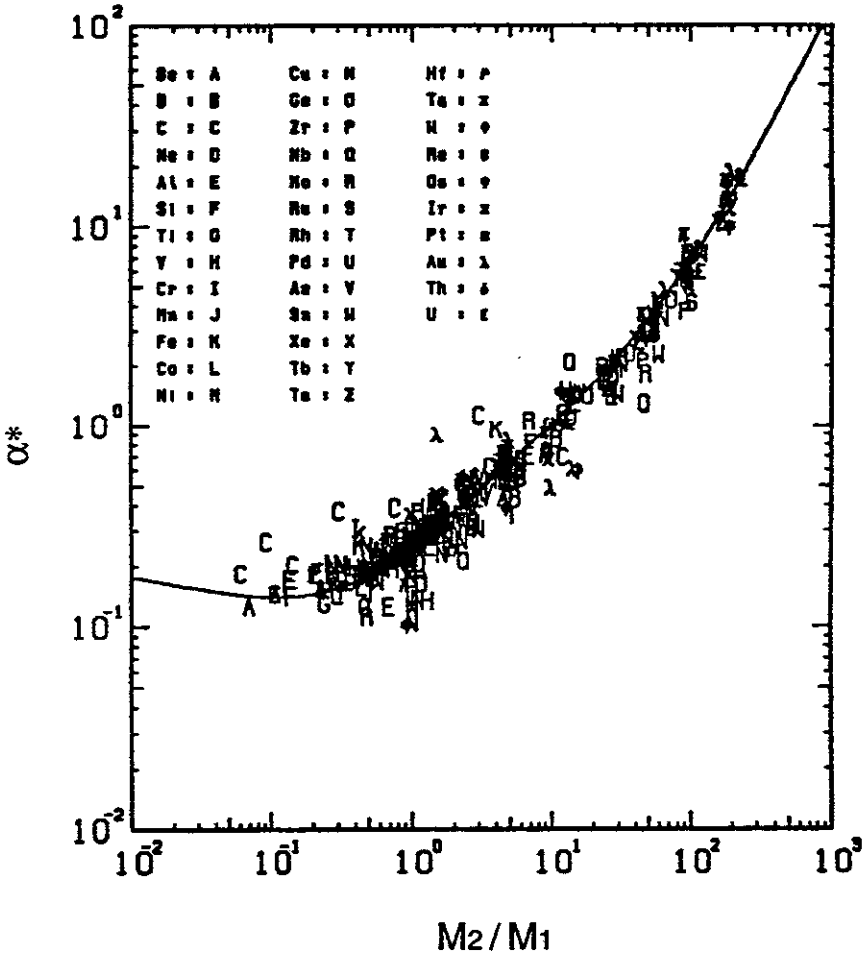


Fig. 1 Plots of the best-fit values of $\alpha^*$ as a function of mass ratio $M_2/M_1$

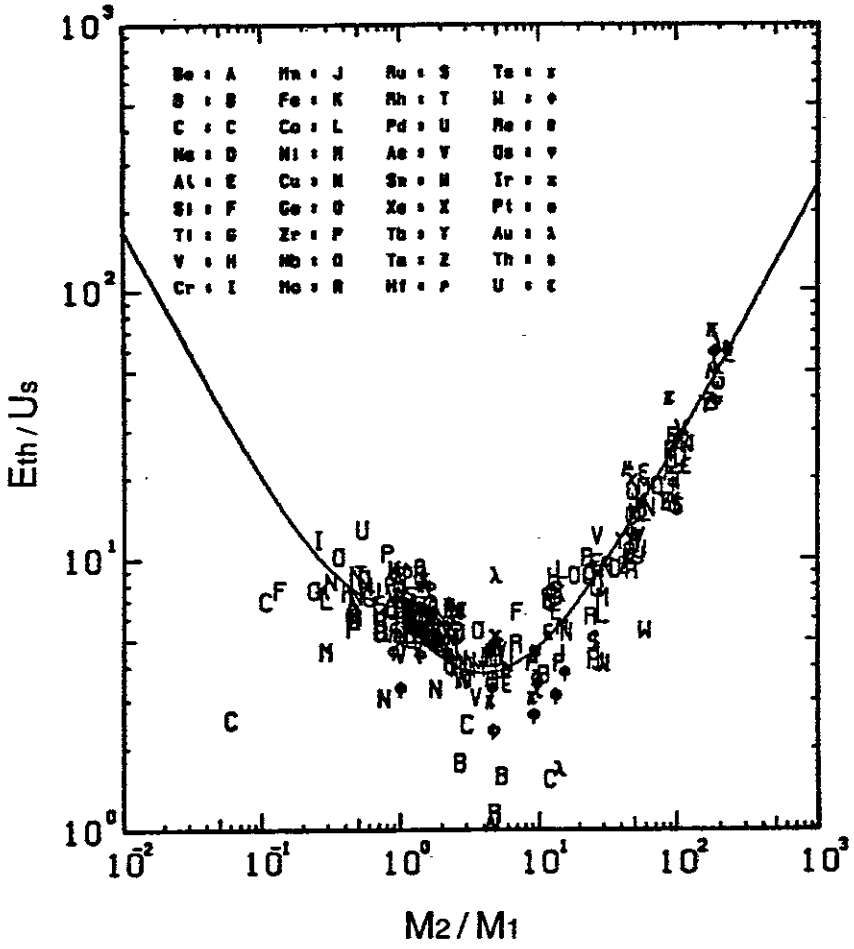


Fig. 2 Plots of the best-fit values of the relative threhold energy $E_{th}/U_s$ as a function of mass ratio $M_2/M_1$

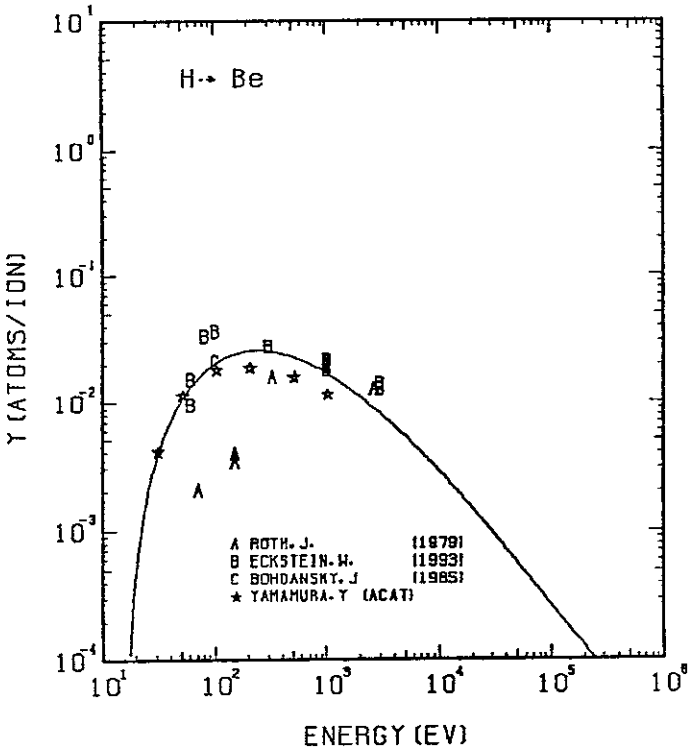


FIG. 3 ENERGY DEPENDENCE OF THE SPUTTERING YIELD OF BE WITH $H^+$.
A= 8.94, Q= 1.66, Us= 3.32EV, s= 2.50,
W= 0.70Us.

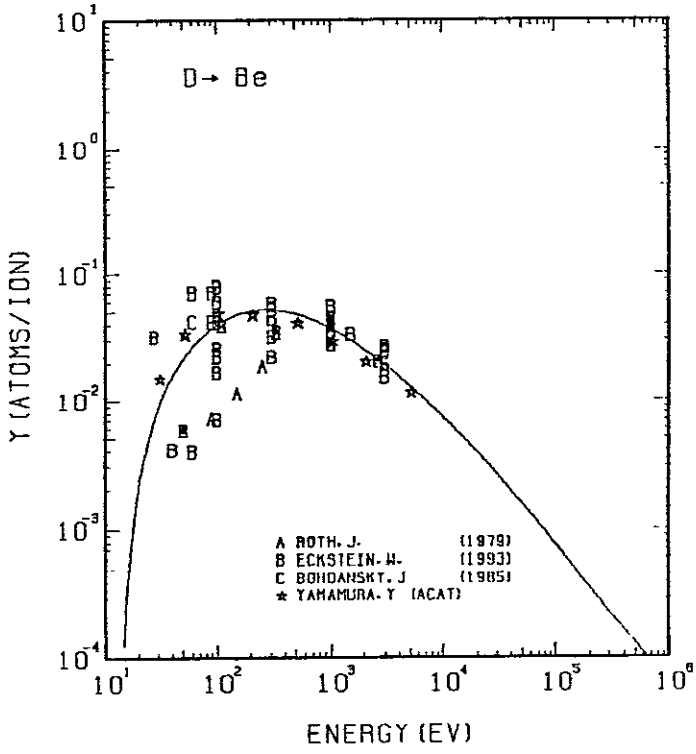


FIG. 4 ENERGY DEPENDENCE OF THE SPUTTERING YIELD OF BE WITH $D^+$.
A= 4.47, Q= 1.66, Us= 3.32EV, s= 2.50,
W= 0.70Us.

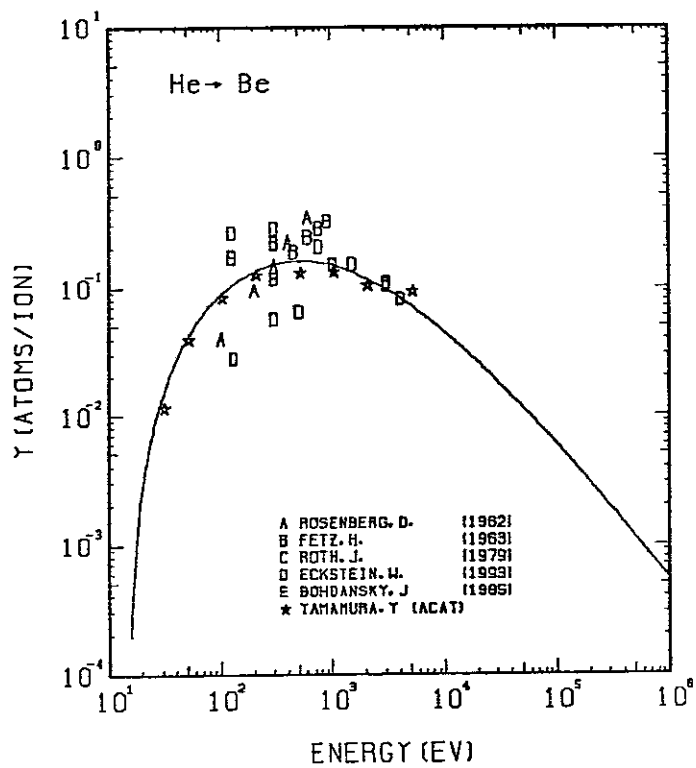


FIG. 5 ENERGY DEPENDENCE OF THE SPUTTERING YIELD OF BE WITH $HE^+$.
A= 2.25, Q= 1.66, Us= 3.32EV, s= 2.50,
W= 0.70Us.

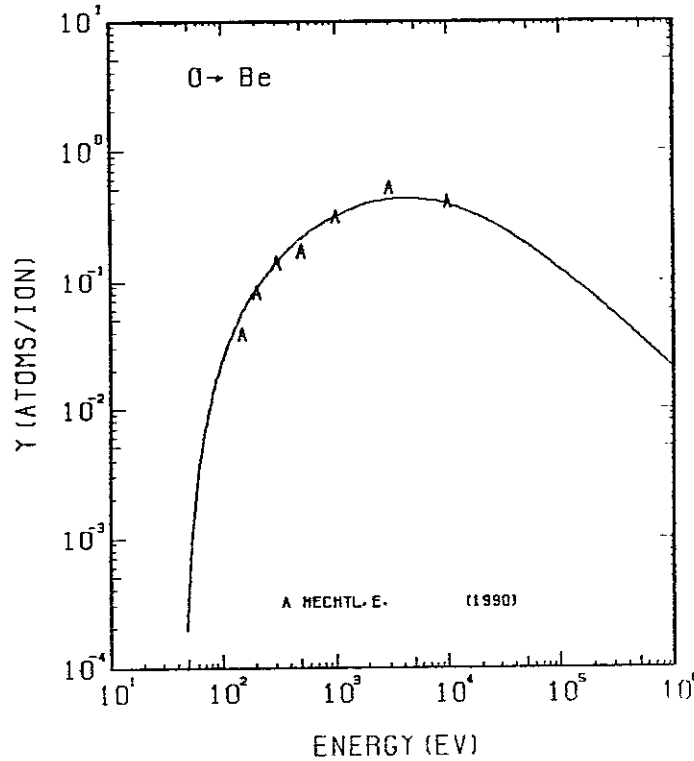


FIG. 6 ENERGY DEPENDENCE OF THE SPUTTERING YIELD OF BE WITH $O^+$.
A= 0.56, Q= 1.66, Us= 5.98EV, s= 2.50,
W= 0.70Us. THE BEST-FIT SURFACE BINDING ENERGY IS USED.

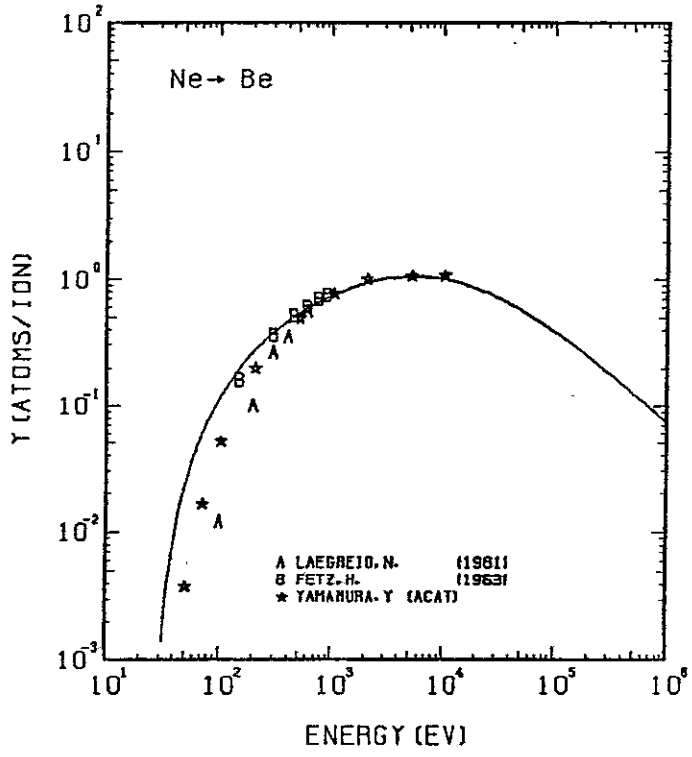


FIG. 7 ENERGY DEPENDENCE OF THE SPUTTERING YIELD OF BE WITH $NE^+$.
A= 0.45, Q= 1.66, Us= 3.32EV, s= 2.50,
W= 0.70Us.

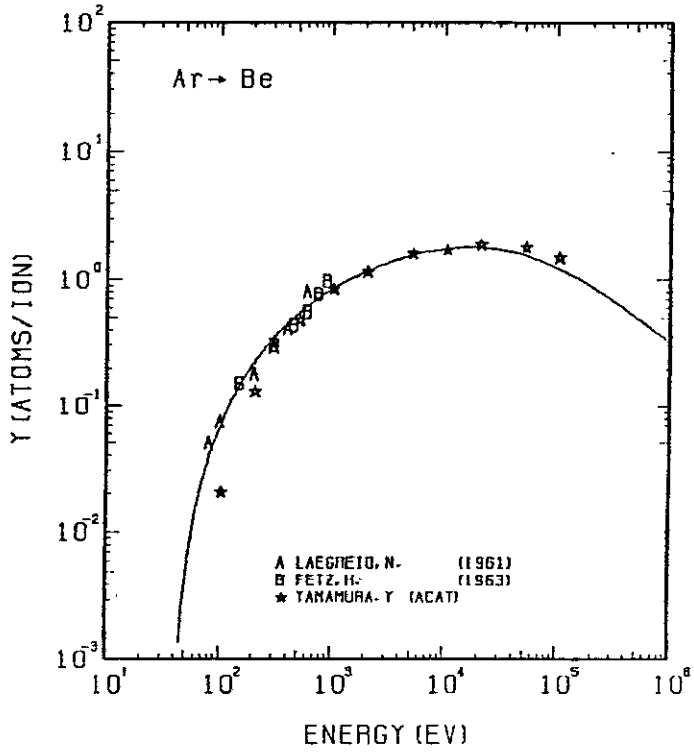


FIG. 8 ENERGY DEPENDENCE OF THE SPUTTERING YIELD OF BE WITH $AR^+$.
A= 0.23, Q= 1.66, Us= 3.32EV, s= 2.50,
W= 0.70Us.

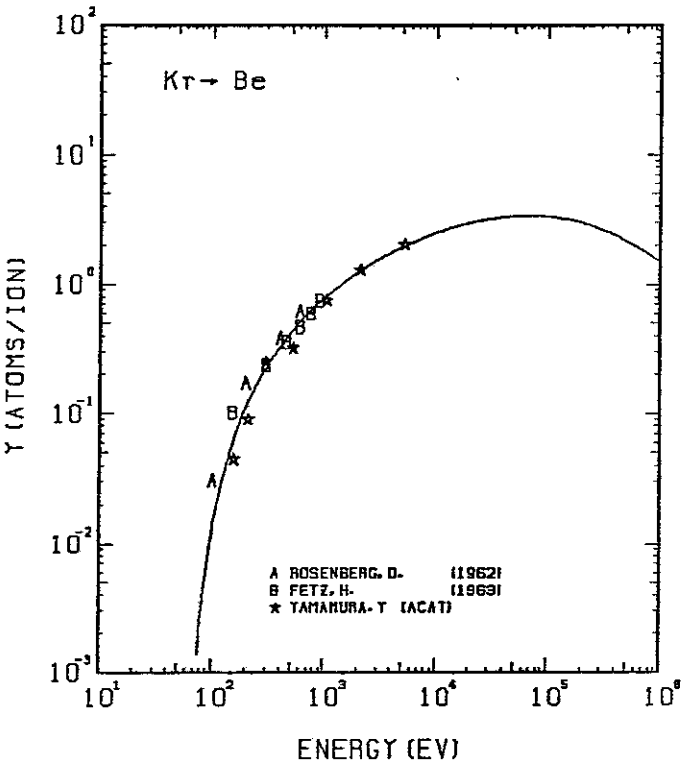


FIG. 9 ENERGY DEPENDENCE OF THE SPUTTERING YIELD OF BE WITH $KR^+$.
A= 0.11, Q= 1.66, Us= 3.32EV, s= 2.50,
W= 0.70Us.

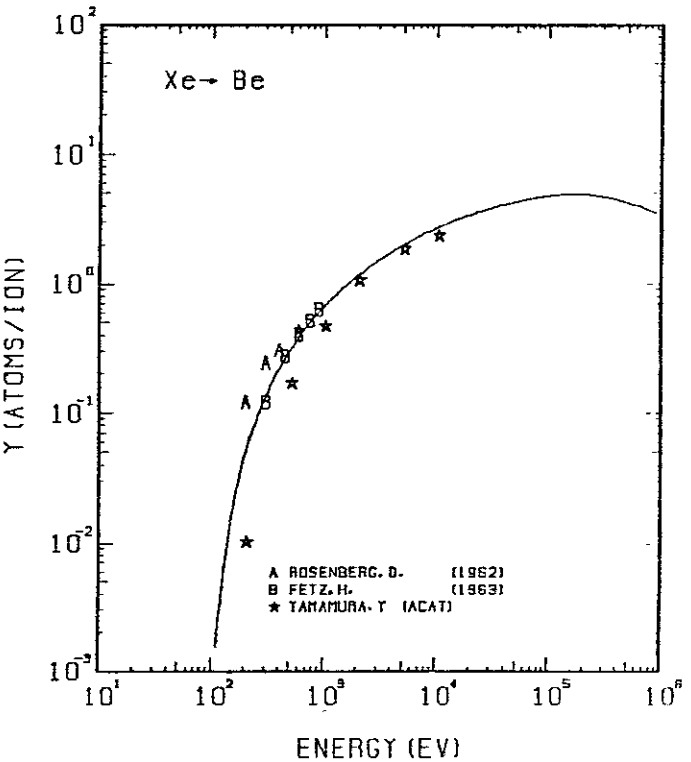


FIG. 10 ENERGY DEPENDENCE OF THE SPUTTERING YIELD OF BE WITH $XE^+$.
A= 0.07, Q= 1.66, Us= 3.32EV, s= 2.50,
W= 0.70Us.

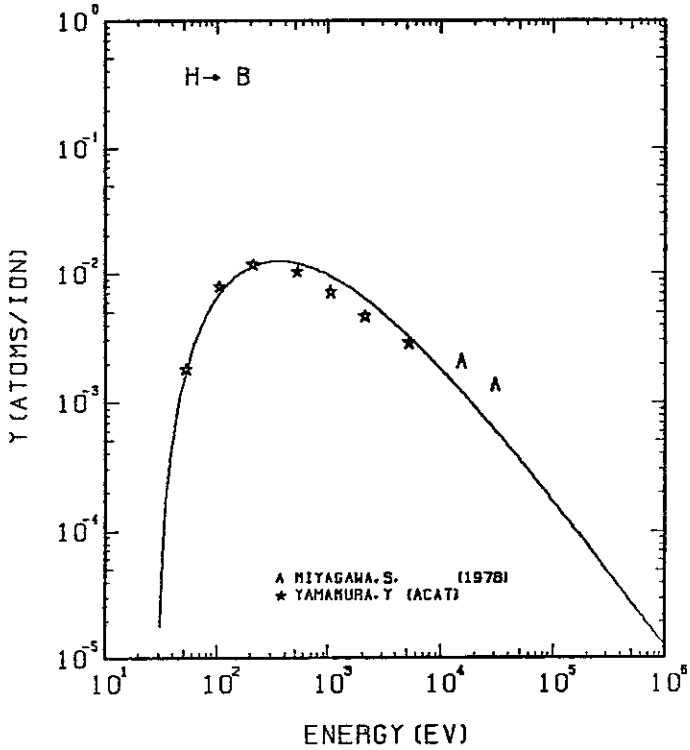


FIG. 11 ENERGY DEPENDENCE OF THE SPUTTERING YIELD OF B WITH $H^+$.
A= 10.72, Q= 2.62, Us= 5.77EV, s= 2.50,
W= 0.76Us.

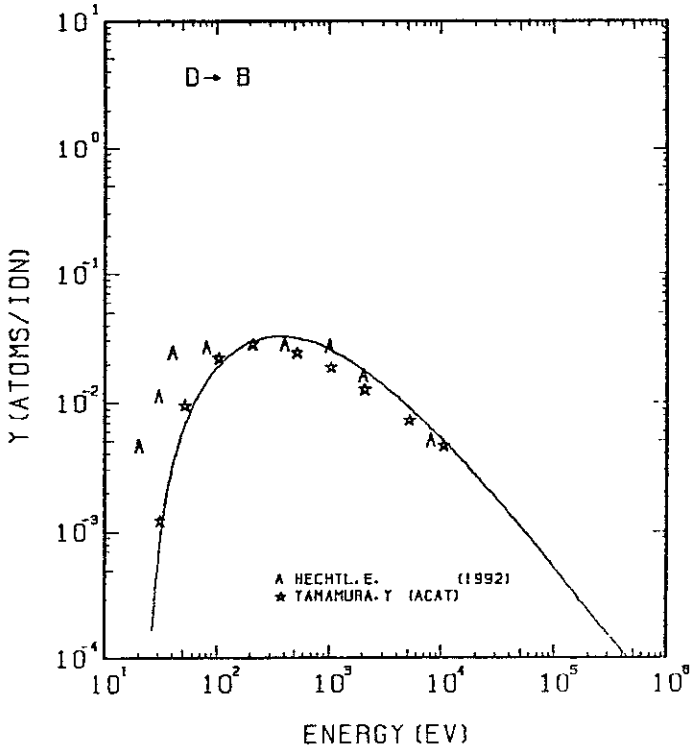


FIG. 12 ENERGY DEPENDENCE OF THE SPUTTERING YIELD OF B WITH $D^+$.
A= 5.37, Q= 2.62, Us= 5.77EV, s= 2.50,
W= 0.76Us.

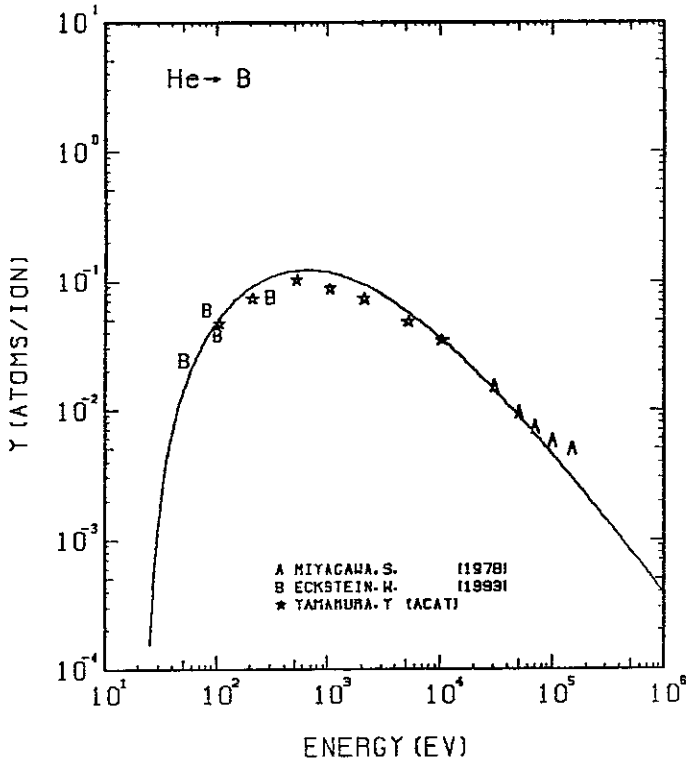


FIG. 13 ENERGY DEPENDENCE OF THE SPUTTERING YIELD OF B WITH $HE^+$.
A= 2.70, Q= 2.62, Us= 5.77EV, s= 2.50,
W= 0.76Us.

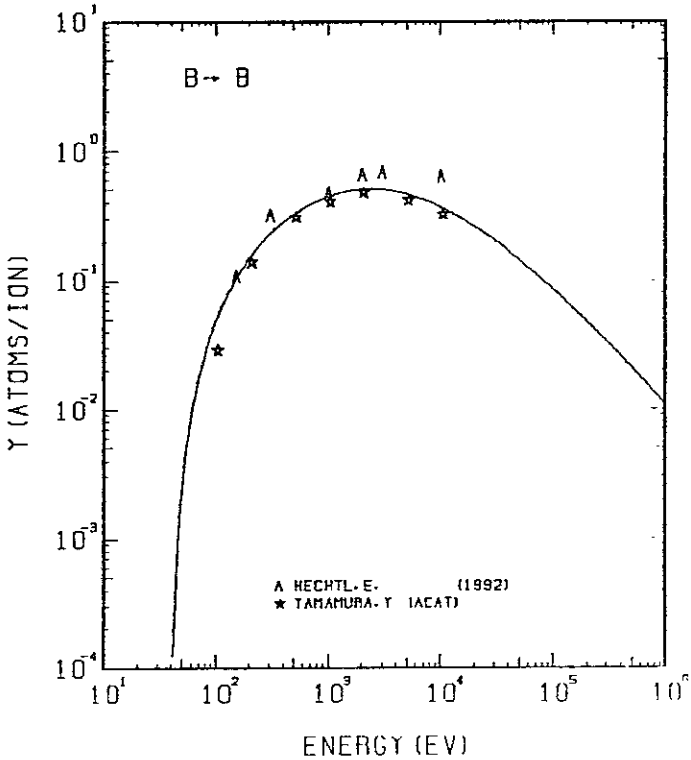


FIG. 14 ENERGY DEPENDENCE OF THE SPUTTERING YIELD OF B WITH $B^+$.
A= 1.00, Q= 2.62, Us= 5.77EV, s= 2.50,
W= 0.76Us.

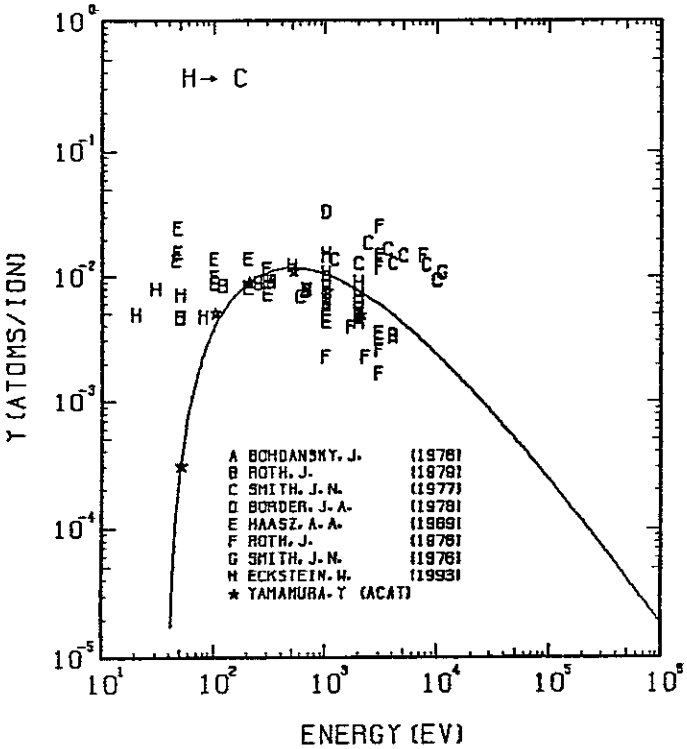


FIG. 15 ENERGY DEPENDENCE OF THE SPUTTERING YIELD OF C WITH $H^+$. A= 11.91, Q= 1.70, Us= 7.37eV, s= 2.50, W= 0.25Us. EXPERIMENTAL DATA FOR DIFFERENT KINDS OF GRAPHITE ARE INCLUDED. THE CHEMICAL EROSION IS FOUND EVEN AT ROOM TEMPERATURE.

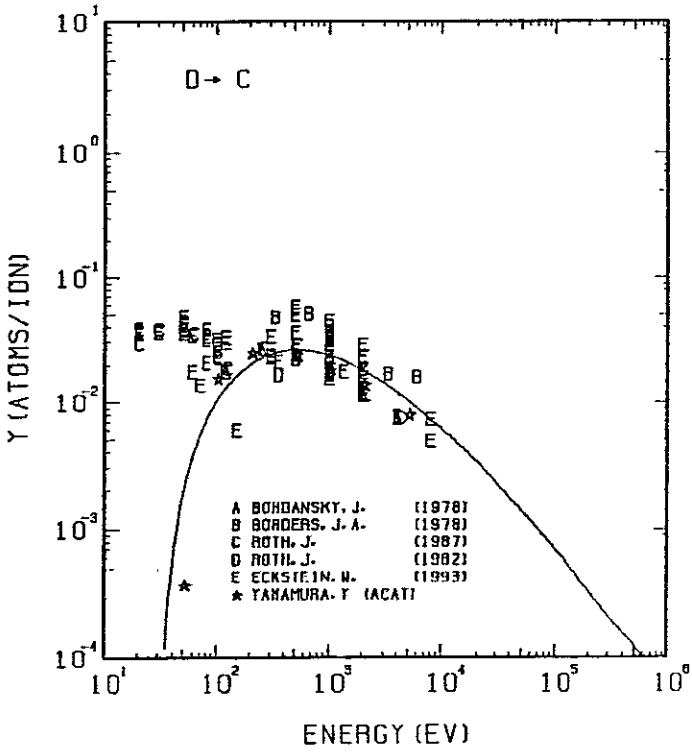


FIG. 16 ENERGY DEPENDENCE OF THE SPUTTERING YIELD OF C WITH $D^+$. A= 5.96, Q= 1.70, Us= 7.37eV, s= 2.50, W= 0.25Us. EXPERIMENTAL DATA FOR DIFFERENT KINDS OF GRAPHITE ARE INCLUDED. THE CHEMICAL EROSION IS FOUND EVEN AT ROOM TEMPERATURE.

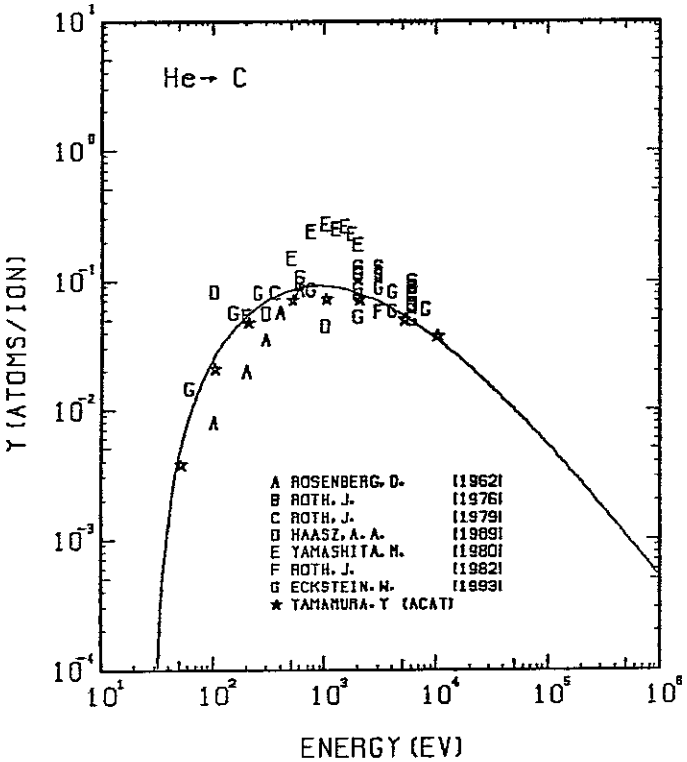


FIG. 17 ENERGY DEPENDENCE OF THE SPUTTERING YIELD OF C WITH $HE^+$. A= 3.00, Q= 1.70, Us= 7.37eV, s= 2.50, W= 0.25Us. EXPERIMENTAL DATA FOR DIFFERENT KINDS OF GRAPHITE ARE INCLUDED.

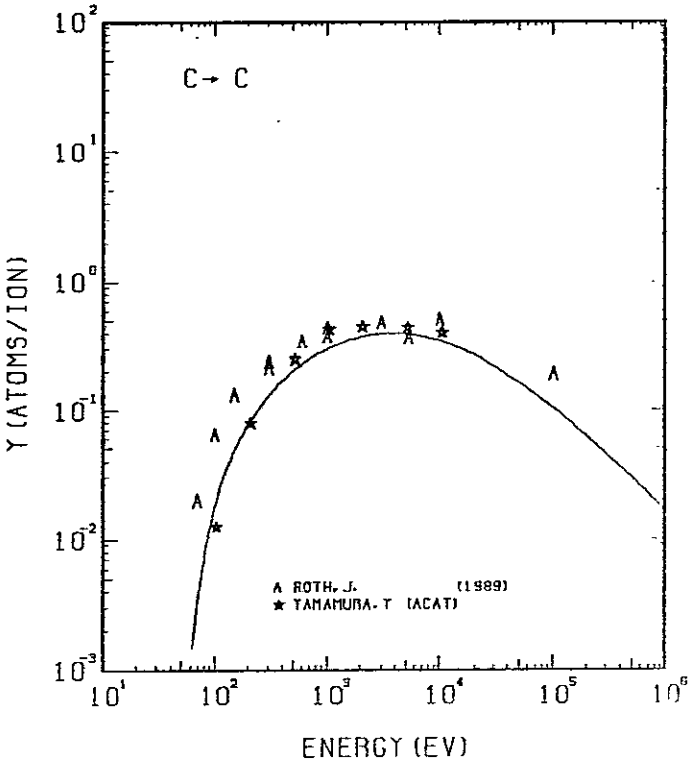


FIG. 18 ENERGY DEPENDENCE OF THE SPUTTERING YIELD OF C WITH $C^+$. A= 1.00, Q= 1.70, Us= 7.37eV, s= 2.50, W= 0.25Us. EXPERIMENTAL DATA FOR DIFFERENT KINDS OF GRAPHITE ARE INCLUDED.

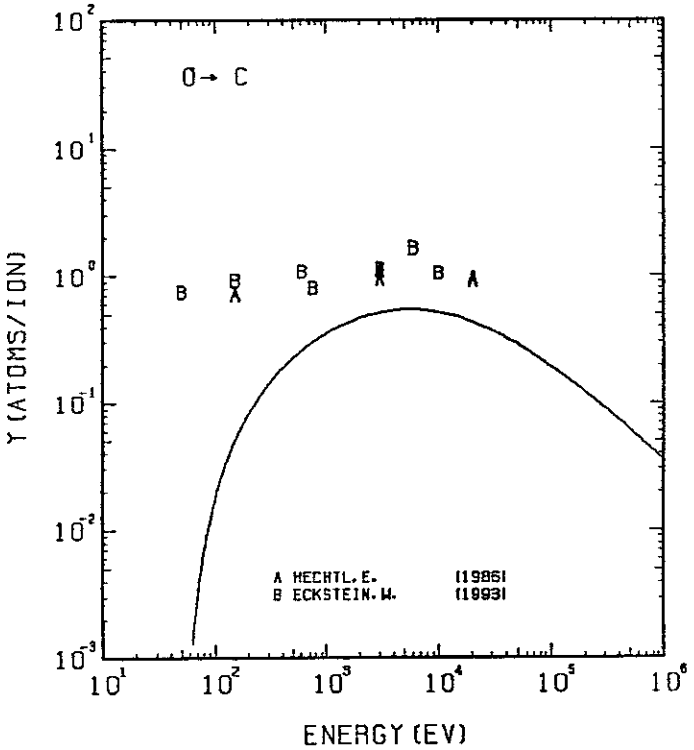


FIG. 19 ENERGY DEPENDENCE OF THE SPUTTERING YIELD OF C WITH $O^+$. A= 0.75, D= 1.70, Us= 7.37EV, S= 2.50, W= 0.25Us. EXPERIMENTAL DATA FOR DIFFERENT KINDS OF GRAPHITE ARE INCLUDED. THE CHEMICAL EROSION IS FOUND EVEN AT ROOM TEMPERATURE.

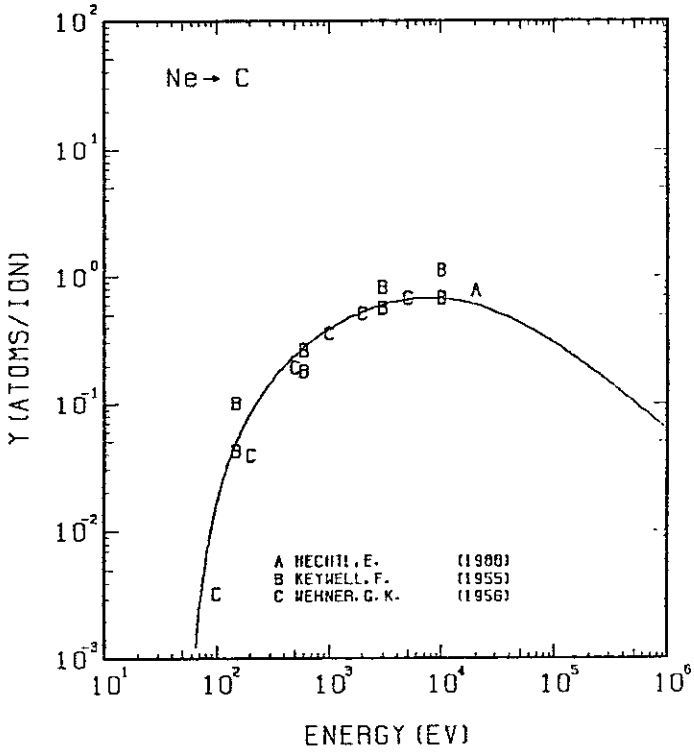


FIG. 20 ENERGY DEPENDENCE OF THE SPUTTERING YIELD OF C WITH $NE^+$. A= 0.60, D= 1.70, Us= 7.37EV, S= 2.50, W= 0.25Us. EXPERIMENTAL DATA FOR DIFFERENT KINDS OF GRAPHITE ARE INCLUDED.

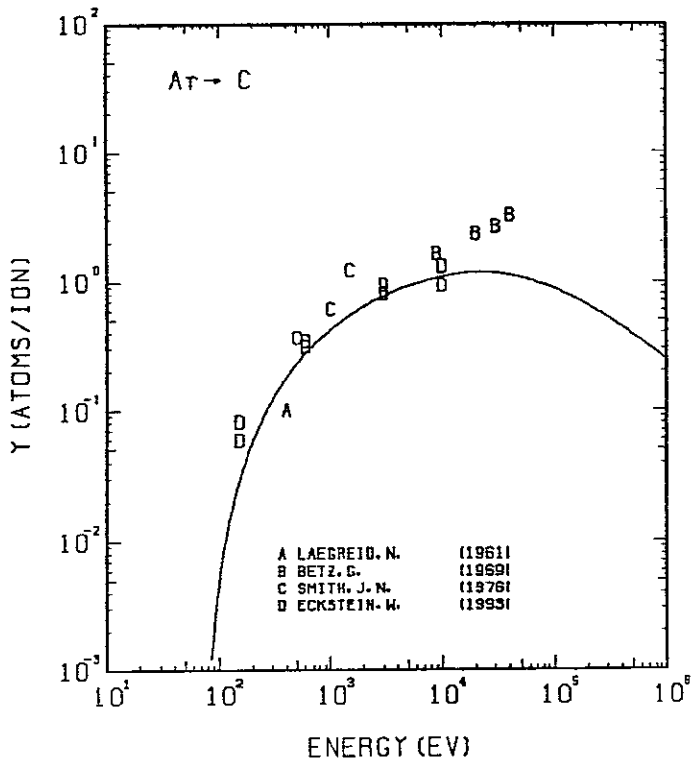


FIG. 21 ENERGY DEPENDENCE OF THE SPUTTERING YIELD OF C WITH $AR^+$. A= 0.30, D= 1.70, Us= 7.37EV, S= 2.50, W= 0.25Us. EXPERIMENTAL DATA FOR DIFFERENT KINDS OF GRAPHITE ARE INCLUDED.

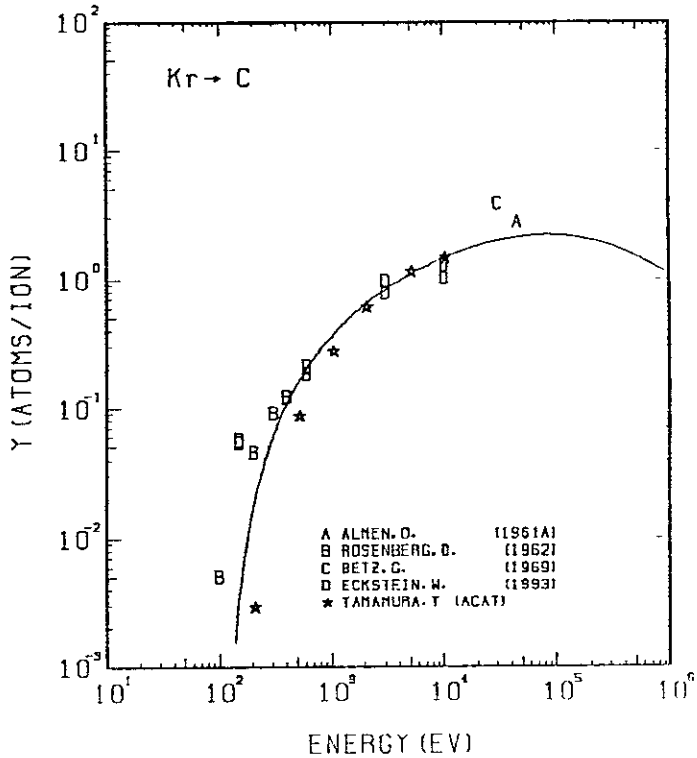


FIG. 22 ENERGY DEPENDENCE OF THE SPUTTERING YIELD OF C WITH $KR^+$. A= 0.14, D= 1.70, Us= 7.37EV, S= 2.50, W= 0.25Us. EXPERIMENTAL DATA FOR DIFFERENT KINDS OF GRAPHITE ARE INCLUDED.

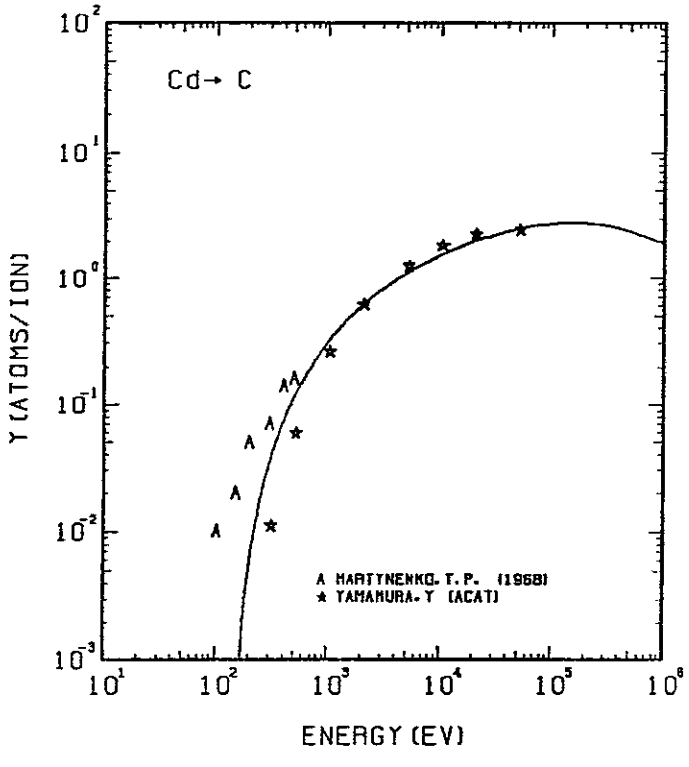


FIG. 23 ENERGY DEPENDENCE OF THE SPUTTERING YIELD OF C WITH $CD^+$. A= 0.11, Q= 1.70, Us=. 7.37EV, S= 2.50, W= 0.25Us.

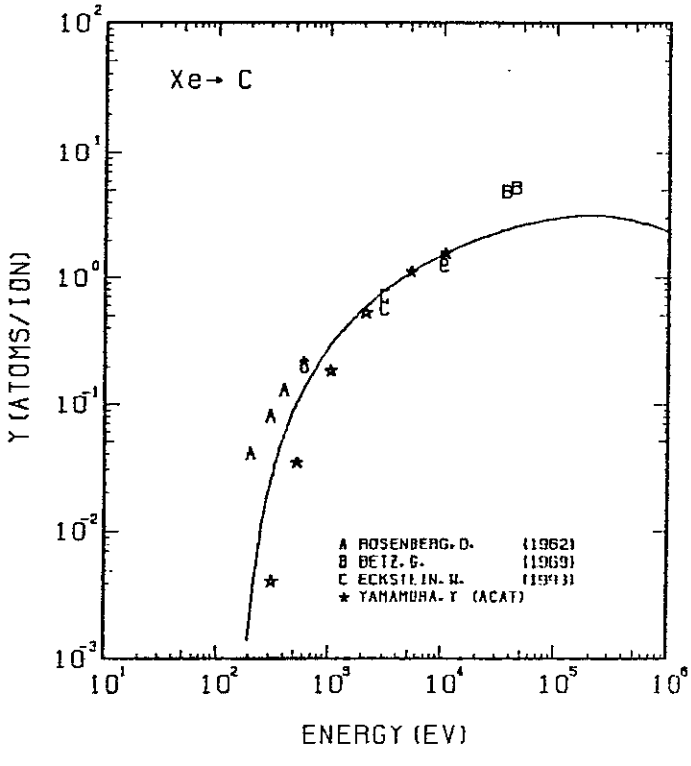


FIG. 24 ENERGY DEPENDENCE OF THE SPUTTERING YIELD OF C WITH $XE^+$. A= 0.09, Q= 1.70, Us= 7.37EV, S= 2.50, W= 0.25Us. EXPERIMENTAL DATA FOR DIFFERENT KINDS OF GRAPHITE ARE INCLUDED.

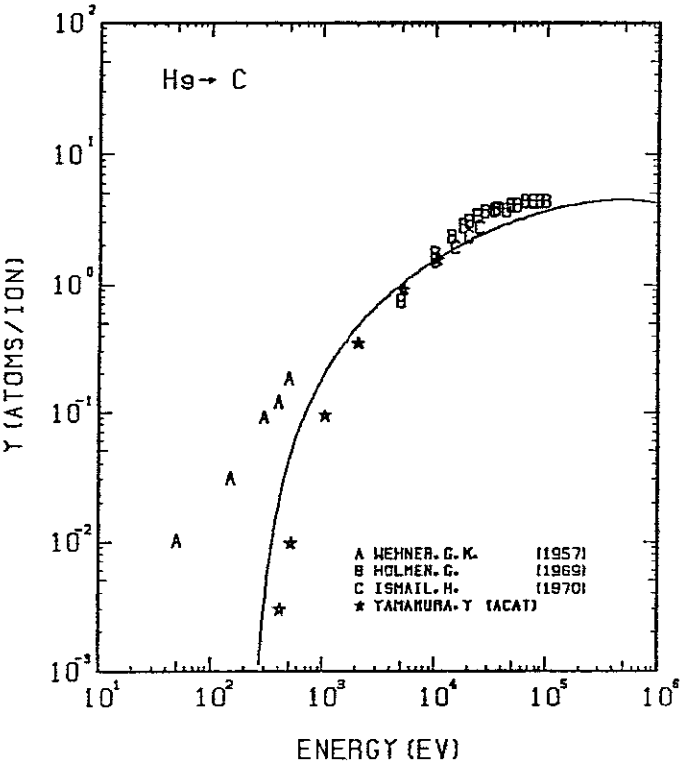


FIG. 25 ENERGY DEPENDENCE OF THE SPUTTERING YIELD OF C WITH $HG^+$. A= 0.06, Q= 1.70, Us= 7.37EV, S= 2.50, W= 0.25Us. EXPERIMENTAL DATA FOR DIFFERENT KINDS OF GRAPHITE ARE INCLUDED.

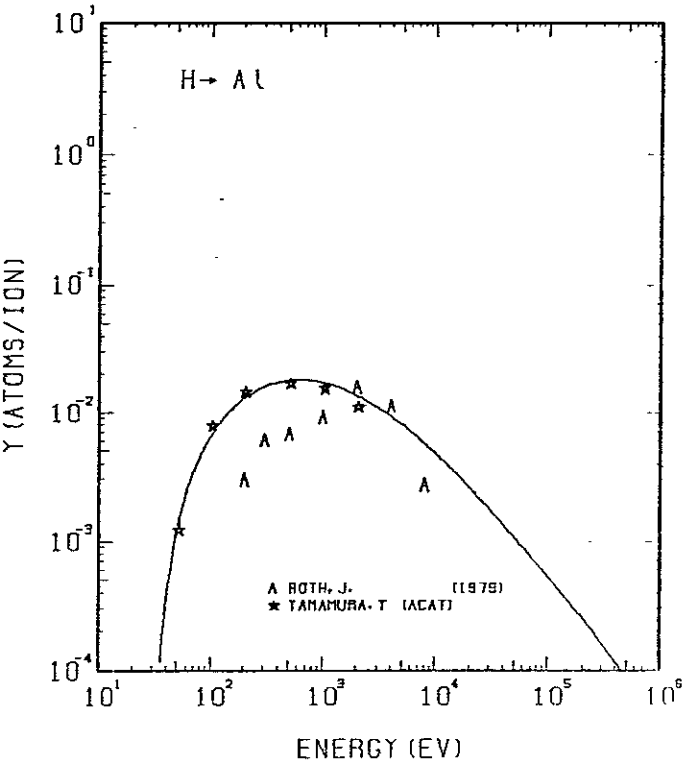


FIG. 26 ENERGY DEPENDENCE OF THE SPUTTERING YIELD OF AL WITH $H^+$. A= 26.77, Q= 1.00, Us= 3.39EV, S= 2.50, W= 0.64Us. EXPERIMENTAL DATA MIGHT BE AFFCTED BY OXIDE FORMAION DURING SPUTTERING.

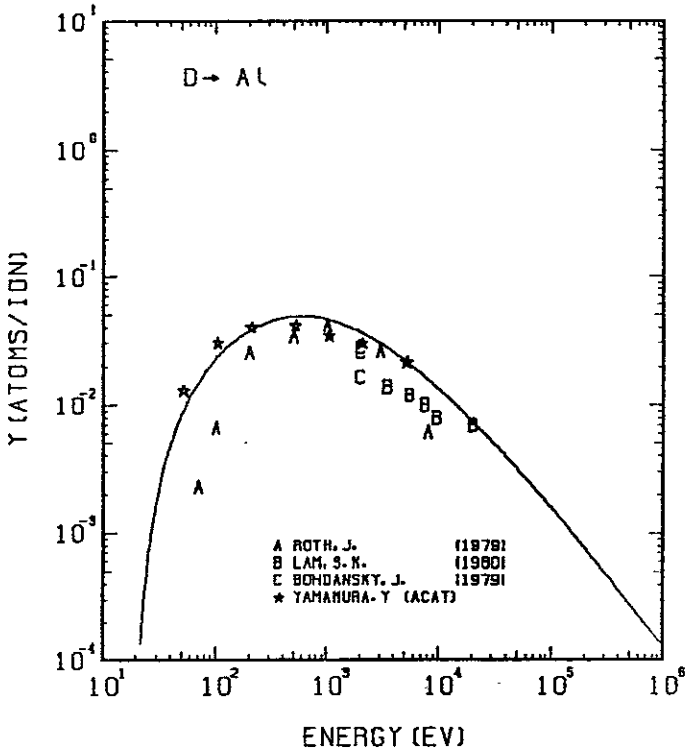


FIG. 27 ENERGY DEPENDENCE OF THE SPUTTERING YIELD OF AL WITH $D^+$. A= 13.40, Q= 1.00, Us= 3.39EV, s= 2.50, W= 0.64Us. EXPERIMENTAL DATA MIGHT BE AFFCTED BY OXIDE FORMAION DURING SPUTTERING.

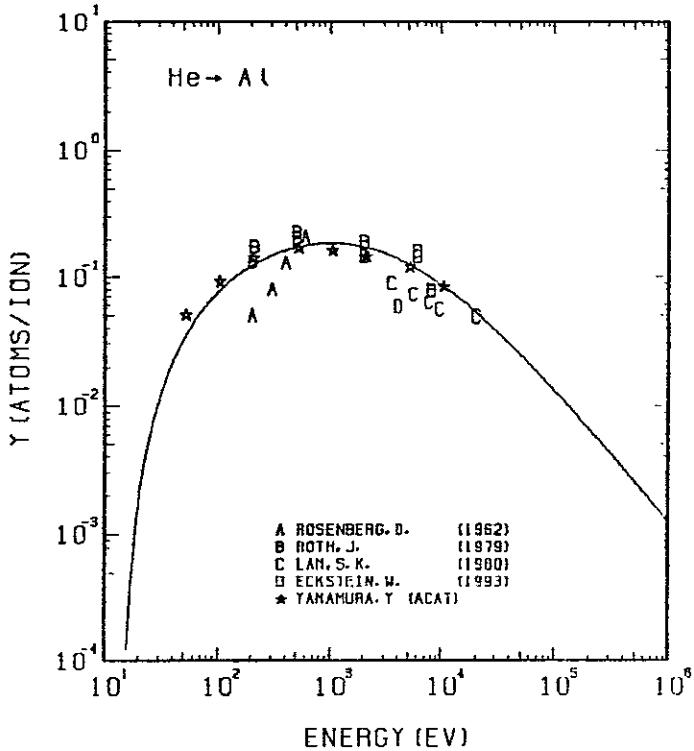


FIG. 28 ENERGY DEPENDENCE OF THE SPUTTERING YIELD OF AL WITH $HE^+$. A= 6.74, Q= 1.00, Us= 3.39EV, s= 2.50, W= 0.64Us. EXPERIMENTAL DATA MIGHT BE AFFCTED BY OXIDE FORMAION DURING SPUTTERING.

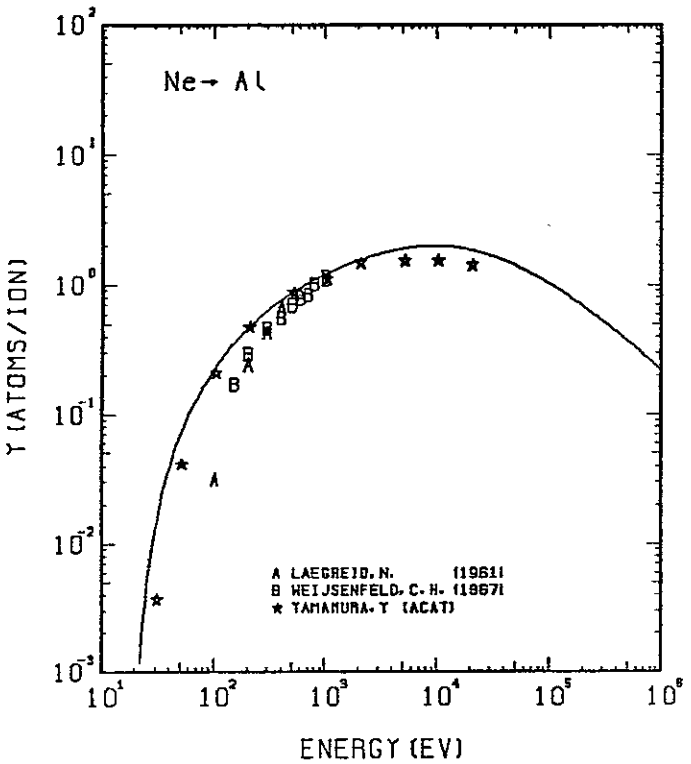


FIG. 29 ENERGY DEPENDENCE OF THE SPUTTERING YIELD OF AL WITH $NE^+$. A= 1.34, Q= 1.00, Us= 3.39EV, s= 2.50, W= 0.64Us. EXPERIMENTAL DATA MIGHT BE AFFCTED BY OXIDE FORMAION DURING SPUTTERING.

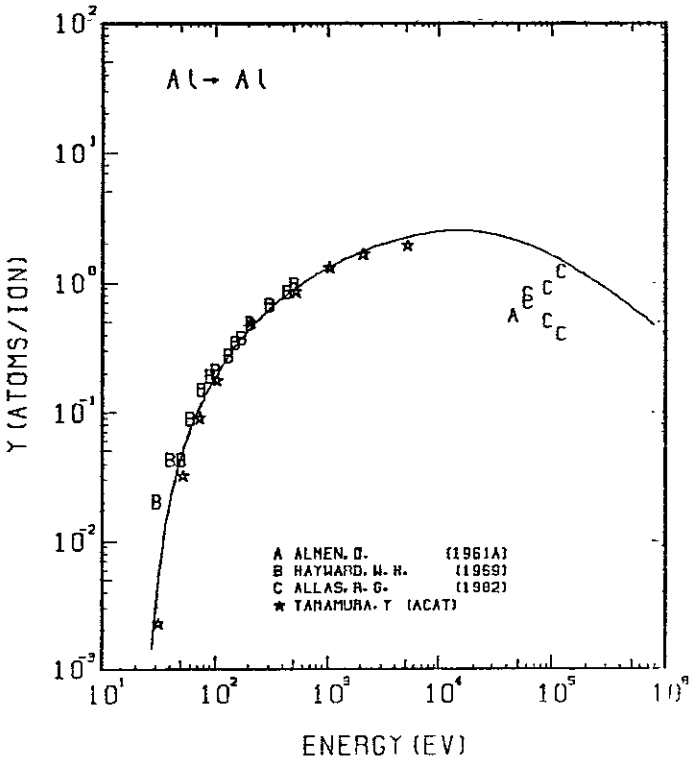


FIG. 30 ENERGY DEPENDENCE OF THE SPUTTERING YIELD OF AL WITH $AL^+$. A= 1.00, Q= 1.00, Us= 3.39EV, s= 2.50, W= 0.64Us.

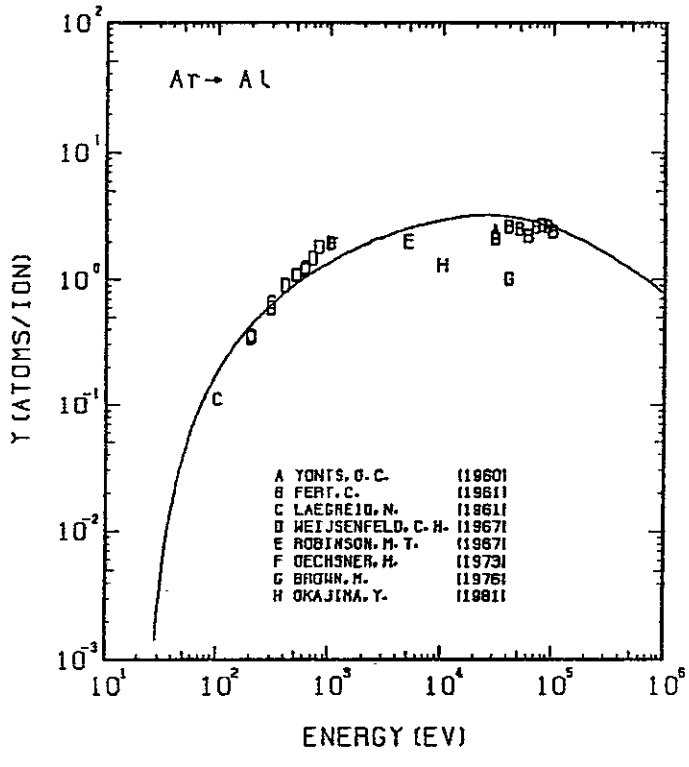


FIG. 31 ENERGY DEPENDENCE OF THE SPUTTERING YIELD OF AL WITH AR+.
A= 0.68, Q= 1.00, Us= 3.39EV, s= 2.50,
W= 0.64Us.

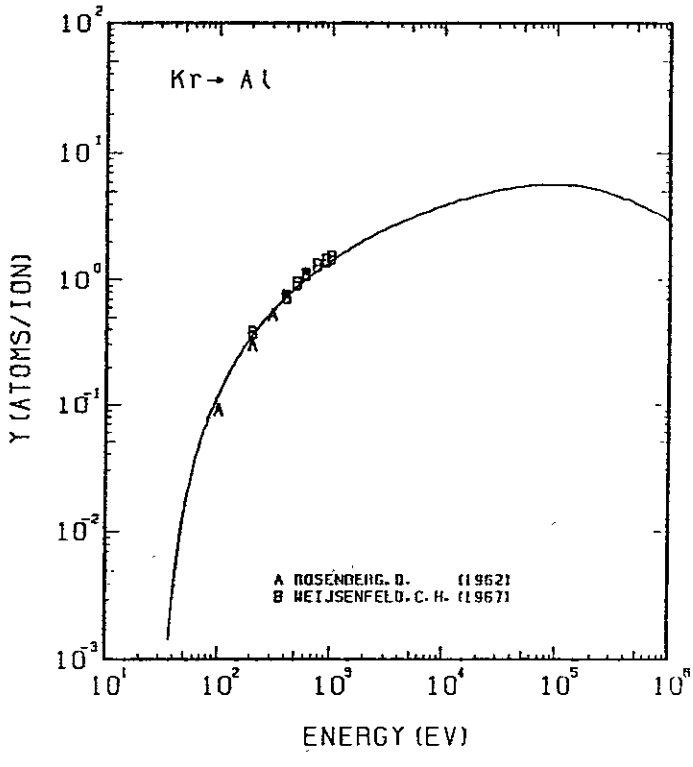


FIG. 32 ENERGY DEPENDENCE OF THE SPUTTERING YIELD OF AL WITH KR+.
A= 0.32, Q= 1.00, Us= 3.39EV, s= 2.50,
W= 0.64Us.

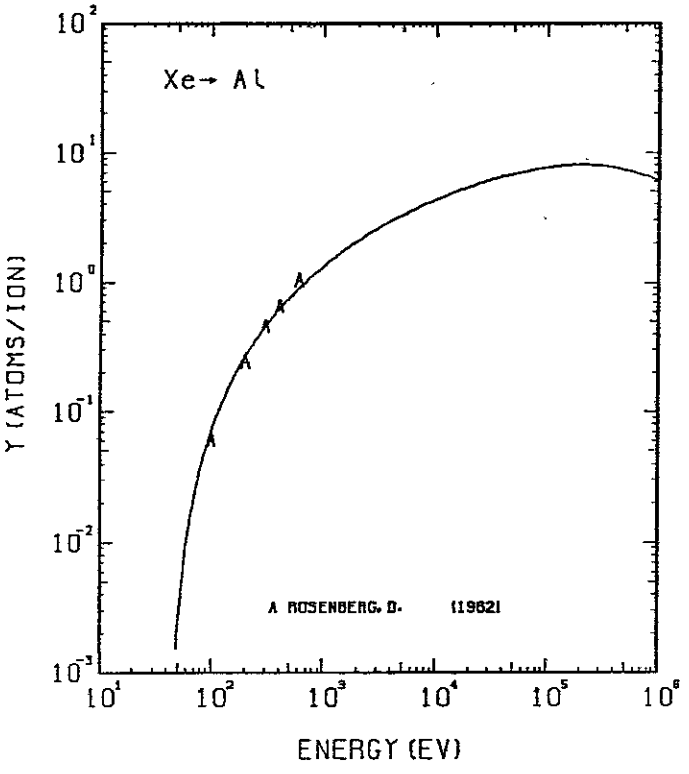


FIG. 33 ENERGY DEPENDENCE OF THE SPUTTERING YIELD OF AL WITH XE+.
A= 0.21, Q= 1.00, Us= 3.39EV, s= 2.50,
W= 0.64Us.

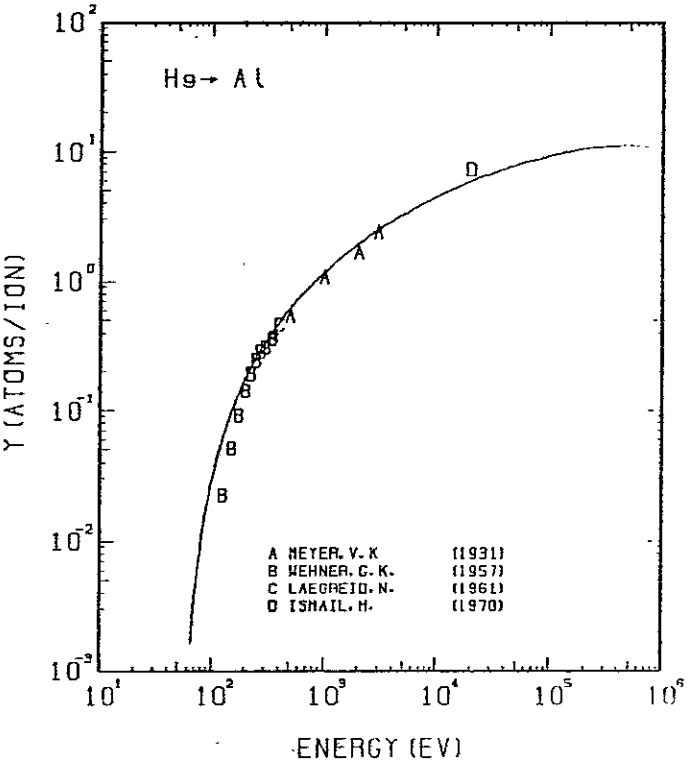


FIG. 34 ENERGY DEPENDENCE OF THE SPUTTERING YIELD OF AL WITH HG+.
A= 0.13, Q= 1.00, Us= 3.39EV, s= 2.50,
W= 0.64Us.

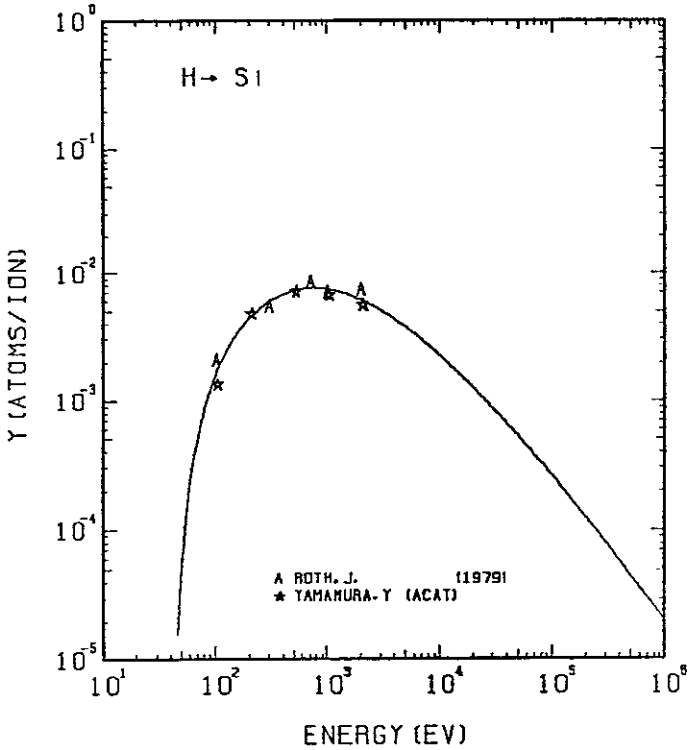


FIG. 35 ENERGY DEPENDENCE OF THE SPUTTERING YIELD OF SI WITH $H^+$.
A= 27.86, Q= 0.66, Us= 4.63EV, s= 2.50,
W= 0.50Us.

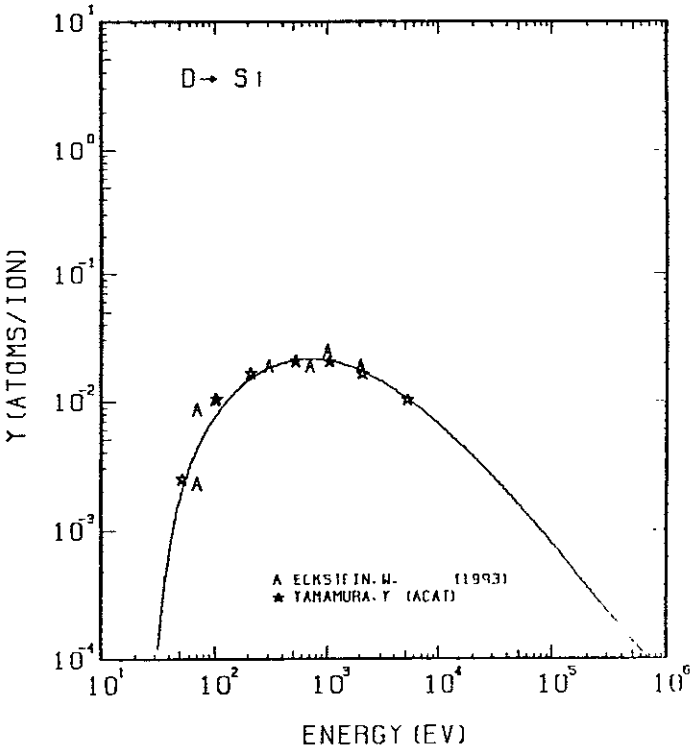


FIG. 36 ENERGY DEPENDENCE OF THE SPUTTERING YIELD OF SI WITH $D^+$.
A= 13.94, Q= 0.66, Us= 4.63EV, s= 2.50,
W= 0.50Us.

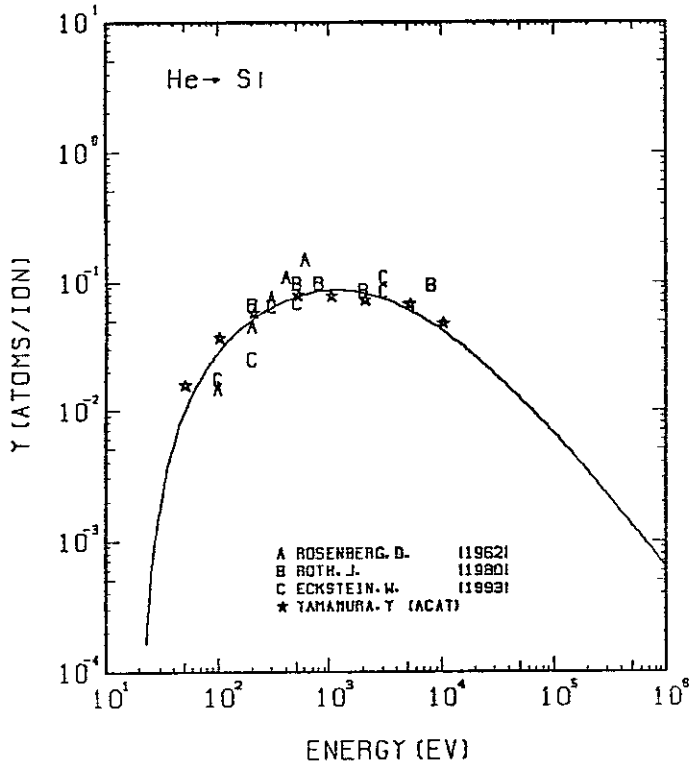


FIG. 37 ENERGY DEPENDENCE OF THE SPUTTERING YIELD OF SI WITH $HE^+$.
A= 7.01, Q= 0.66, Us= 4.63EV, s= 2.50,
W= 0.50Us.

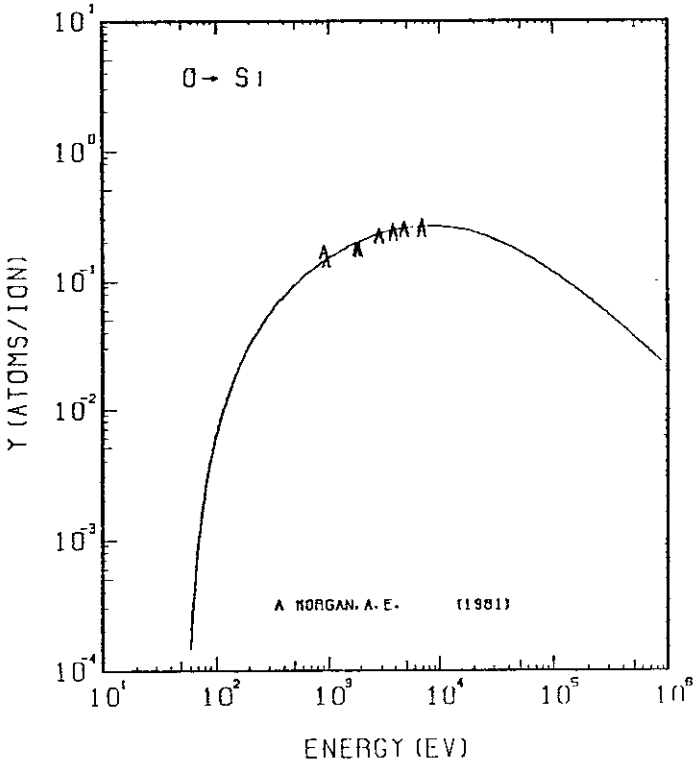


FIG. 38 ENERGY DEPENDENCE OF THE SPUTTERING YIELD OF SI WITH $O^+$.
A= 1.75, Q= 0.66, Us= 11.57EV, s= 2.50,
W= 0.50Us. THE BEST-FIT SURFACE BINDING ENERGY IS USED.

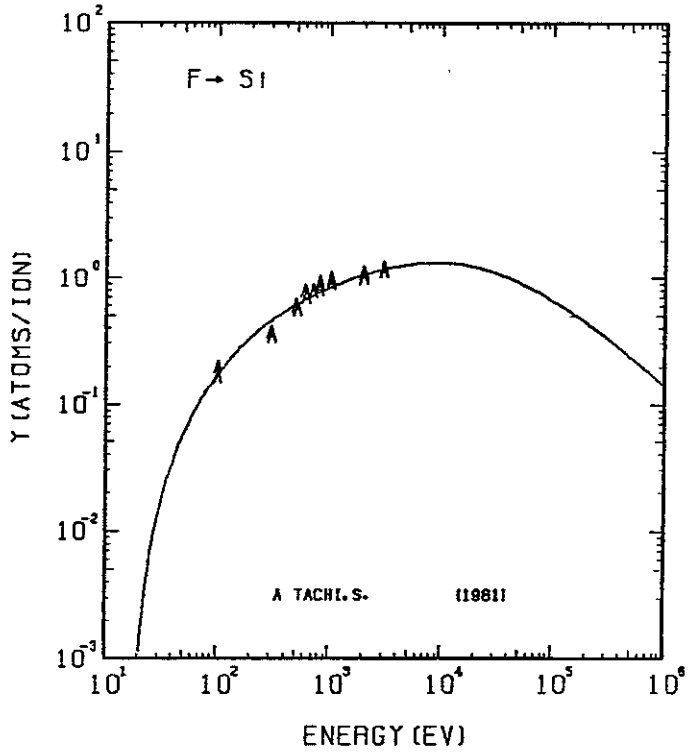


FIG. 39 ENERGY DEPENDENCE OF THE SPUTTERING YIELD OF SI WITH $F^+$. A= 1.48, D= 0.66, Us= 3.24EV, s= 2.50. W= 0.50Us. THE BEST-FIT SURFACE BINDING ENERGY IS USED.

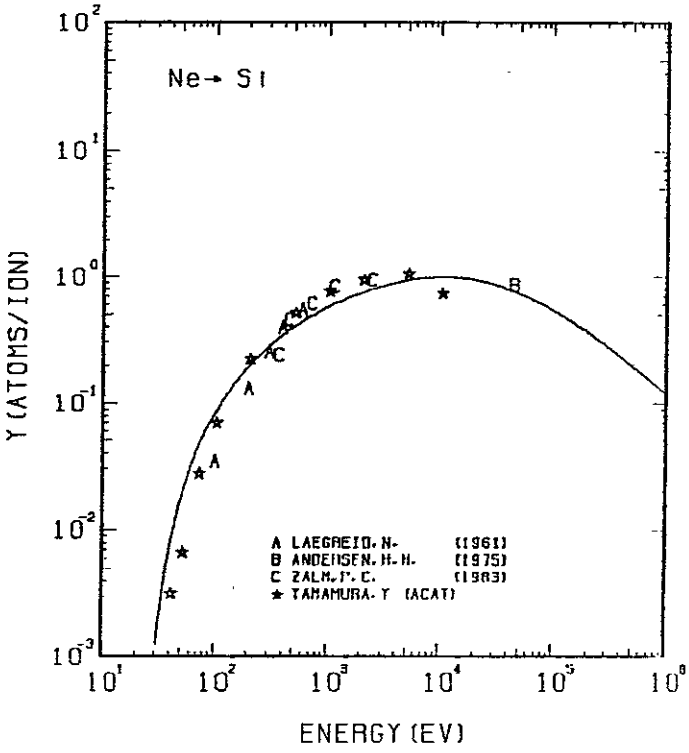


FIG. 40 ENERGY DEPENDENCE OF THE SPUTTERING YIELD OF SI WITH $NE^+$. A= 1.39, D= 0.66, Us= 4.63EV, s= 2.50. W= 0.50Us.

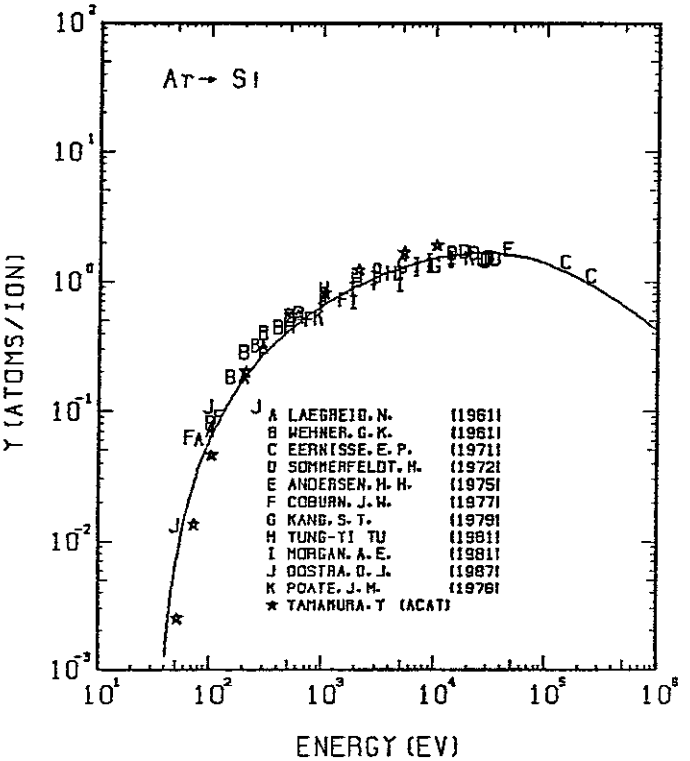


FIG. 41 ENERGY DEPENDENCE OF THE SPUTTERING YIELD OF SI WITH $AR^+$. A= 0.70, D= 0.66, Us= 4.63EV, s= 2.50, W= 0.50Us.

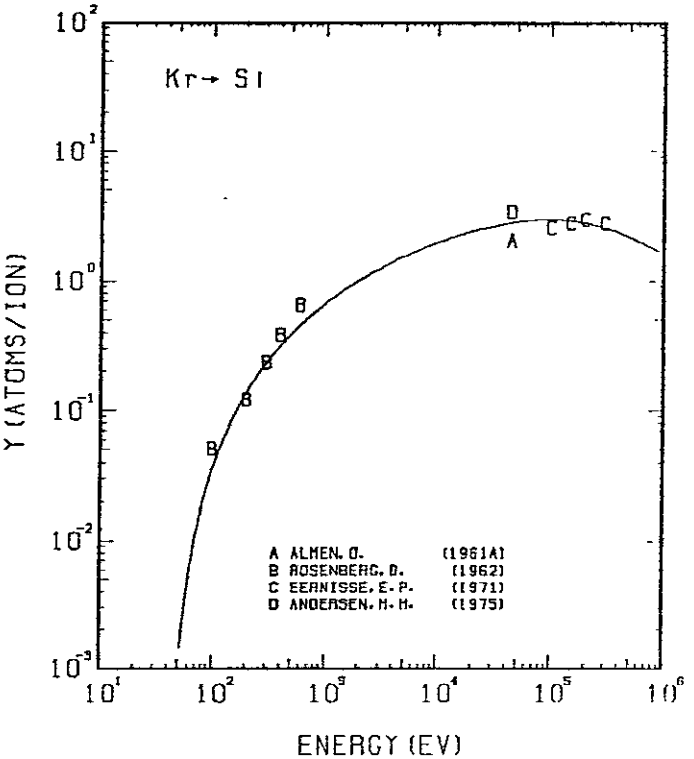


FIG. 42 ENERGY DEPENDENCE OF THE SPUTTERING YIELD OF SI WITH $KR^+$. A= 0.34, D= 0.66, Us= 4.63EV, s= 2.50, W= 0.50Us.

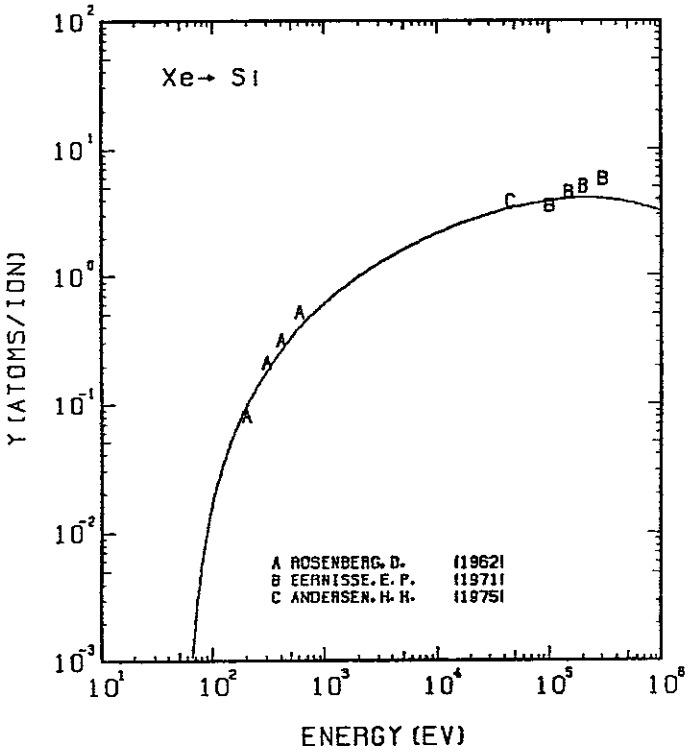


FIG. 43 ENERGY DEPENDENCE OF THE SPUTTERING YIELD OF SI WITH $XE^{+}$.
A= 0.21, 0= 0.66, Us= 4.63EV, s= 2.50.
W= 0.50Us.

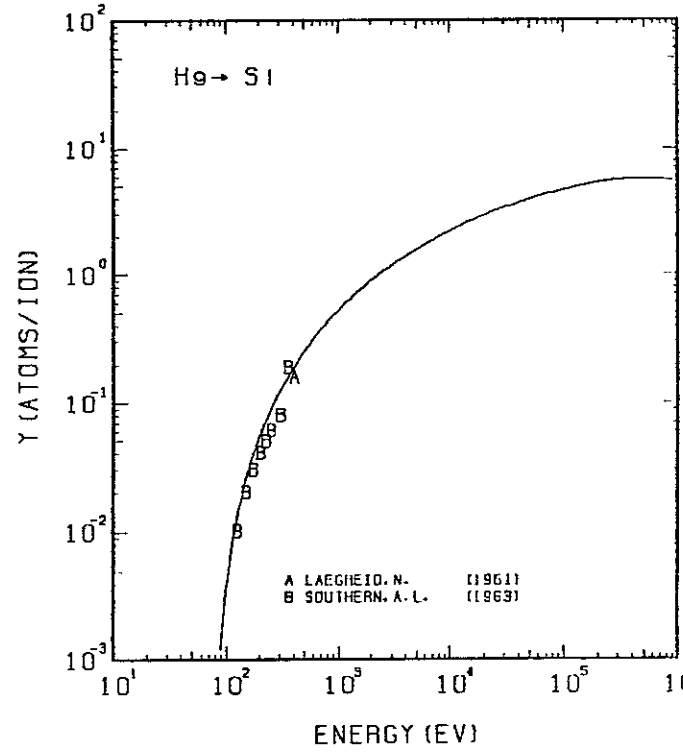


FIG. 44 ENERGY DEPENDENCE OF THE SPUTTERING YIELD OF SI WITH $HG^{+}$.
A= 0.14, 0= 0.66, Us= 4.63EV, s= 2.50.
W= 0.50Us.

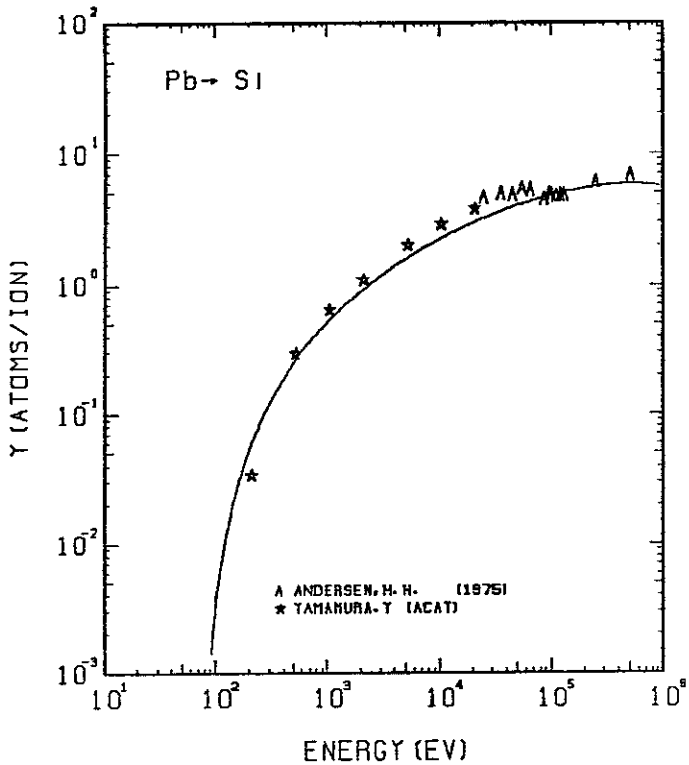


FIG. 45 ENERGY DEPENDENCE OF THE SPUTTERING YIELD OF SI WITH $PB^{+}$.
A= 0.14, 0= 0.66, Us= 4.63EV, s= 2.50.
W= 0.50Us.

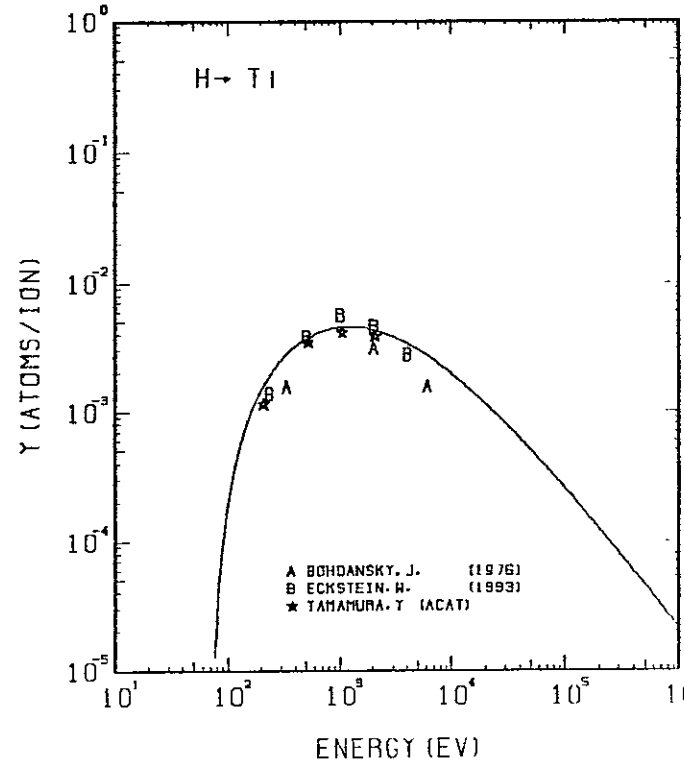


FIG. 46 ENERGY DEPENDENCE OF THE SPUTTERING YIELD OF TI WITH $H^{+}$.
A= 47.52, 0= 0.54, Us= 4.85EV, s= 2.50.
W= 0.53Us.

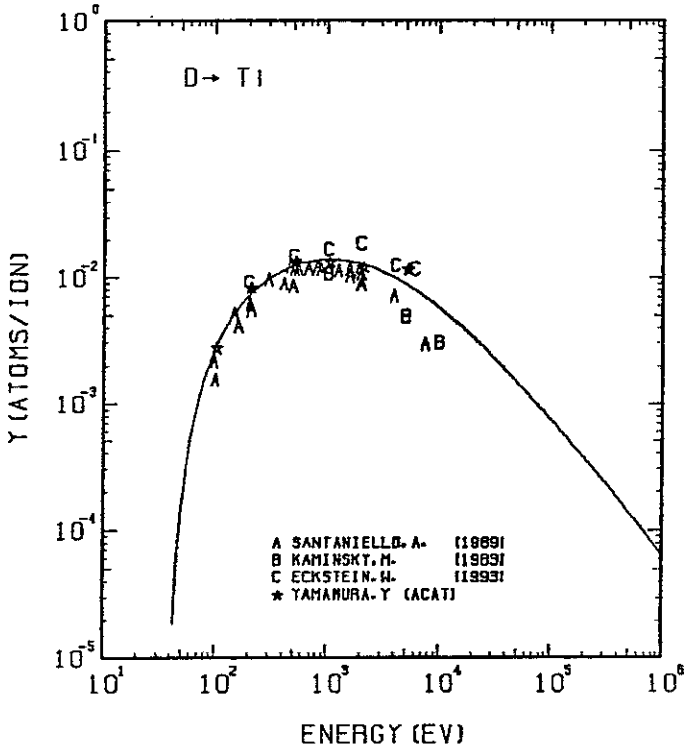


FIG. 47 ENERGY DEPENDENCE OF THE SPUTTERING YIELD OF TI WITH $D^+$.
A= 23.78, Q= 0.54, Us= 4.85EV, s= 2.50,
W= 0.53Us.

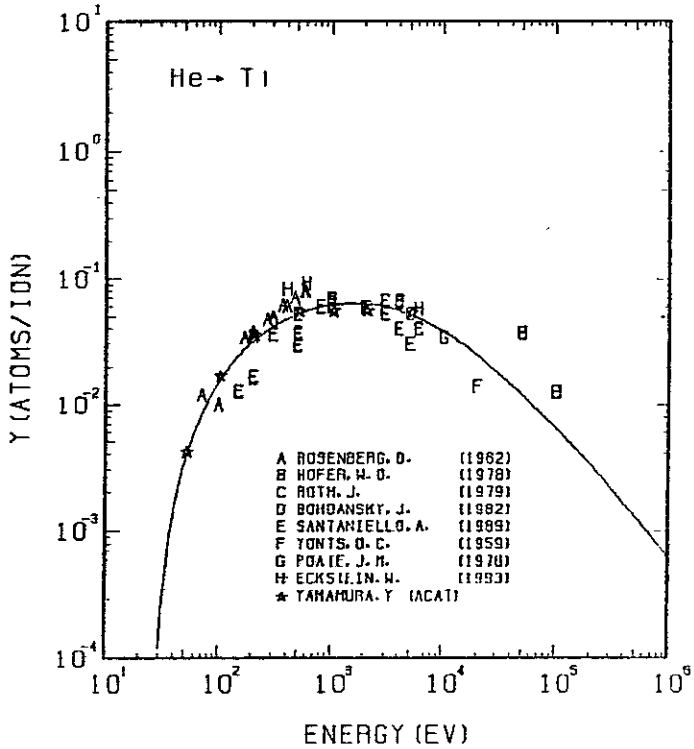


FIG. 48 ENERGY DEPENDENCE OF THE SPUTTERING YIELD OF TI WITH $HE^+$.
A= 11.97, Q= 0.54, Us= 4.85EV, s= 2.50,
W= 0.53Us.

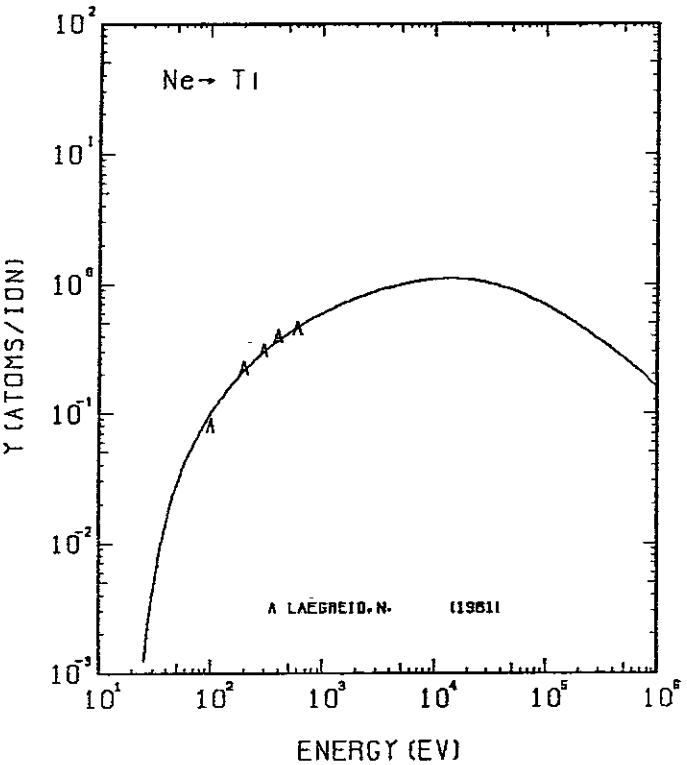


FIG. 49 ENERGY DEPENDENCE OF THE SPUTTERING YIELD OF TI WITH $NE^+$.
A= 2.37, Q= 0.54, Us= 4.85EV, s= 2.50,
W= 0.53Us.

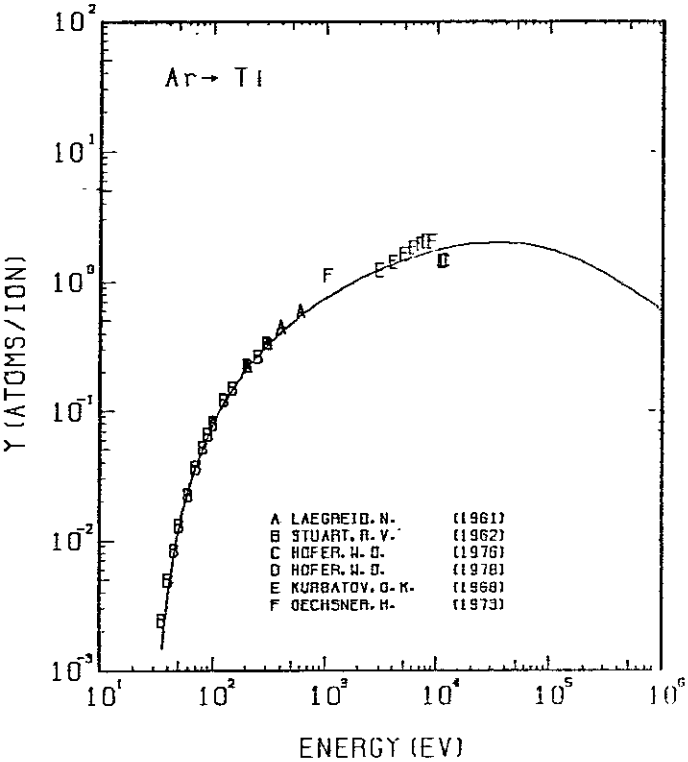


FIG. 50 ENERGY DEPENDENCE OF THE SPUTTERING YIELD OF TI WITH $AR^+$.
A= 1.20, Q= 0.54, Us= 4.85EV, s= 2.50,
W= 0.53Us.

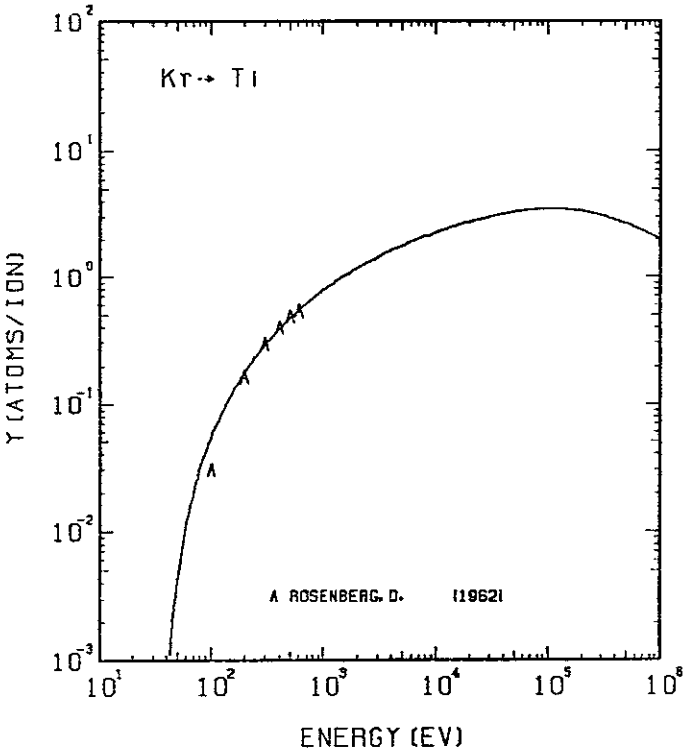


FIG. 51 ENERGY DEPENDENCE OF THE SPUTTERING YIELD OF TI WITH $KR^+$.
A= 0.57, 0= 0.54, Us= 4.85EV, s= 2.50,
W= 0.53Us.

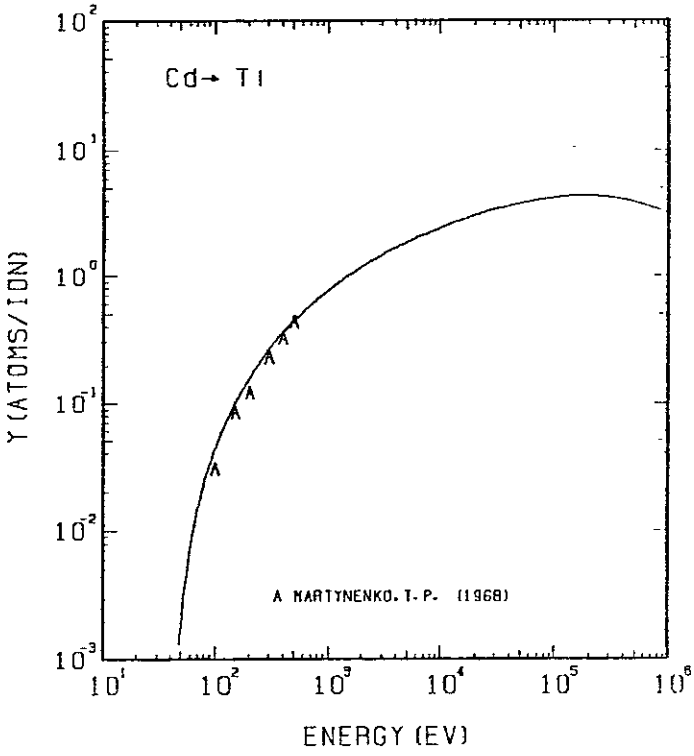


FIG. 52 ENERGY DEPENDENCE OF THE SPUTTERING YIELD OF TI WITH $CD^+$.
A= 0.43, 0= 0.54, Us= 4.85EV, s= 2.50,
W= 0.53Us.

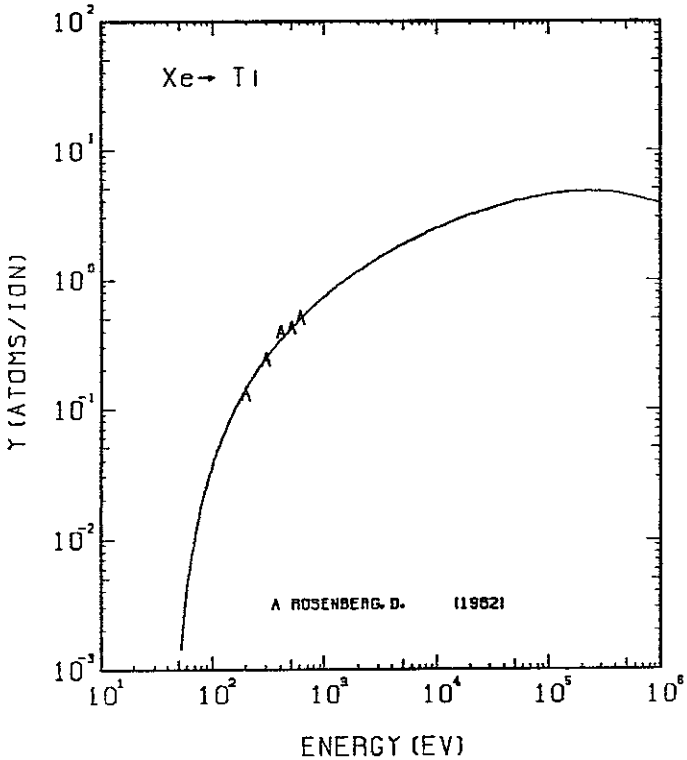


FIG. 53 ENERGY DEPENDENCE OF THE SPUTTERING YIELD OF TI WITH $XE^+$.
A= 0.36, 0= 0.54, Us= 4.85EV, s= 2.50,
W= 0.53Us.

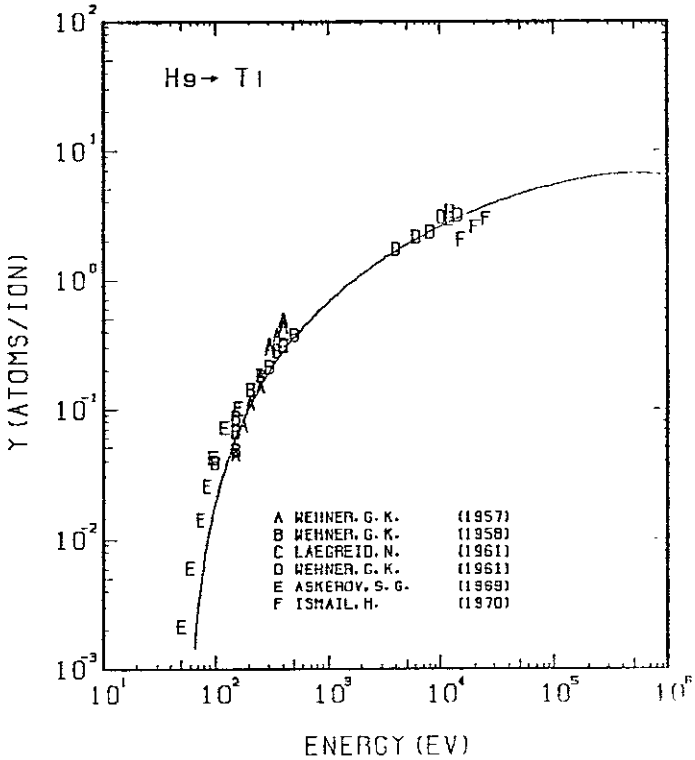


FIG. 54 ENERGY DEPENDENCE OF THE SPUTTERING YIELD OF TI WITH $HG^+$.
A= 0.24, 0= 0.54, Us= 4.85EV, s= 2.50,
W= 0.53Us.

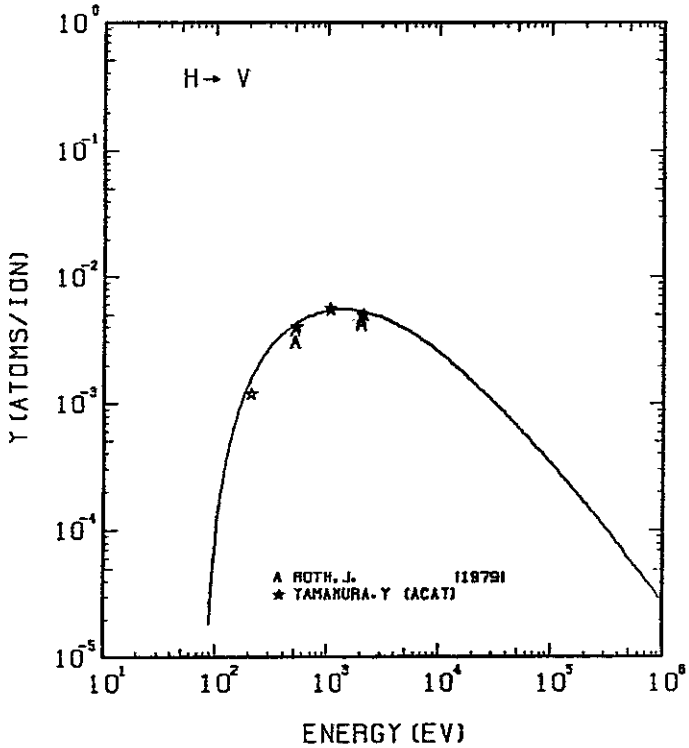


FIG. 55 ENERGY DEPENDENCE OF THE SPUTTERING YIELD OF V WITH $H^+$.
A= 50.54, Q= 0.72, Us= 5.31eV, s= 2.50,
W= 0.45Us.

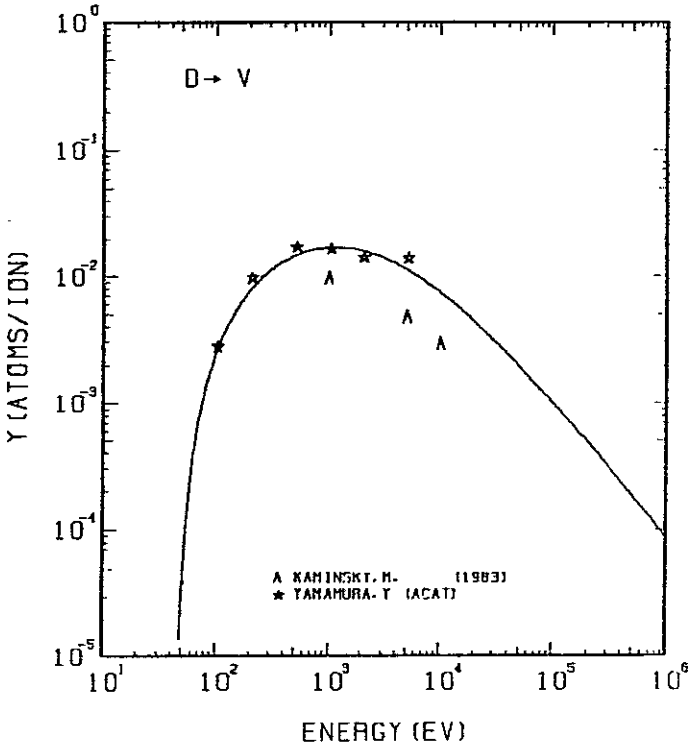


FIG. 56 ENERGY DEPENDENCE OF THE SPUTTERING YIELD OF V WITH $D^+$.
A= 25.29, Q= 0.72, Us= 5.31eV, s= 2.50,
W= 0.45Us.

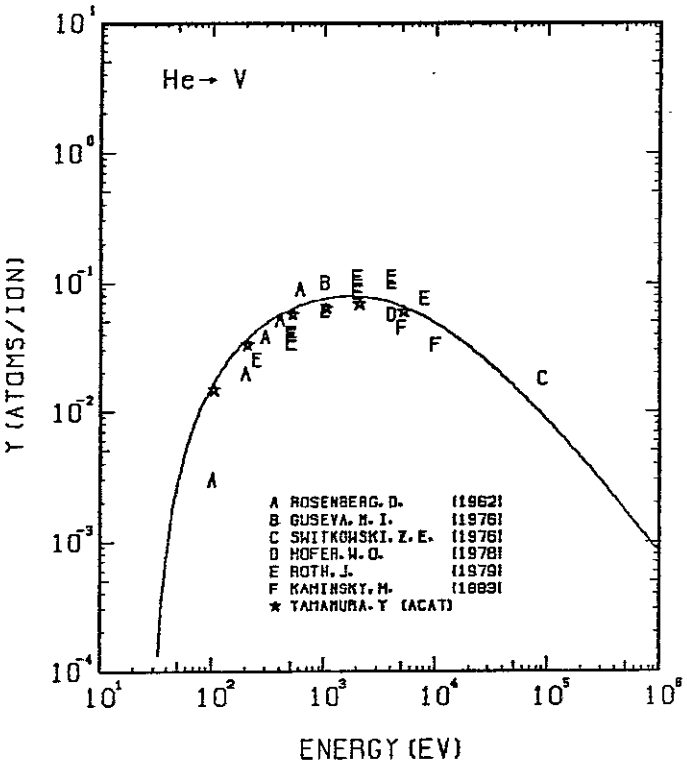


FIG. 57 ENERGY DEPENDENCE OF THE SPUTTERING YIELD OF V WITH $HE^+$.
A= 12.73, Q= 0.72, Us= 5.31eV, s= 2.50,
W= 0.45Us.

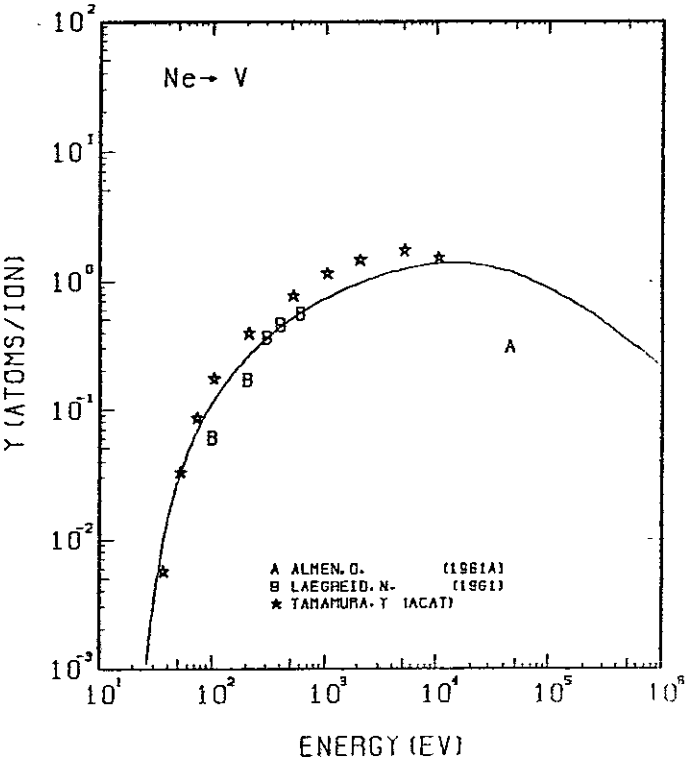


FIG. 58 ENERGY DEPENDENCE OF THE SPUTTERING YIELD OF V WITH $NE^+$.
A= 2.53, Q= 0.72, Us= 5.31eV, s= 2.50,
W= 0.45Us.

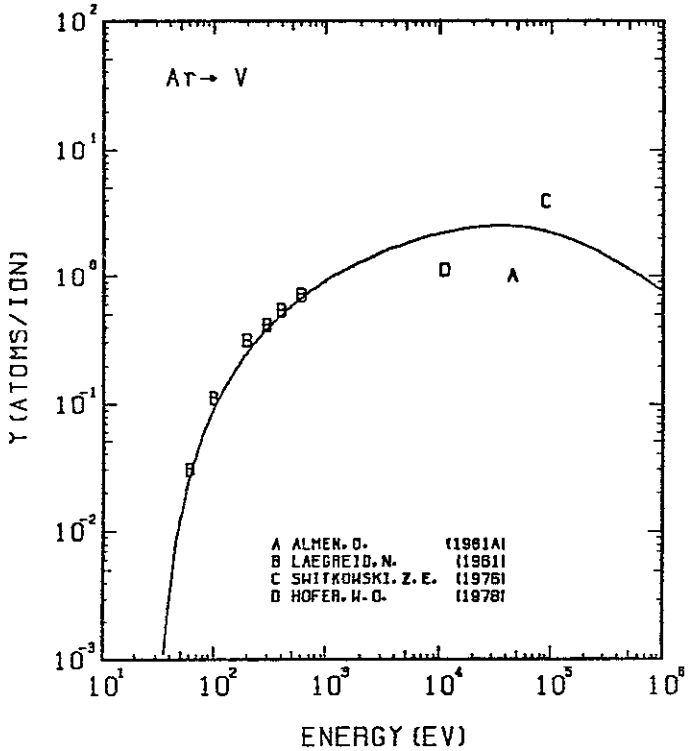


FIG. 59 ENERGY DEPENDENCE OF THE SPUTTERING YIELD OF V WITH $AR^+$.
A= 1.28, D= 0.72, Us= 5.31EV, S= 2.50,
W= 0.45Us.

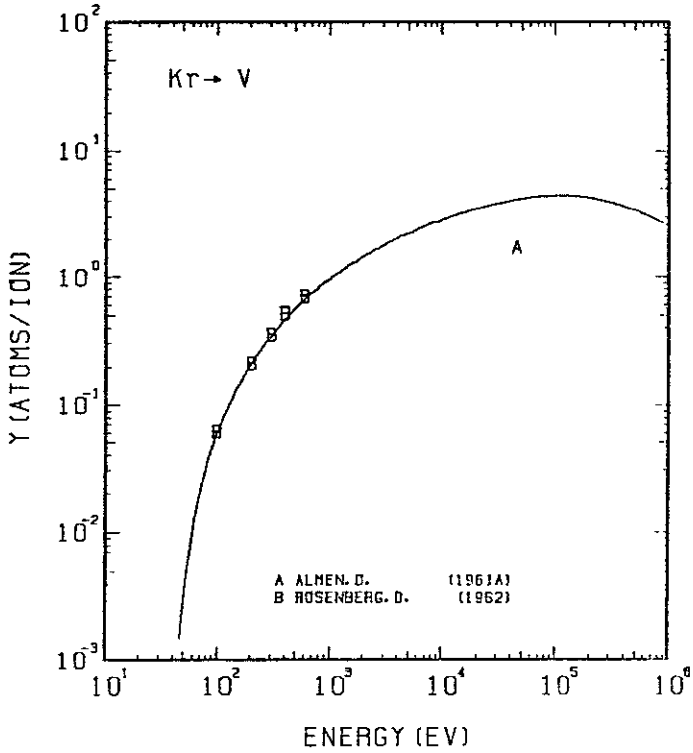


FIG. 60 ENERGY DEPENDENCE OF THE SPUTTERING YIELD OF V WITH $KR^+$.
A= 0.61, D= 0.72, Us= 5.31EV, S= 2.50,
W= 0.45Us.

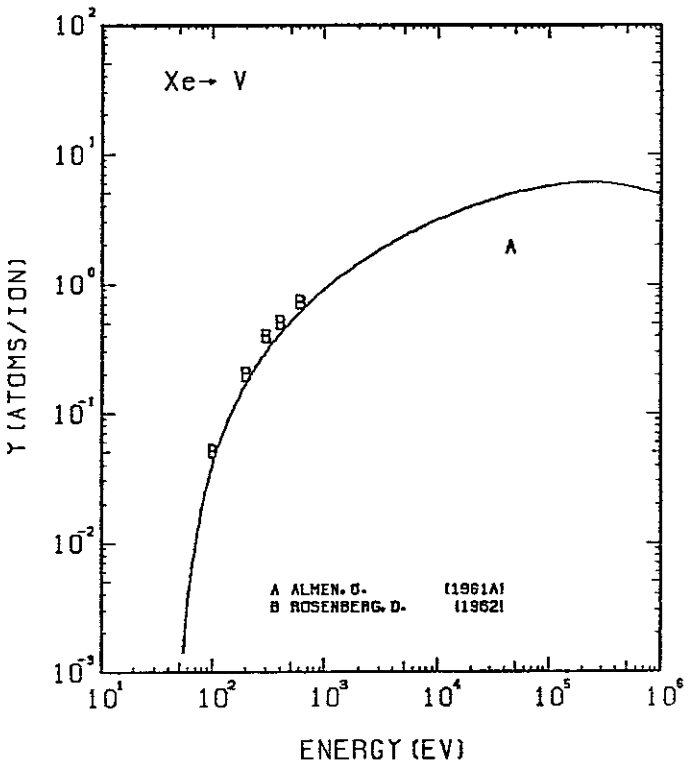


FIG. 61 ENERGY DEPENDENCE OF THE SPUTTERING YIELD OF V WITH $XE^+$.
A= 0.39, D= 0.72, Us= 5.31EV, S= 2.50,
W= 0.45Us.

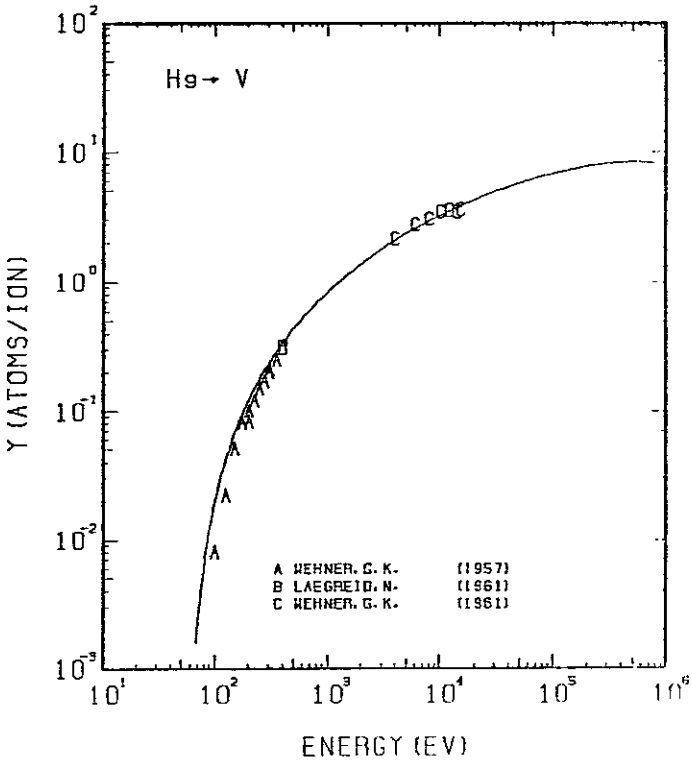


FIG. 62 ENERGY DEPENDENCE OF THE SPUTTERING YIELD OF V WITH $HG^+$.
A= 0.25, D= 0.72, Us= 5.31EV, S= 2.50,
W= 0.45Us.

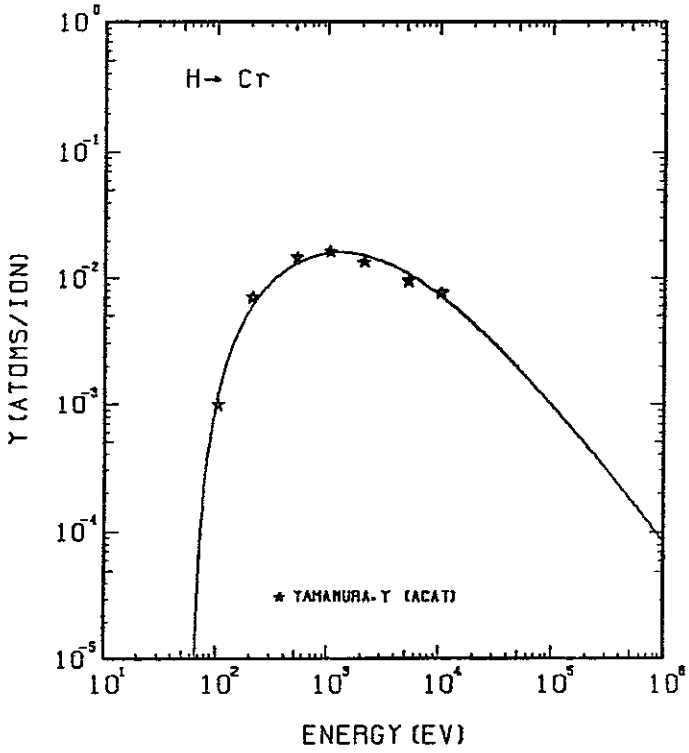


FIG. 63 ENERGY DEPENDENCE OF THE SPUTTERING YIELD OF CR WITH $H^+$.
A= 51.59, Q= 0.93, Us= 4.10EV, s= 2.50,
W= 0.35Us.

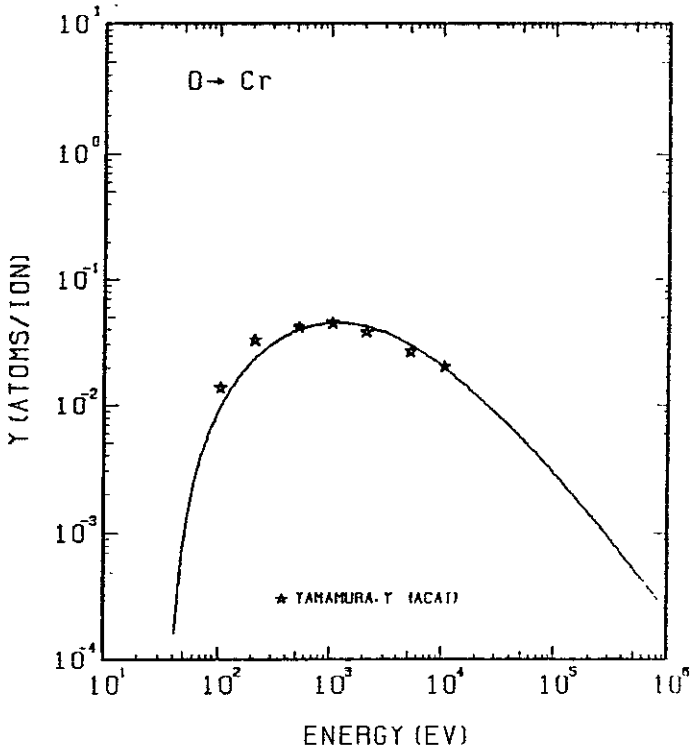


FIG. 64 ENERGY DEPENDENCE OF THE SPUTTERING YIELD OF CR WITH $D^+$.
A= 25.82, Q= 0.93, Us= 4.10EV, s= 2.50,
W= 0.35Us.

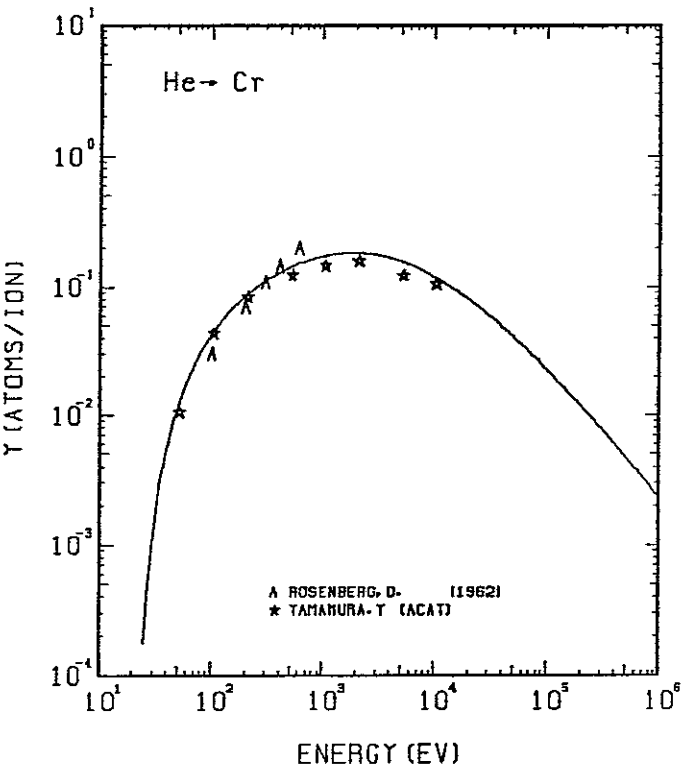


FIG. 65 ENERGY DEPENDENCE OF THE SPUTTERING YIELD OF CR WITH $HE^+$.
A= 12.99, Q= 0.93, Us= 4.10EV, s= 2.50,
W= 0.35Us.

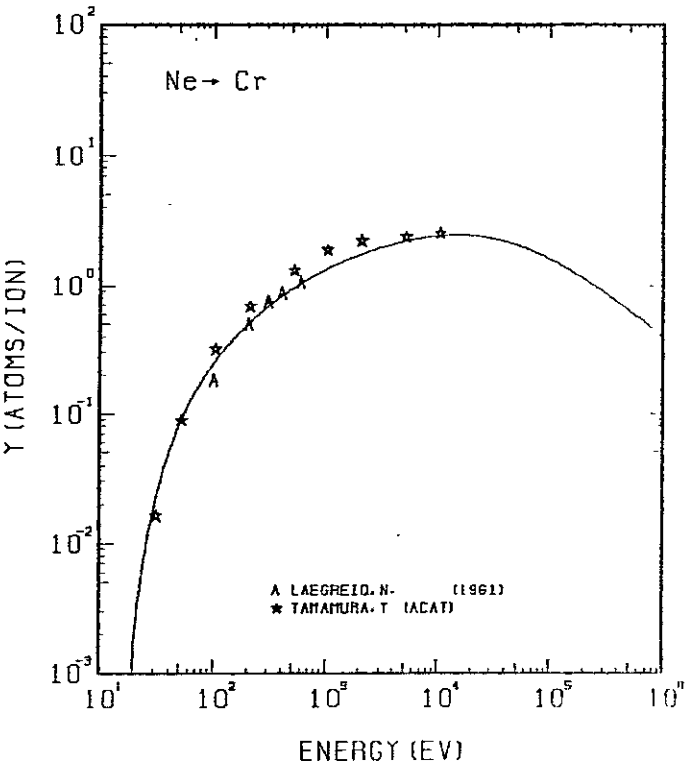


FIG. 66 ENERGY DEPENDENCE OF THE SPUTTERING YIELD OF CR WITH $NE^+$.
A= 2.58, Q= 0.93, Us= 4.10EV, s= 2.50,
W= 0.35Us.

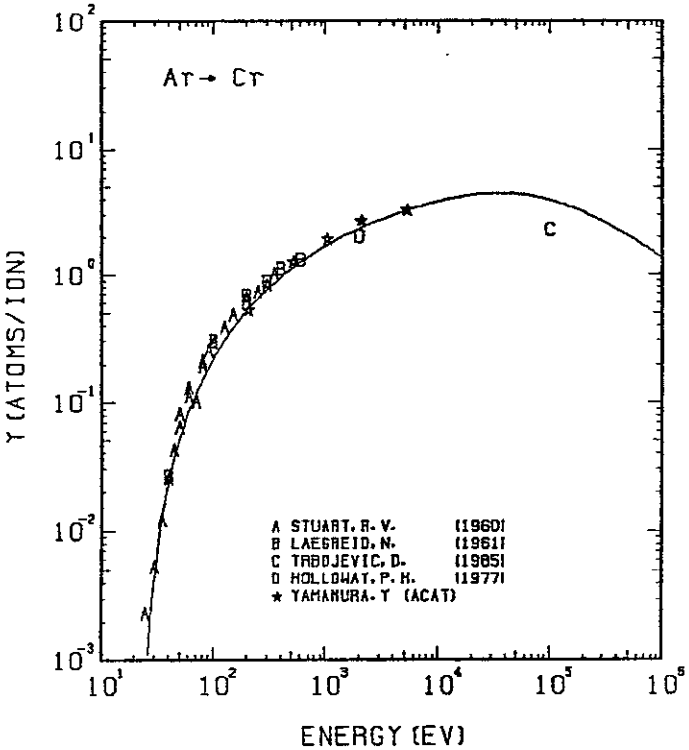


FIG. 67 ENERGY DEPENDENCE OF THE SPUTTERING YIELD OF CR WITH $AR^+$.
A= 1.30, D= 0.93, Us= 4.10EV, S= 2.50,
W= 0.35Us.

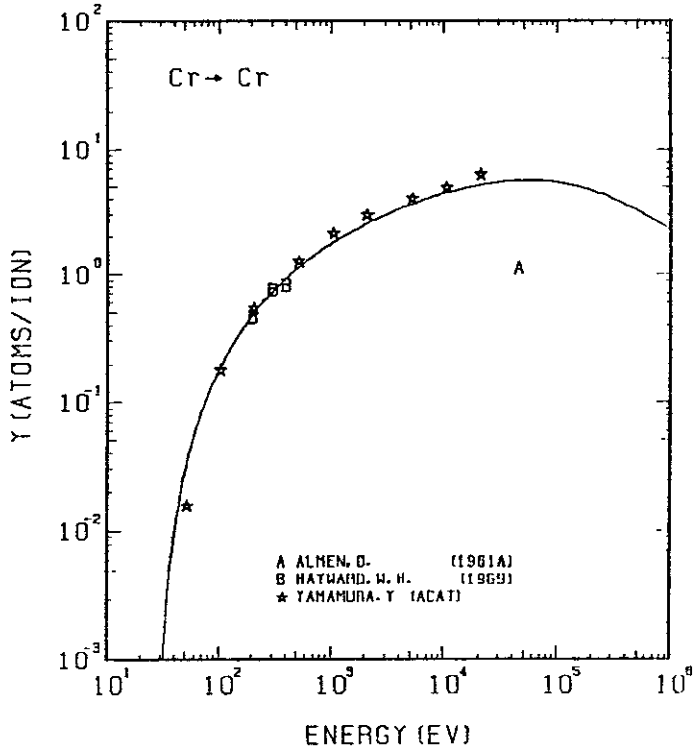


FIG. 68 ENERGY DEPENDENCE OF THE SPUTTERING YIELD OF CR WITH $CR^+$.
A= 1.00, D= 0.93, Us= 4.10EV, S= 2.50,
W= 0.35Us.

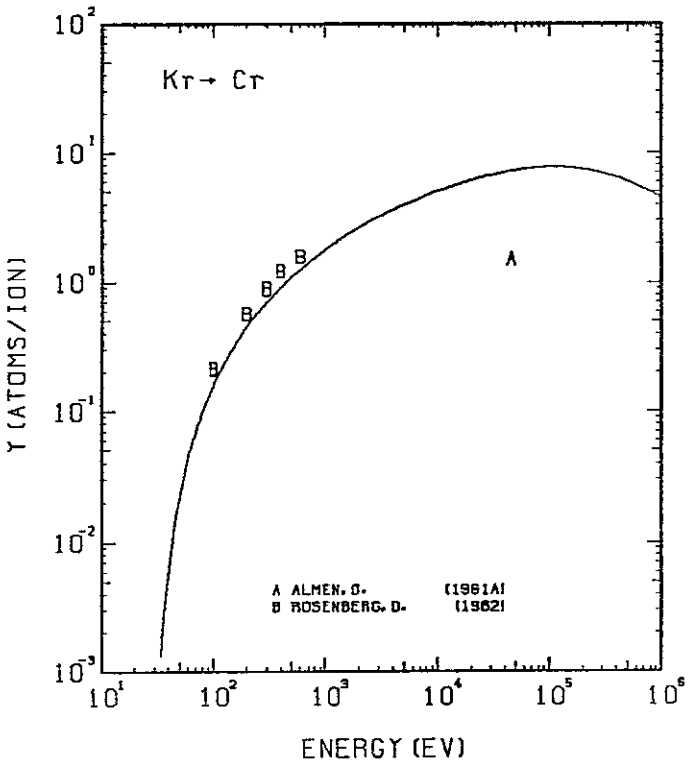


FIG. 69 ENERGY DEPENDENCE OF THE SPUTTERING YIELD OF CR WITH $KR^+$.
A= 0.62, D= 0.93, Us= 4.10EV, S= 2.50,
W= 0.35Us.

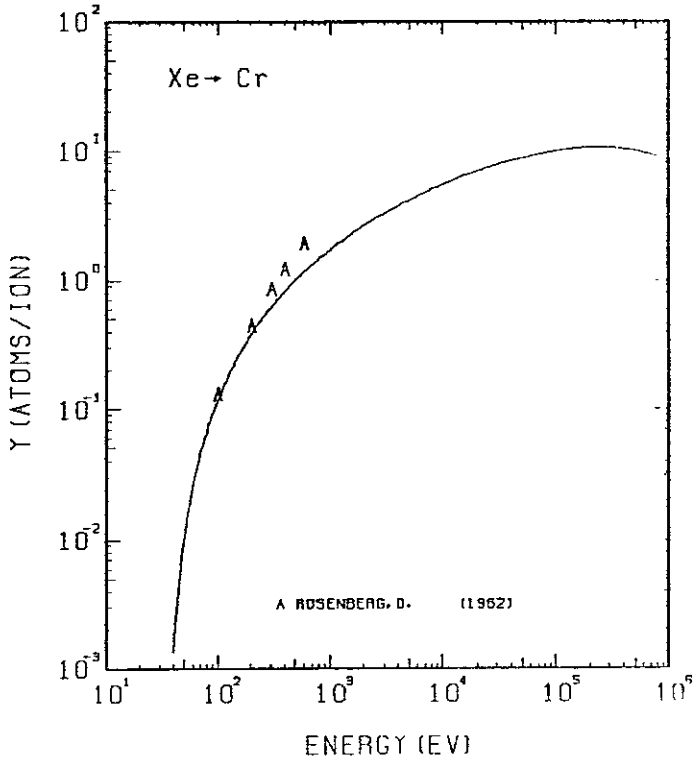


FIG. 70 ENERGY DEPENDENCE OF THE SPUTTERING YIELD OF CR WITH $XE^+$.
A= 0.40, D= 0.93, Us= 4.10EV, S= 2.50,
W= 0.35Us.

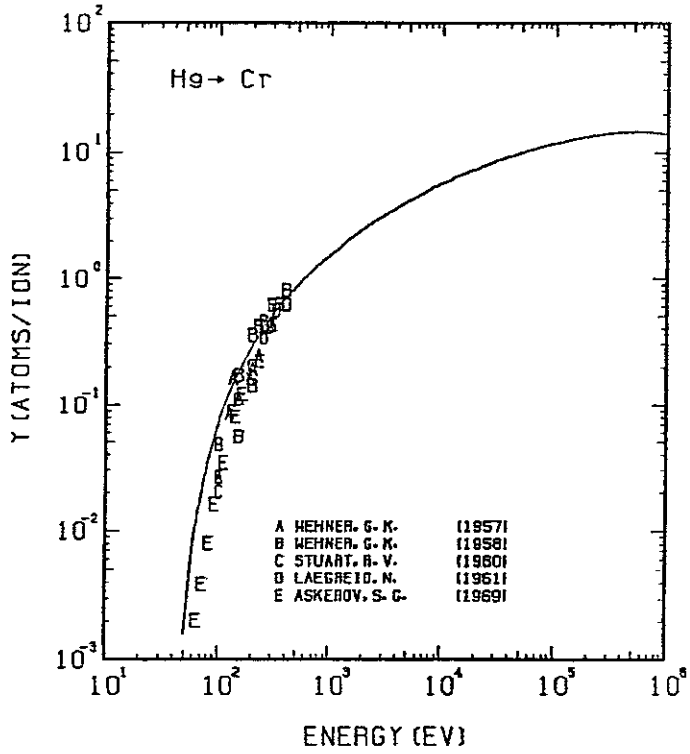


FIG. 71 ENERGY DEPENDENCE OF THE SPUTTERING YIELD OF CR WITH $HG^+$.
A= 0.26, 0= 0.93, Us= 4.10EV, s= 2.50,
W= 0.35Us.

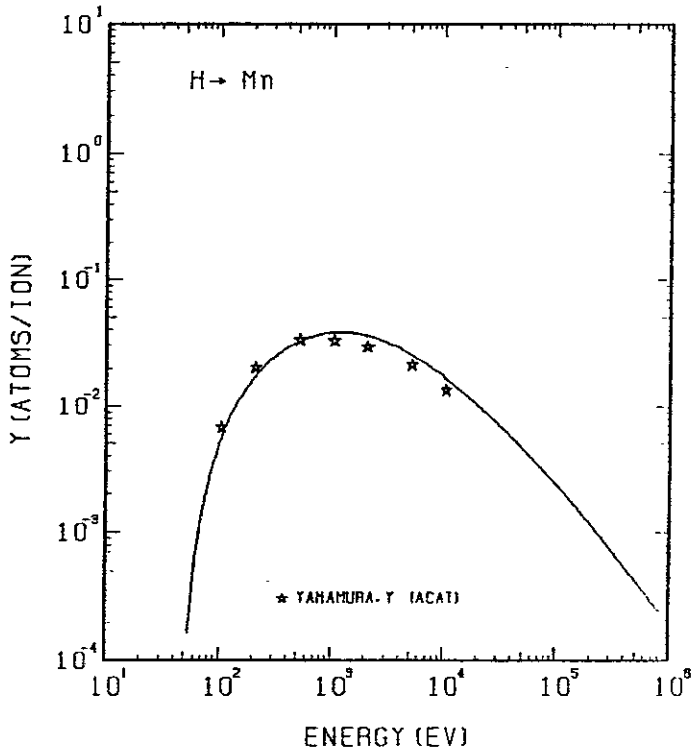


FIG. 72 ENERGY DEPENDENCE OF THE SPUTTERING YIELD OF MN WITH $H^+$.
A= 54.49, 0= 0.95, Us= 2.92EV, s= 2.50,
W= 0.30Us.

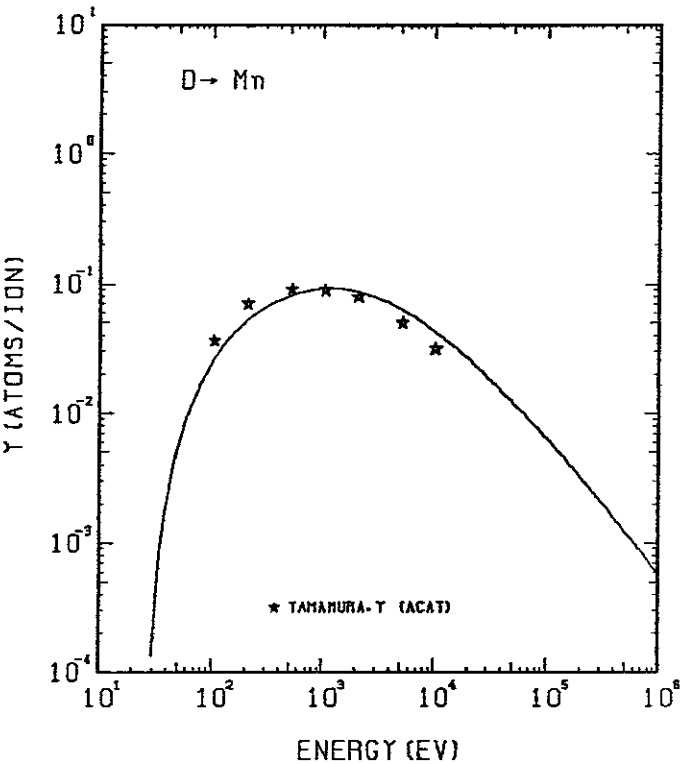


FIG. 73 ENERGY DEPENDENCE OF THE SPUTTERING YIELD OF MN WITH $D^+$.
A= 27.27, 0= 0.95, Us= 2.92EV, s= 2.50,
W= 0.30Us.

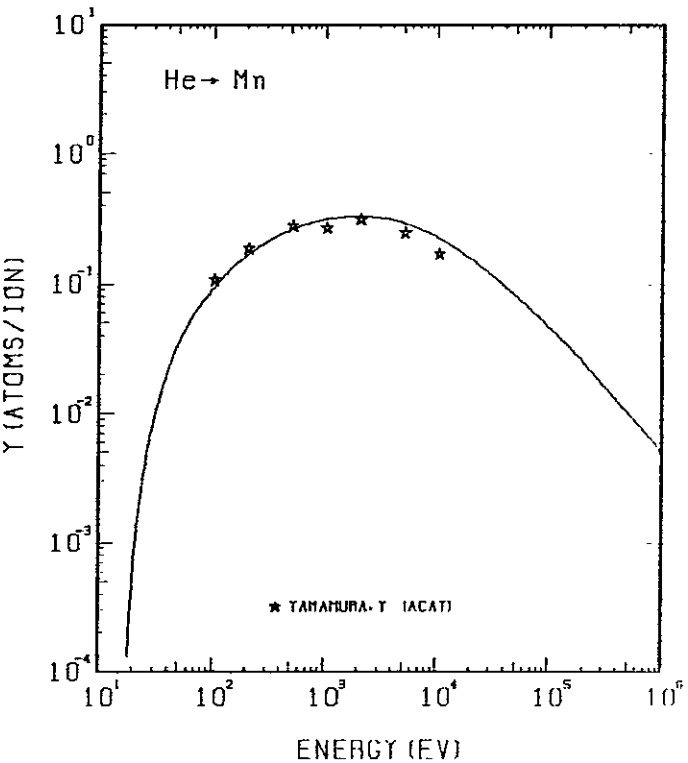


FIG. 74 ENERGY DEPENDENCE OF THE SPUTTERING YIELD OF MN WITH $HE^+$.
A= 13.72, 0= 0.95, Us= 2.92EV, s= 2.50,
W= 0.30Us.

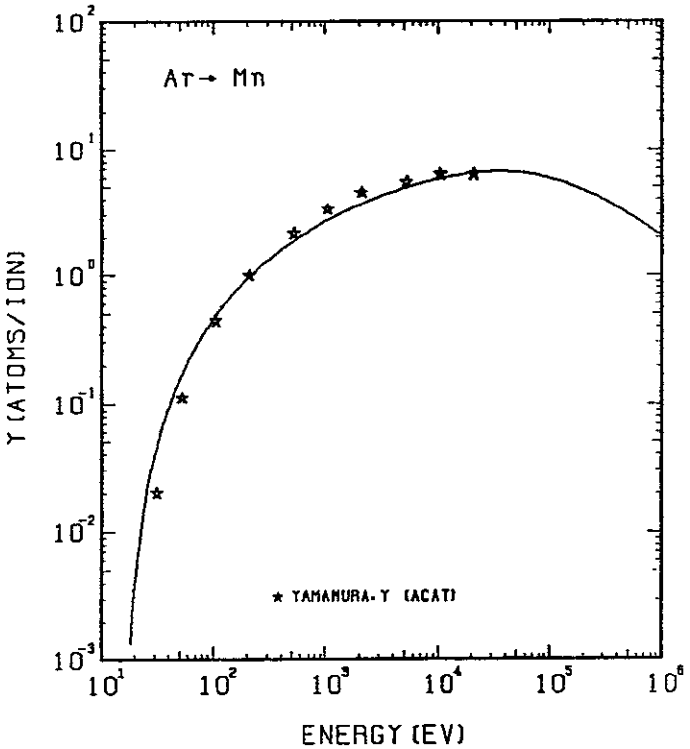


FIG. 75 ENERGY DEPENDENCE OF THE SPUTTERING YIELD OF MN WITH $AR^+$.
A= 1.38, D= 0.95, Us= 2.92EV, S= 2.50.
W= 0.30Us.

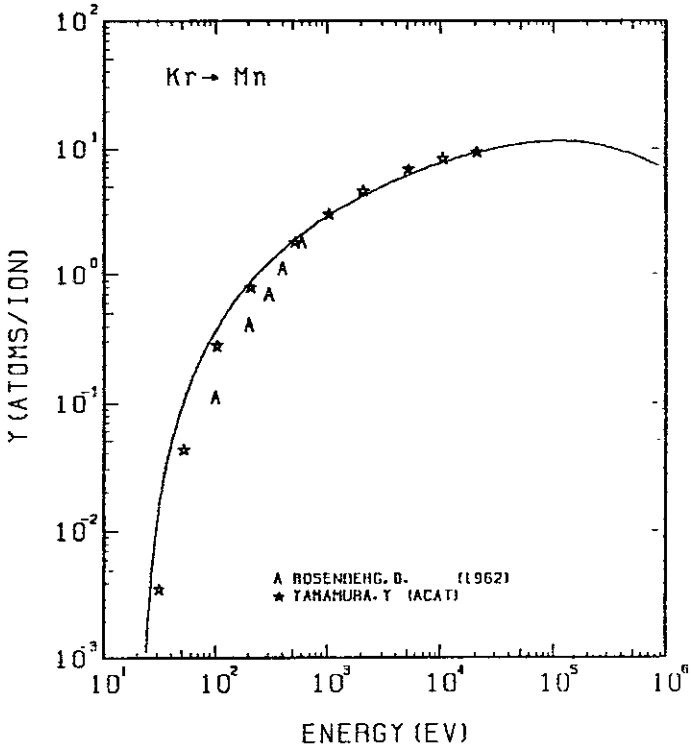


FIG. 76 ENERGY DEPENDENCE OF THE SPUTTERING YIELD OF MN WITH $KR^+$.
A= 0.66, D= 0.95, Us= 2.92EV, S= 2.50.
W= 0.30Us.

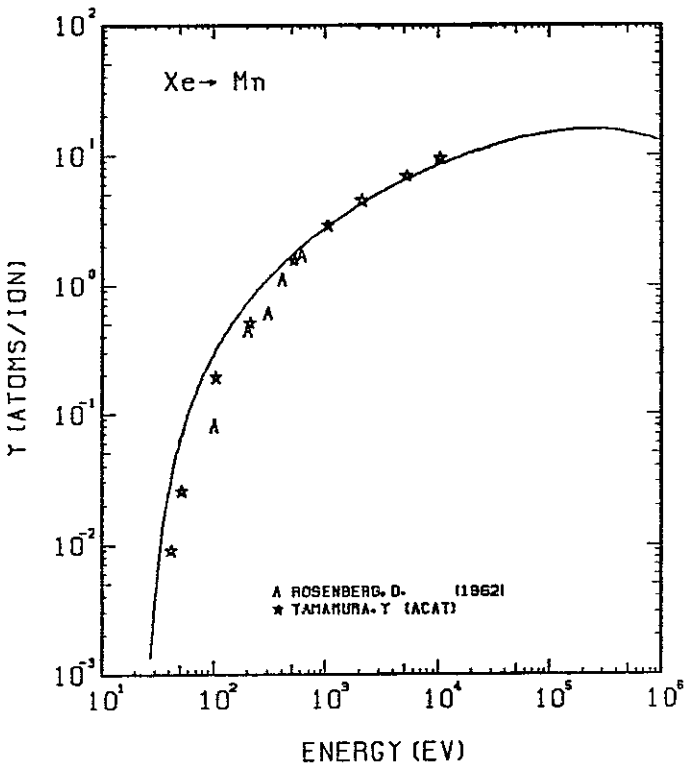


FIG. 77 ENERGY DEPENDENCE OF THE SPUTTERING YIELD OF MN WITH $XE^+$.
A= 0.42, D= 0.95, Us= 2.92EV, S= 2.50.
W= 0.30Us.

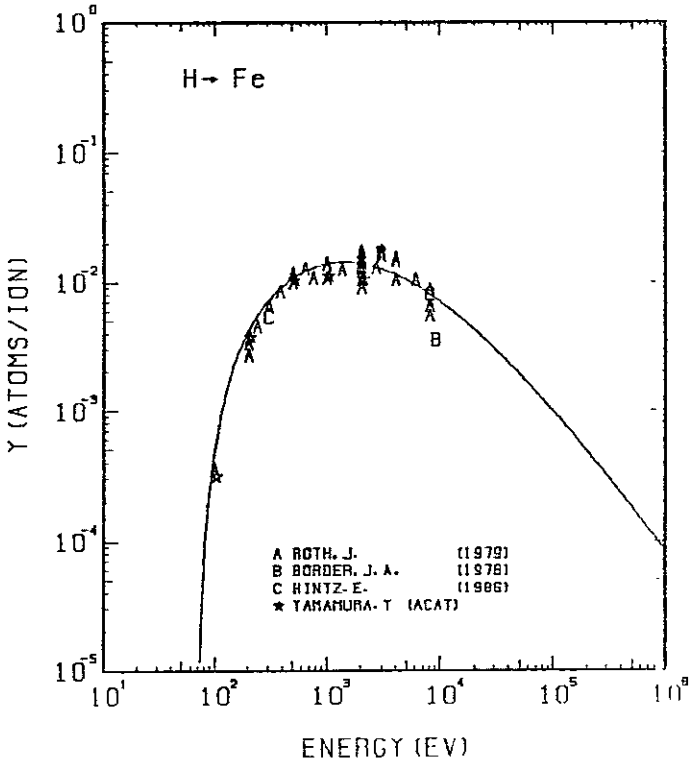


FIG. 78 ENERGY DEPENDENCE OF THE SPUTTERING YIELD OF FE WITH $H^+$.
A= 55.41, D= 0.75, Us= 4.28EV, S= 2.50.
W= 0.28Us.

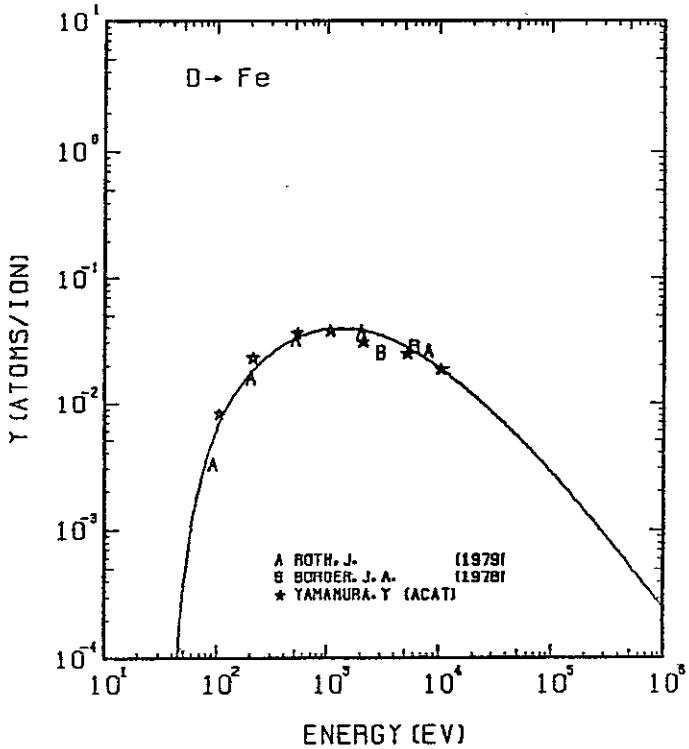


FIG. 79 ENERGY DEPENDENCE OF THE SPUTTERING YIELD OF FE WITH $D^+$.
A= 27.73, Q= 0.75, Us= 4.28EV, s= 2.50.
W= 0.28Us.

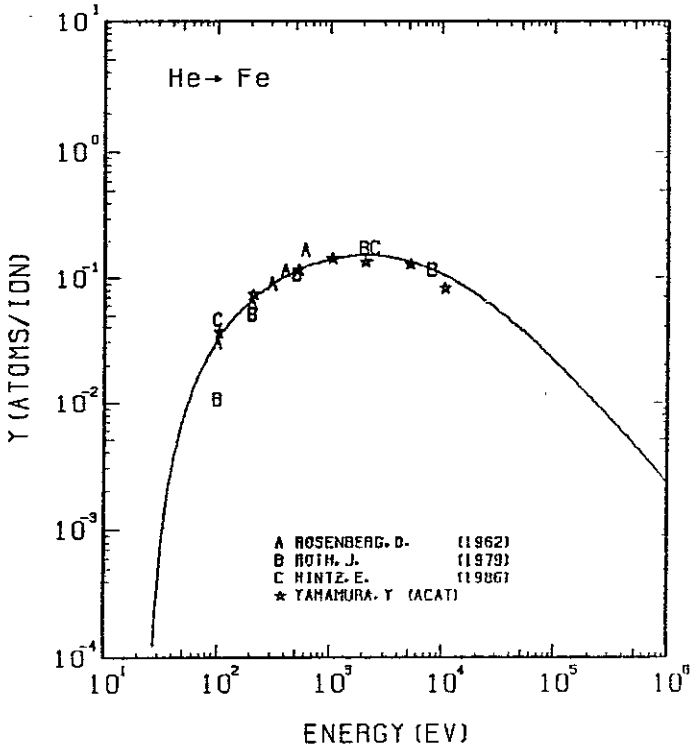


FIG. 80 ENERGY DEPENDENCE OF THE SPUTTERING YIELD OF FE WITH $HE^+$.
A= 13.95, Q= 0.75, Us= 4.28EV, s= 2.50.
W= 0.28Us.

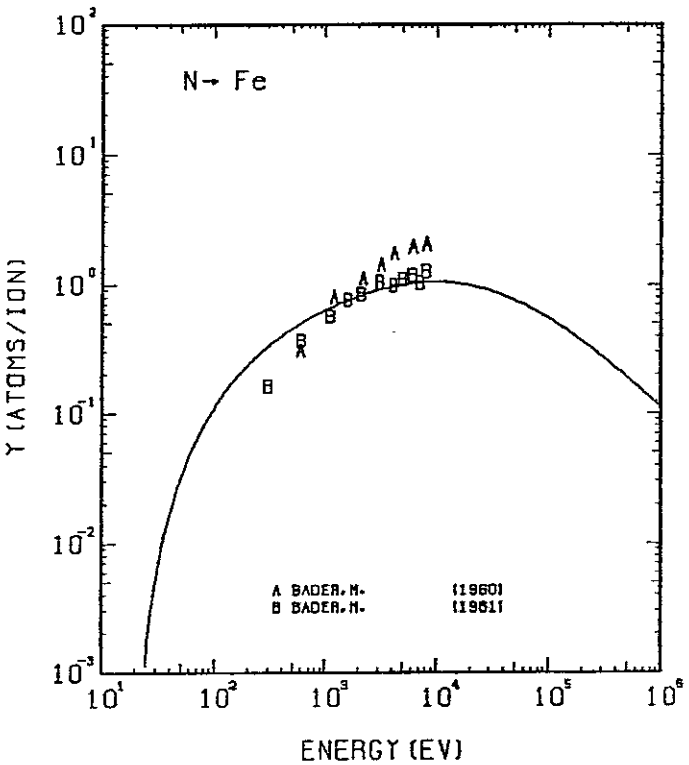


FIG. 81 ENERGY DEPENDENCE OF THE SPUTTERING YIELD OF FE WITH $N^+$.
A= 3.99, Q= 0.75, Us= 5.14EV, s= 2.50,
W= 0.28Us. THE BEST-FIT SURFACE BINDING ENERGY IS USED.

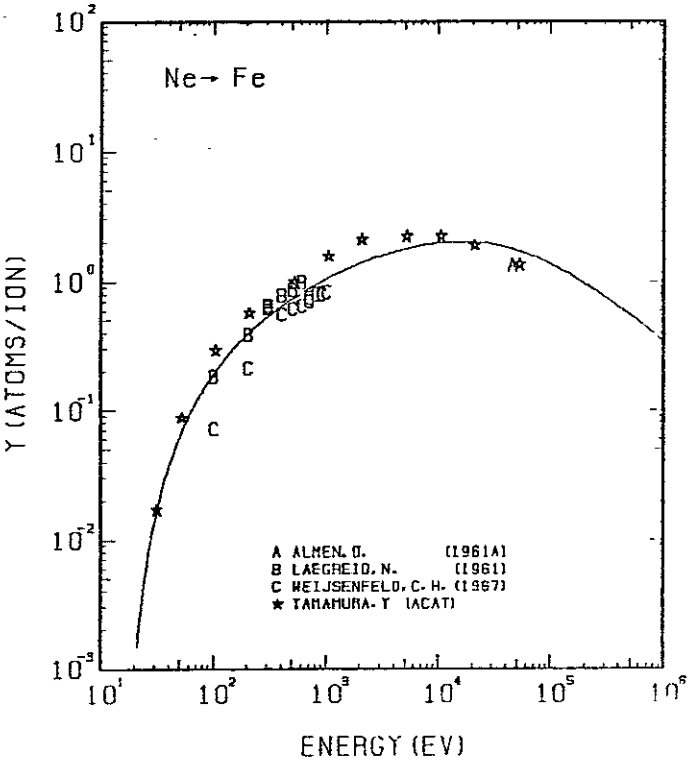


FIG. 82 ENERGY DEPENDENCE OF THE SPUTTERING YIELD OF FE WITH $NE^+$.
A= 2.77, Q= 0.75, Us= 4.28EV, s= 2.50,
W= 0.28Us.

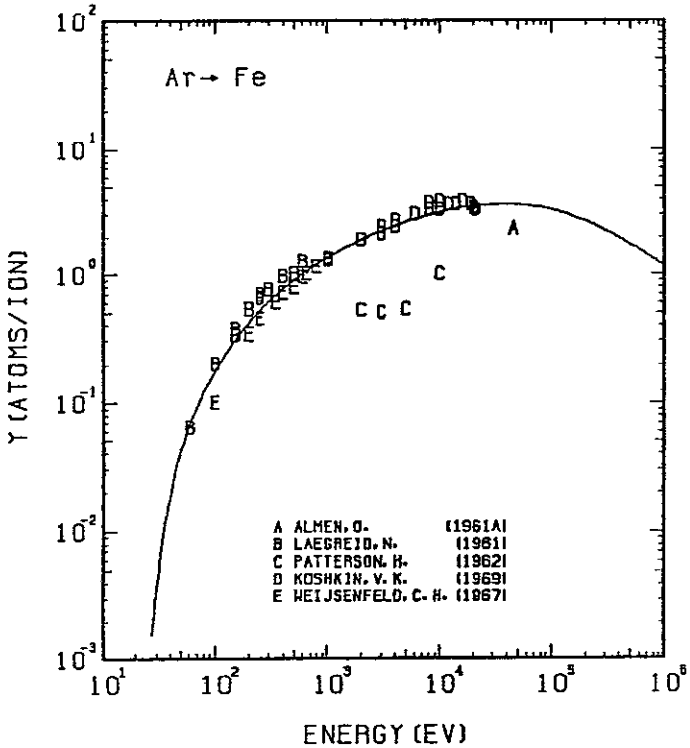


FIG. 83 ENERGY DEPENDENCE OF THE SPUTTERING YIELD OF FE WITH $AR^+$.
A= 1.40, D= 0.75, Us= 4.28EV, S= 2.50, W= 0.28Us.

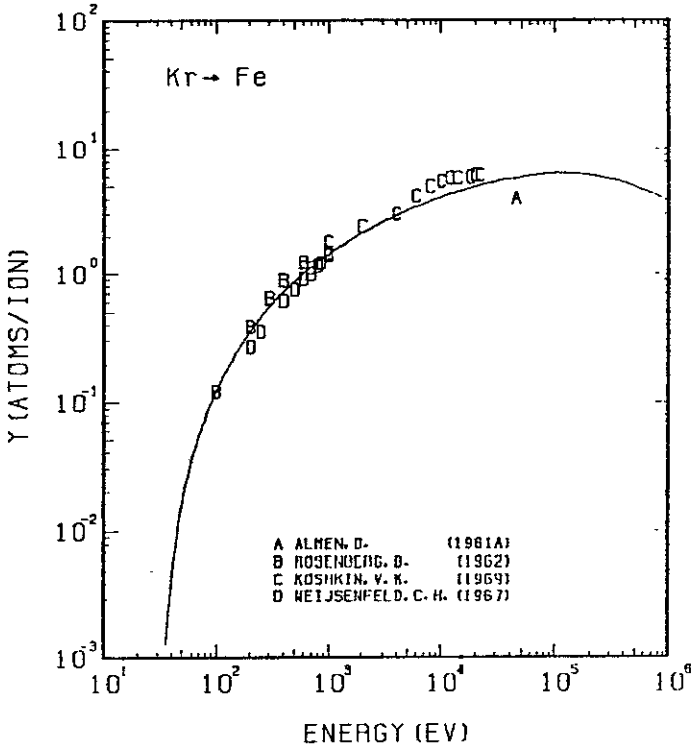


FIG. 84 ENERGY DEPENDENCE OF THE SPUTTERING YIELD OF FE WITH $KR^+$.
A= 0.67, D= 0.75, Us= 4.28EV, S= 2.50, W= 0.28Us.

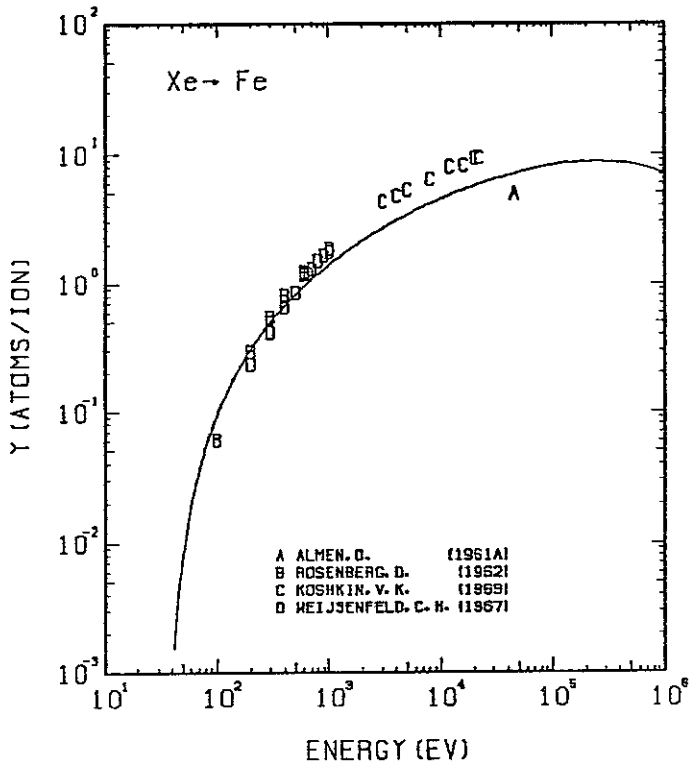


FIG. 85 ENERGY DEPENDENCE OF THE SPUTTERING YIELD OF FE WITH $XE^+$.
A= 0.43, D= 0.75, Us= 4.28EV, S= 2.50, W= 0.28Us.

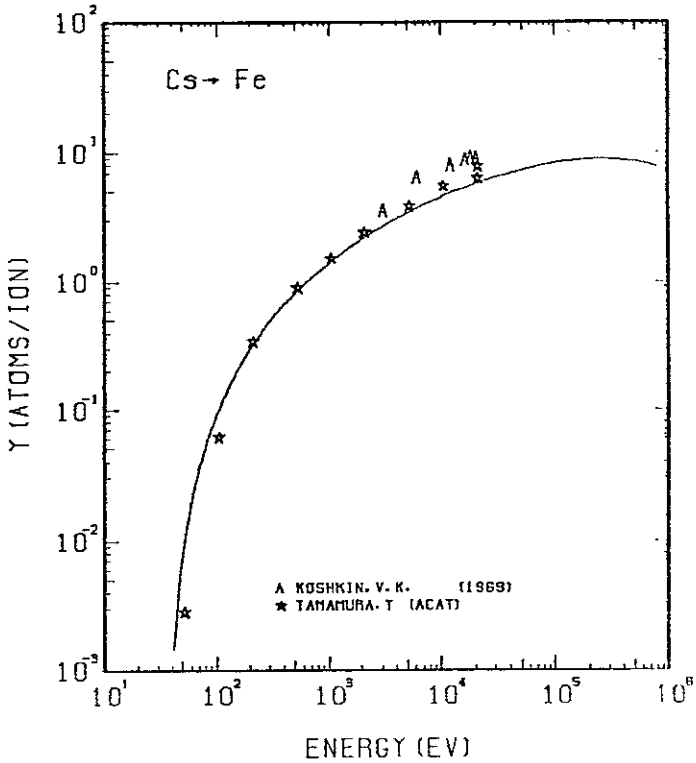


FIG. 86 ENERGY DEPENDENCE OF THE SPUTTERING YIELD OF FE WITH $CS^+$.
A= 0.42, D= 0.75, Us= 4.28EV, S= 2.50, W= 0.28Us.

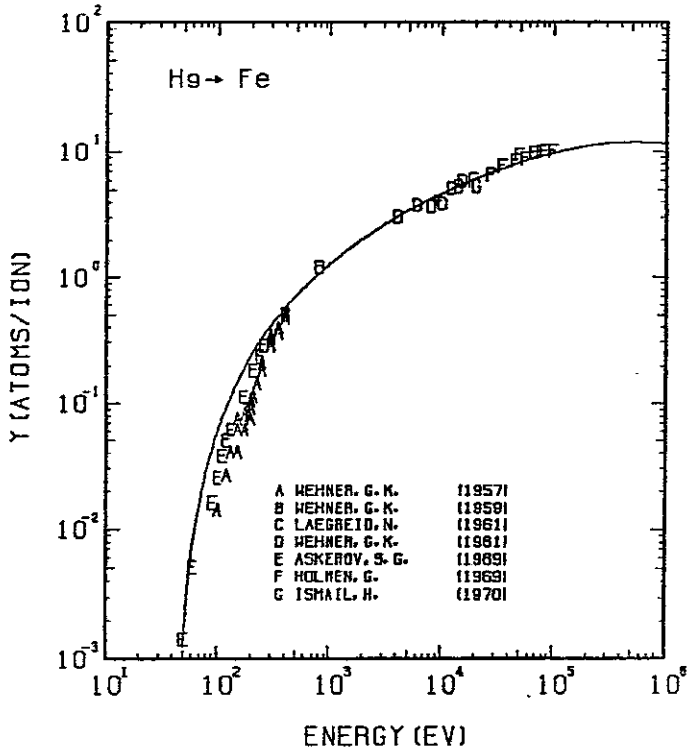


FIG. 87 ENERGY DEPENDENCE OF THE SPUTTERING YIELD OF FE WITH $HG^+$.
A= 0.28, 0= 0.75, Us= 4.28EV, s= 2.50,
W= 0.28Us.

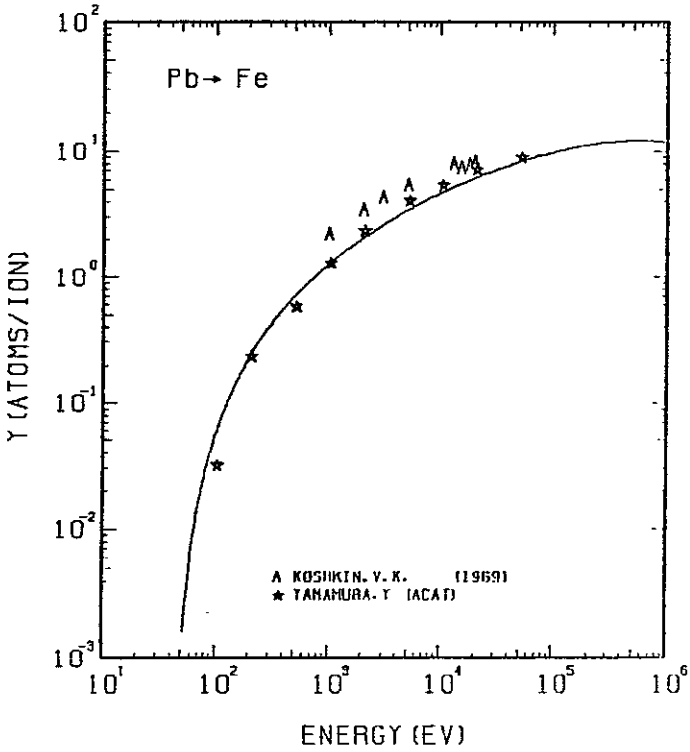


FIG. 88 ENERGY DEPENDENCE OF THE SPUTTERING YIELD OF FE WITH $PB^+$.
A= 0.27, 0= 0.75, Us= 4.28EV, s= 2.50,
W= 0.28Us.

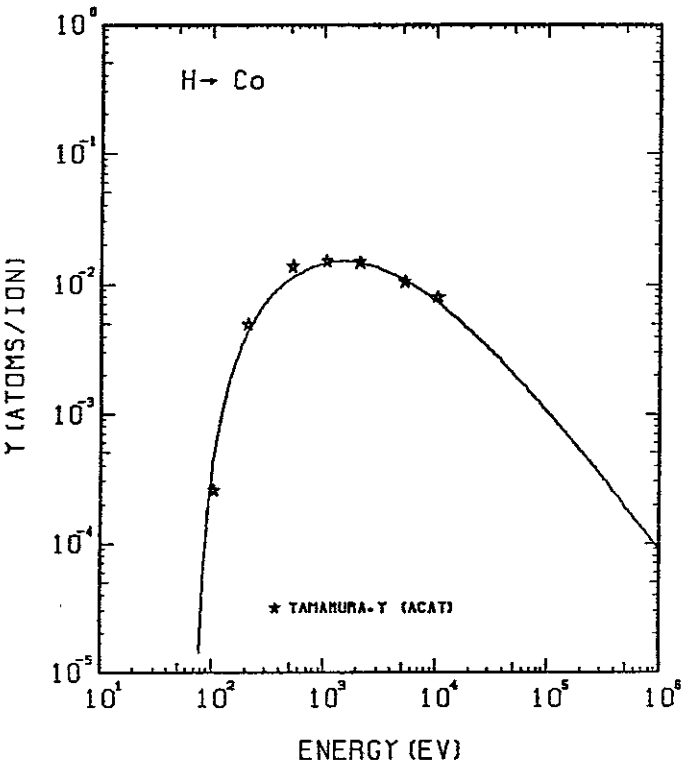


FIG. 89 ENERGY DEPENDENCE OF THE SPUTTERING YIELD OF CO WITH $H^+$.
A= 58.46, 0= 1.02, Us= 4.39EV, s= 2.50,
W= 0.35Us.

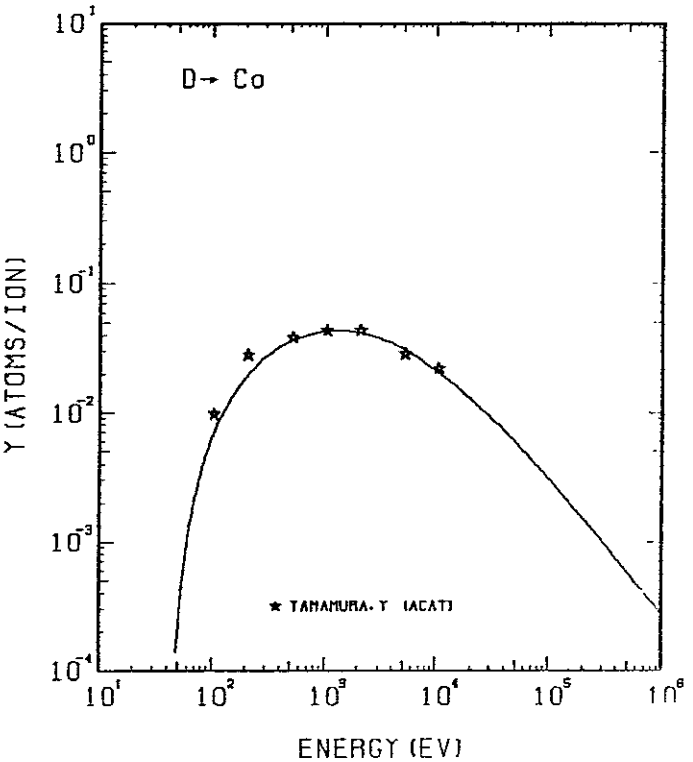


FIG. 90 ENERGY DEPENDENCE OF THE SPUTTERING YIELD OF CO WITH $D^+$.
A= 29.26, 0= 1.02, Us= 4.39EV, s= 2.50,
W= 0.35Us.

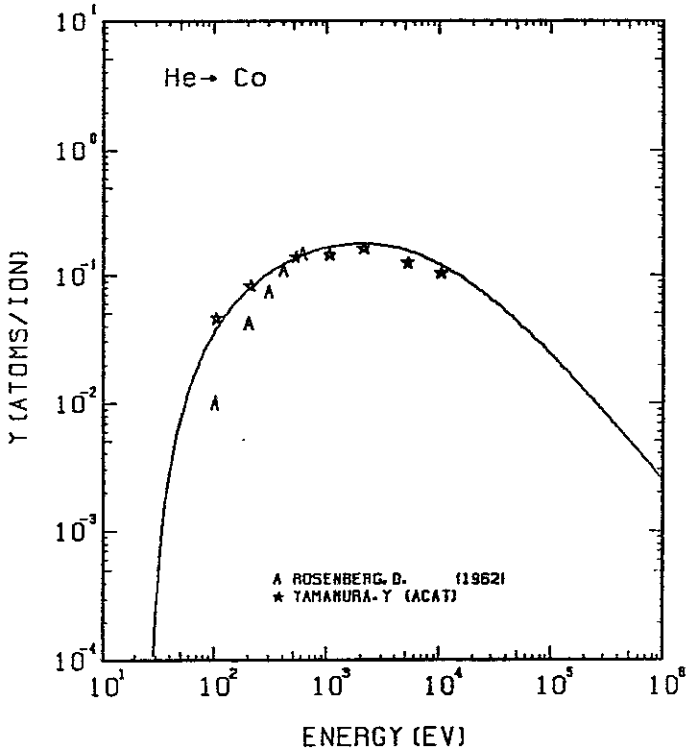


FIG. 91 ENERGY DEPENDENCE OF THE SPUTTERING YIELD OF CO WITH $HE^+$.
A= 14.72, D= 1.02, Us= 4.39EV, S= 2.50,
W= 0.35Us.

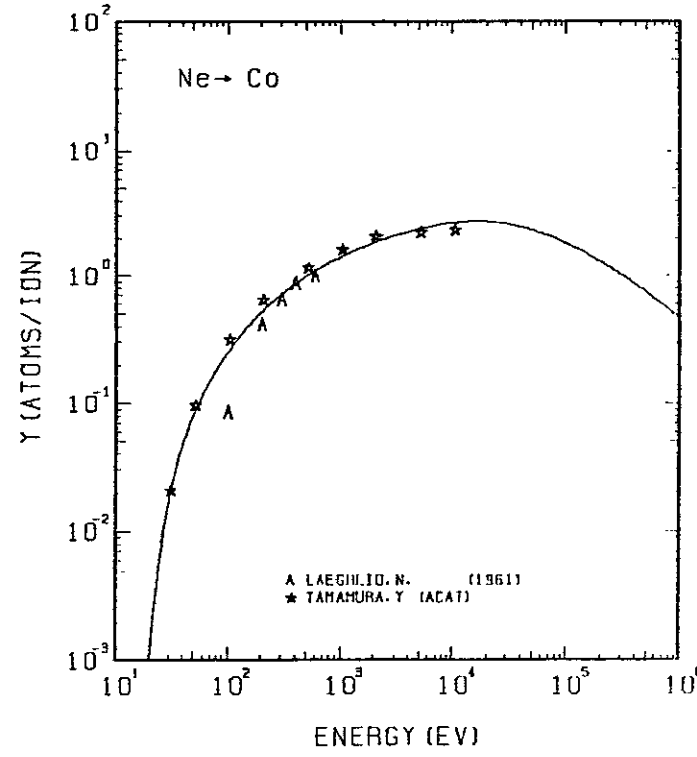


FIG. 92 ENERGY DEPENDENCE OF THE SPUTTERING YIELD OF CO WITH $NE^+$.
A= 2.92, D= 1.02, Us= 4.39EV, S= 2.50,
W= 0.35Us.

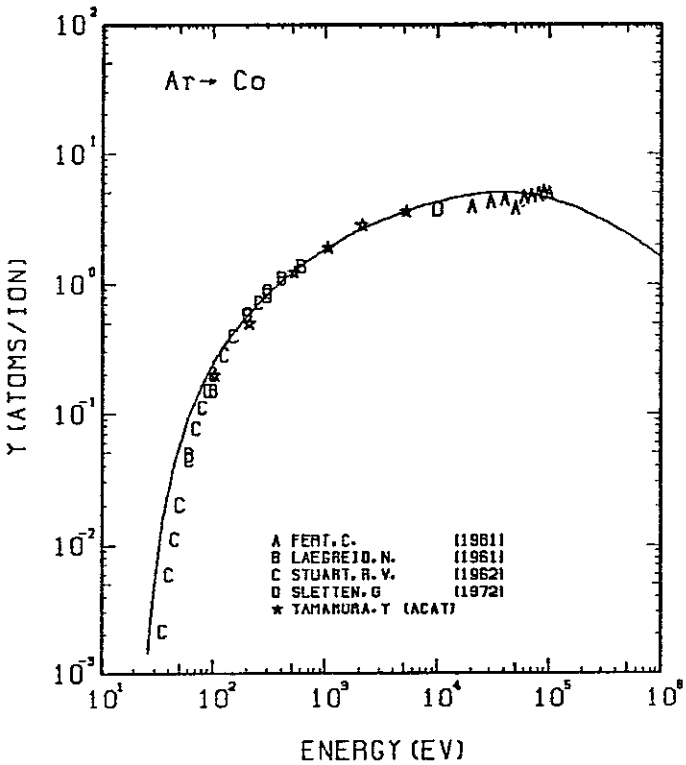


FIG. 93 ENERGY DEPENDENCE OF THE SPUTTERING YIELD OF CO WITH $AR^+$.
A= 1.48, D= 1.02, Us= 4.39EV, S= 2.50,
W= 0.35Us.

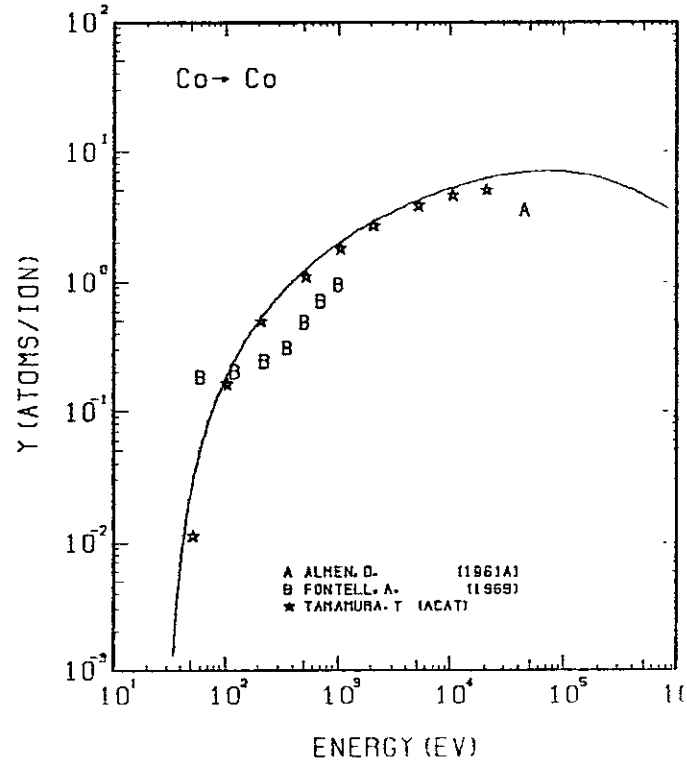


FIG. 94 ENERGY DEPENDENCE OF THE SPUTTERING YIELD OF CO WITH $CO^+$.
A= 1.00, D= 1.02, Us= 4.39EV, S= 2.50,
W= 0.35Us.

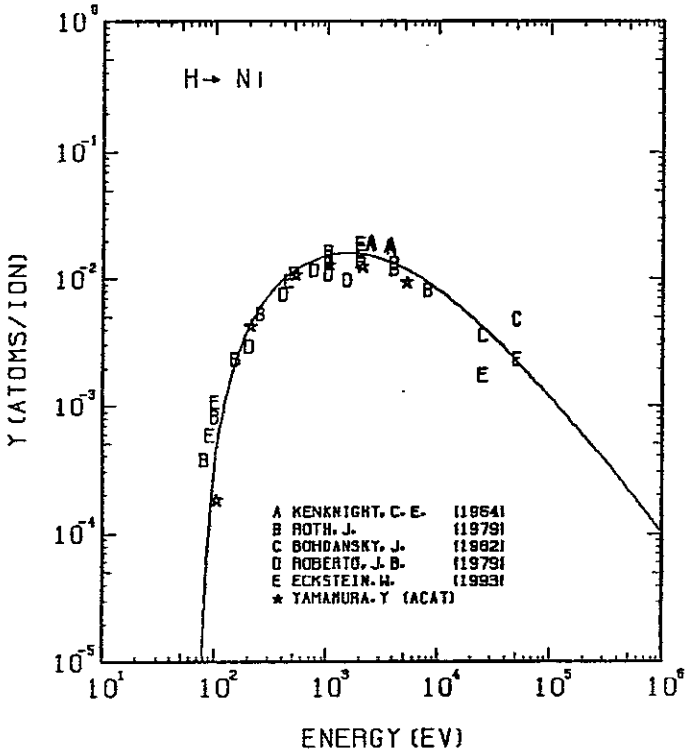


FIG. 99 ENERGY DEPENDENCE OF THE SPUTTERING YIELD OF NI WITH $H^+$.
A= 58.24, Q= 0.94, Us= 4.44EV, s= 2.50,
W= 0.30Us.

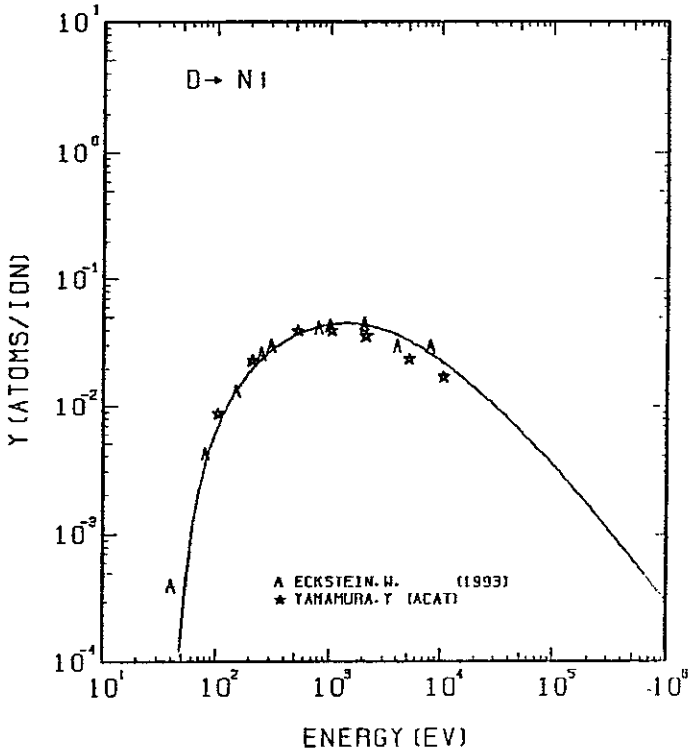


FIG. 100 ENERGY DEPENDENCE OF THE SPUTTERING YIELD OF NI WITH $D^+$.
A= 29.15, Q= 0.94, Us= 4.44EV, s= 2.50,
W= 0.30Us.

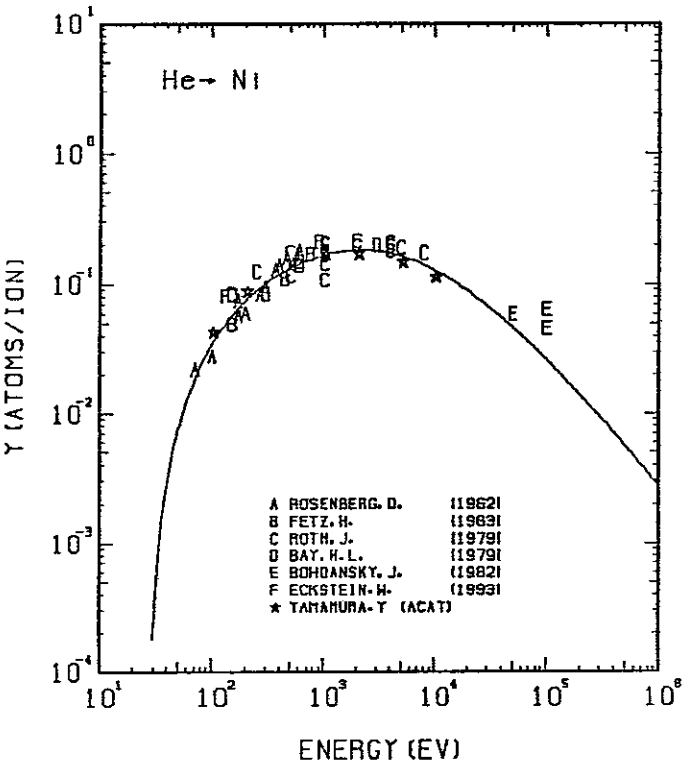


FIG. 101 ENERGY DEPENDENCE OF THE SPUTTERING YIELD OF NI WITH $HE^+$.
A= 14.67, Q= 0.94, Us= 4.44EV, s= 2.50,
W= 0.30Us.

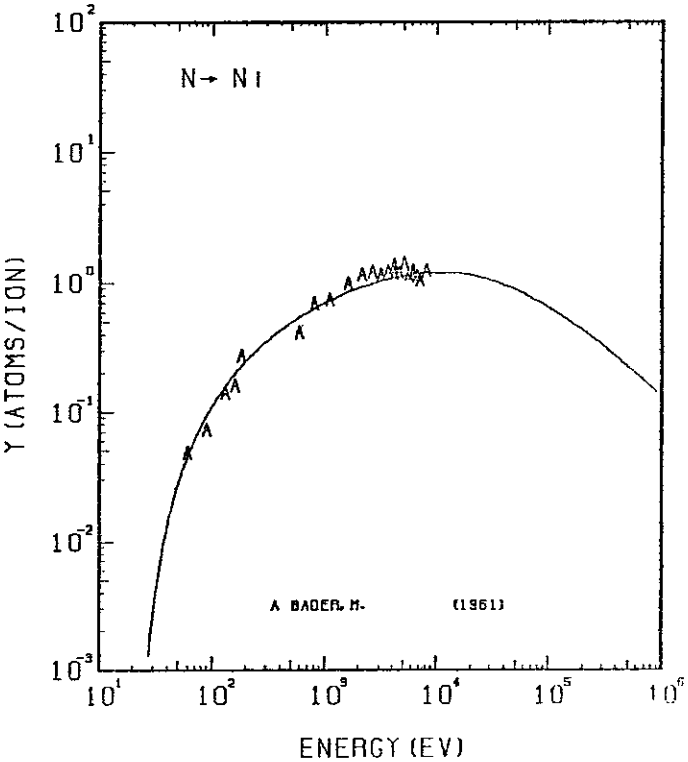


FIG. 102 ENERGY DEPENDENCE OF THE SPUTTERING YIELD OF NI WITH $N^+$.
A= 4.19, Q= 0.94, Us= 5.77EV, s= 2.50,
W= 0.30Us. THE BEST-FIT SURFACE BINDING ENERGY IS USED.

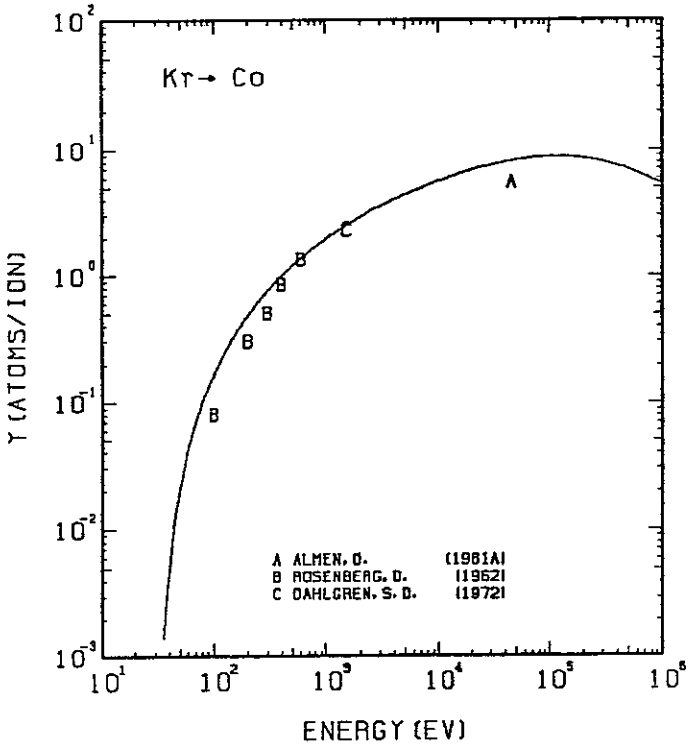


FIG. 95 ENERGY DEPENDENCE OF THE SPUTTERING YIELD OF CO WITH $KR^+$.
A= 0.70, 0= 1.02, Us= 4.39EV, S= 2.50,
W= 0.35Us.

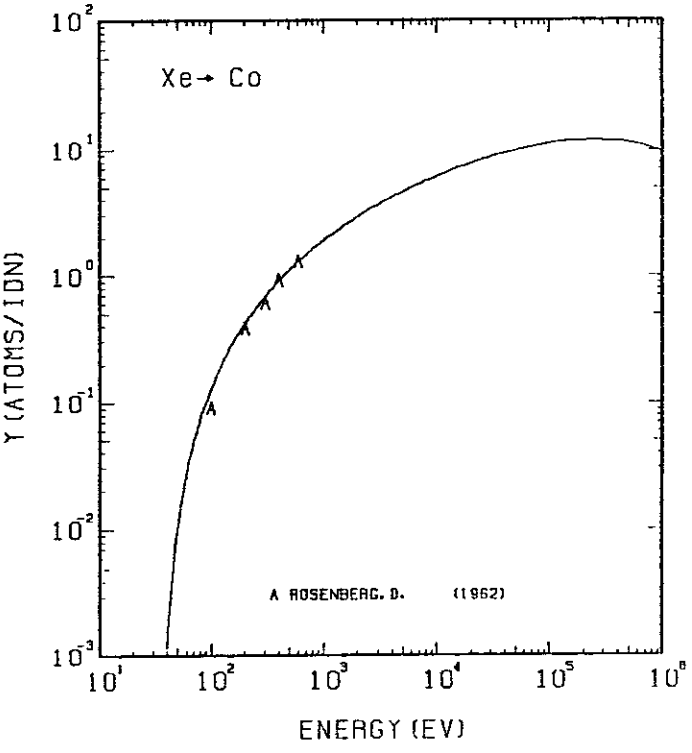


FIG. 96 ENERGY DEPENDENCE OF THE SPUTTERING YIELD OF CO WITH $XE^+$.
A= 0.45, 0= 1.02, Us= 4.39EV, S= 2.50,
W= 0.35Us.

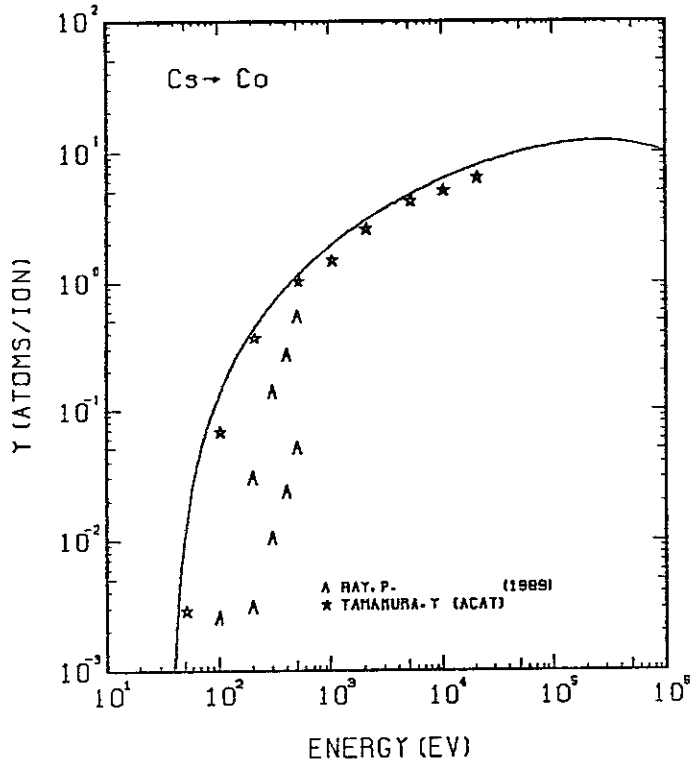


FIG. 97 ENERGY DEPENDENCE OF THE SPUTTERING YIELD OF CO WITH $CS^+$.
A= 0.44, 0= 1.02, Us= 4.39EV, S= 2.50,
W= 0.35Us.

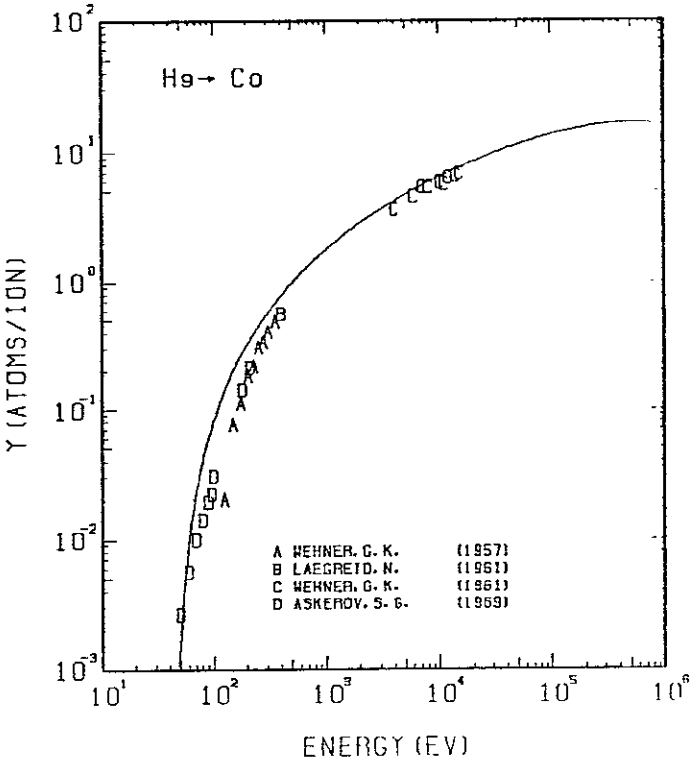


FIG. 98 ENERGY DEPENDENCE OF THE SPUTTERING YIELD OF CO WITH $HG^+$.
A= 0.29, 0= 1.02, Us= 4.39EV, S= 2.50,
W= 0.35Us.

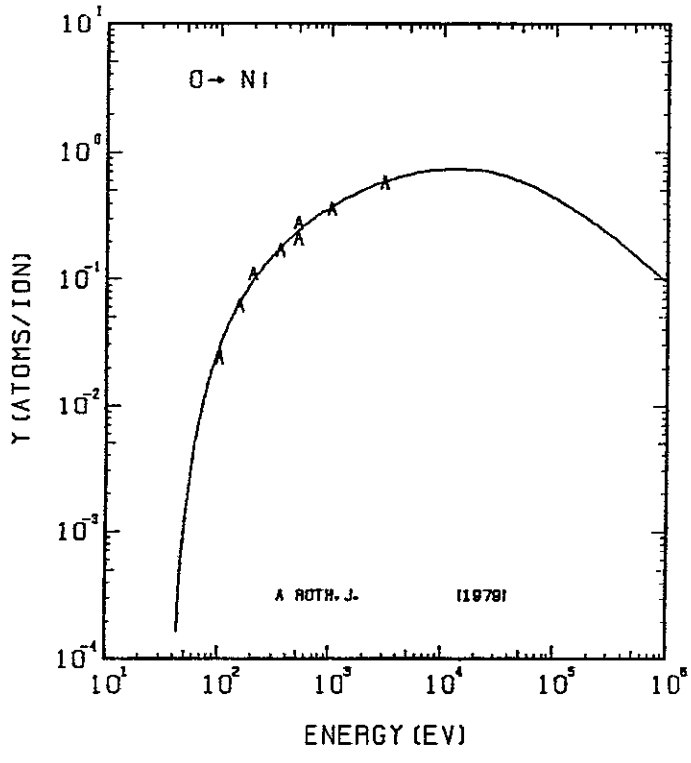


FIG. 103 ENERGY DEPENDENCE OF THE SPUTTERING YIELD OF NI WITH $O^+$. A= 3.67, O= 0.94, Us= 10.21EV, S= 2.50, W= 0.30Us. THE BEST-FIT SURFACE BINDING ENERGY IS USED.

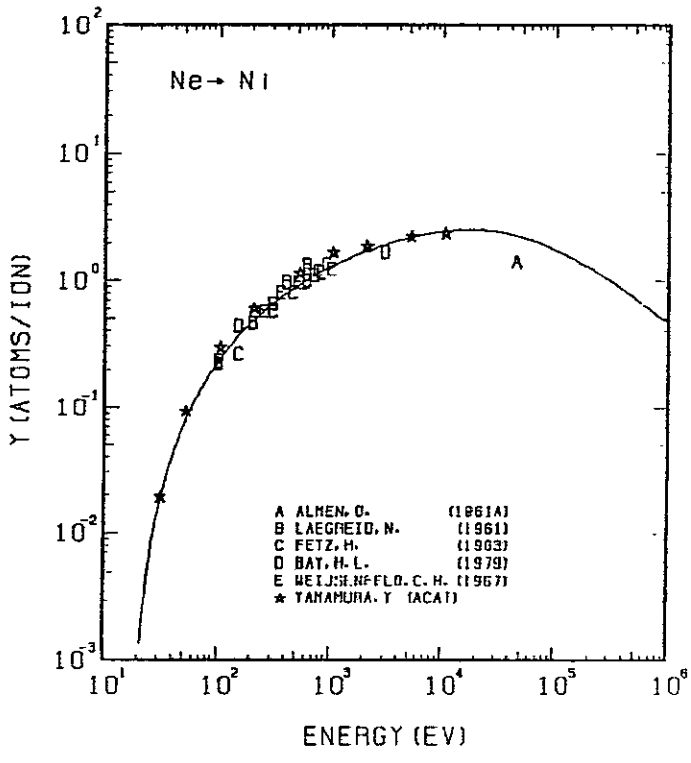


FIG. 104 ENERGY DEPENDENCE OF THE SPUTTERING YIELD OF NI WITH $NE^+$. A= 2.91, O= 0.94, Us= 4.44EV, S= 2.50, W= 0.30Us.

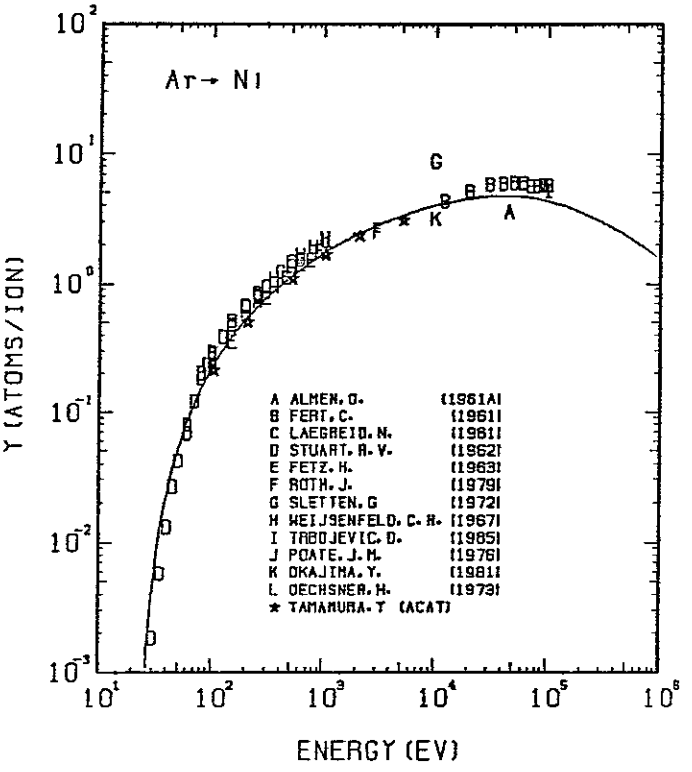


FIG. 105 ENERGY DEPENDENCE OF THE SPUTTERING YIELD OF NI WITH $AR^+$. A= 1.47, O= 0.94, Us= 4.44EV, S= 2.50, W= 0.30Us.

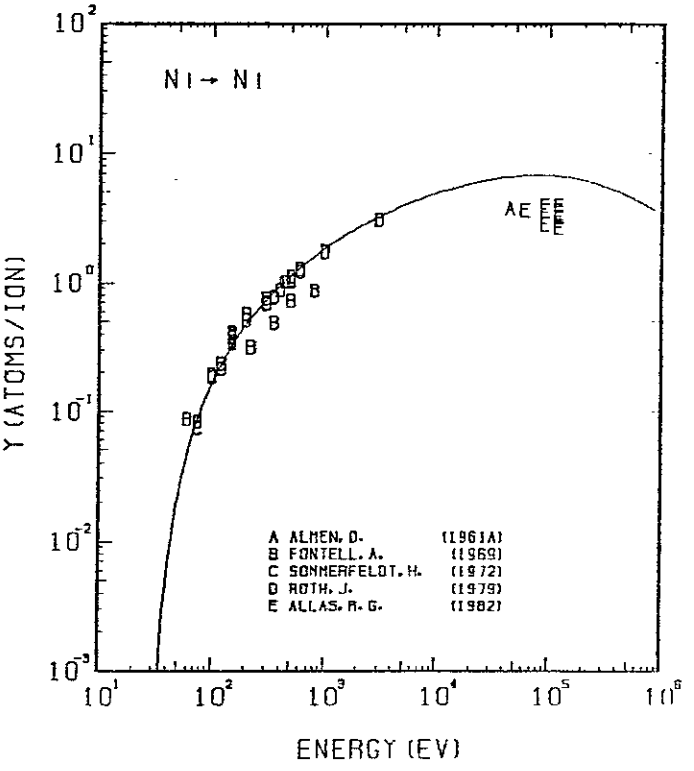


FIG. 106 ENERGY DEPENDENCE OF THE SPUTTERING YIELD OF NI WITH $NI^+$. A= 1.00, O= 0.94, Us= 4.44EV, S= 2.50, W= 0.30Us.

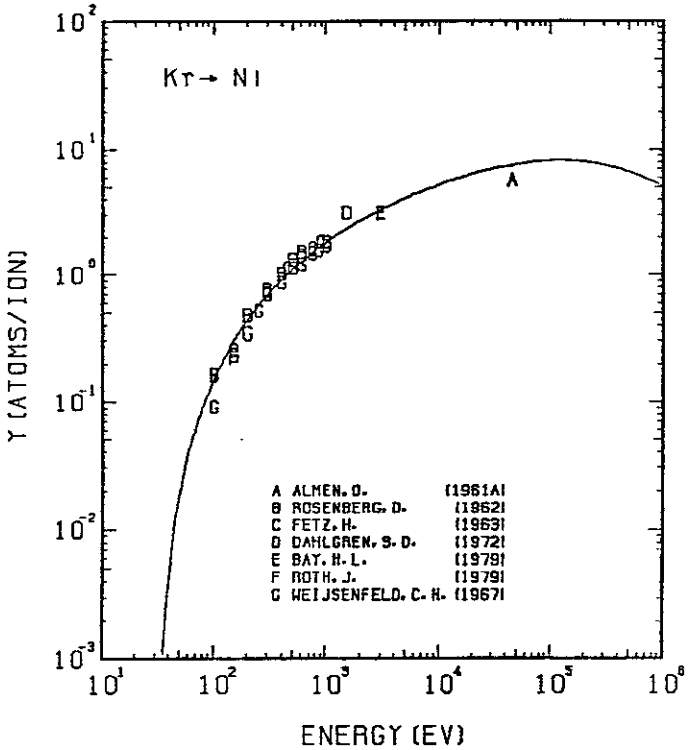


FIG. 107 ENERGY DEPENDENCE OF THE SPUTTERING YIELD OF NI WITH $KR^+$.
A= 0.70, D= 0.94, Us= 4.44EV, S= 2.50,
W= 0.30Us.

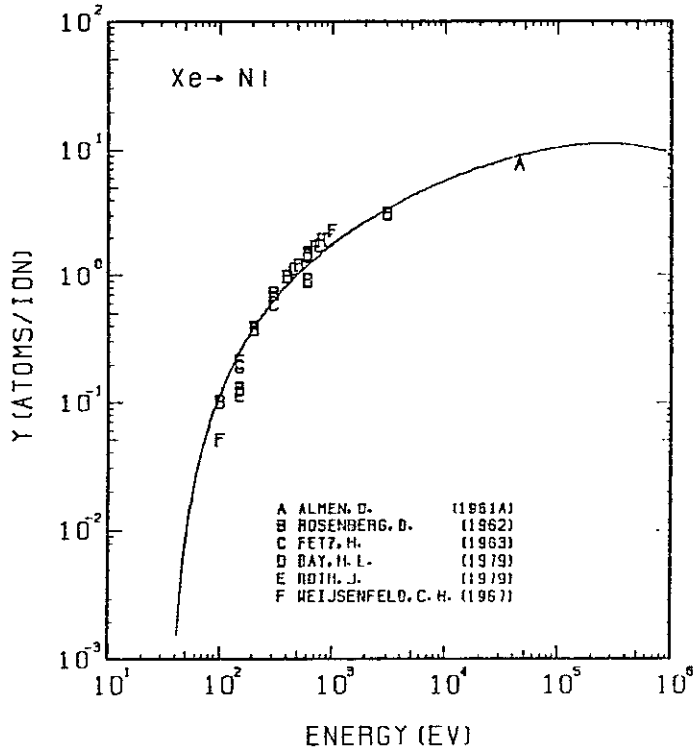


FIG. 108 ENERGY DEPENDENCE OF THE SPUTTERING YIELD OF NI WITH $XE^+$.
A= 0.45, D= 0.94, Us= 4.44EV, S= 2.50,
W= 0.30Us.

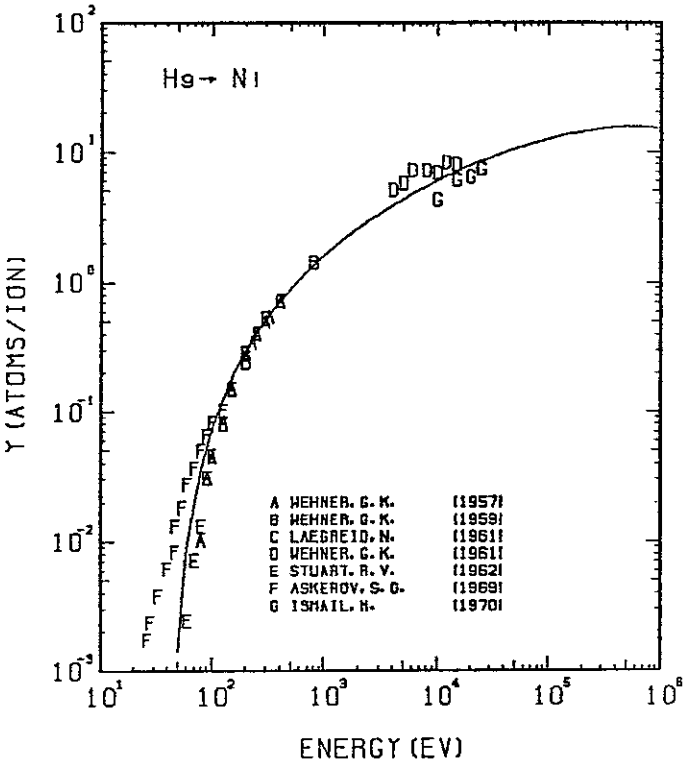


FIG. 109 ENERGY DEPENDENCE OF THE SPUTTERING YIELD OF NI WITH $HG^+$.
A= 0.29, D= 0.94, Us= 4.44EV, S= 2.50,
W= 0.30Us.

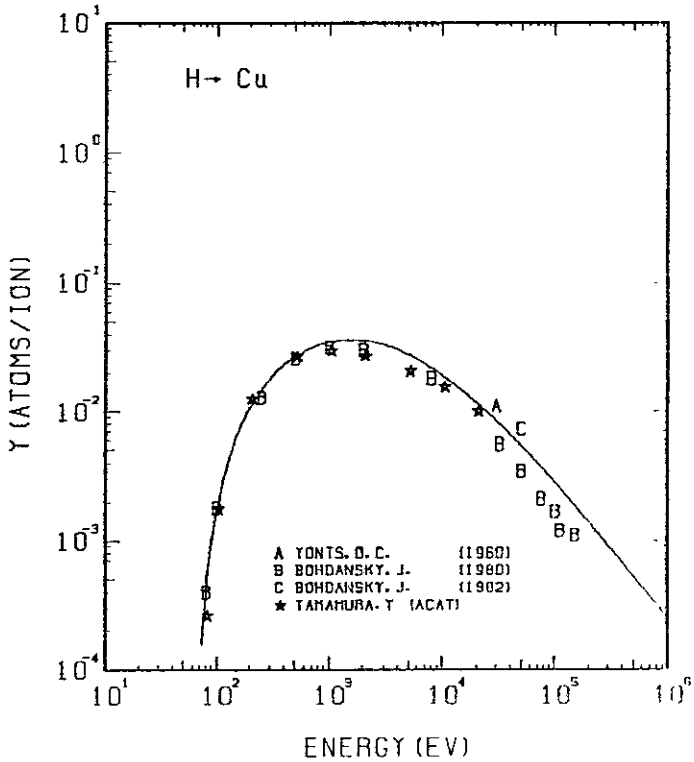


FIG. 110 ENERGY DEPENDENCE OF THE SPUTTERING YIELD OF CU WITH $H^+$.
A= 63.05, D= 1.00, Us= 3.49EV, S= 2.50,
W= 0.21Us.

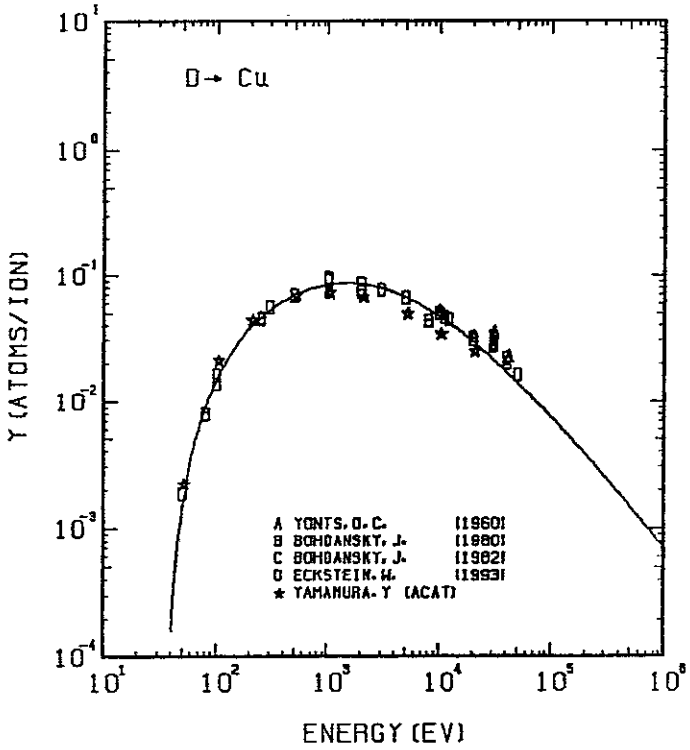


FIG. 111 ENERGY DEPENDENCE OF THE SPUTTERING YIELD OF CU WITH $D^+$.
A= 31.55, Q= 1.00, Us= 3.49EV, s= 2.50.
W= 0.21Us.

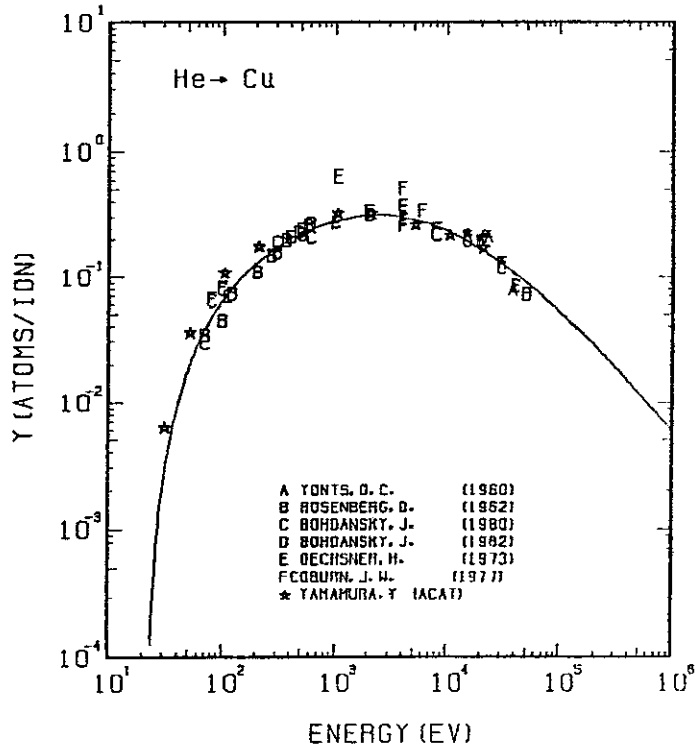


FIG. 112 ENERGY DEPENDENCE OF THE SPUTTERING YIELD OF CU WITH $HE^+$.
A= 15.88, Q= 1.00, Us= 3.49EV, s= 2.50.
W= 0.21Us.

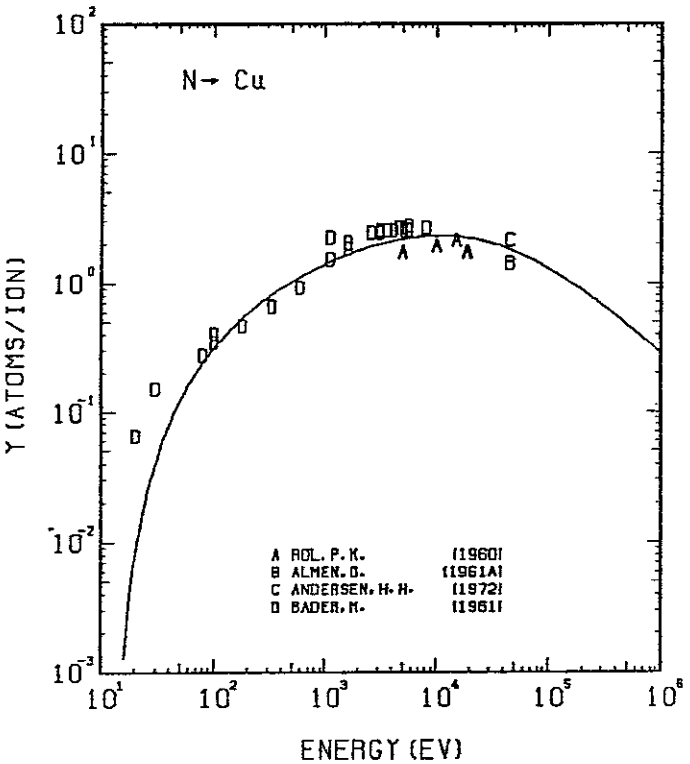


FIG. 113 ENERGY DEPENDENCE OF THE SPUTTERING YIELD OF CU WITH $N^+$.
A= 4.54, Q= 1.00, Us= 3.49EV, s= 2.50.
W= 0.21Us. THE BEST-FIT SURFACE BINDING ENERGY IS USED.

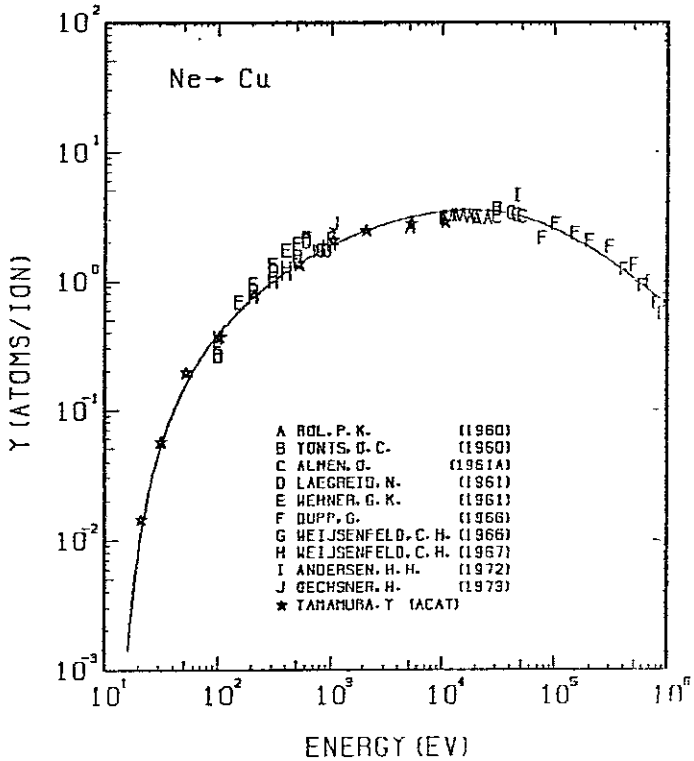


FIG. 114 ENERGY DEPENDENCE OF THE SPUTTERING YIELD OF CU WITH $NE^+$.
A= 3.15, Q= 1.00, Us= 3.49EV, s= 2.50.
W= 0.21Us.

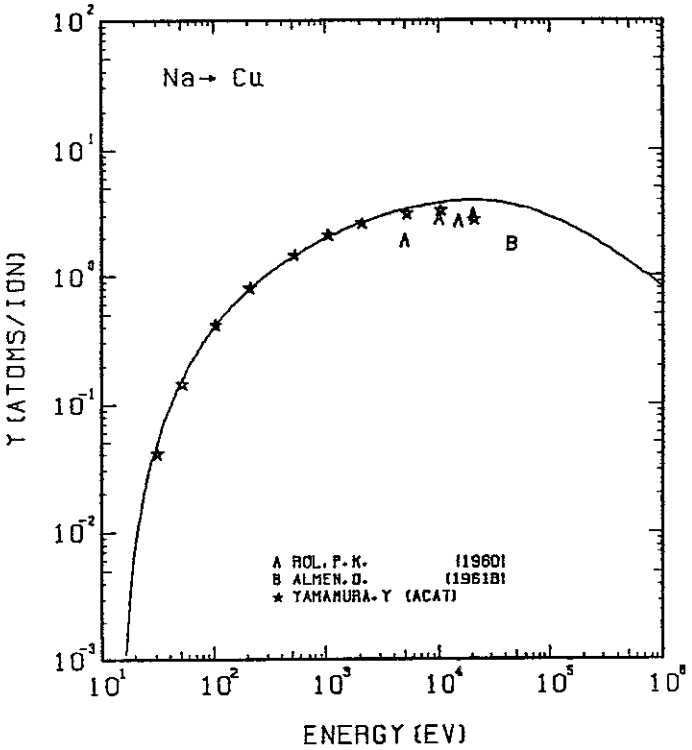


FIG. 115 ENERGY DEPENDENCE OF THE SPUTTERING YIELD OF CU WITH $NA^+$.
A= 2.76, D= 1.00, Us= 3.49EV, S= 2.50,
W= 0.21Us.

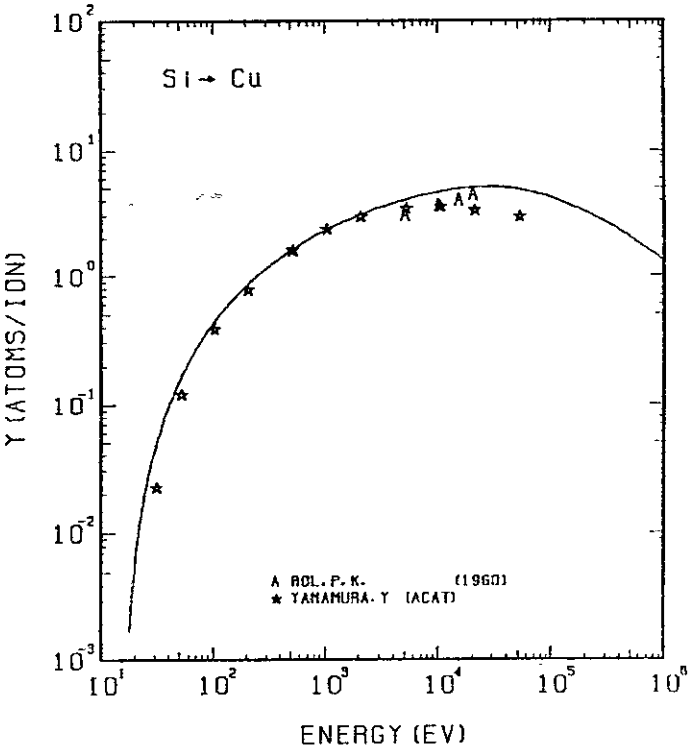


FIG. 116 ENERGY DEPENDENCE OF THE SPUTTERING YIELD OF CU WITH $SI^+$.
A= 2.26, D= 1.00, Us= 3.49EV, S= 2.50,
W= 0.21Us.

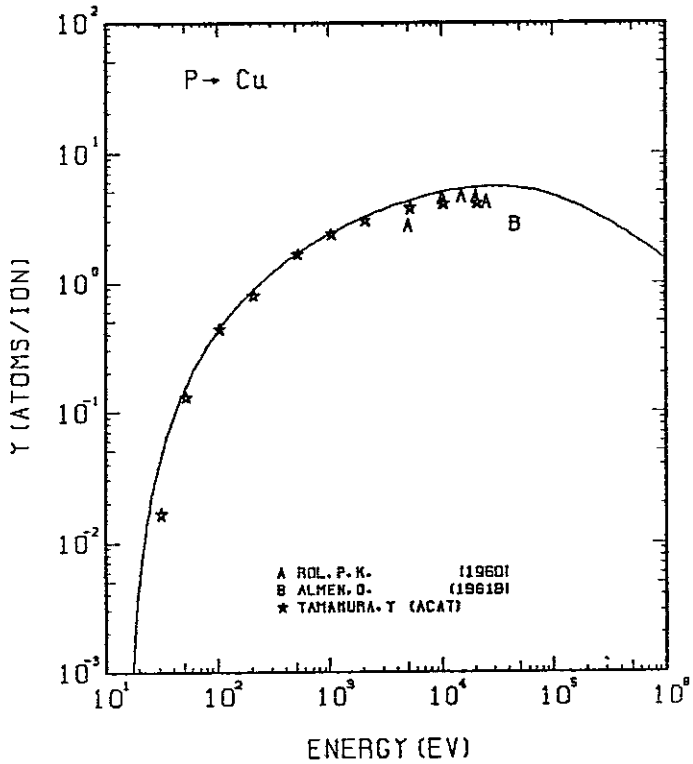


FIG. 117 ENERGY DEPENDENCE OF THE SPUTTERING YIELD OF CU WITH $P^+$.
A= 2.05, D= 1.00, Us= 3.49EV, S= 2.50,
W= 0.21Us.

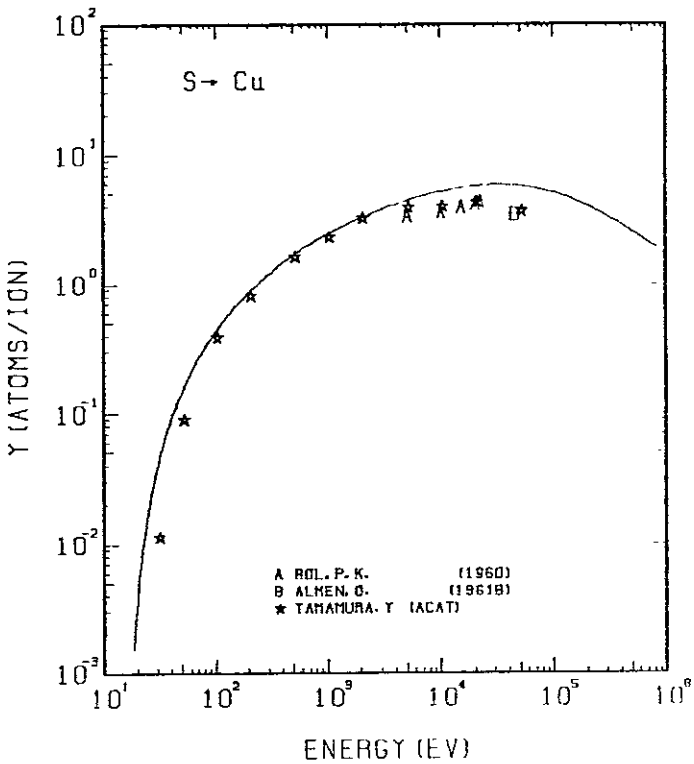


FIG. 118 ENERGY DEPENDENCE OF THE SPUTTERING YIELD OF CU WITH $S^+$.
A= 1.98, D= 1.00, Us= 3.49EV, S= 2.50,
W= 0.21Us.

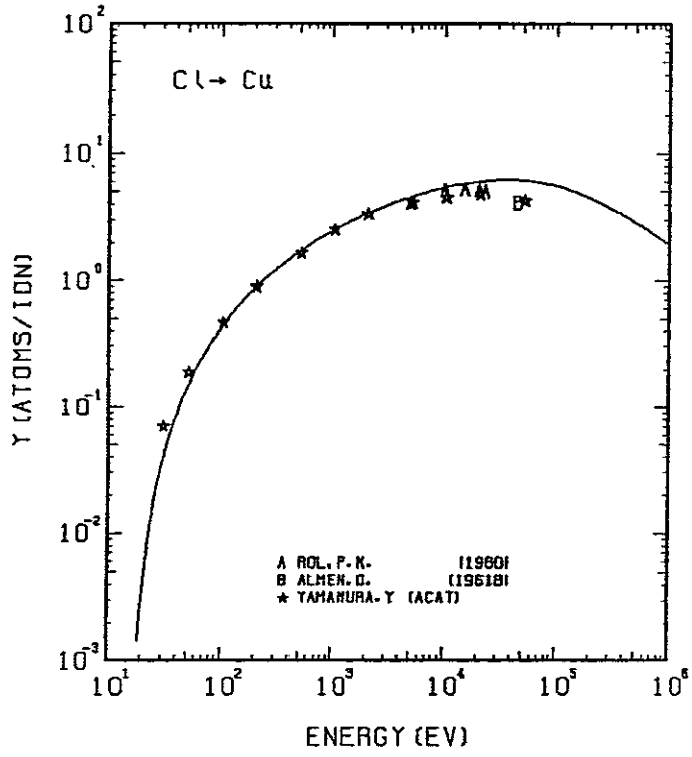


FIG. 119 ENERGY DEPENDENCE OF THE SPUTTERING YIELD OF CU WITH $CL^+$.
A= 1.79, Q= 1.00, Us= 3.49EV, S= 2.50,
W= 0.21Us.

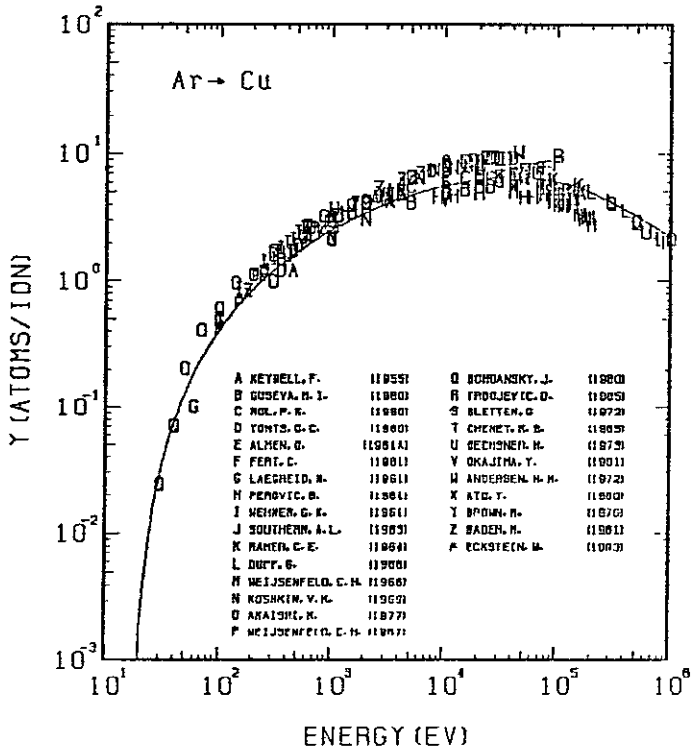


FIG. 120 ENERGY DEPENDENCE OF THE SPUTTERING YIELD OF CU WITH $AR^+$.
A= 1.59, Q= 1.00, Us= 3.49EV, S= 2.50,
W= 0.21Us.

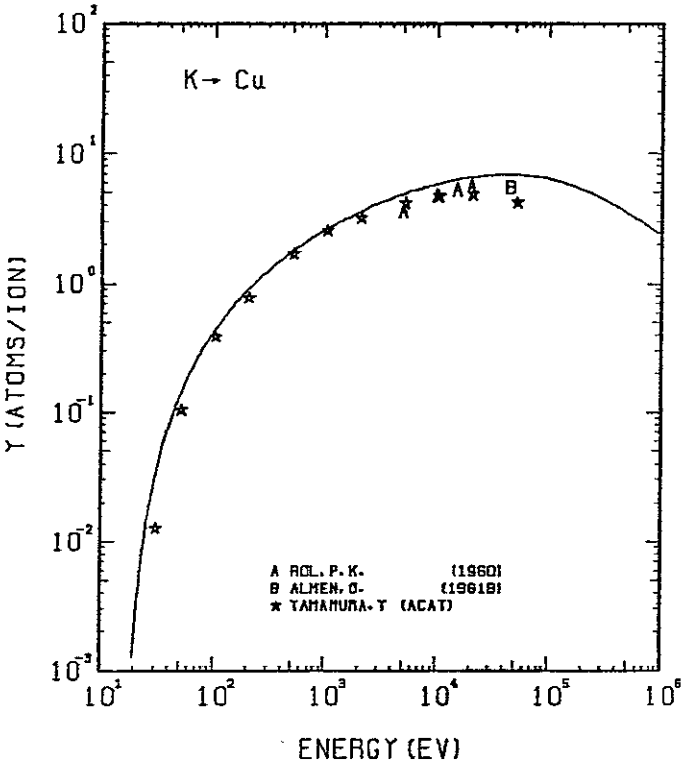


FIG. 121 ENERGY DEPENDENCE OF THE SPUTTERING YIELD OF CU WITH $K^+$.
A= 1.63, Q= 1.00, Us= 3.49EV, S= 2.50,
W= 0.21Us.

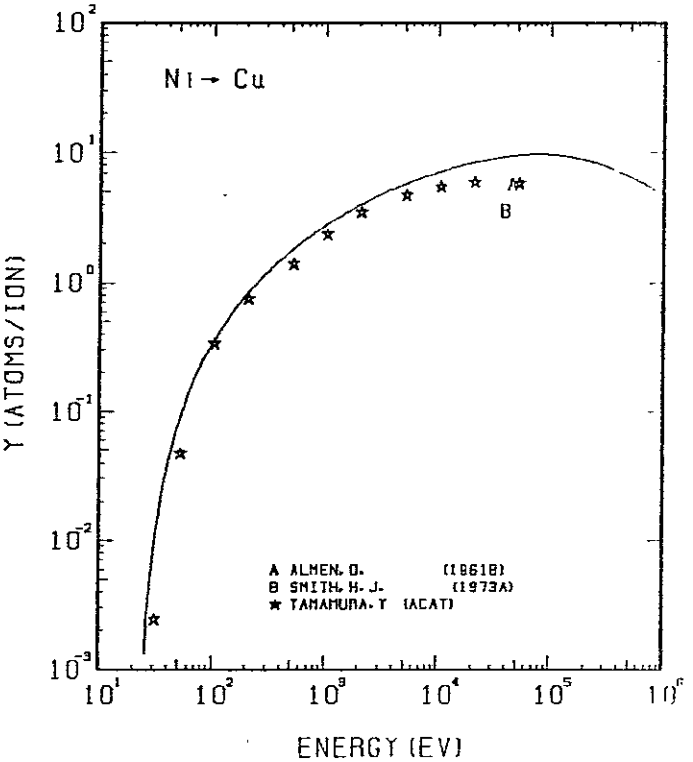


FIG. 122 ENERGY DEPENDENCE OF THE SPUTTERING YIELD OF CU WITH $NI^+$.
A= 1.08, Q= 1.00, Us= 3.49EV, S= 2.50,
W= 0.21Us.

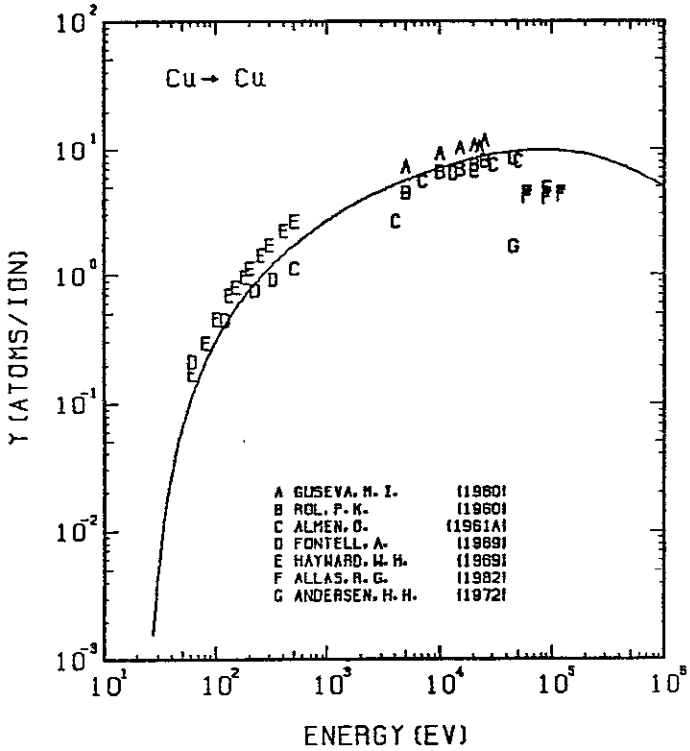


FIG. 123 ENERGY DEPENDENCE OF THE SPUTTERING YIELD OF CU WITH $CU^+$.
A= 1.00, D= 1.00, Us= 3.49EV, S= 2.50,
W= 0.21Us.

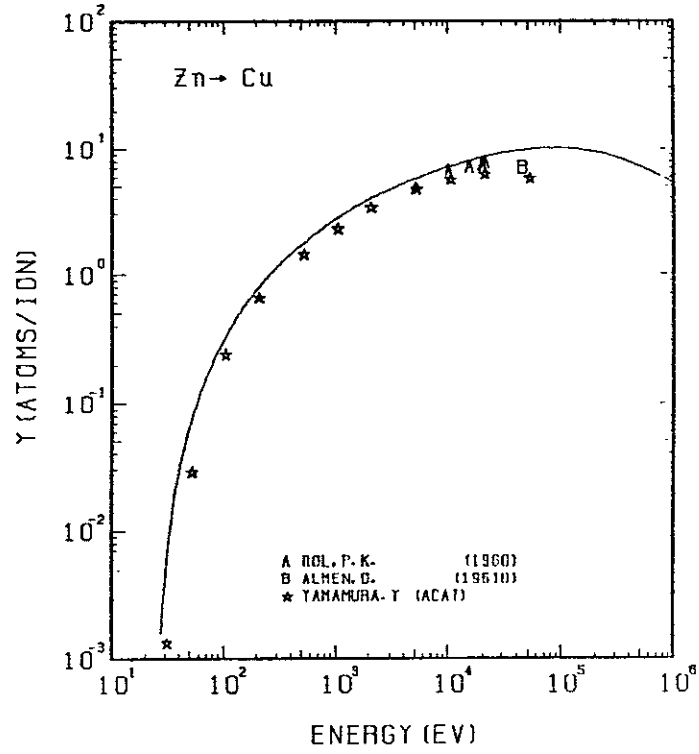


FIG. 124 ENERGY DEPENDENCE OF THE SPUTTERING YIELD OF CU WITH $ZN^+$.
A= 0.97, D= 1.00, Us= 3.49EV, S= 2.50,
W= 0.21Us.

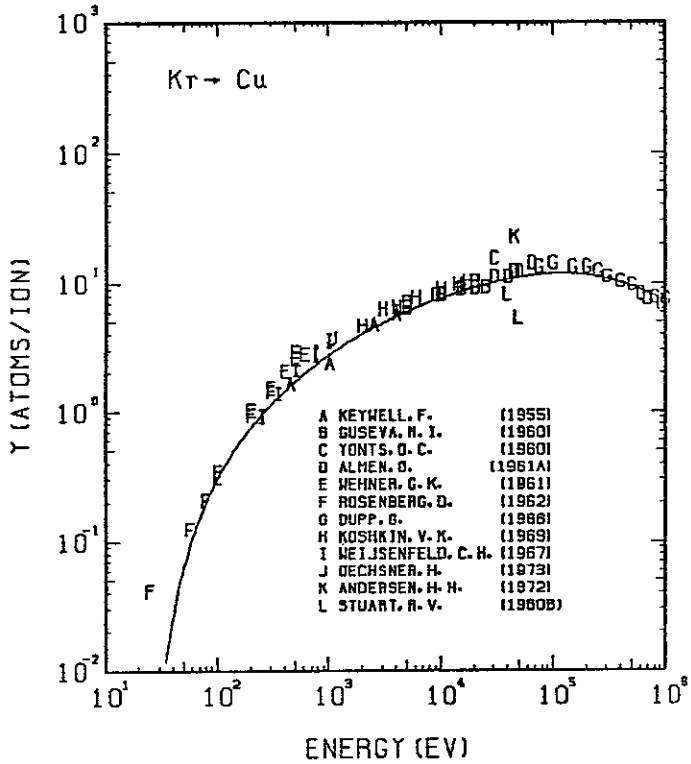


FIG. 125 ENERGY DEPENDENCE OF THE SPUTTERING YIELD OF CU WITH $KR^+$.
A= 0.76, D= 1.00, Us= 3.49EV, S= 2.50,
W= 0.21Us.

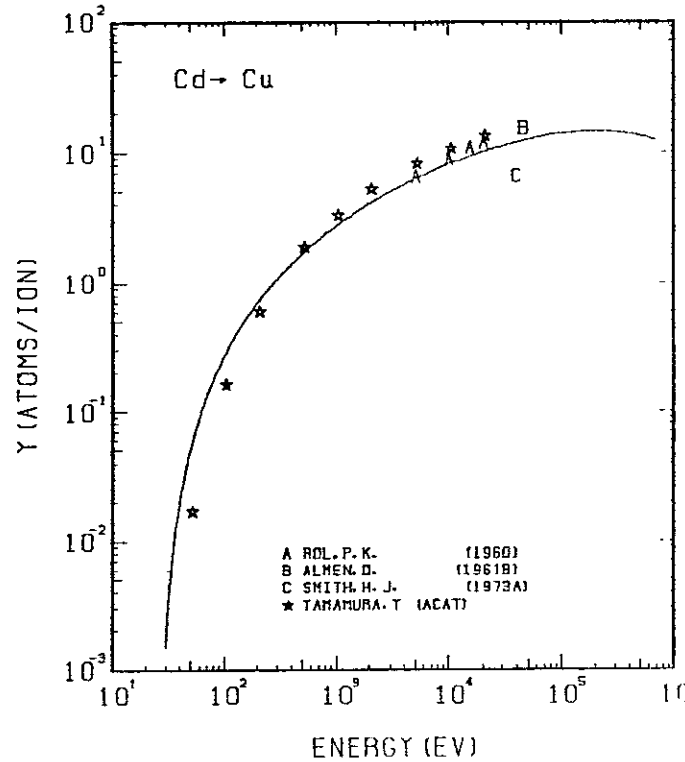


FIG. 126 ENERGY DEPENDENCE OF THE SPUTTERING YIELD OF CU WITH $CD^+$.
A= 0.57, D= 1.00, Us= 3.49EV, S= 2.50,
W= 0.21Us.

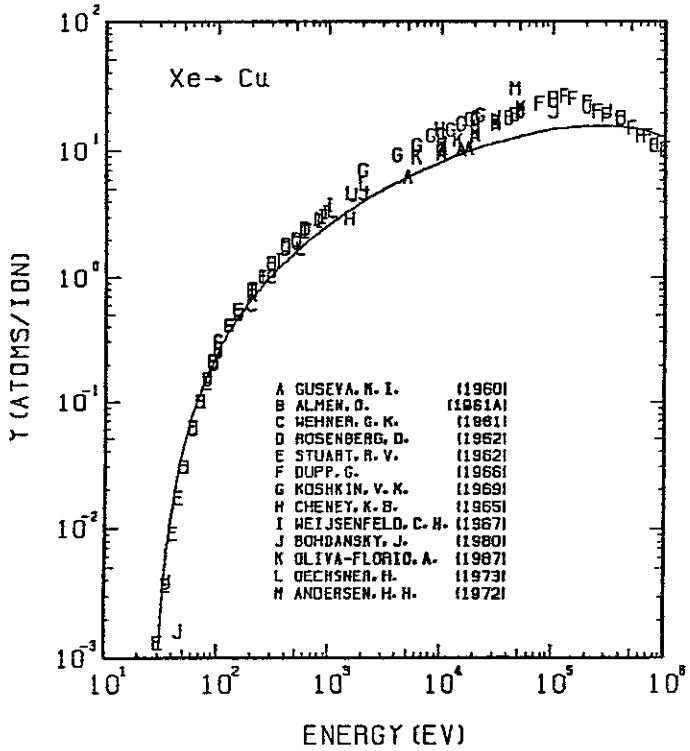


FIG. 127 ENERGY DEPENDENCE OF THE SPUTTERING YIELD OF CU WITH $XE^+$.
A= 0.48, 0= 1.00, Us= 3.49EV, s= 2.50.
W= 0.21Us.

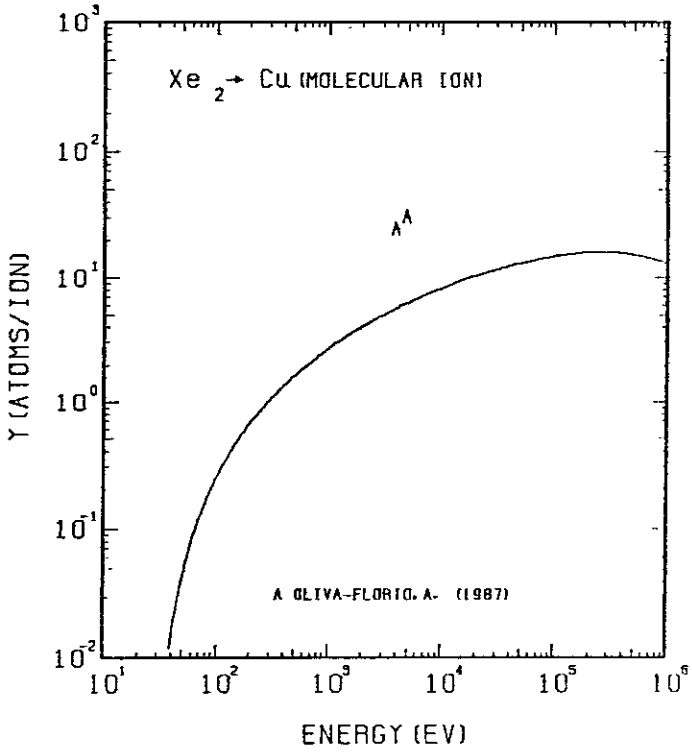


FIG. 128 ENERGY DEPENDENCE OF THE SPUTTERING YIELD OF CU WITH $XE_2^+$.
A= 0.48, 0= 1.00, Us= 3.49EV, s= 2.50.
W= 0.21Us. THE NON-LINEAR EFFECT IS OBSERVED DUE TO MOLECULAR IONS.

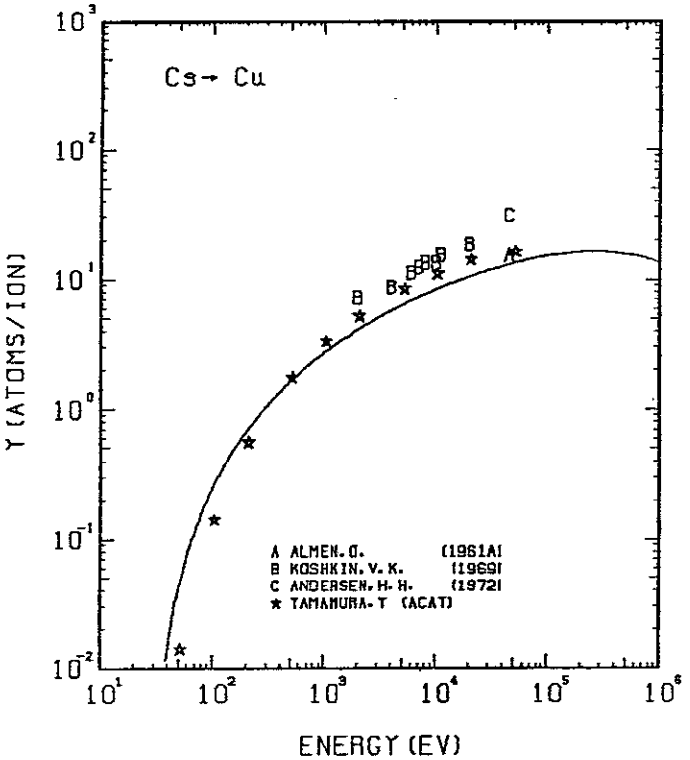


FIG. 129 ENERGY DEPENDENCE OF THE SPUTTERING YIELD OF CU WITH $CS^+$.
A= 0.48, 0= 1.00, Us= 3.49EV, s= 2.50.
W= 0.21Us.

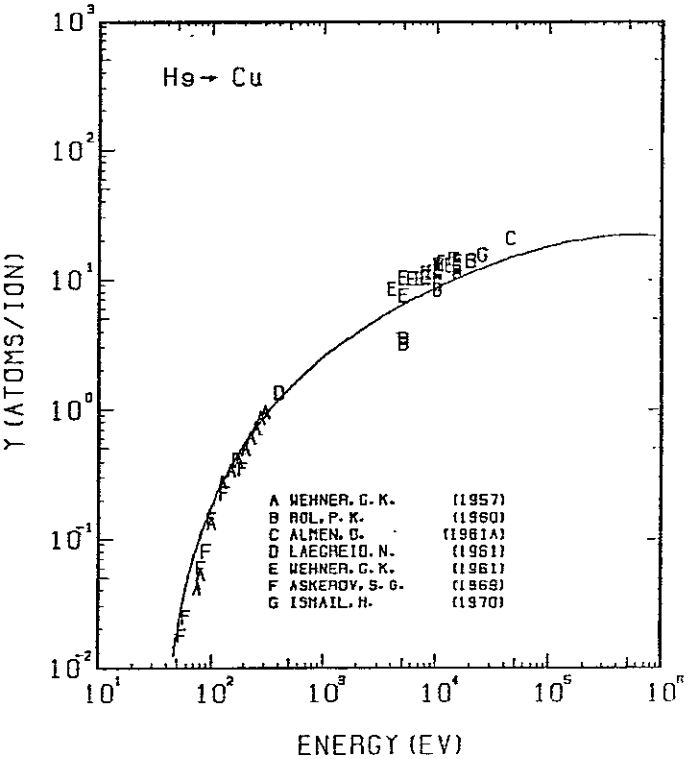


FIG. 130 ENERGY DEPENDENCE OF THE SPUTTERING YIELD OF CU WITH $HG^+$.
A= 0.32, 0= 1.00, Us= 3.49EV, s= 2.50.
W= 0.21Us.

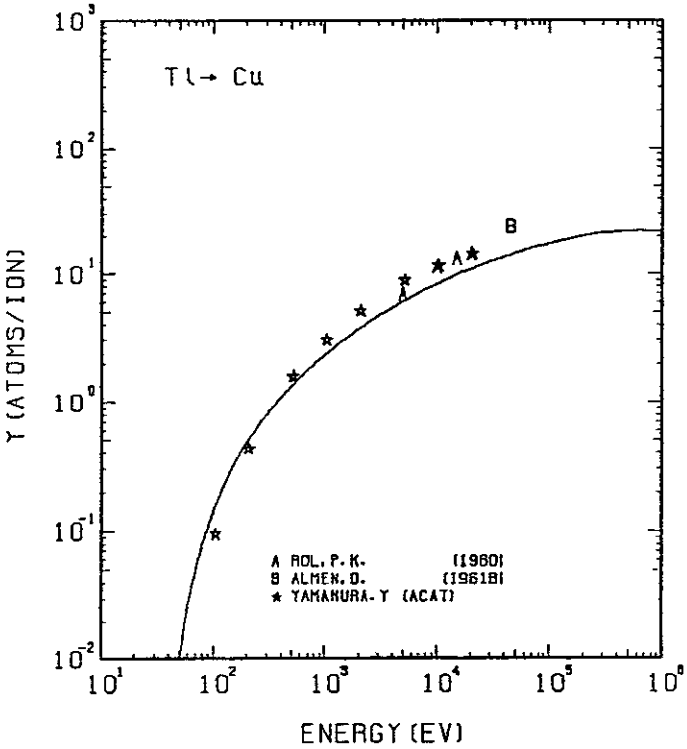


FIG. 131 ENERGY DEPENDENCE OF THE SPUTTERING YIELD OF CU WITH $TL^+$.
A= 0.26, Q= 1.00, Us= 3.49EV, s= 2.50,
W= 0.21Us.

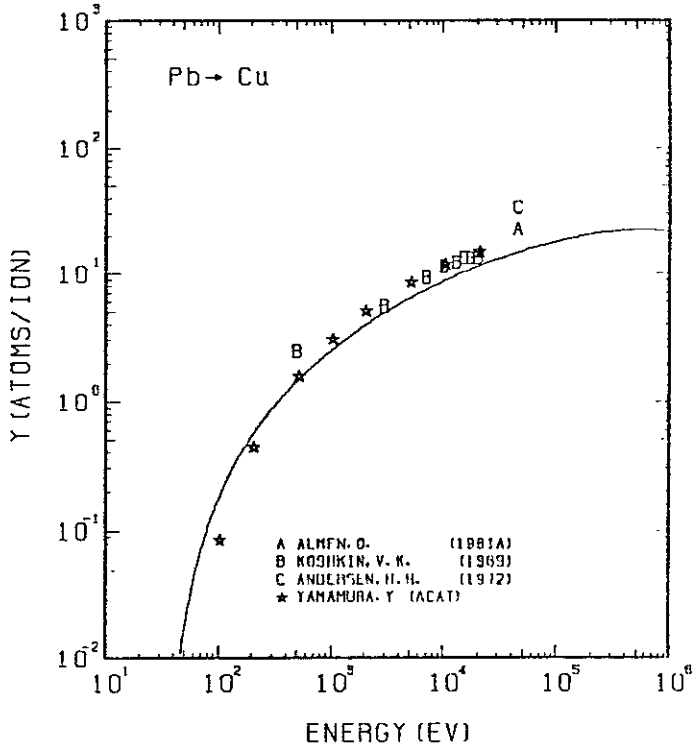


FIG. 132 ENERGY DEPENDENCE OF THE SPUTTERING YIELD OF CU WITH $PB^+$.
A= 0.31, Q= 1.00, Us= 3.49EV, s= 2.50,
W= 0.21Us.

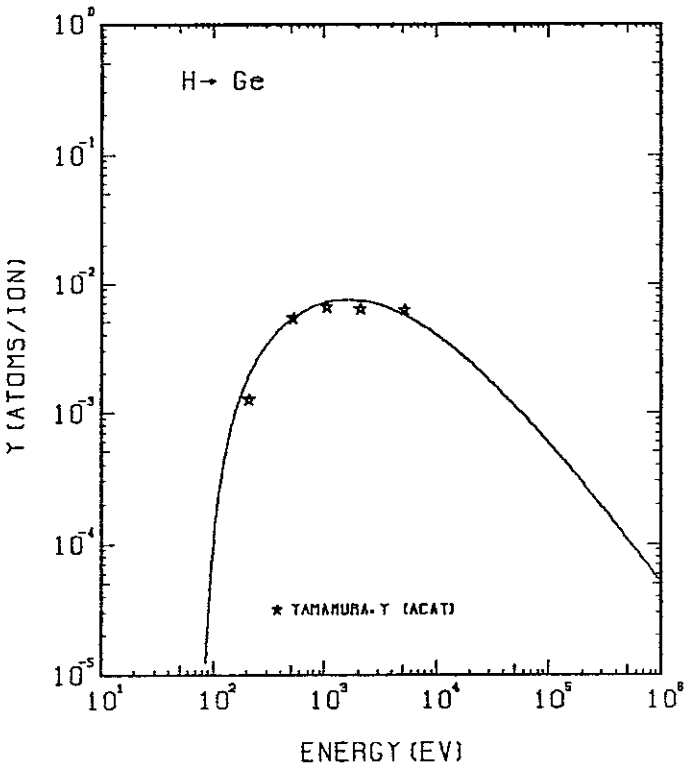


FIG. 133 ENERGY DEPENDENCE OF THE SPUTTERING YIELD OF GE WITH $H^+$.
A= 72.01, Q= 0.59, Us= 3.85EV, s= 2.50,
W= 0.54Us.

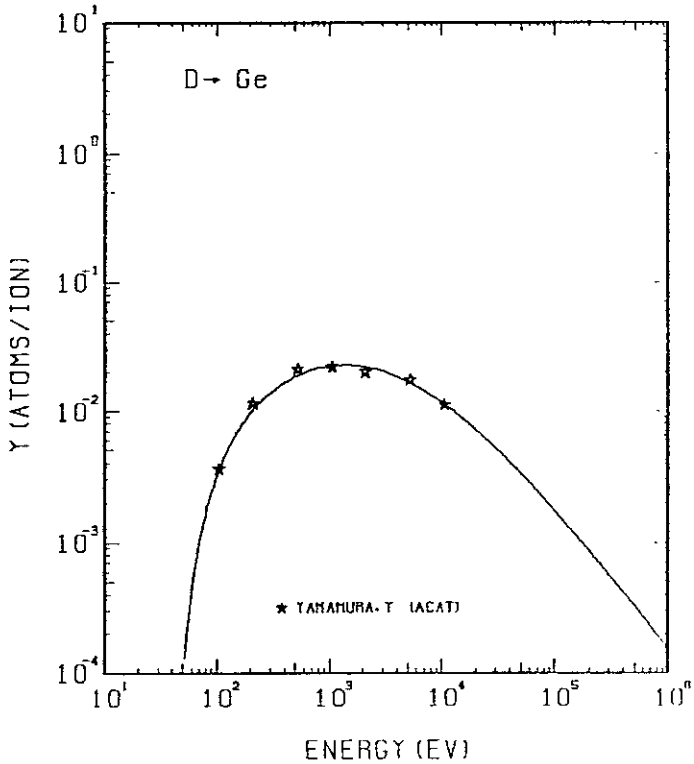


FIG. 134 ENERGY DEPENDENCE OF THE SPUTTERING YIELD OF GE WITH $D^+$.
A= 36.04, Q= 0.59, Us= 3.85EV, s= 2.50,
W= 0.54Us.

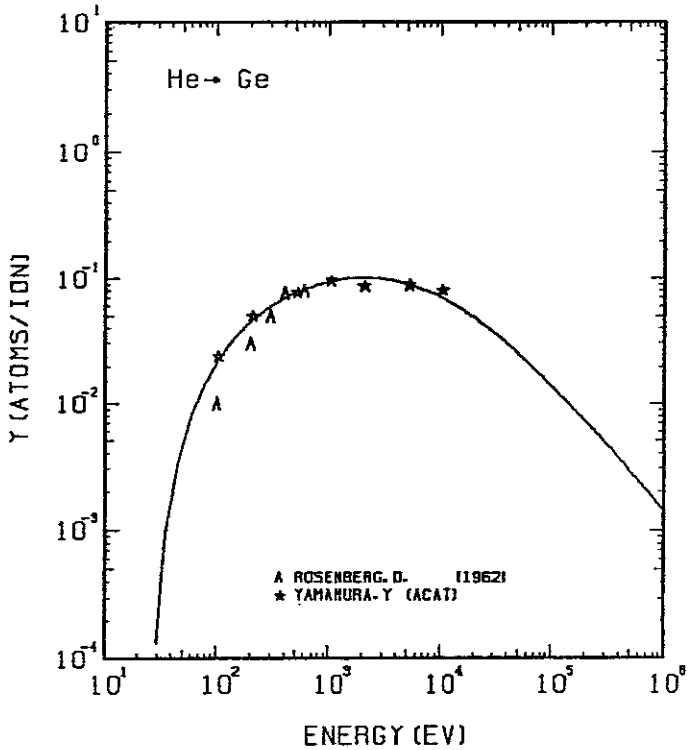


FIG. 135 ENERGY DEPENDENCE OF THE SPUTTERING YIELD OF GE WITH HE+.
A= 18.13, D= 0.59, Us= 3.85EV, s= 2.50,
W= 0.54Us.

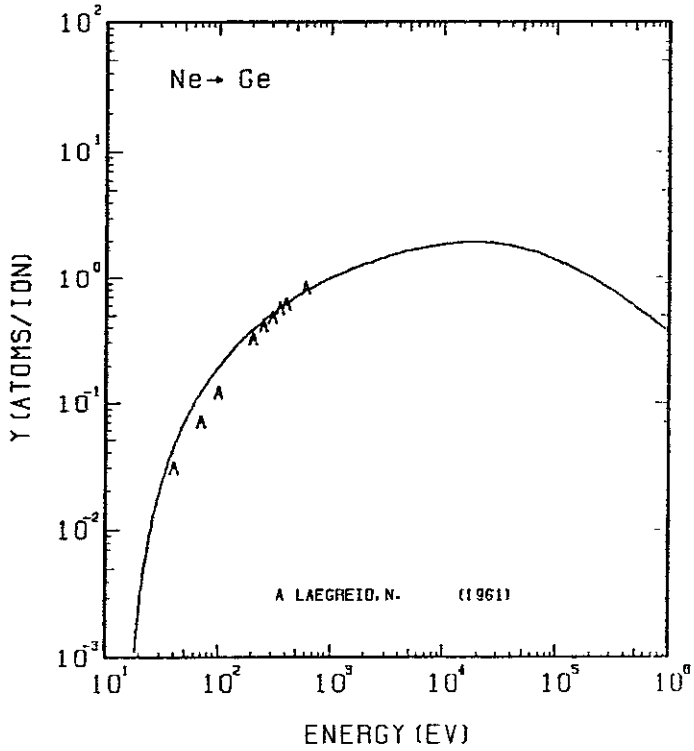


FIG. 136 ENERGY DEPENDENCE OF THE SPUTTERING YIELD OF GE WITH NE+.
A= 3.60, D= 0.59, Us= 3.85EV, s= 2.50,
W= 0.54Us.

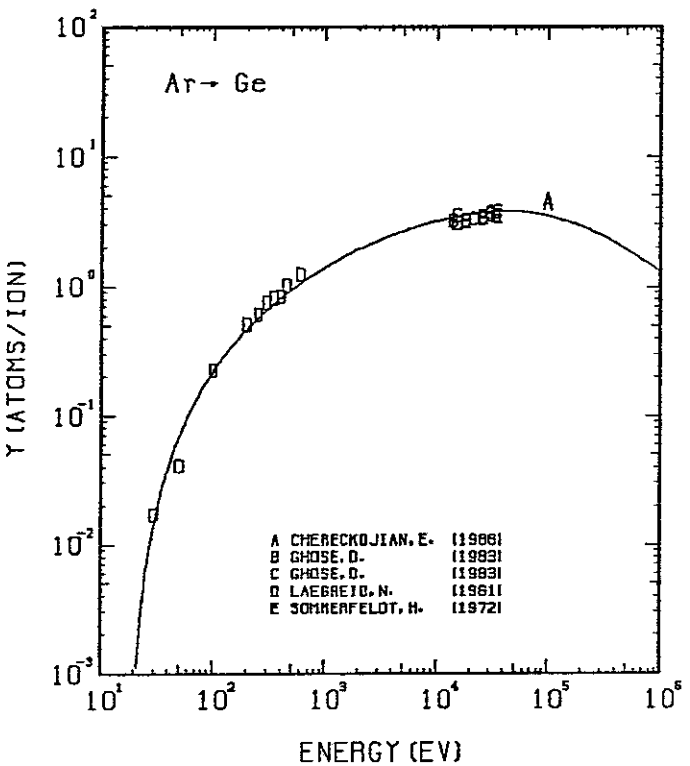


FIG. 137 ENERGY DEPENDENCE OF THE SPUTTERING YIELD OF GE WITH AR+.
A= 1.82, D= 0.59, Us= 3.85EV, s= 2.50,
W= 0.54Us.

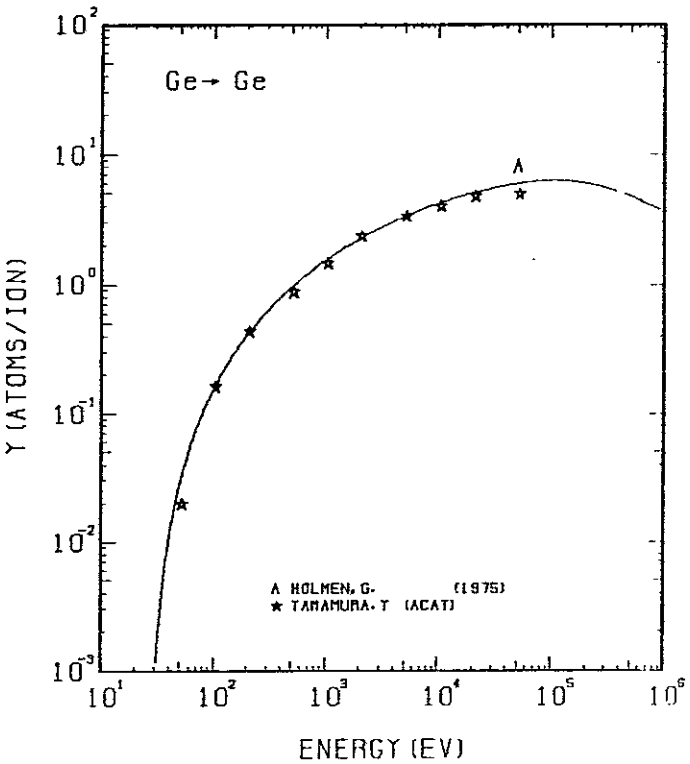


FIG. 138 ENERGY DEPENDENCE OF THE SPUTTERING YIELD OF GE WITH GE+.
A= 1.00, D= 0.59, Us= 3.85EV, s= 2.50,
W= 0.54Us.

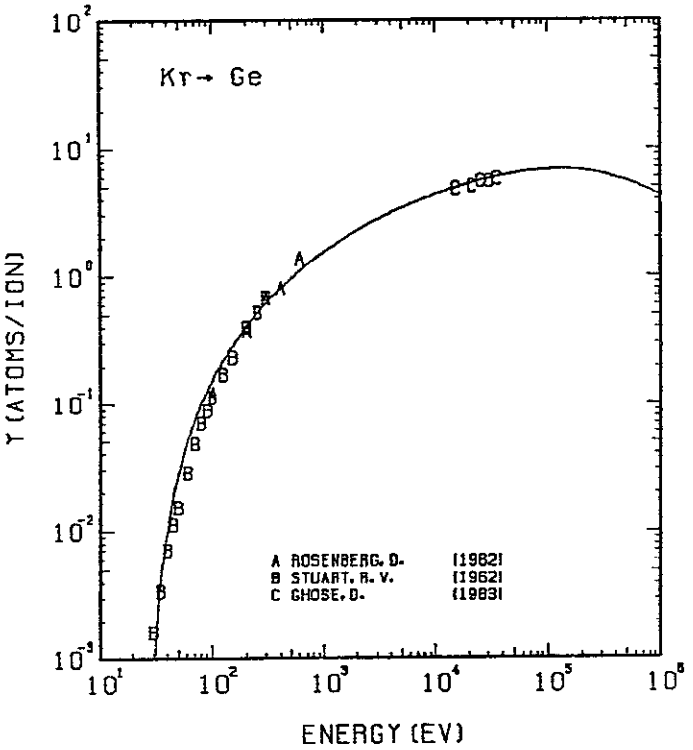


FIG. 139 ENERGY DEPENDENCE OF THE SPUTTERING YIELD OF GE WITH KR⁺.
A= 0.87, 0= 0.59, Us= 3.85EV, s= 2.50,
W= 0.54Us.

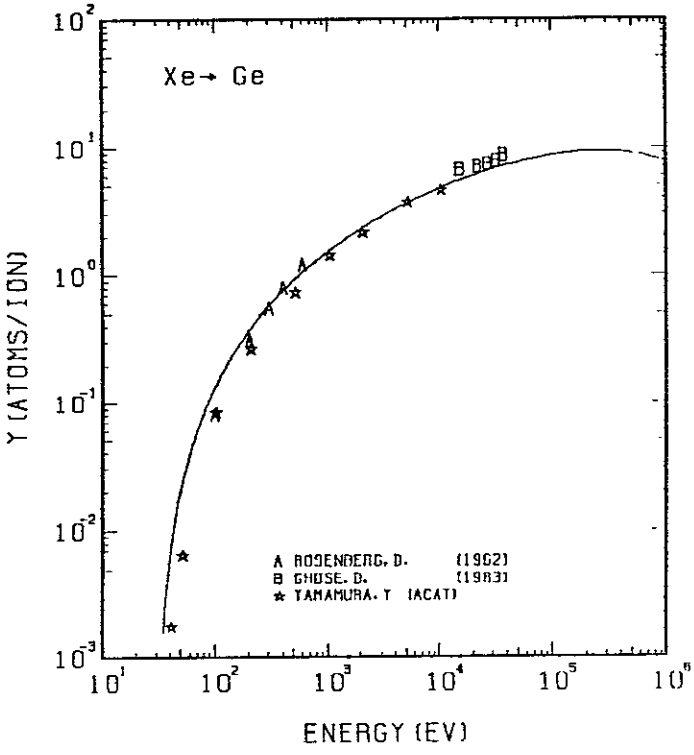


FIG. 140 ENERGY DEPENDENCE OF THE SPUTTERING YIELD OF GE WITH XE⁺.
A= 0.55, 0= 0.59, Us= 3.85EV, s= 2.50,
W= 0.54Us.

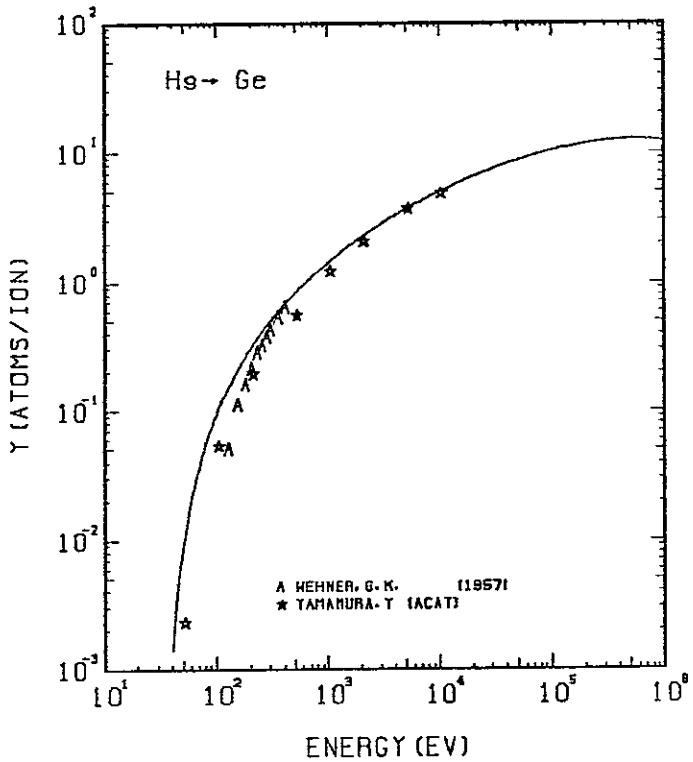


FIG. 141 ENERGY DEPENDENCE OF THE SPUTTERING YIELD OF GE WITH HG⁺.
A= 0.36, 0= 0.59, Us= 3.85EV, s= 2.50,
W= 0.54Us.

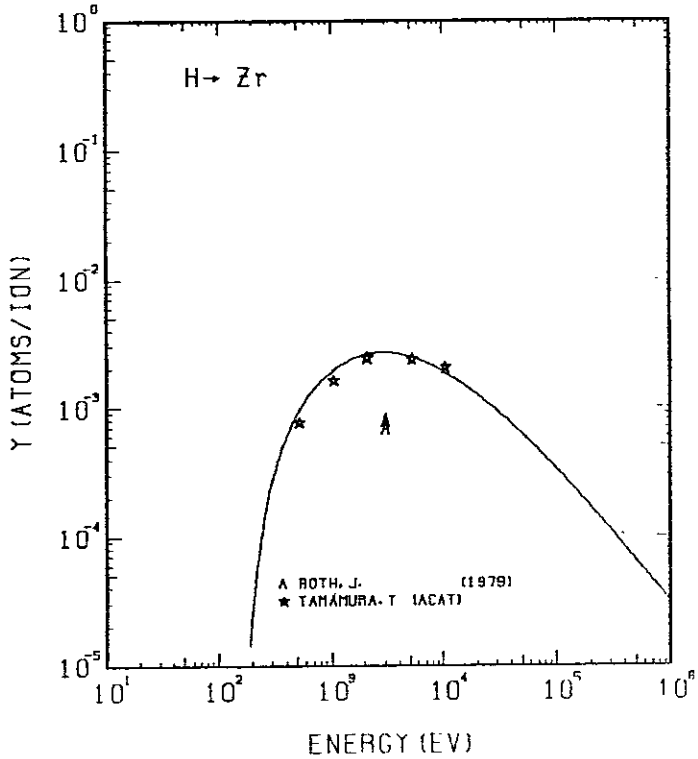


FIG. 142 ENERGY DEPENDENCE OF THE SPUTTERING YIELD OF ZR WITH H⁺.
A= 90.50, 0= 0.54, Us= 6.25EV, s= 2.80,
W= 0.40Us.

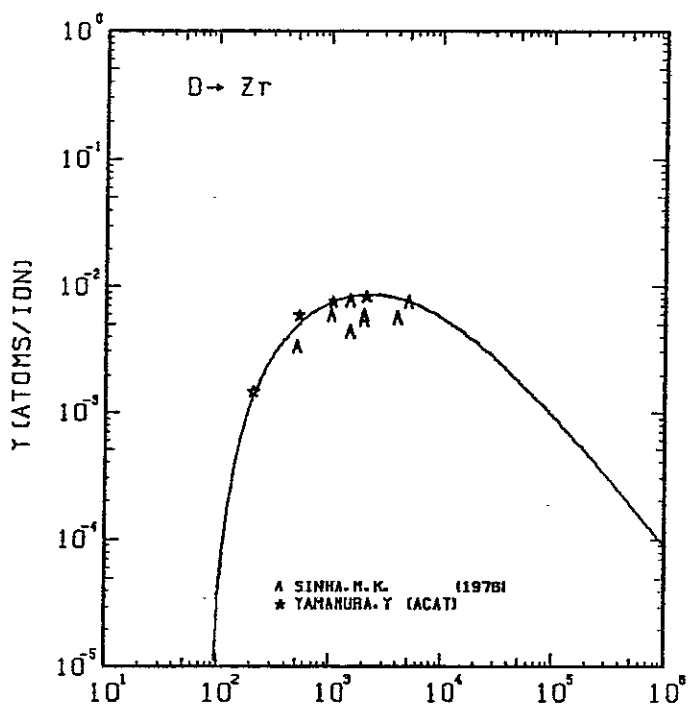


FIG. 143 ENERGY DEPENDENCE OF THE SPUTTERING YIELD OF ZR WITH $D^+$.
A= 45.29, Q= 0.54, Us= 6.25EV, s= 2.80,
W= 0.40Us.

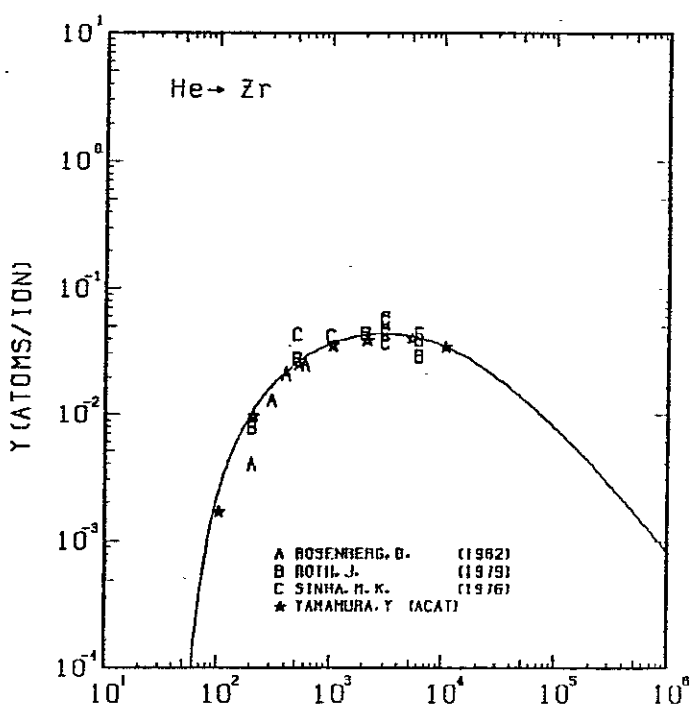


FIG. 144 ENERGY DEPENDENCE OF THE SPUTTERING YIELD OF ZR WITH $HE^+$.
A= 22.79, Q= 0.54, Us= 6.25EV, s= 2.80,
W= 0.40Us.

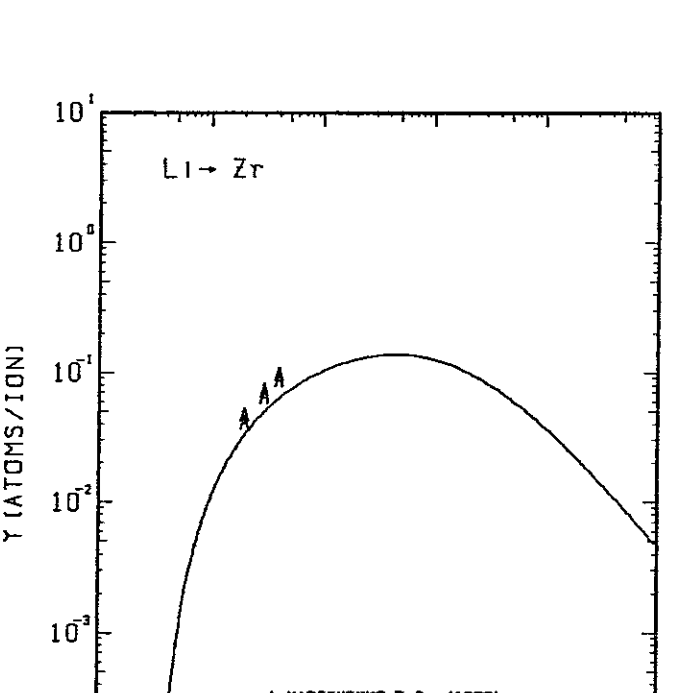


FIG. 145 ENERGY DEPENDENCE OF THE SPUTTERING YIELD OF ZR WITH $LI^+$.
A= 13.14, Q= 0.54, Us= 6.25EV, s= 2.80,
W= 0.40Us.

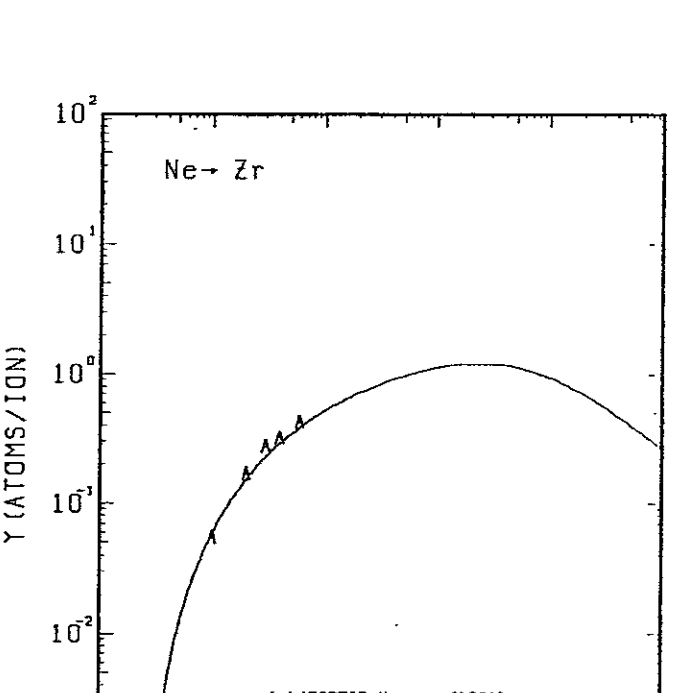


FIG. 146 ENERGY DEPENDENCE OF THE SPUTTERING YIELD OF ZR WITH $NE^+$.
A= 4.52, Q= 0.54, Us= 6.25EV, s= 2.80,
W= 0.40Us.

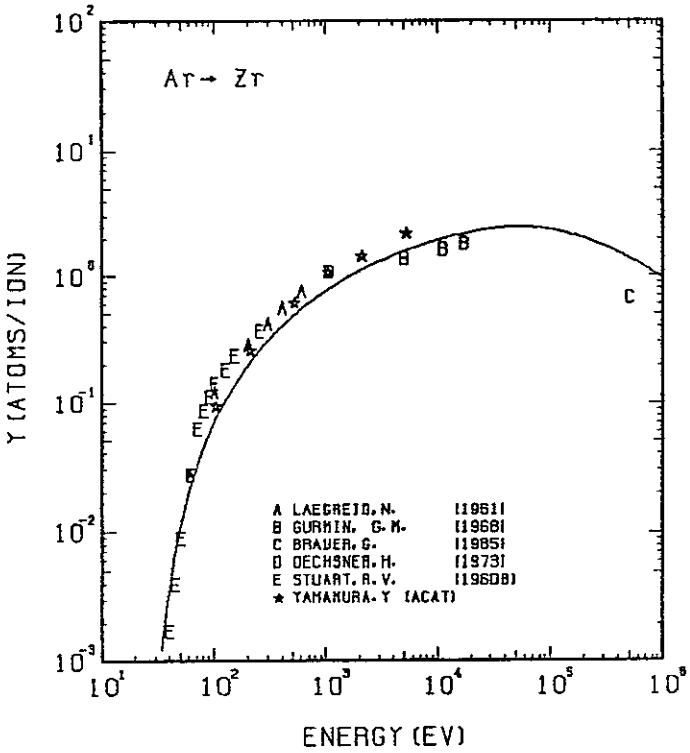


FIG. 147 ENERGY DEPENDENCE OF THE SPUTTERING YIELD OF ZR WITH $AR^+$.
A= 2.28, D= 0.54, Us= 6.25eV, s= 2.80,
W= 0.40Us.

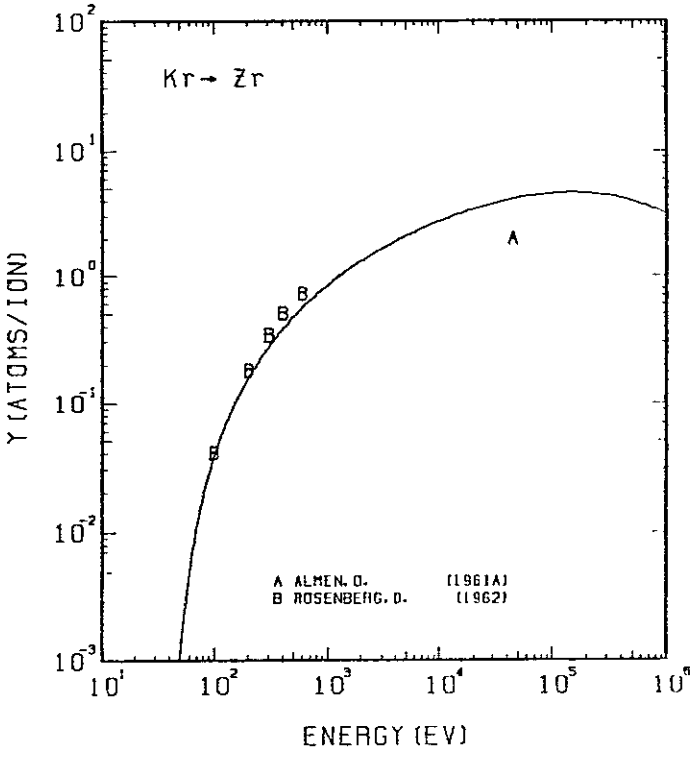


FIG. 148 ENERGY DEPENDENCE OF THE SPUTTERING YIELD OF ZR WITH $KR^+$.
A= 1.09, D= 0.54, Us= 6.25eV, s= 2.80,
W= 0.40Us.

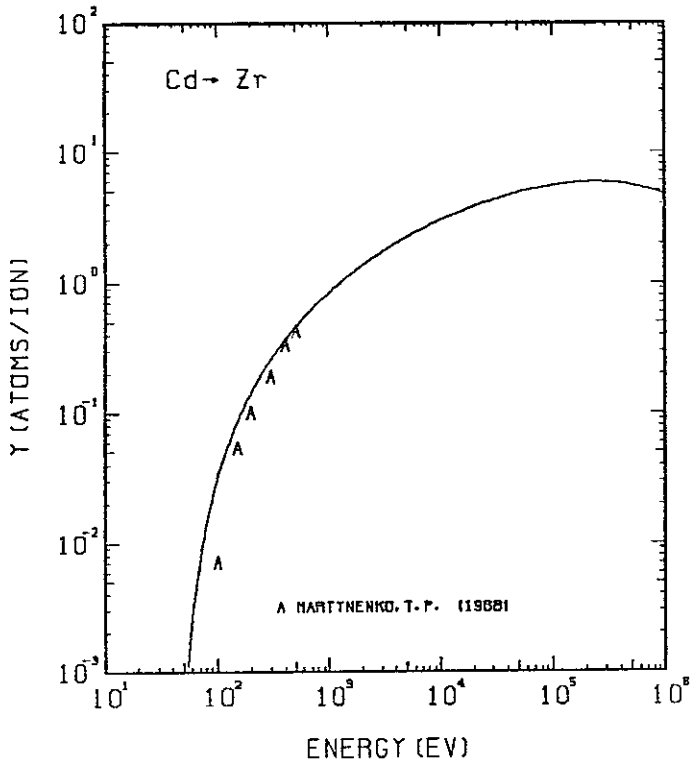


FIG. 149 ENERGY DEPENDENCE OF THE SPUTTERING YIELD OF ZR WITH $CD^+$.
A= 0.81, D= 0.54, Us= 6.25eV, s= 2.80,
W= 0.40Us.

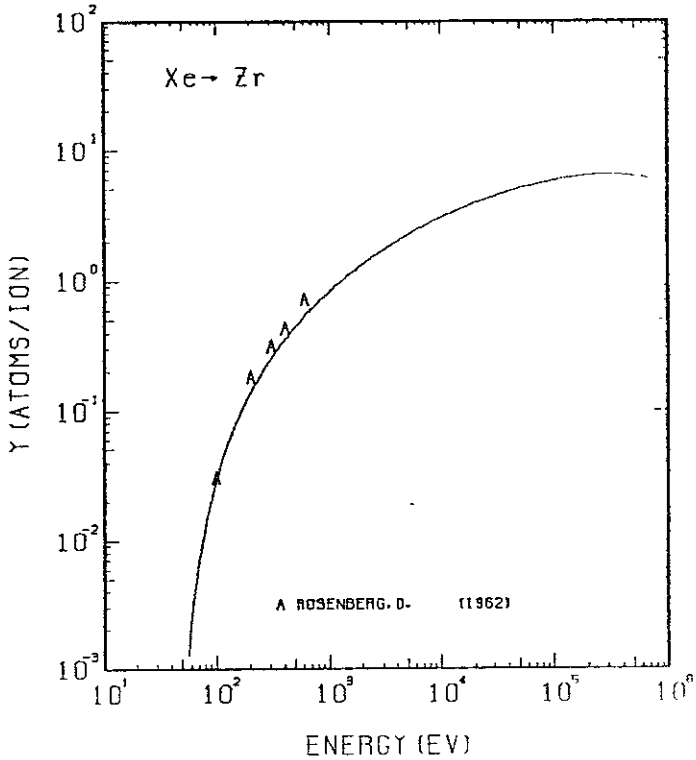


FIG. 150 ENERGY DEPENDENCE OF THE SPUTTERING YIELD OF ZR WITH $XE^+$.
A= 0.69, D= 0.54, Us= 6.25eV, s= 2.80,
W= 0.40Us.

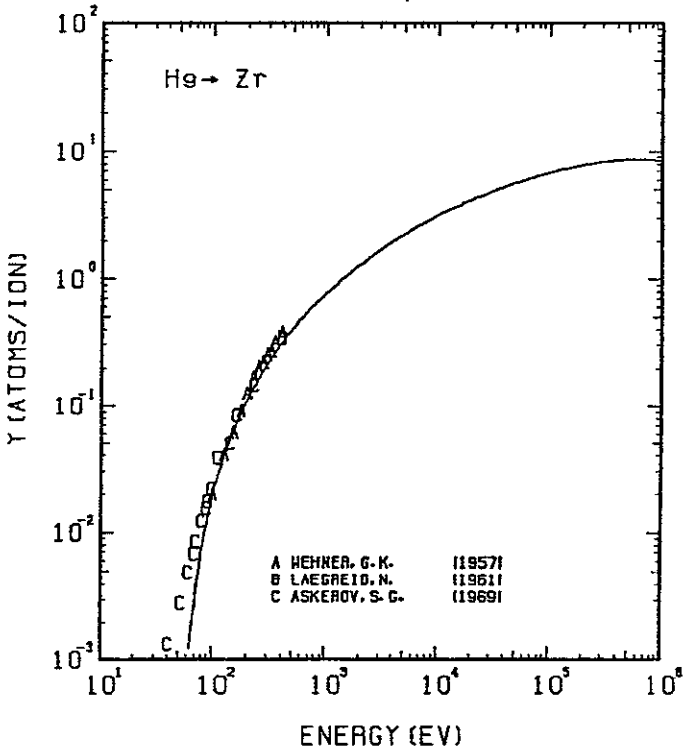


FIG. 151 ENERGY DEPENDENCE OF THE SPUTTERING YIELD OF ZR WITH $HG^+$.
A= 0.45, 0= 0.54, Us= 6.25EV, s= 2.80,
W= 0.40Us.

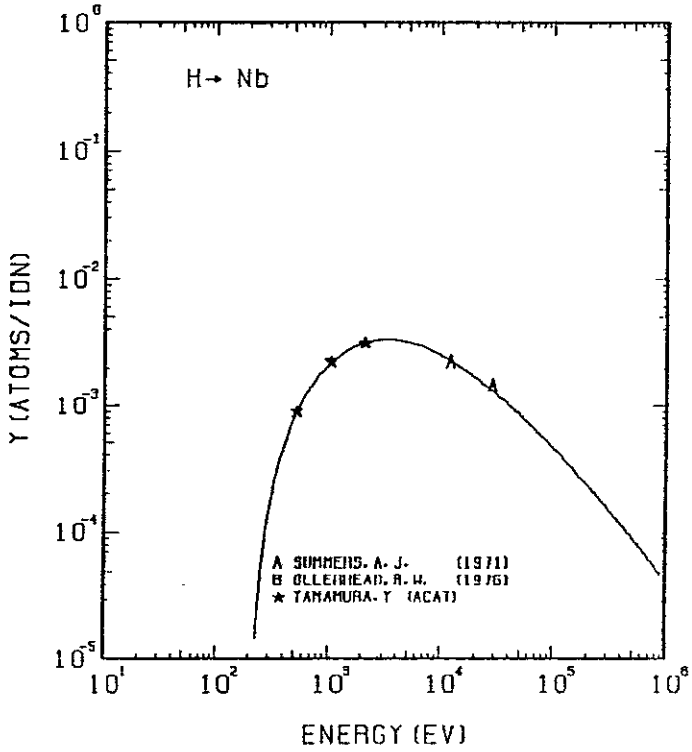


FIG. 152 ENERGY DEPENDENCE OF THE SPUTTERING YIELD OF NB WITH $H^+$.
A= 92.17, 0= 0.93, Us= 7.57EV, s= 2.80,
W= 0.35Us.

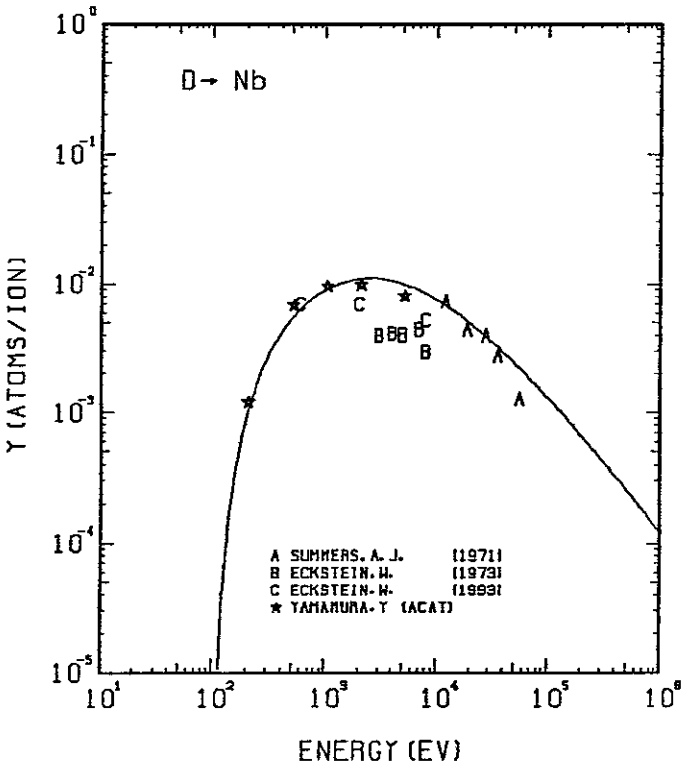


FIG. 153 ENERGY DEPENDENCE OF THE SPUTTERING YIELD OF NB WITH $D^+$.
A= 46.13, 0= 0.93, Us= 7.57EV, s= 2.80,
W= 0.35Us.

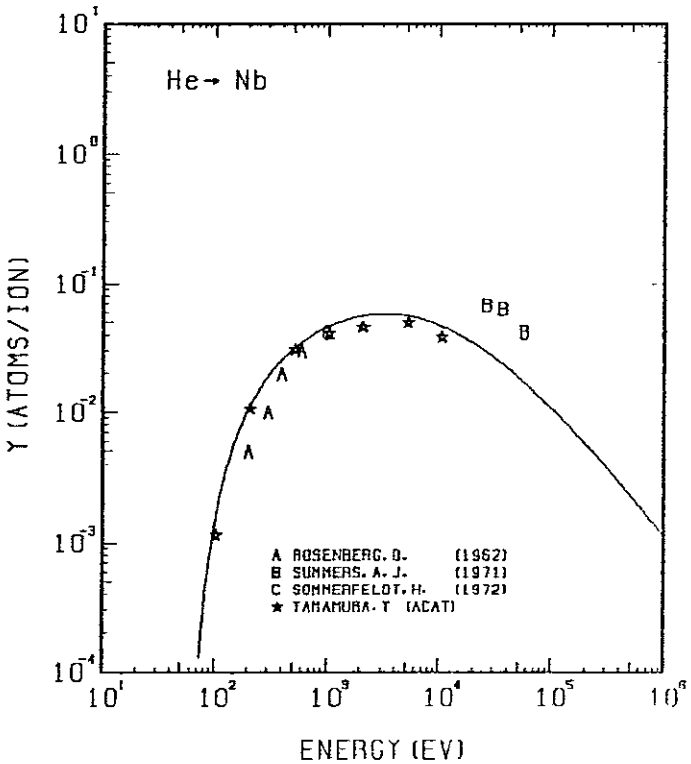


FIG. 154 ENERGY DEPENDENCE OF THE SPUTTERING YIELD OF NB WITH $HE^+$.
A= 23.21, 0= 0.93, Us= 7.57EV, s= 2.80,
W= 0.35Us.

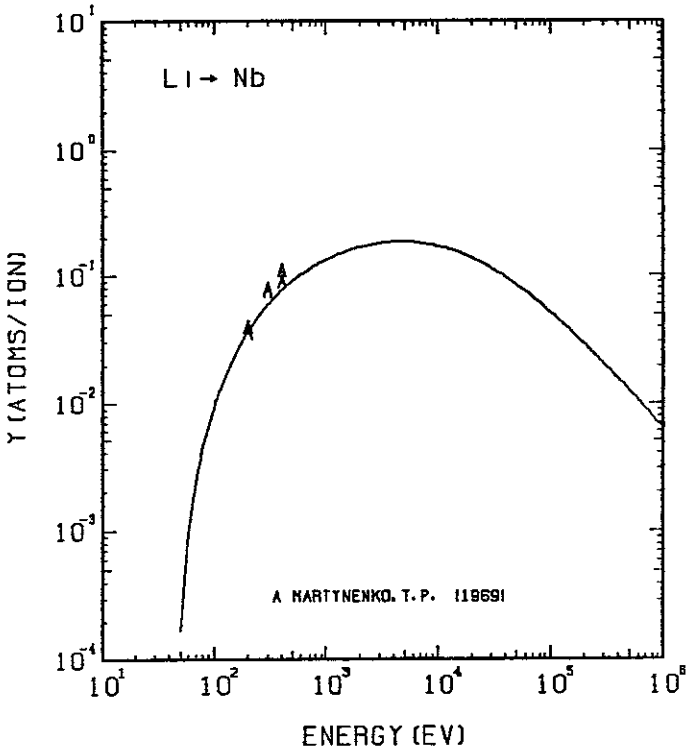


FIG. 155 ENERGY DEPENDENCE OF THE SPUTTERING YIELD OF NB WITH $LI^+$.
A= 13.39, D= 0.93, Us= 7.57EV, S= 2.80,
W= 0.35Us.

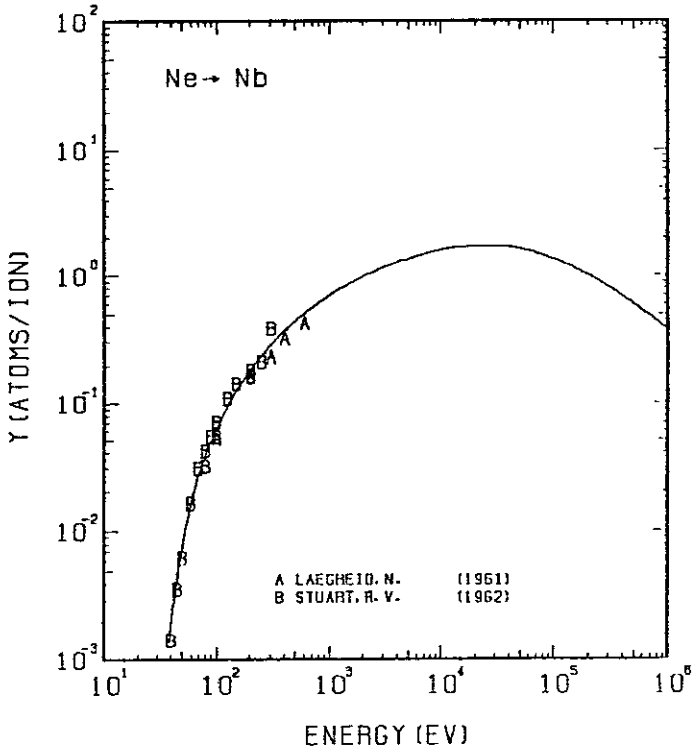


FIG. 156 ENERGY DEPENDENCE OF THE SPUTTERING YIELD OF NB WITH $NE^+$.
A= 4.60, D= 0.93, Us= 7.57EV, S= 2.80,
W= 0.35Us.

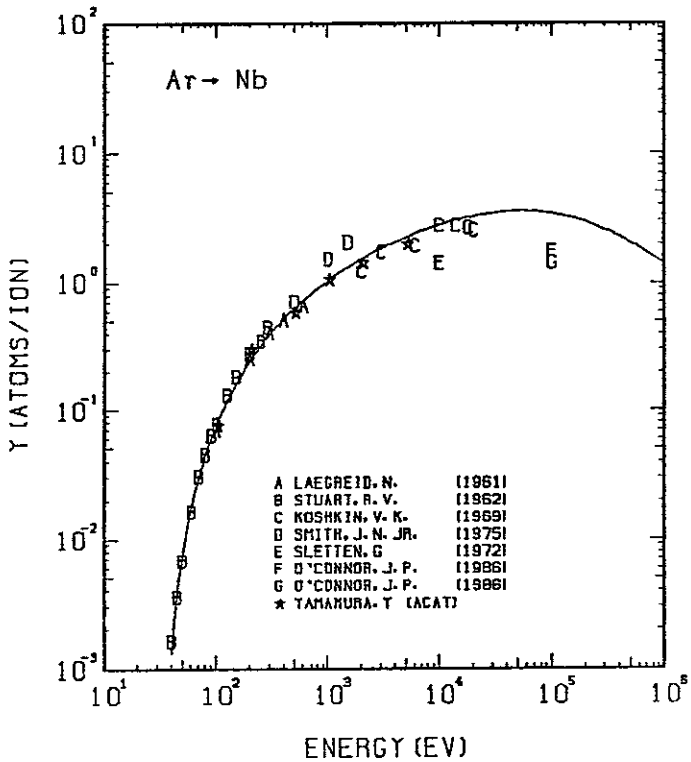


FIG. 157 ENERGY DEPENDENCE OF THE SPUTTERING YIELD OF NB WITH $AR^+$.
A= 2.33, D= 0.93, Us= 7.57EV, S= 2.80,
W= 0.35Us.

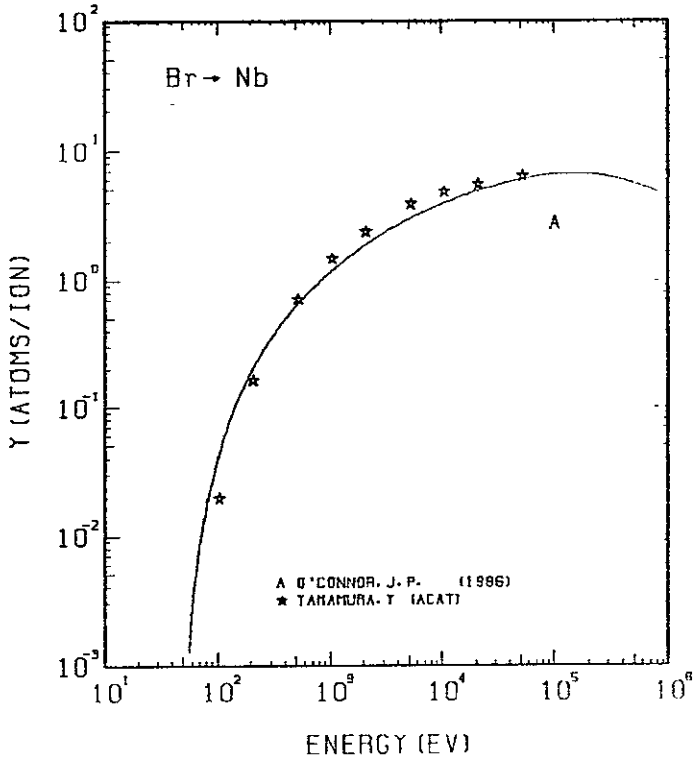


FIG. 158 ENERGY DEPENDENCE OF THE SPUTTERING YIELD OF NB WITH $BR^+$.
A= 1.16, D= 0.93, Us= 7.57EV, S= 2.80,
W= 0.35Us.

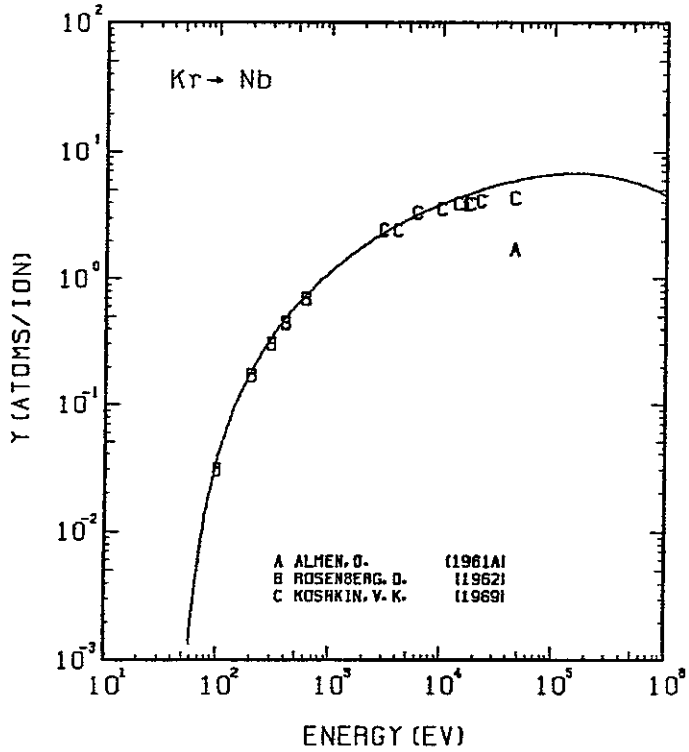


FIG. 159 ENERGY DEPENDENCE OF THE SPUTTERING YIELD OF NB WITH $KR^+$.
A= 1.11, D= 0.93, Us= 7.57EV, S= 2.80,
W= 0.35Us.

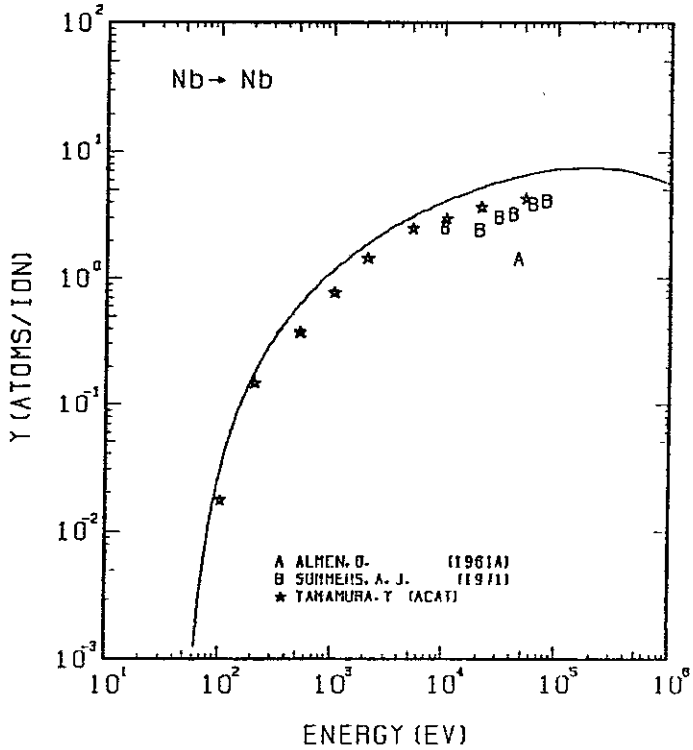


FIG. 160 ENERGY DEPENDENCE OF THE SPUTTERING YIELD OF NB WITH $NB^+$.
A= 1.00, D= 0.93, Us= 7.57EV, S= 2.80,
W= 0.35Us.

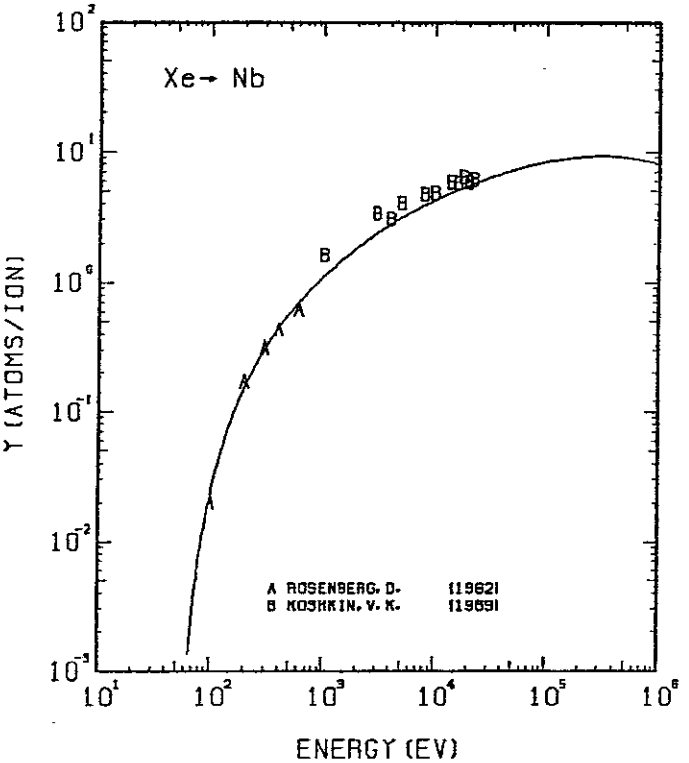


FIG. 161 ENERGY DEPENDENCE OF THE SPUTTERING YIELD OF NB WITH $XE^+$.
A= 0.71, D= 0.93, Us= 7.57EV, S= 2.80,
W= 0.35Us.

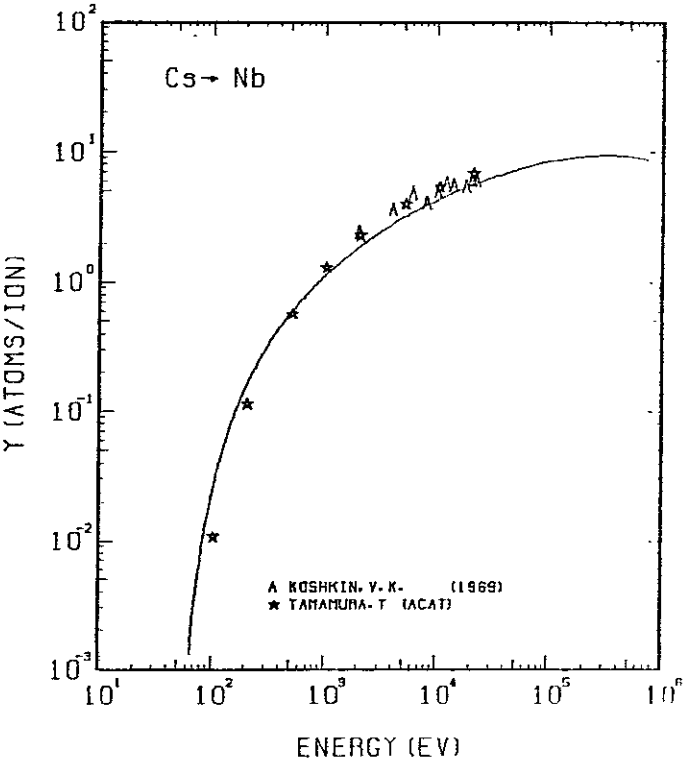


FIG. 162 ENERGY DEPENDENCE OF THE SPUTTERING YIELD OF NB WITH $CS^+$.
A= 0.70, D= 0.93, Us= 7.57EV, S= 2.80,
W= 0.35Us.

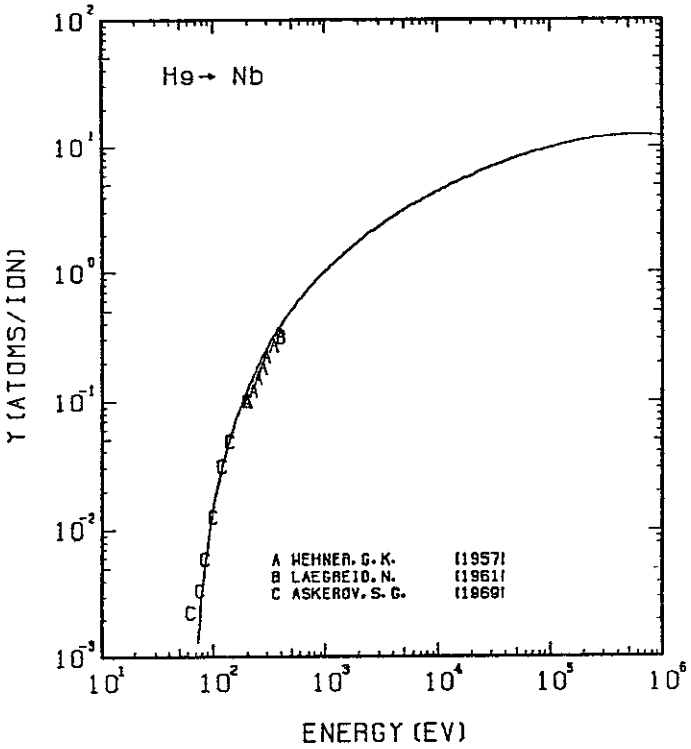


FIG. 163 ENERGY DEPENDENCE OF THE SPUTTERING YIELD OF NB WITH HG$^+$.
A= 0.46, D= 0.93, Us= 7.57EV, s= 2.80, W= 0.35Us.

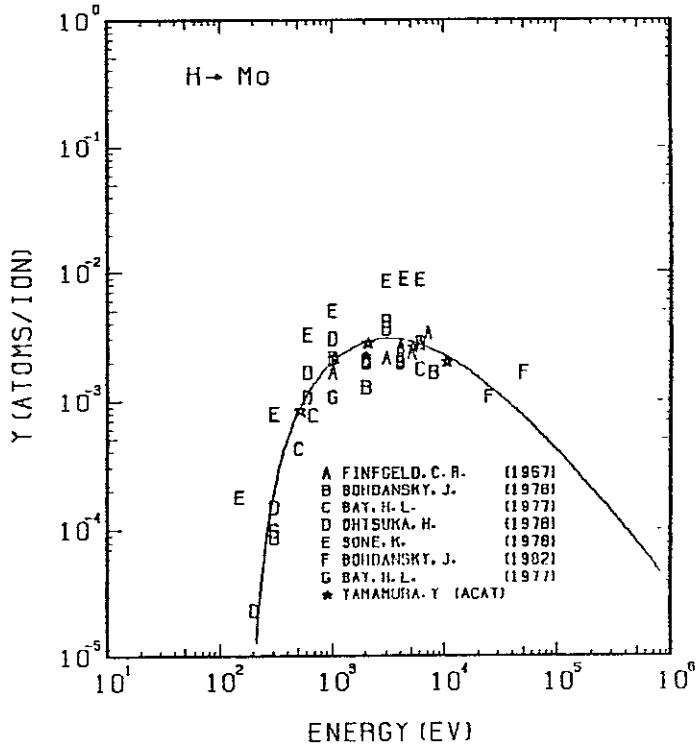


FIG. 164 ENERGY DEPENDENCE OF THE SPUTTERING YIELD OF MO WITH H$^+$.
A= 95.18, D= 0.85, Us= 6.82EV, s= 2.80, W= 0.45Us.

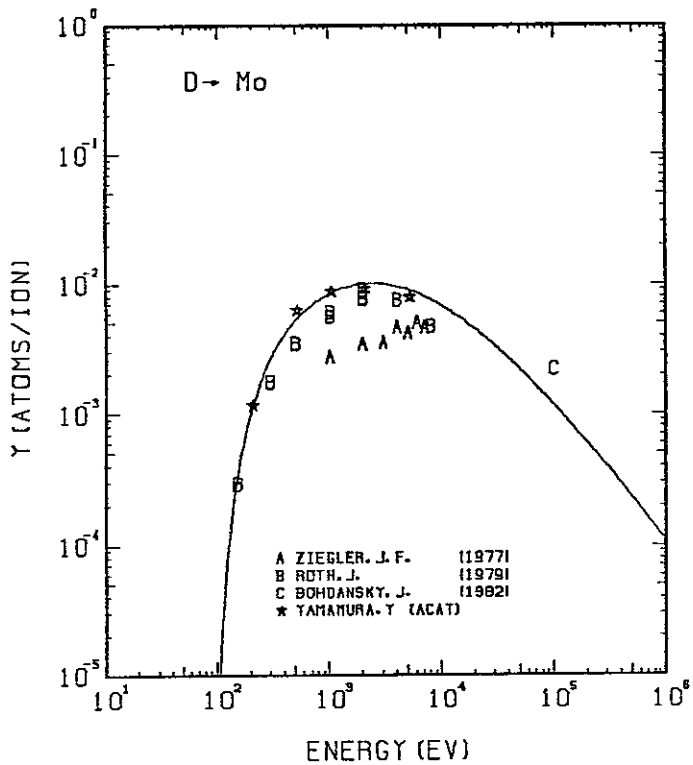


FIG. 165 ENERGY DEPENDENCE OF THE SPUTTERING YIELD OF MO WITH D$^+$.
A= 47.64, D= 0.85, Us= 6.82EV, s= 2.80, W= 0.45Us.

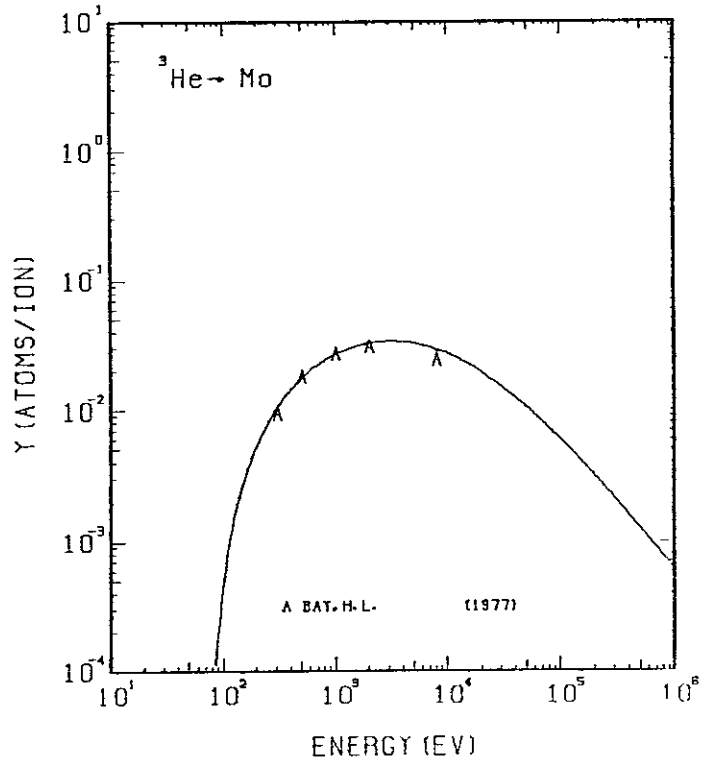


FIG. 166 ENERGY DEPENDENCE OF THE SPUTTERING YIELD OF MO WITH $^3$HE$^+$.
A= 31.81, D= 0.85, Us= 6.82EV, s= 2.80, W= 0.45Us.

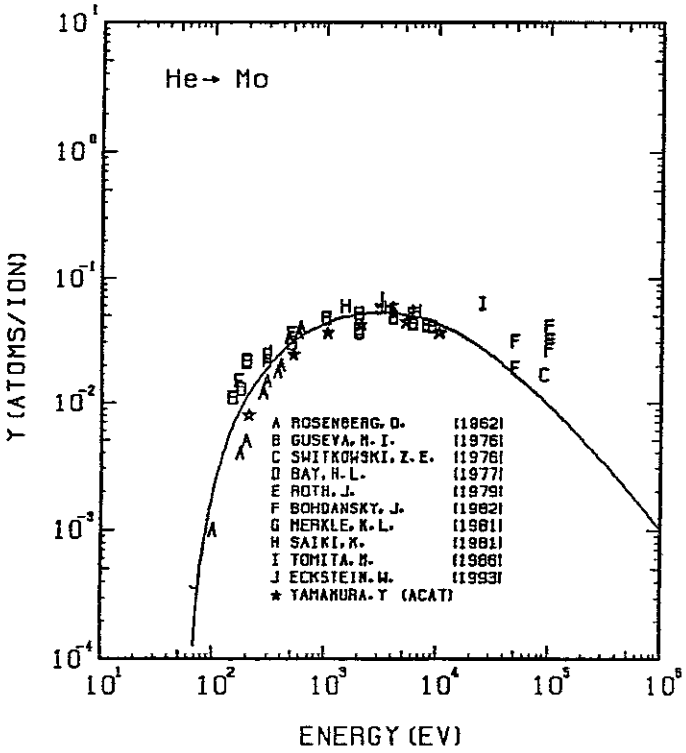


FIG. 167 ENERGY DEPENDENCE OF THE SPUTTERING YIELD OF MO WITH $HE^+$.
A= 23.97, D= 0.85, Us= 6.82EV, s= 2.80,
W= 0.45Us.

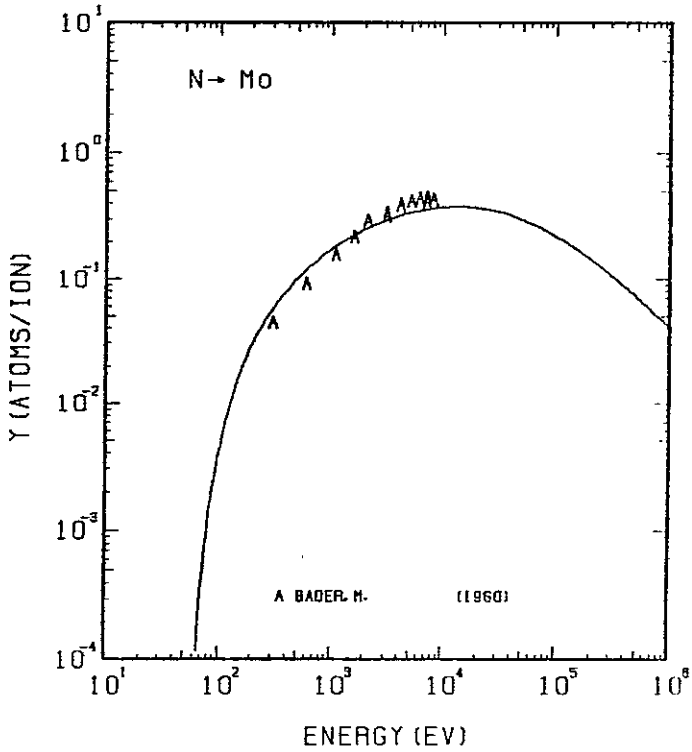


FIG. 168 ENERGY DEPENDENCE OF THE SPUTTERING YIELD OF MO WITH $N^+$.
A= 6.85, D= 0.85, Us= 13.64EV, s= 2.80,
W= 0.45Us. THE BEST-FIT SURFACE BINDING ENERGY IS USED.

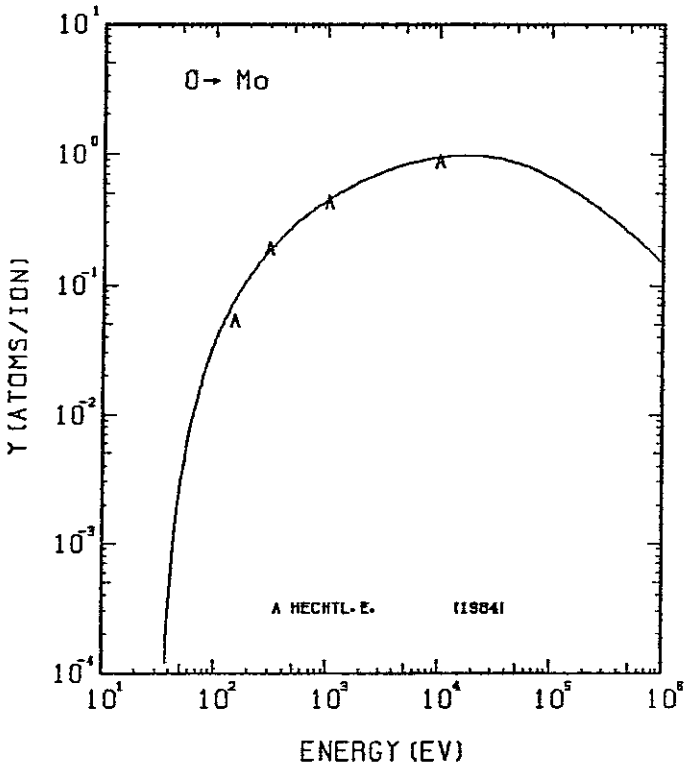


FIG. 169 ENERGY DEPENDENCE OF THE SPUTTERING YIELD OF MO WITH $O^+$.
A= 6.00, D= 0.85, Us= 8.18EV, s= 2.80,
W= 0.45Us. THE BEST-FIT SURFACE BINDING ENERGY IS USED.

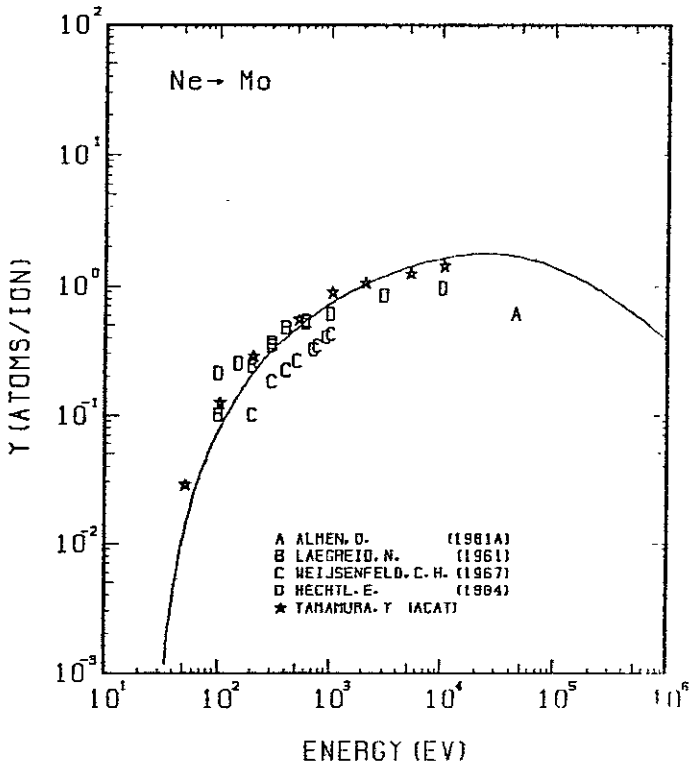


FIG. 170 ENERGY DEPENDENCE OF THE SPUTTERING YIELD OF MO WITH $NE^+$.
A= 4.75, D= 0.85, Us= 6.82EV, s= 2.80,
W= 0.45Us.

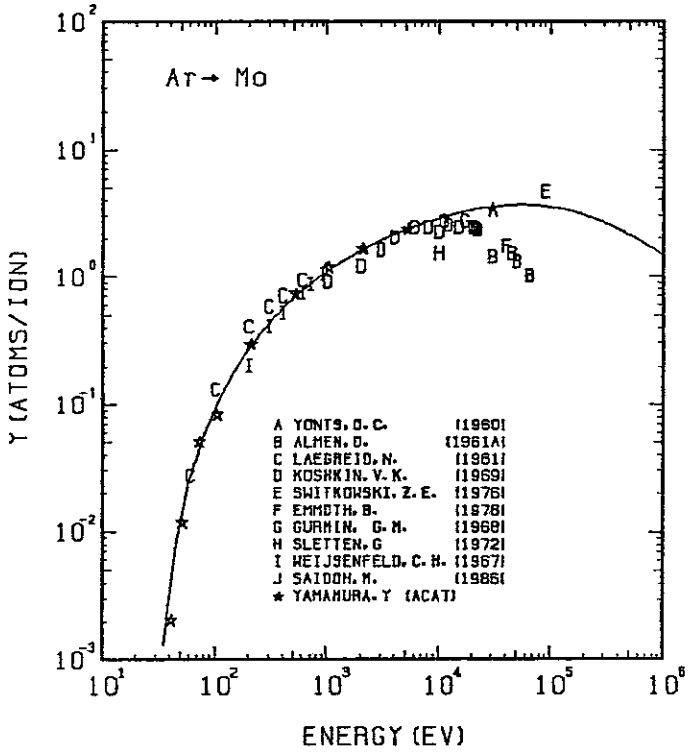


FIG. 171 ENERGY DEPENDENCE OF THE SPUTTERING YIELD OF MO WITH $AR^+$.
A= 2.40, D= 0.85, Us= 6.82EV, S= 2.80,
W= 0.45Us.

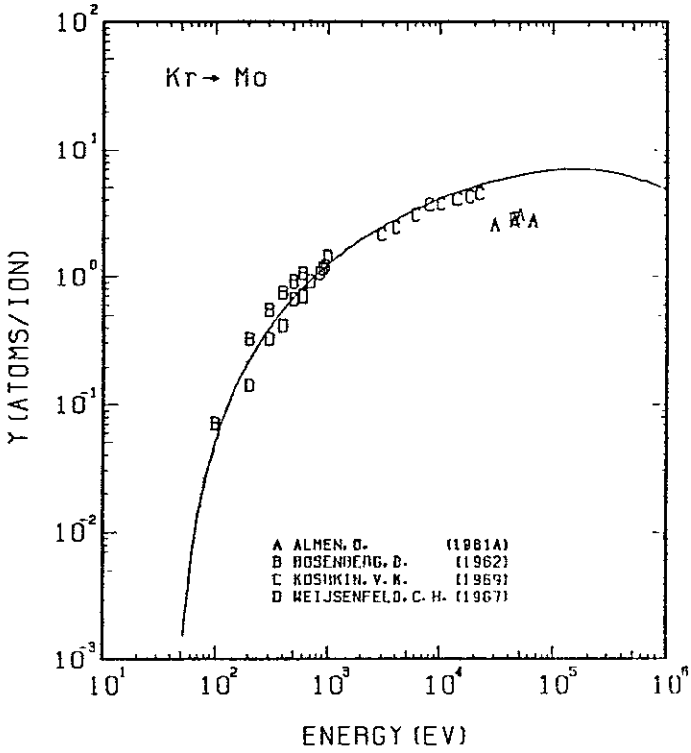


FIG. 172 ENERGY DEPENDENCE OF THE SPUTTERING YIELD OF MO WITH $KR^+$.
A= 1.14, D= 0.85, Us= 6.82EV, S= 2.80,
W= 0.45Us.

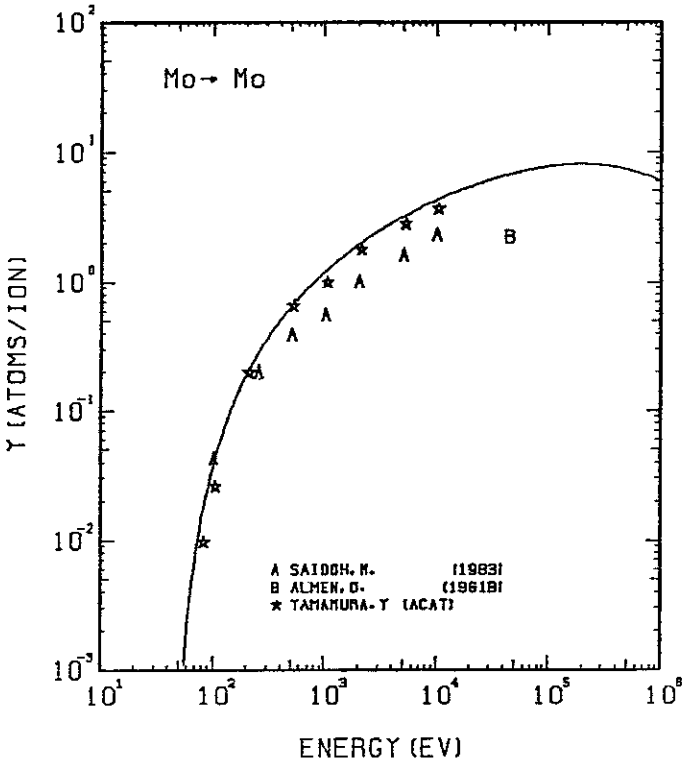


FIG. 173 ENERGY DEPENDENCE OF THE SPUTTERING YIELD OF MO WITH $MO^+$.
A= 1.00, D= 0.85, Us= 6.82EV, S= 2.80,
W= 0.45Us.

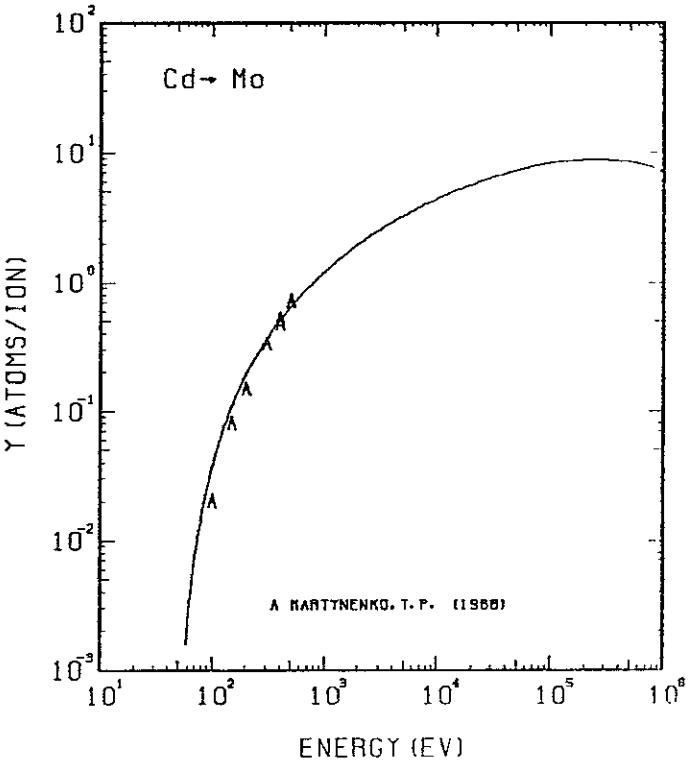


FIG. 174 ENERGY DEPENDENCE OF THE SPUTTERING YIELD OF MO WITH $CD^+$.
A= 0.85, D= 0.85, Us= 6.82EV, S= 2.80,
W= 0.45Us.

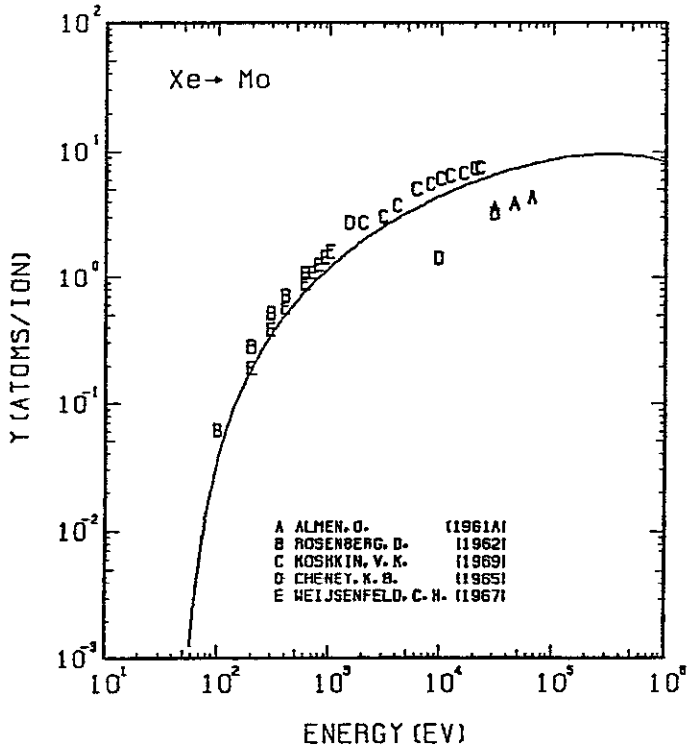


FIG. 175 ENERGY DEPENDENCE OF THE SPUTTERING YIELD OF MO WITH $XE^+$.
A= 0.73, D= 0.85, Us= 6.82EV, s= 2.80,
W= 0.45Us.

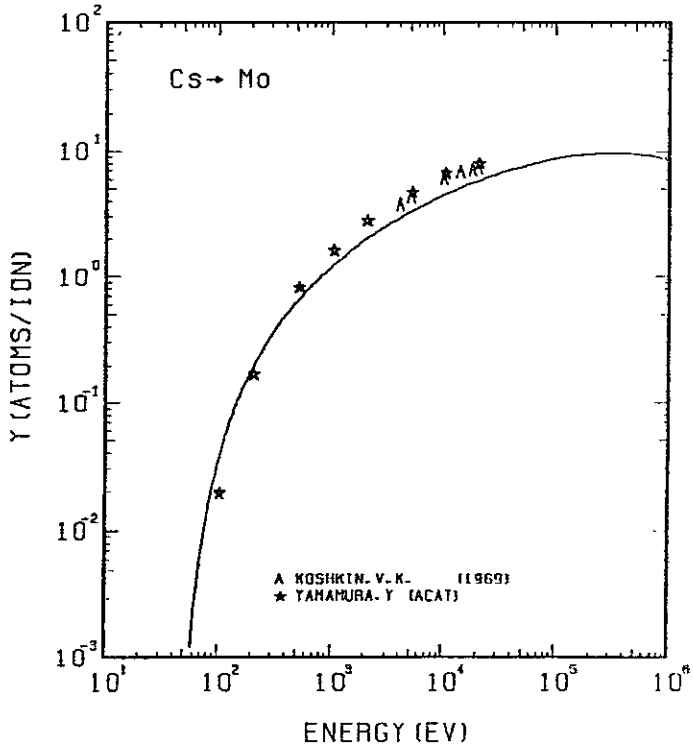


FIG. 176 ENERGY DEPENDENCE OF THE SPUTTERING YIELD OF MO WITH $CS^+$.
A= 0.72, D= 0.85, Us= 6.82EV, s= 2.80,
W= 0.45Us.

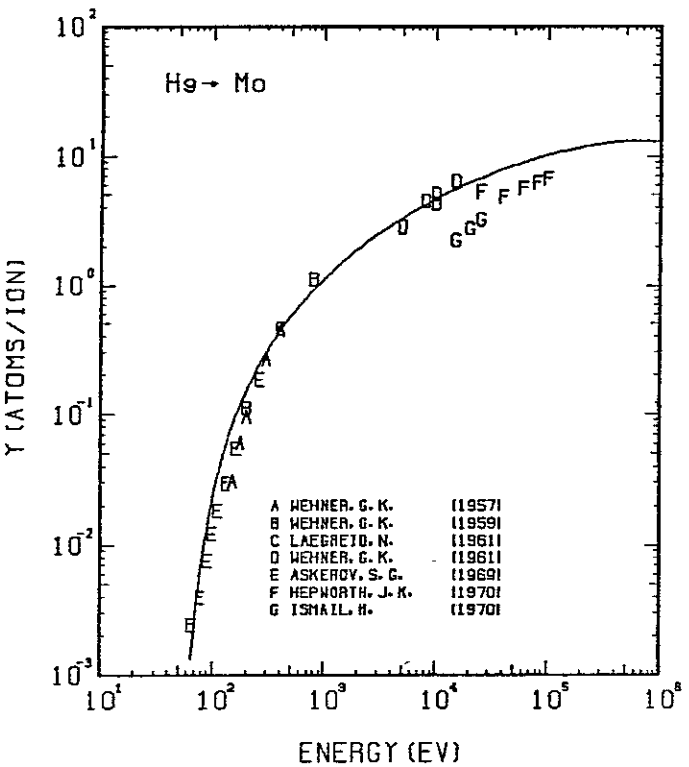


FIG. 177 ENERGY DEPENDENCE OF THE SPUTTERING YIELD OF MO WITH $HG^+$.
A= 0.48, D= 0.85, Us= 6.82EV, s= 2.80,
W= 0.45Us.

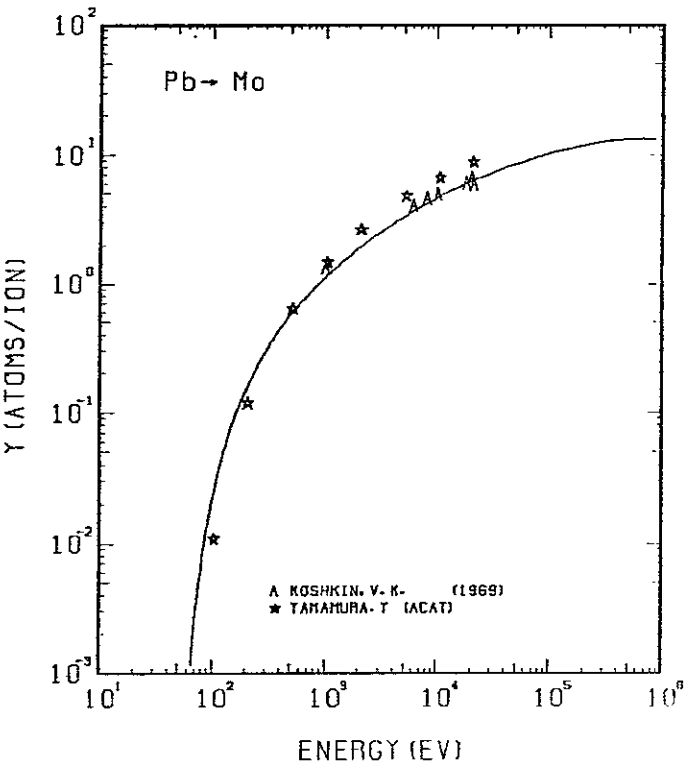


FIG. 178 ENERGY DEPENDENCE OF THE SPUTTERING YIELD OF MO WITH $PB^+$.
A= 0.46, D= 0.85, Us= 6.82EV, s= 2.80,
W= 0.45Us.

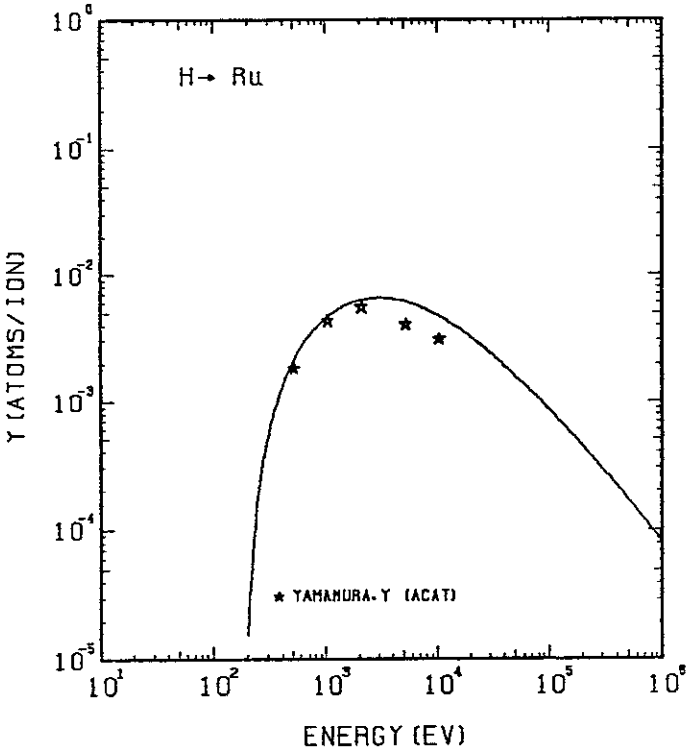


FIG. 179 ENERGY DEPENDENCE OF THE SPUTTERING YIELD OF RU WITH $H^+$.
A= 100.20, Q= 1.31, Us= 6.74EV, s= 2.50.
W= 0.35Us.

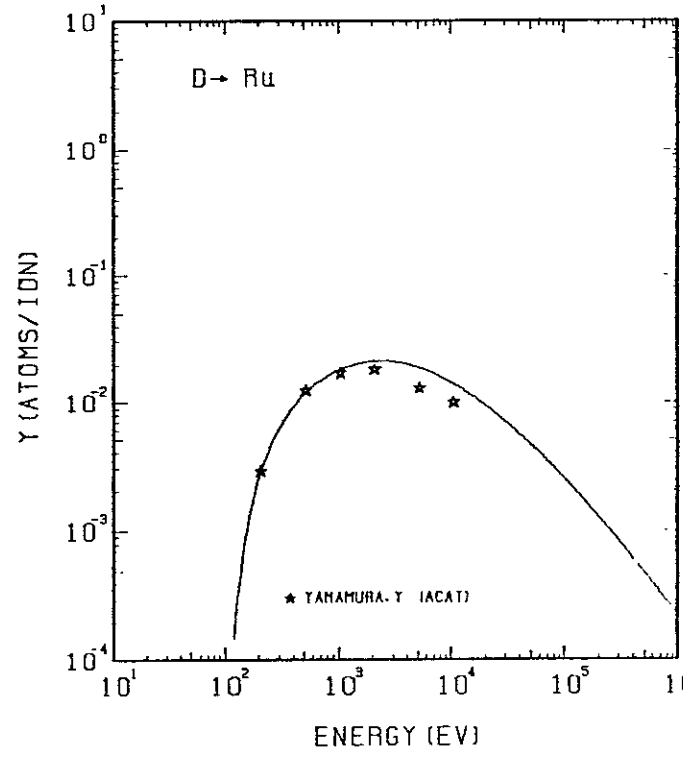


FIG. 180 ENERGY DEPENDENCE OF THE SPUTTERING YIELD OF RU WITH $D^+$.
A= 50.15, Q= 1.31, Us= 6.74EV, s= 2.50.
W= 0.35Us.

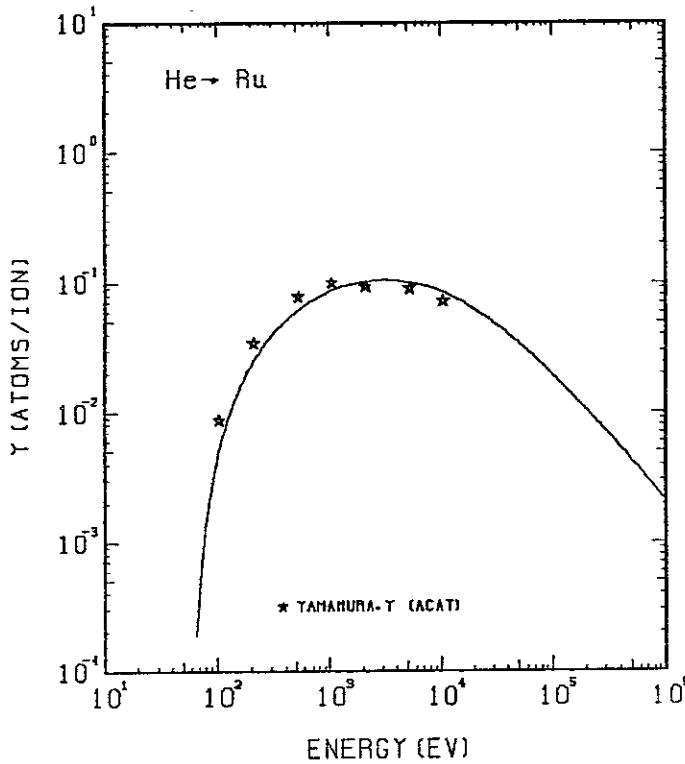


FIG. 181 ENERGY DEPENDENCE OF THE SPUTTERING YIELD OF RU WITH $HE^+$.
A= 25.23, Q= 1.31, Us= 6.74EV, s= 2.50.
W= 0.35Us.

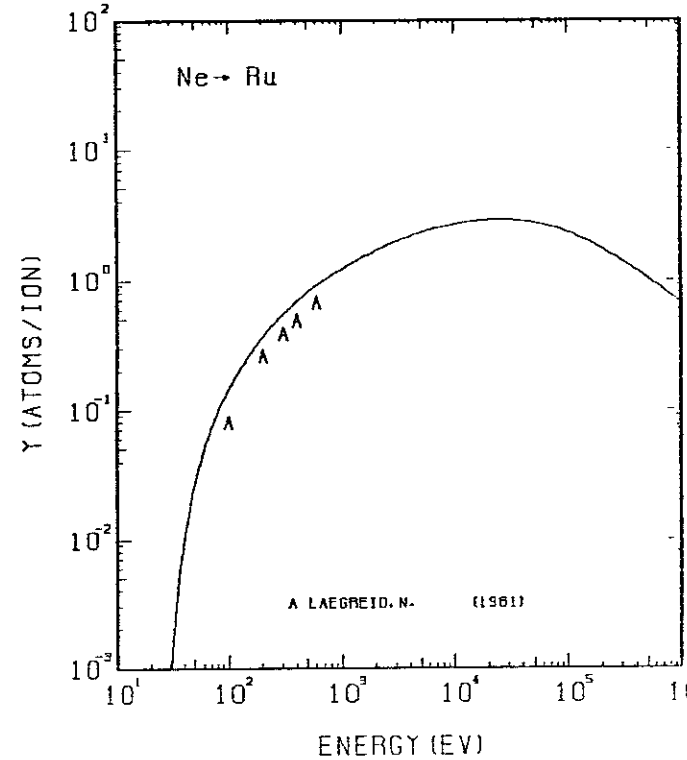


FIG. 182 ENERGY DEPENDENCE OF THE SPUTTERING YIELD OF RU WITH $NE^+$.
A= 5.00, Q= 1.31, Us= 6.74EV, s= 2.50.
W= 0.35Us.

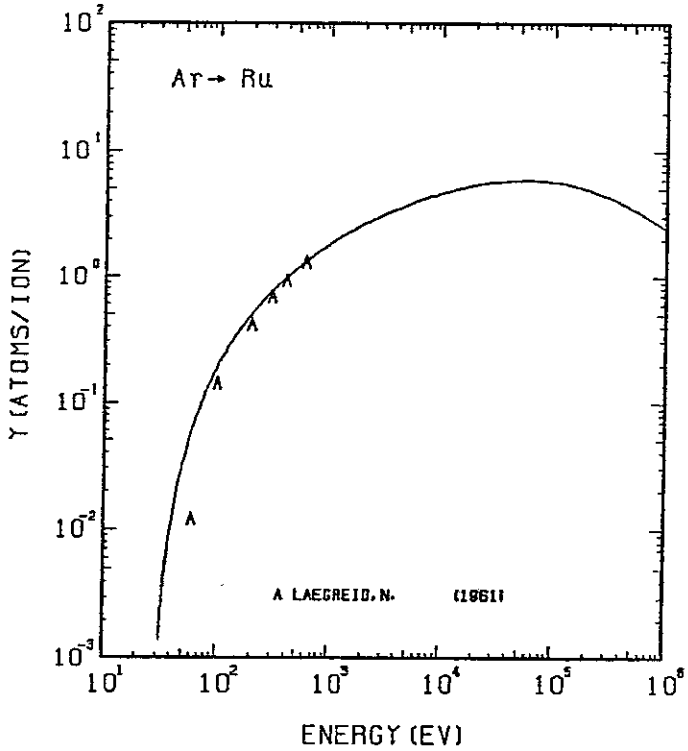


FIG. 183 ENERGY DEPENDENCE OF THE SPUTTERING YIELD OF RU WITH $AR^+$.
A= 2.53, D= 1.31, Us= 6.74EV, s= 2.50,
W= 0.35Us.

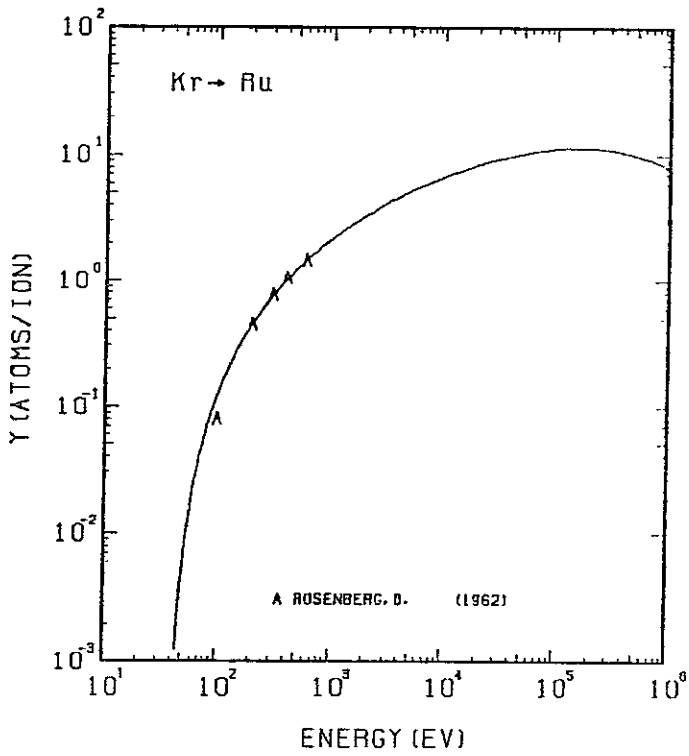


FIG. 184 ENERGY DEPENDENCE OF THE SPUTTERING YIELD OF RU WITH $KR^+$.
A= 1.21, D= 1.31, Us= 6.74EV, s= 2.50,
W= 0.35Us.

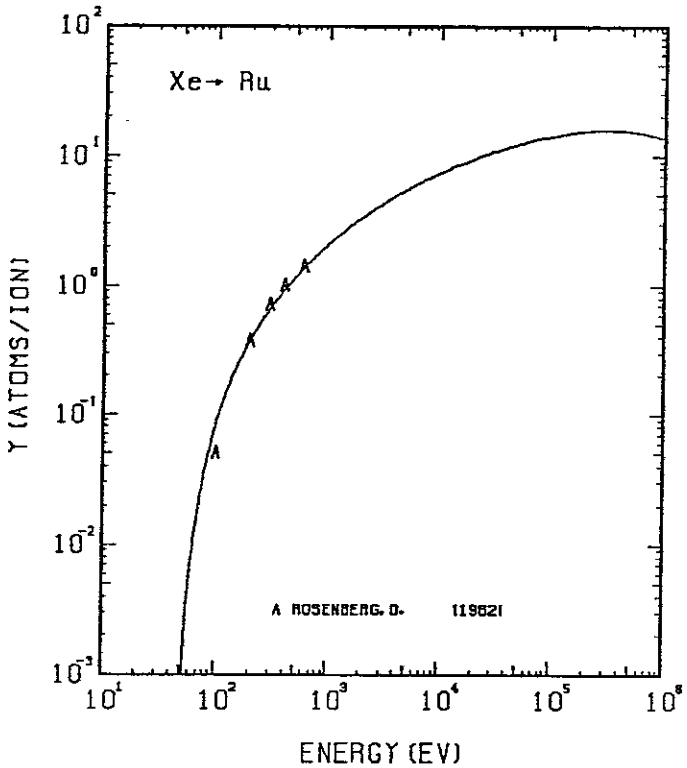


FIG. 185 ENERGY DEPENDENCE OF THE SPUTTERING YIELD OF RU WITH $XE^+$.
A= 0.77, D= 1.31, Us= 6.74EV, s= 2.50,
W= 0.35Us.

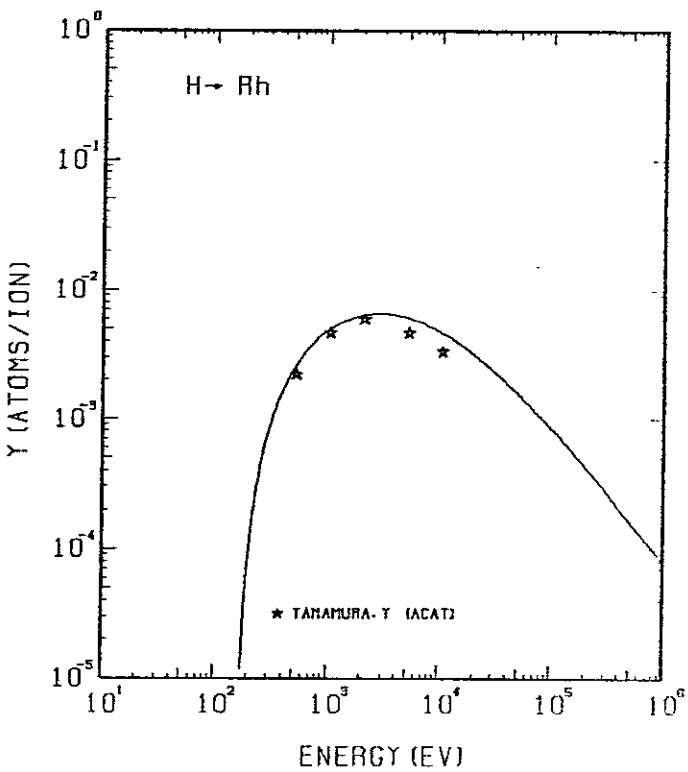


FIG. 186 ENERGY DEPENDENCE OF THE SPUTTERING YIELD OF RH WITH $H^+$.
A= 102.08, D= 1.14, Us= 5.75EV, s= 2.50,
W= 0.45Us.

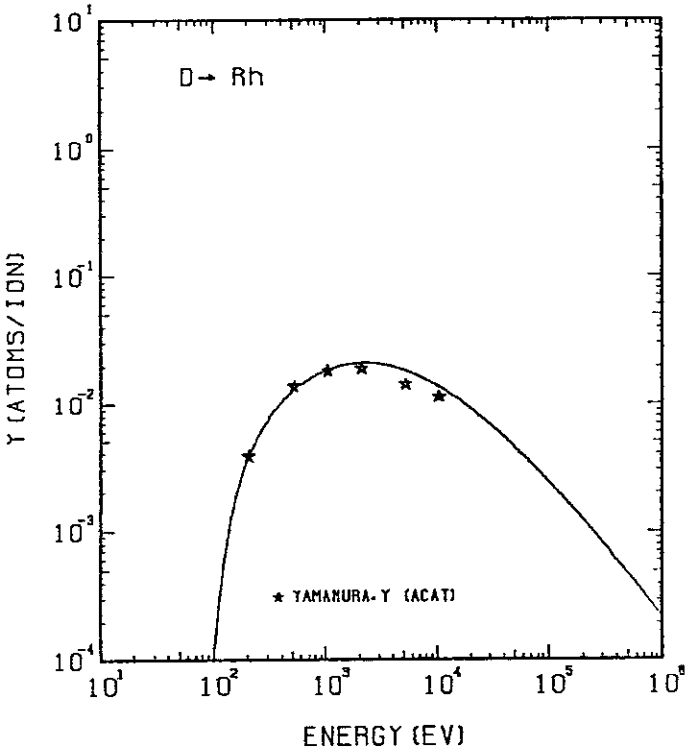


FIG. 187 ENERGY DEPENDENCE OF THE SPUTTERING YIELD OF RH WITH $D^+$.
A= 51.09, Q= 1.14, Us= 5.75EV, s= 2.50.
W= 0.45Us.

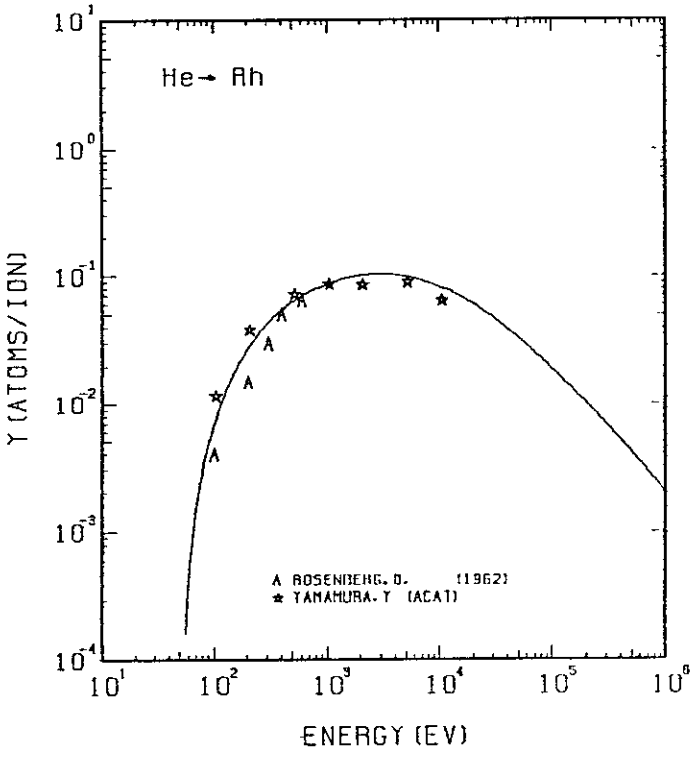


FIG. 188 ENERGY DEPENDENCE OF THE SPUTTERING YIELD OF RH WITH $HE^+$.
A= 25.71, Q= 1.14, Us= 5.75EV, s= 2.50.
W= 0.45Us.

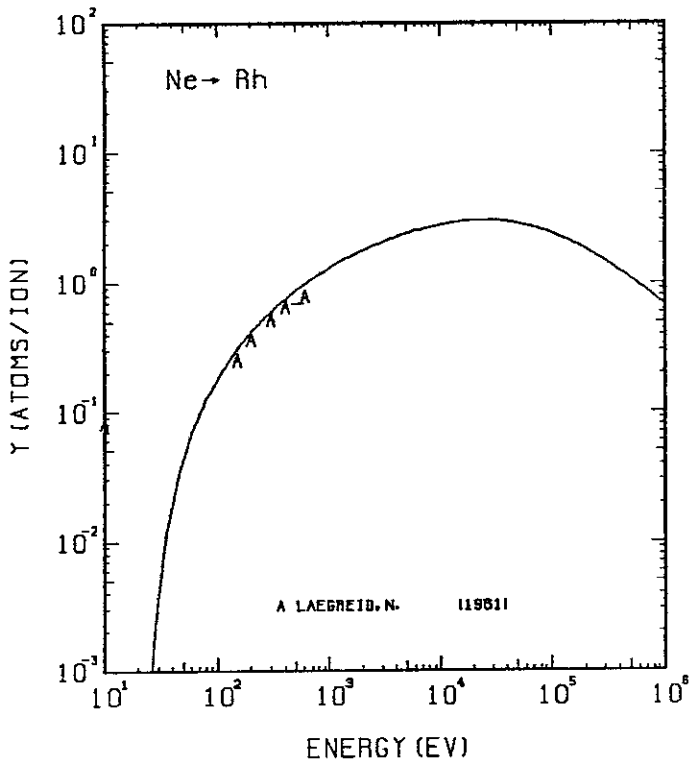


FIG. 189 ENERGY DEPENDENCE OF THE SPUTTERING YIELD OF RH WITH $NE^+$.
A= 5.10, Q= 1.14, Us= 5.75EV, s= 2.50.
W= 0.45Us.

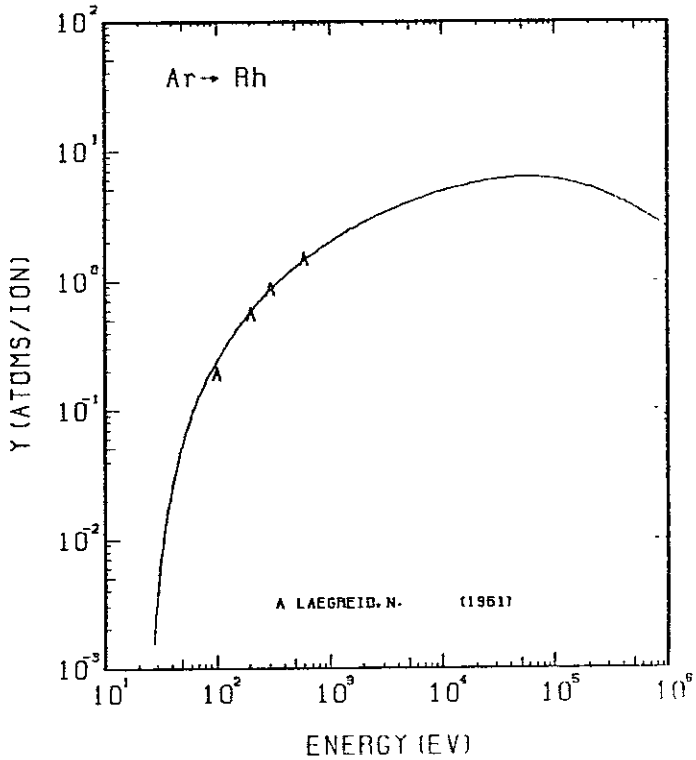


FIG. 190 ENERGY DEPENDENCE OF THE SPUTTERING YIELD OF RH WITH $AR^+$.
A= 2.58, Q= 1.14, Us= 5.75EV, s= 2.50.
W= 0.45Us.

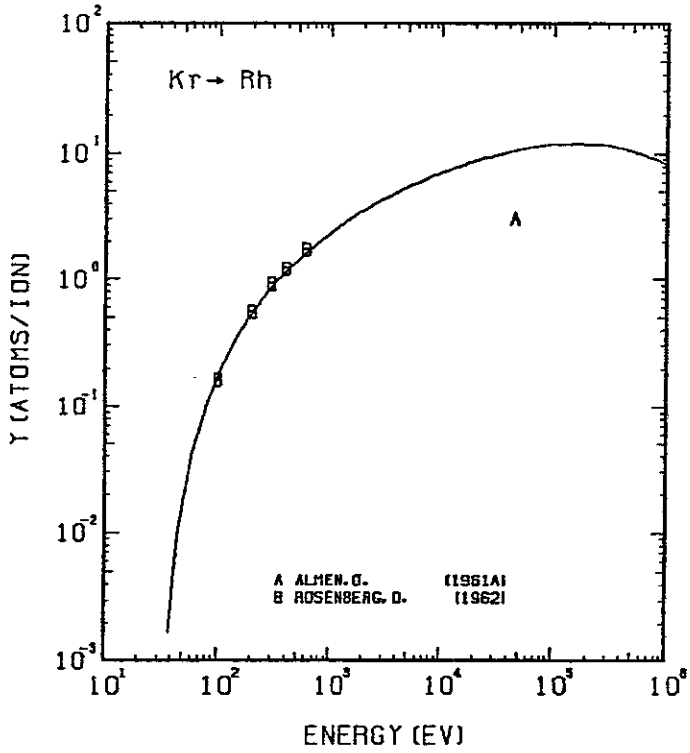


FIG. 191 ENERGY DEPENDENCE OF THE SPUTTERING YIELD OF RH WITH KR+.
A= 1.23, O= 1.14, Us= 5.75EV, S= 2.50,
W= 0.45Us.

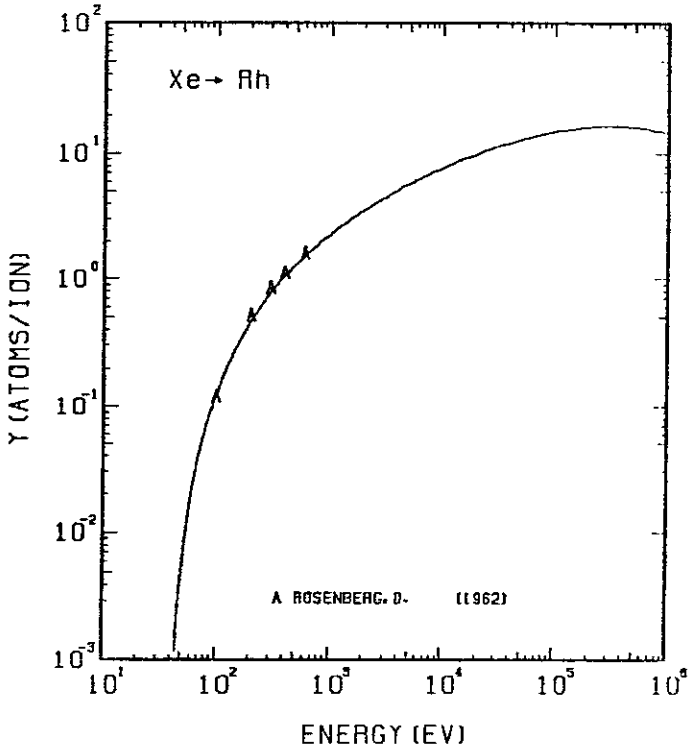


FIG. 192 ENERGY DEPENDENCE OF THE SPUTTERING YIELD OF RH WITH XE+.
A= 0.78, O= 1.14, Us= 5.75EV, S= 2.50,
W= 0.45Us.

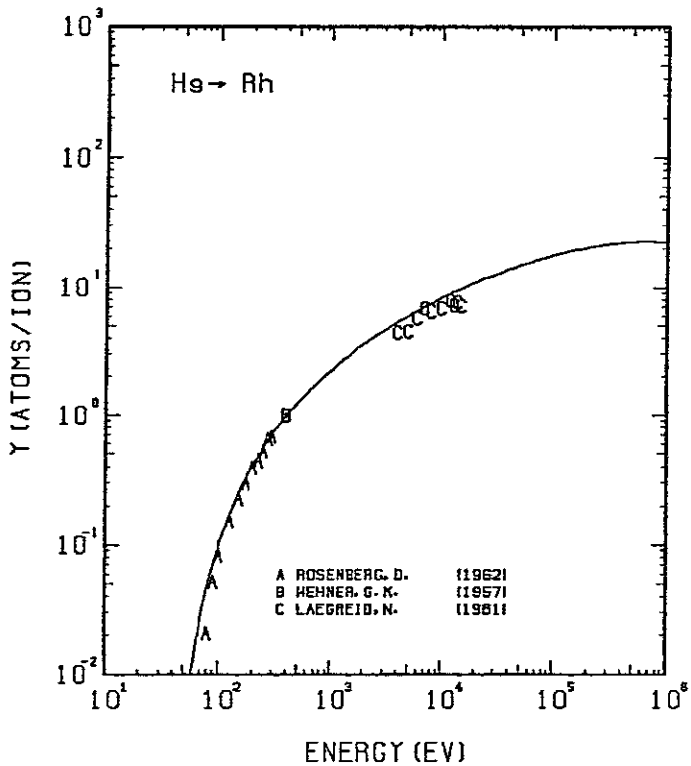


FIG. 193 ENERGY DEPENDENCE OF THE SPUTTERING YIELD OF RH WITH HG+.
A= 0.51, O= 1.14, Us= 5.75EV, S= 2.50,
W= 0.45Us.

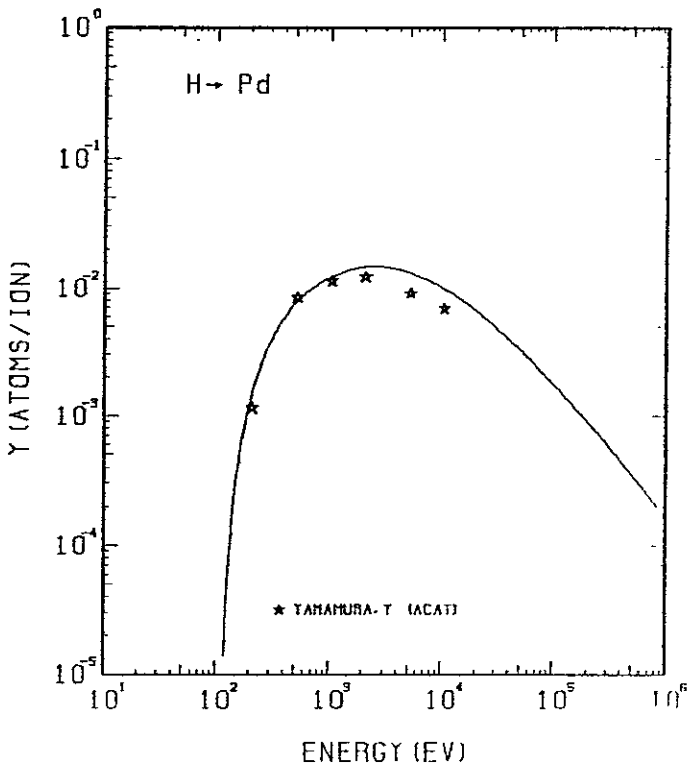


FIG. 194 ENERGY DEPENDENCE OF THE SPUTTERING YIELD OF PD WITH H+.
A= 105.56, O= 0.85, Us= 3.89EV, S= 2.50,
W= 0.35Us.

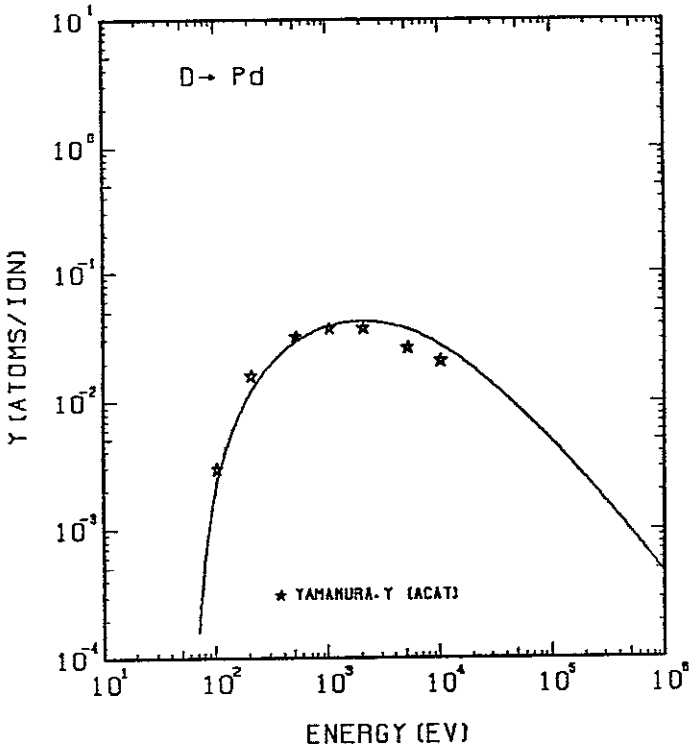


FIG. 195 ENERGY DEPENDENCE OF THE SPUTTERING YIELD OF PD WITH $D^+$.
A= 52.83, D= 0.85, Us= 3.89EV, s= 2.50.
W= 0.35Us.

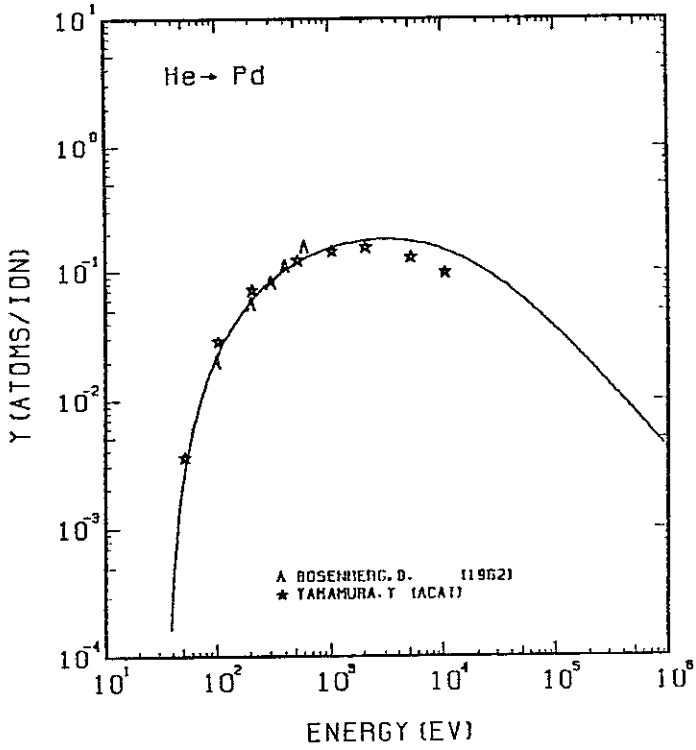


FIG. 196 ENERGY DEPENDENCE OF THE SPUTTERING YIELD OF PD WITH $HE^+$.
A= 26.58, D= 0.85, Us= 3.89EV, s= 2.50.
W= 0.35Us.

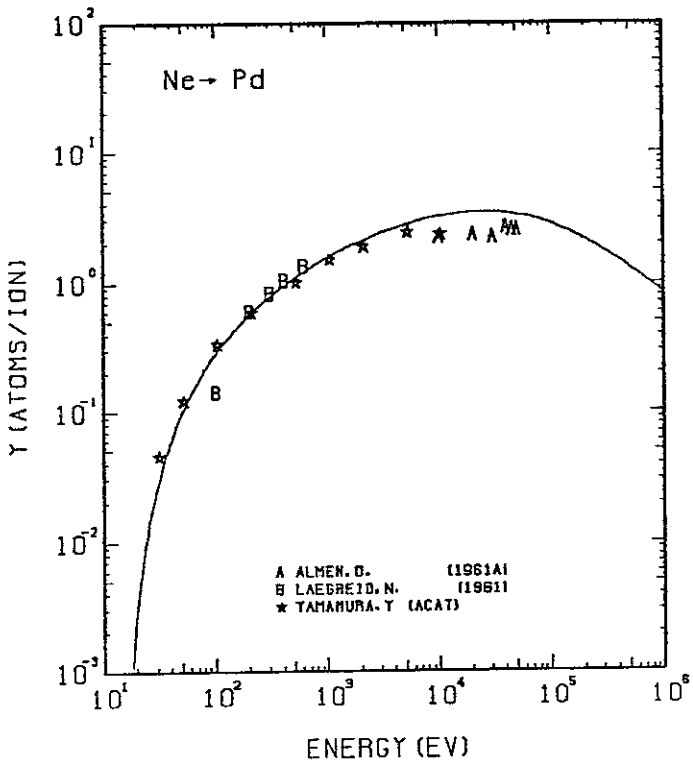


FIG. 197 ENERGY DEPENDENCE OF THE SPUTTERING YIELD OF PD WITH $NE^+$.
A= 5.27, D= 0.85, Us= 3.89EV, s= 2.50,
W= 0.35Us.

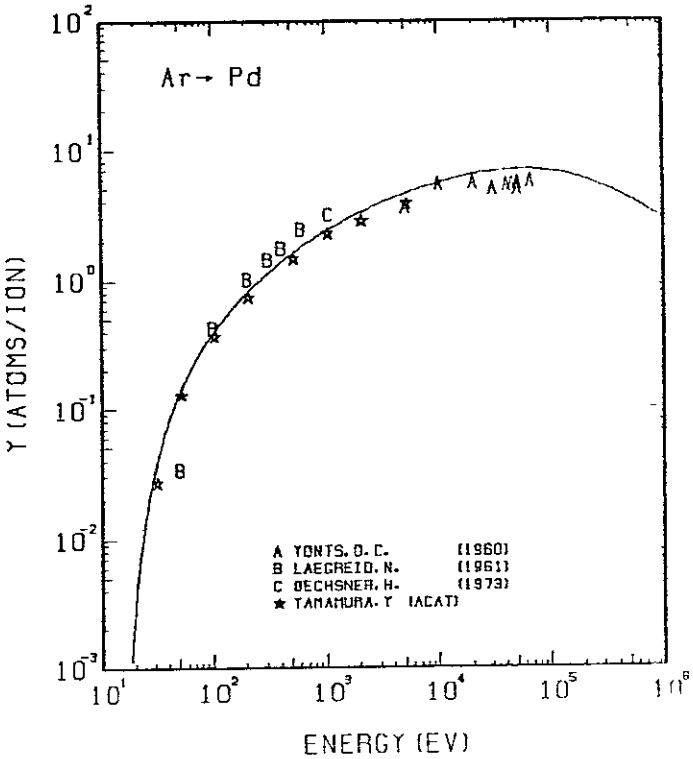


FIG. 198 ENERGY DEPENDENCE OF THE SPUTTERING YIELD OF PD WITH $AR^+$.
A= 2.66, D= 0.85, Us= 3.89EV, s= 2.50,
W= 0.35Us.

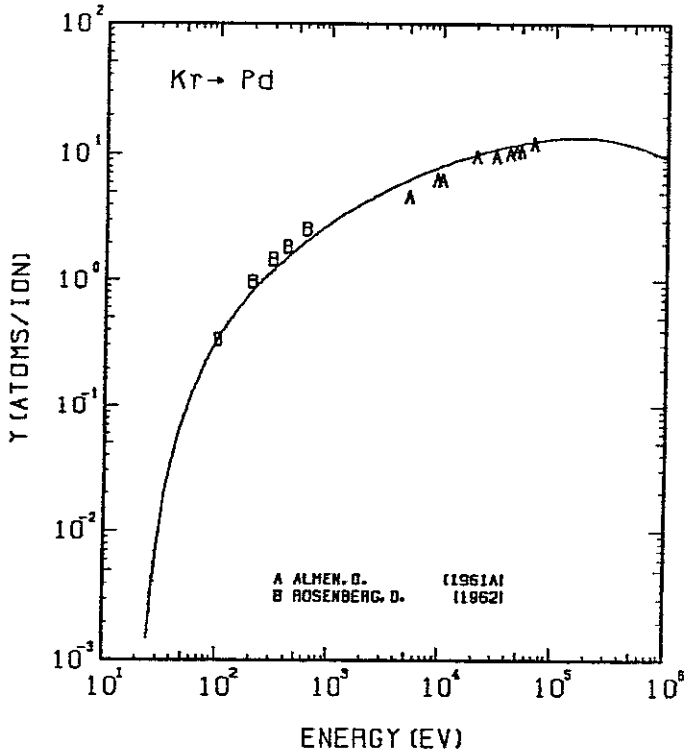


FIG. 199 ENERGY DEPENDENCE OF THE SPUTTERING YIELD OF PD WITH KR+.
A= 1.27, Q= 0.85, Us= 3.89EV, S= 2.50,
W= 0.35Us.

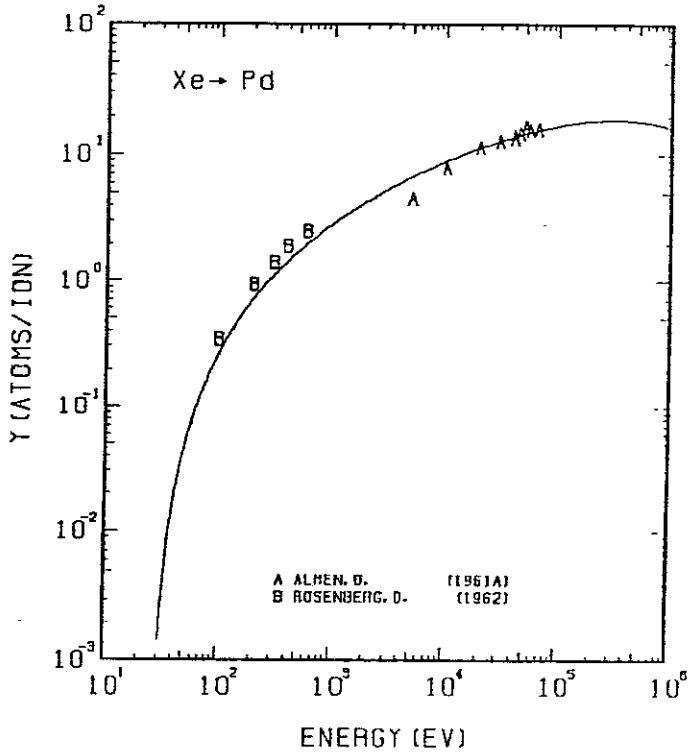


FIG. 200 ENERGY DEPENDENCE OF THE SPUTTERING YIELD OF PD WITH XE+.
A= 0.81, Q= 0.85, Us= 3.89EV, S= 2.50,
W= 0.35Us.

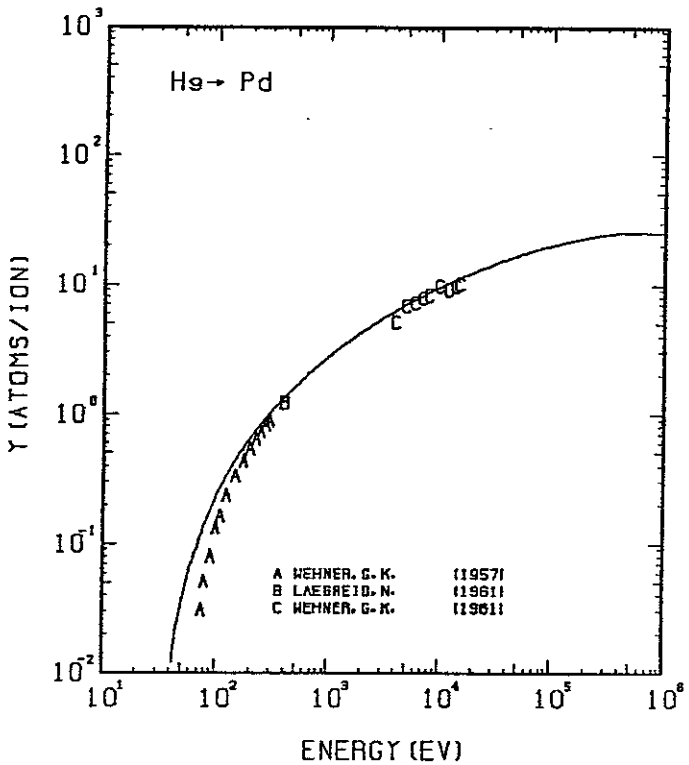


FIG. 201 ENERGY DEPENDENCE OF THE SPUTTERING YIELD OF PD WITH HG+.
A= 0.53, Q= 0.85, Us= 3.89EV, S= 2.50,
W= 0.35Us.

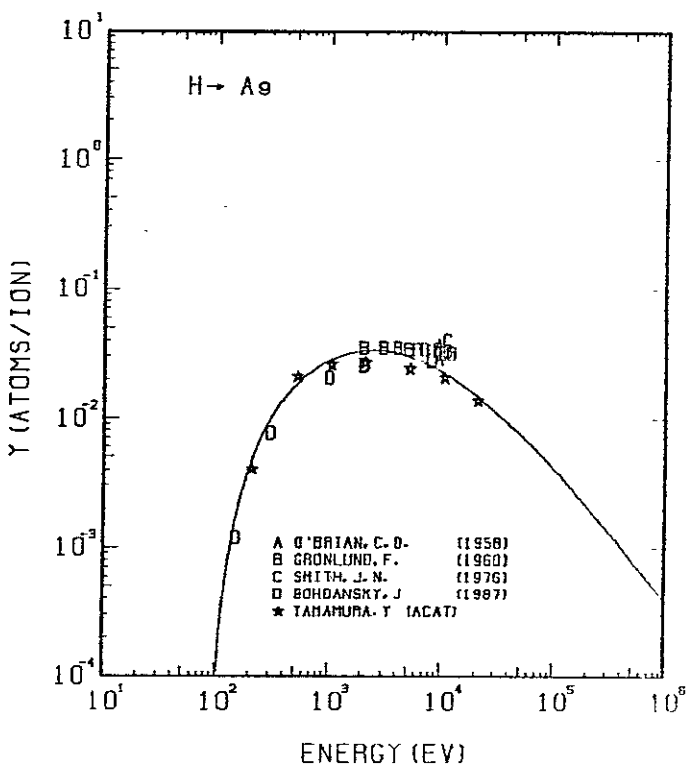


FIG. 202 ENERGY DEPENDENCE OF THE SPUTTERING YIELD OF AG WITH H+.
A= 106.94, Q= 1.08, Us= 2.95EV, S= 2.80,
W= 0.35Us.

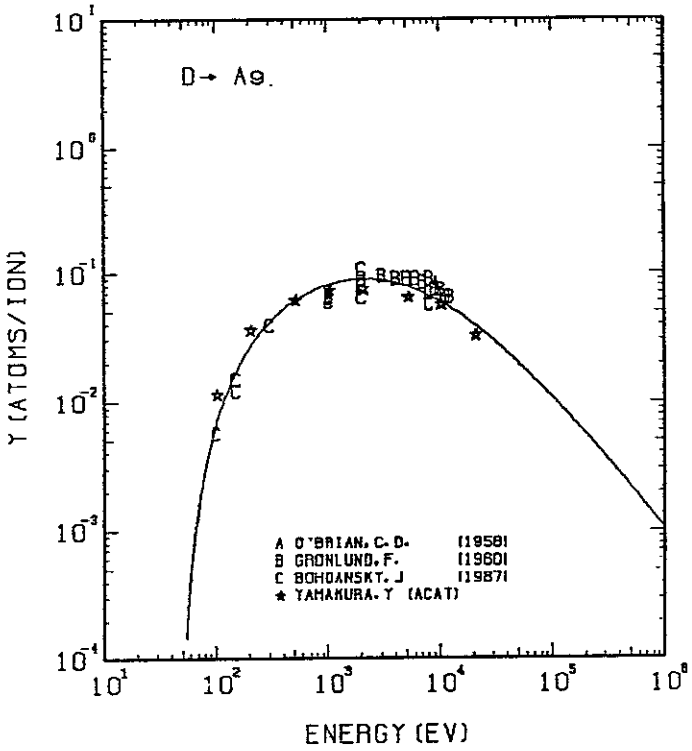


FIG. 203 ENERGY DEPENDENCE OF THE SPUTTERING YIELD OF AG WITH $D^+$.
A= 53.53, Q= 1.08, Us= 2.95EV, s= 2.80,
W= 0.35Us.

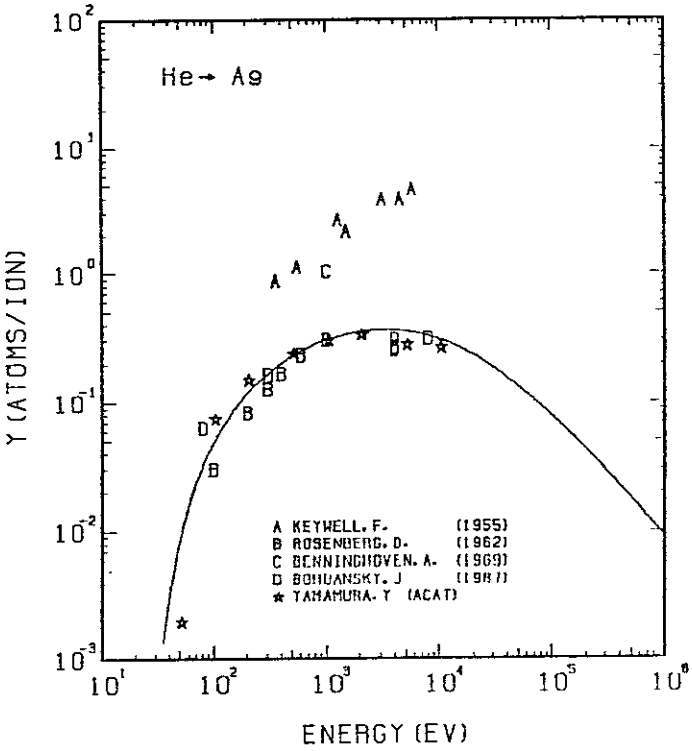


FIG. 204 ENERGY DEPENDENCE OF THE SPUTTERING YIELD OF AG WITH $HE^+$.
A= 26.93, Q= 1.08, Us= 2.95EV, s= 2.80,
W= 0.35Us.

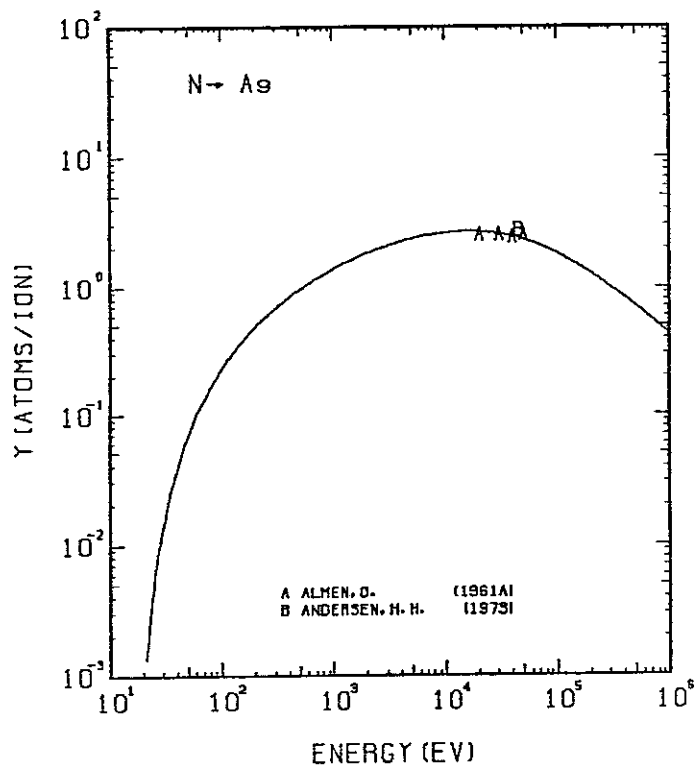


FIG. 205 ENERGY DEPENDENCE OF THE SPUTTERING YIELD OF AG WITH $N^+$.
A= 7.69, Q= 1.08, Us= 3.83EV, s= 2.80,
W= 0.35Us. THE BEST-FIT SURFACE
BINDING ENERGY IS USED.

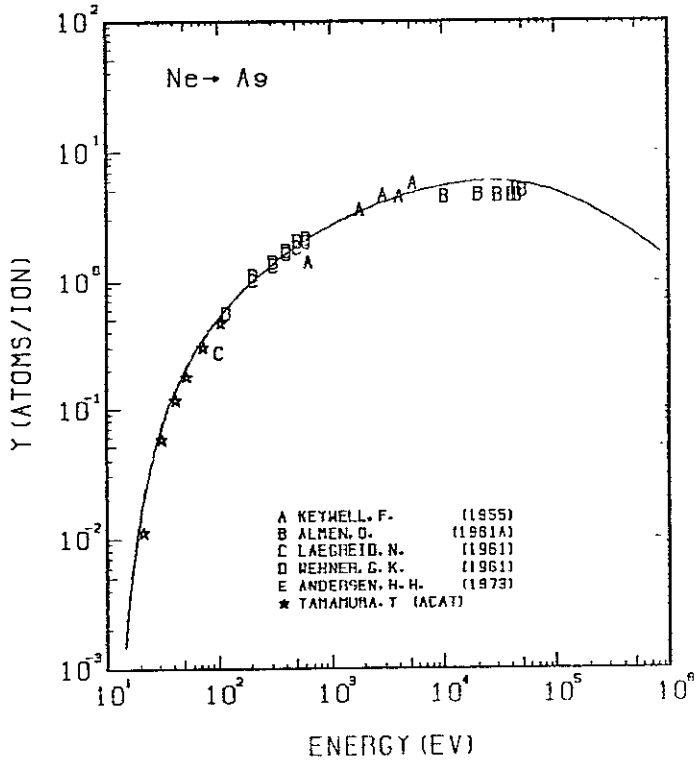


FIG. 206 ENERGY DEPENDENCE OF THE SPUTTERING YIELD OF AG WITH $NE^+$.
A= 5.34, Q= 1.08, Us= 2.95EV, s= 2.80,
W= 0.35Us.

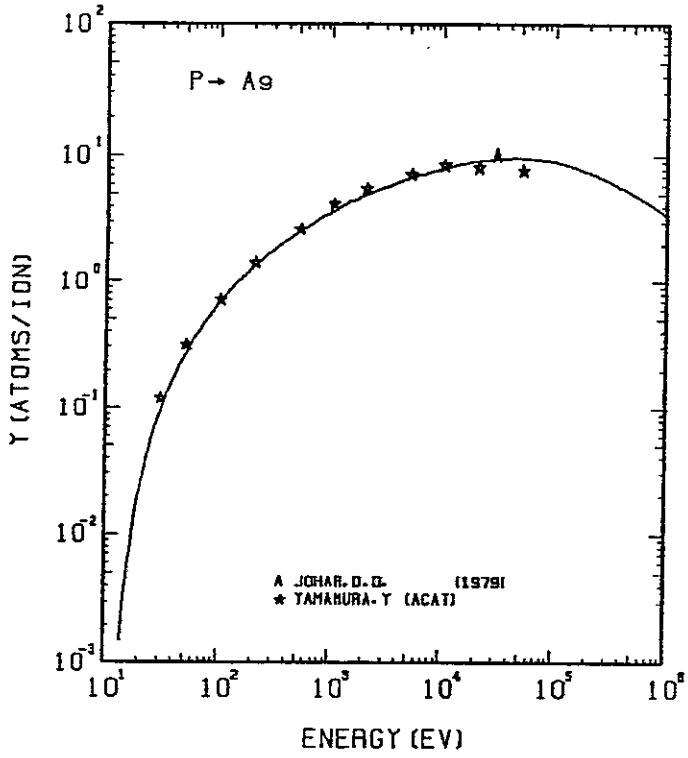


FIG. 207 ENERGY DEPENDENCE OF THE SPUTTERING YIELD OF AG WITH $P^+$.
A= 3.48, O= 1.08, Us= 2.95EV, S= 2.80,
W= 0.35Us.

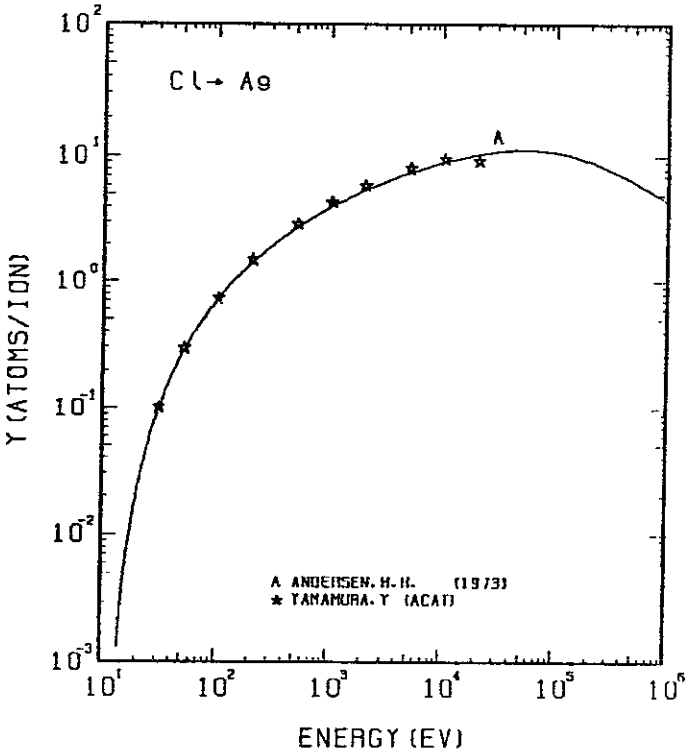


FIG. 208 ENERGY DEPENDENCE OF THE SPUTTERING YIELD OF AG WITH $CL^+$.
A= 3.04, O= 1.08, Us= 2.95EV, S= 2.80,
W= 0.35Us.

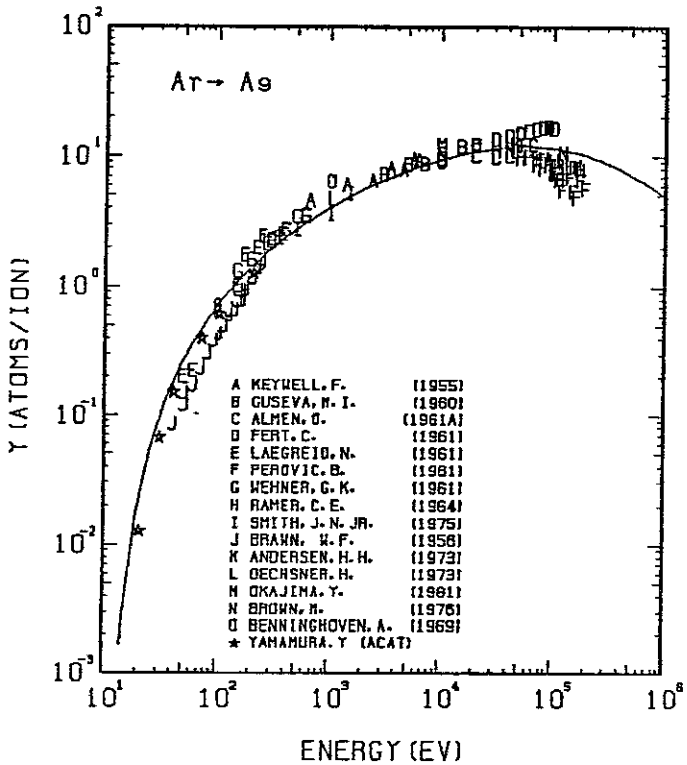


FIG. 209 ENERGY DEPENDENCE OF THE SPUTTERING YIELD OF AG WITH $AR^+$.
A= 2.70, O= 1.08, Us= 2.95EV, S= 2.80,
W= 0.35Us.

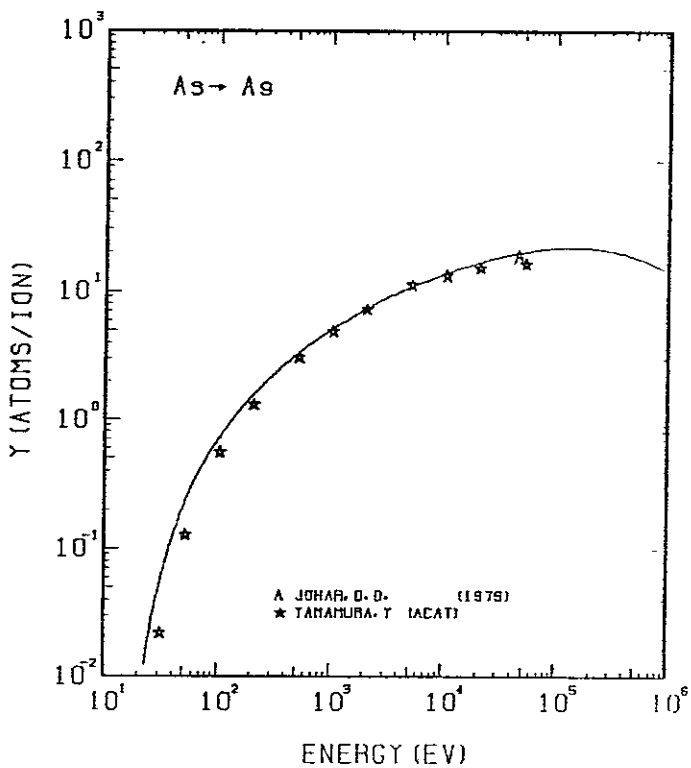


FIG. 210 ENERGY DEPENDENCE OF THE SPUTTERING YIELD OF AG WITH $AS^+$.
A= 1.44, O= 1.08, Us= 2.95EV, S= 2.80,
W= 0.35Us.

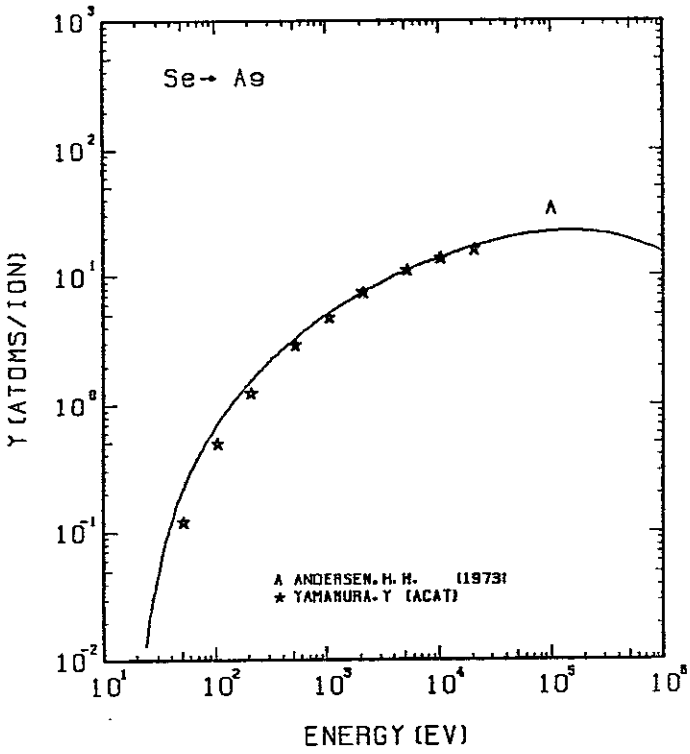


FIG. 211 ENERGY DEPENDENCE OF THE SPUTTERING YIELD OF AG WITH $SE^+$.
A= 1.37, D= 1.08, Us= 2.95EV, s= 2.80,
W= 0.35Us.

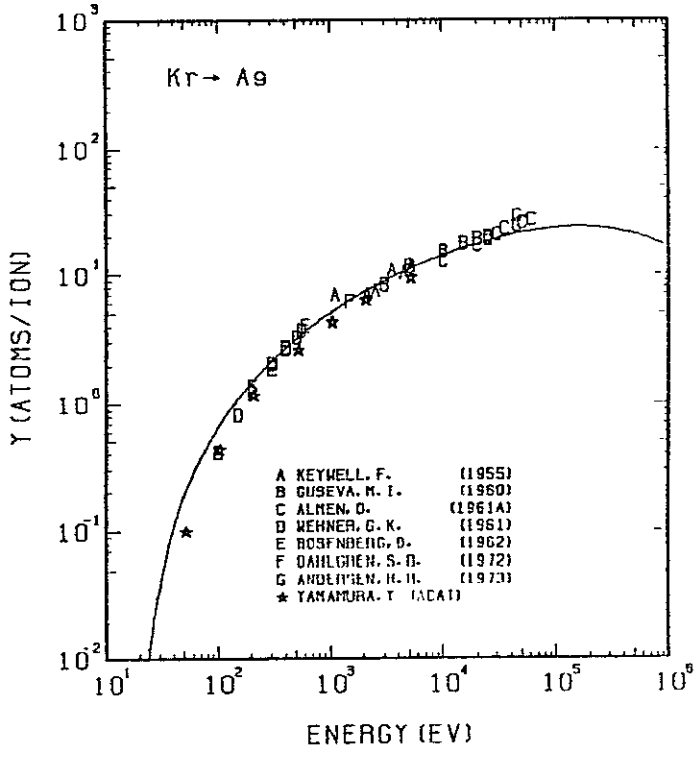


FIG. 212 ENERGY DEPENDENCE OF THE SPUTTERING YIELD OF AG WITH $KR^+$.
A= 1.29, D= 1.08, Us= 2.95EV, s= 2.80,
W= 0.35Us.

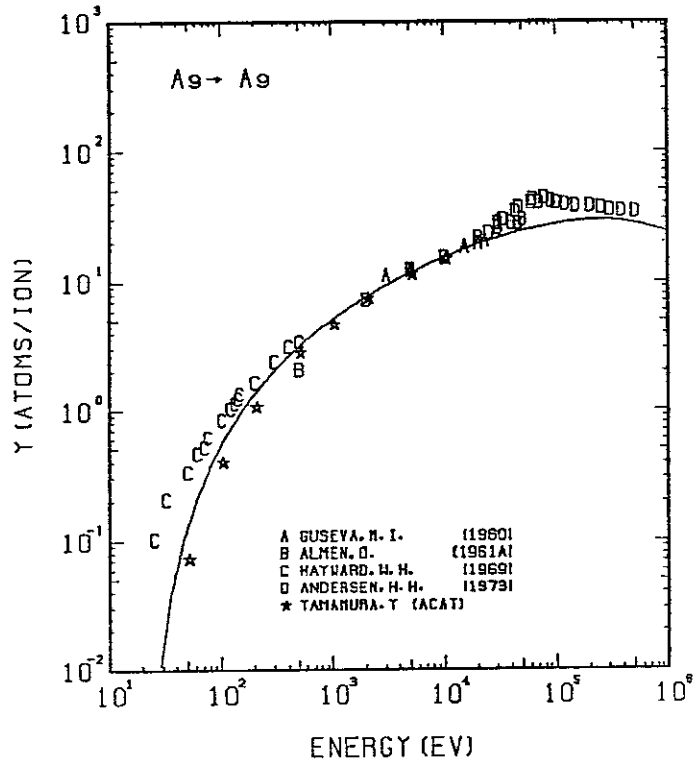


FIG. 213 ENERGY DEPENDENCE OF THE SPUTTERING YIELD OF AG WITH $AG^+$.
A= 1.00, D= 1.08, Us= 2.95EV, s= 2.80,
W= 0.35Us.

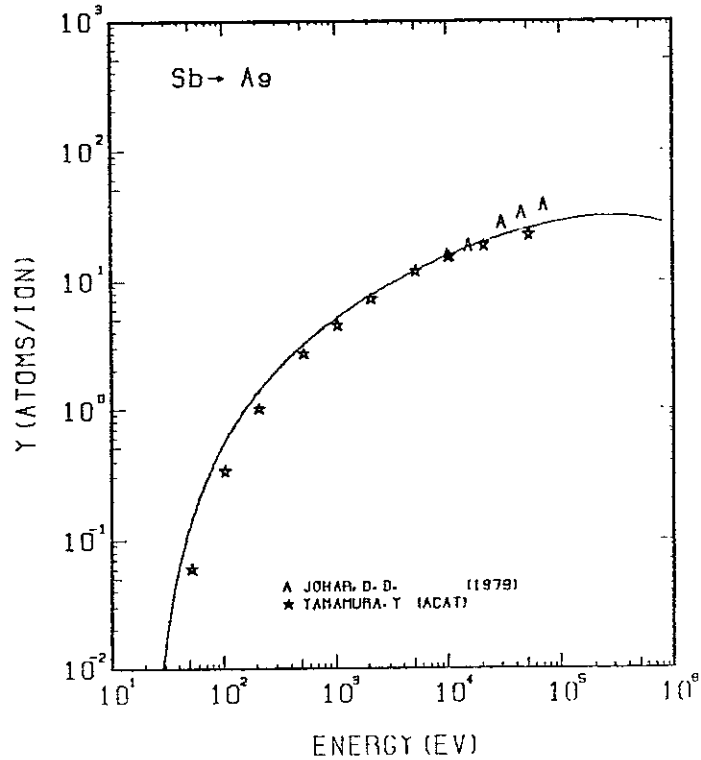


FIG. 214 ENERGY DEPENDENCE OF THE SPUTTERING YIELD OF AG WITH $SB^+$.
A= 0.89, D= 1.08, Us= 2.95EV, s= 2.80,
W= 0.35Us.

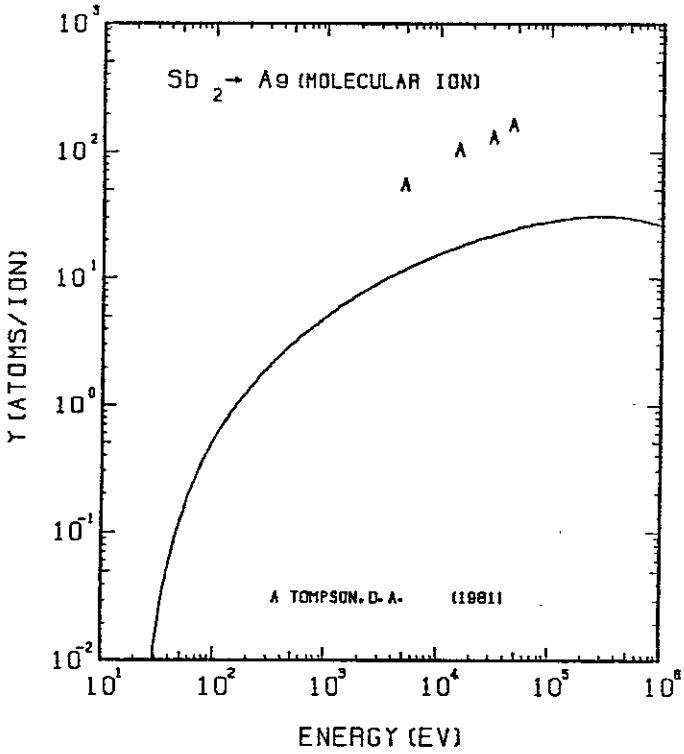


FIG. 215 ENERGY DEPENDENCE OF THE SPUTTERING YIELD OF AG WITH SB $_2^+$. A= 0.89, D= 1.08, Us= 2.95EV, S= 2.80, W= 0.35Us. THE NON-LINEAR EFFECT IS OBSERVED DUE TO MOLECULAR IONS.

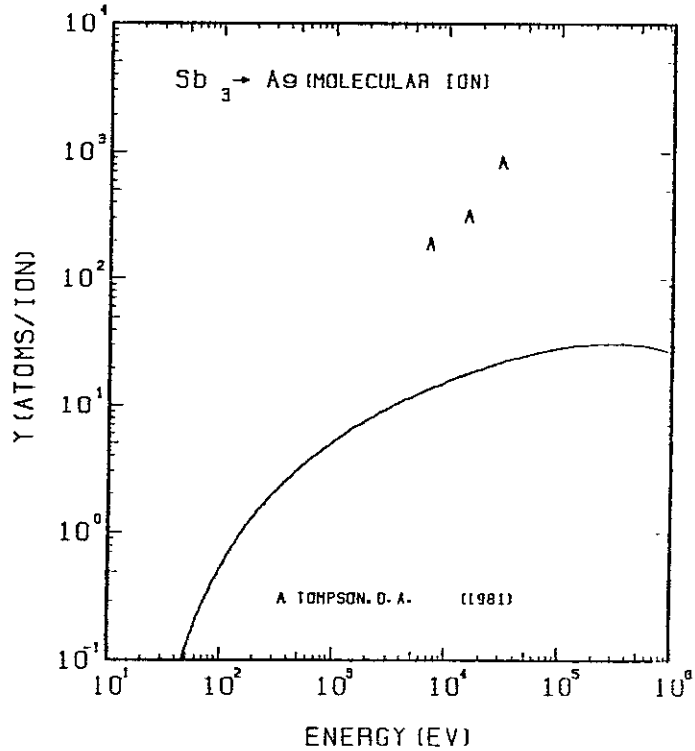


FIG. 216 ENERGY DEPENDENCE OF THE SPUTTERING YIELD OF AG WITH SB $_3^+$. A= 0.89, D= 1.08, Us= 2.95EV, S= 2.80, W= 0.35Us. THE NON-LINEAR EFFECT IS OBSERVED DUE TO MOLECULAR IONS.

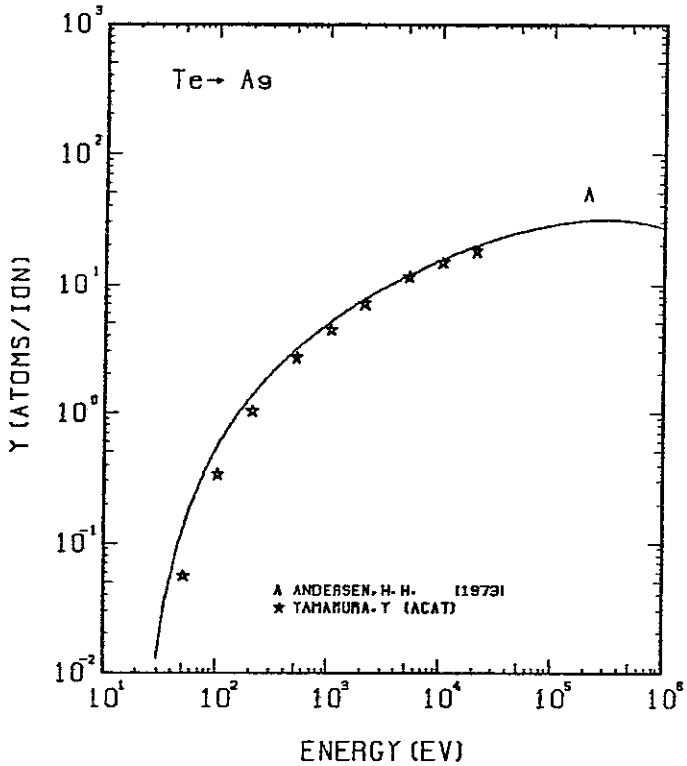


FIG. 217 ENERGY DEPENDENCE OF THE SPUTTERING YIELD OF AG WITH TE$^+$. A= 0.84, D= 1.08, Us= 2.95EV, S= 2.80, W= 0.35Us.

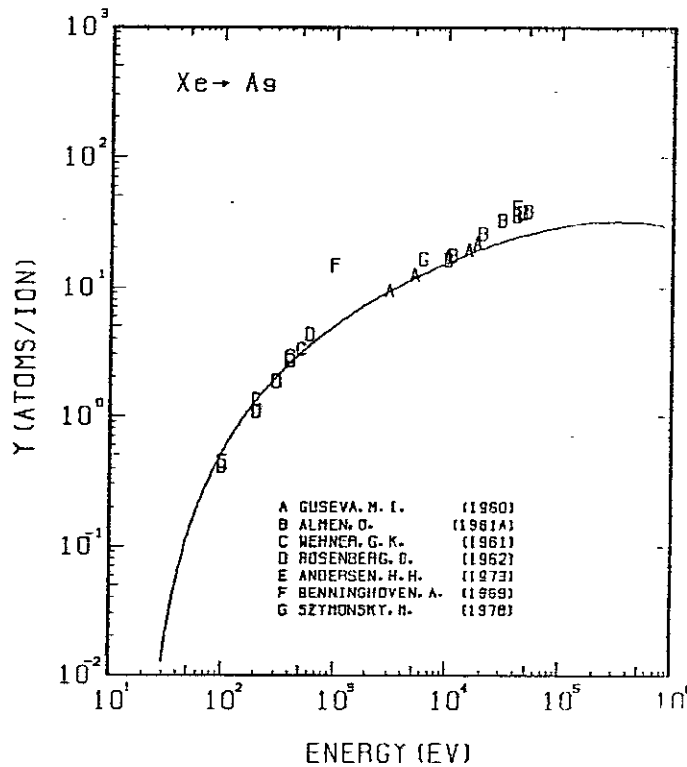


FIG. 218 ENERGY DEPENDENCE OF THE SPUTTERING YIELD OF AG WITH XE$^+$. A= 0.82, D= 1.08, Us= 2.95EV, S= 2.80, W= 0.35Us.

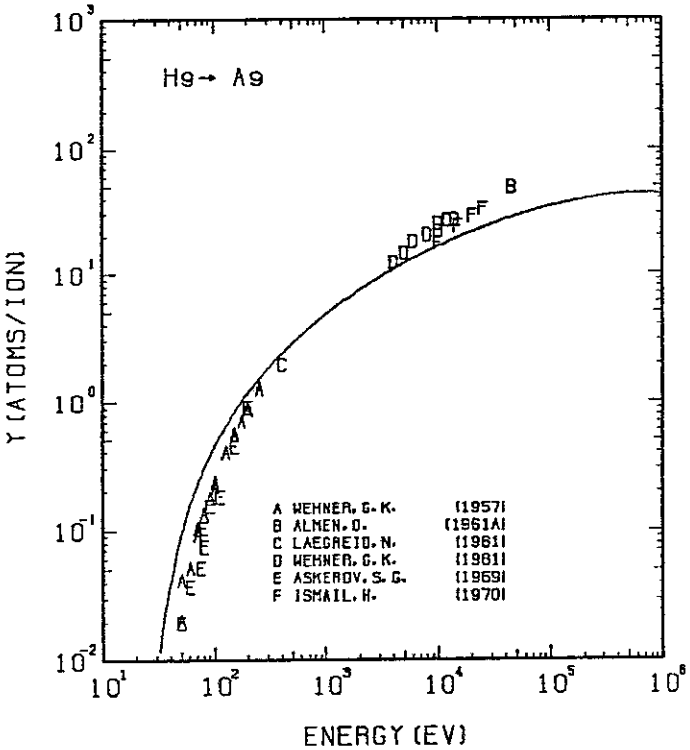


FIG. 219 ENERGY DEPENDENCE OF THE SPUTTERING YIELD OF AG WITH $HG^{+}$.
A= 0.54, D= 1.08, Us= 2.95EV, s= 2.80,
W= 0.35Us.

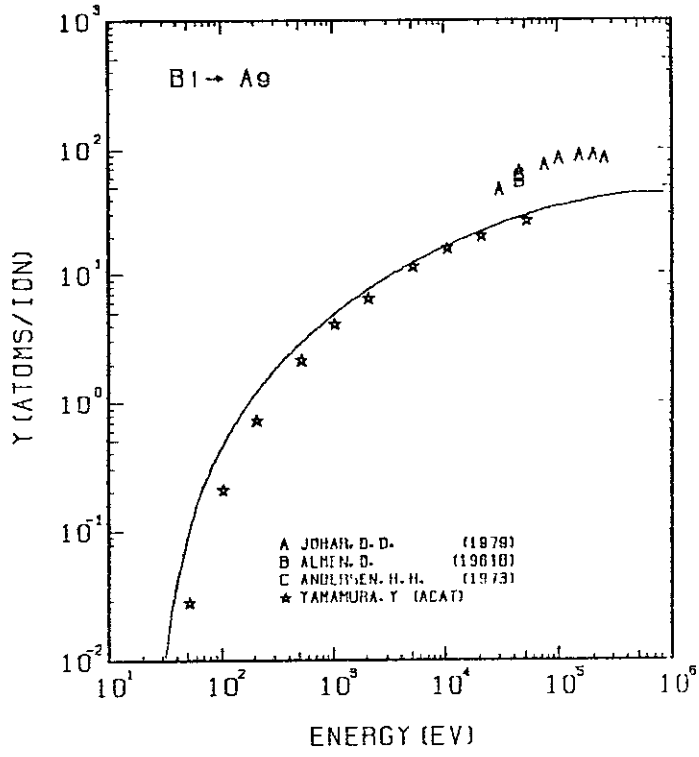


FIG. 220 ENERGY DEPENDENCE OF THE SPUTTERING YIELD OF AG WITH $BI^{+}$.
A= 0.52, D= 1.08, Us= 2.95EV, s= 2.80,
W= 0.35Us.

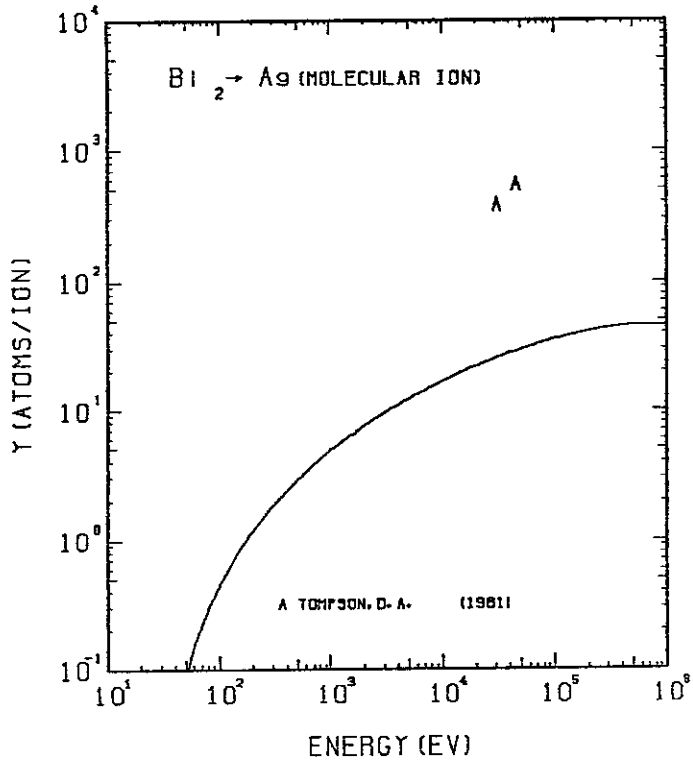


FIG. 221 ENERGY DEPENDENCE OF THE SPUTTERING YIELD OF AG WITH $BI_2^{+}$.
A= 0.52, D= 1.08, Us= 2.95EV, s= 2.80,
W= 0.35Us. THE NON-LINEAR EFFECT IS OBSERVED DUE TO MOLECULAR IONS.

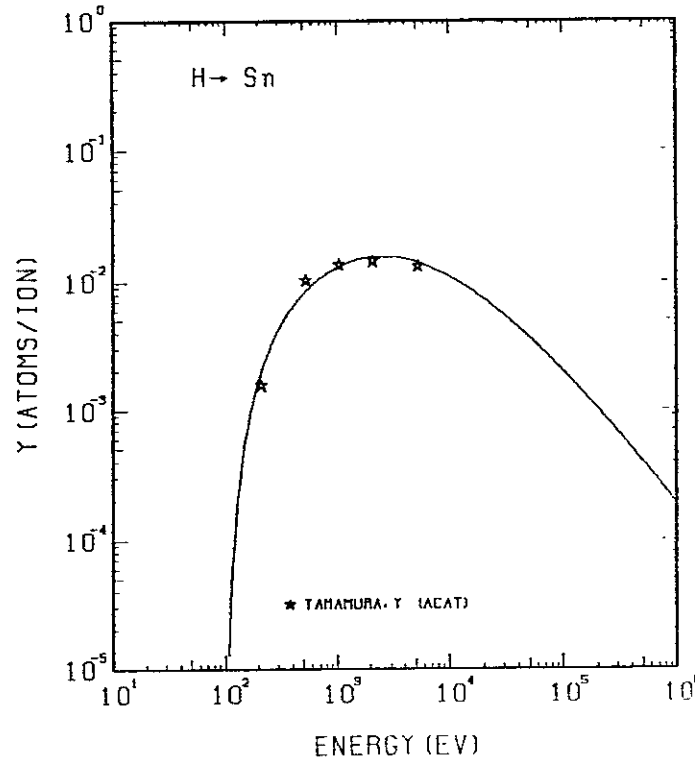


FIG. 222 ENERGY DEPENDENCE OF THE SPUTTERING YIELD OF SN WITH $H^{+}$.
A= 117.66, D= 0.47, Us= 3.14EV, s= 2.50,
W= 0.28Us.

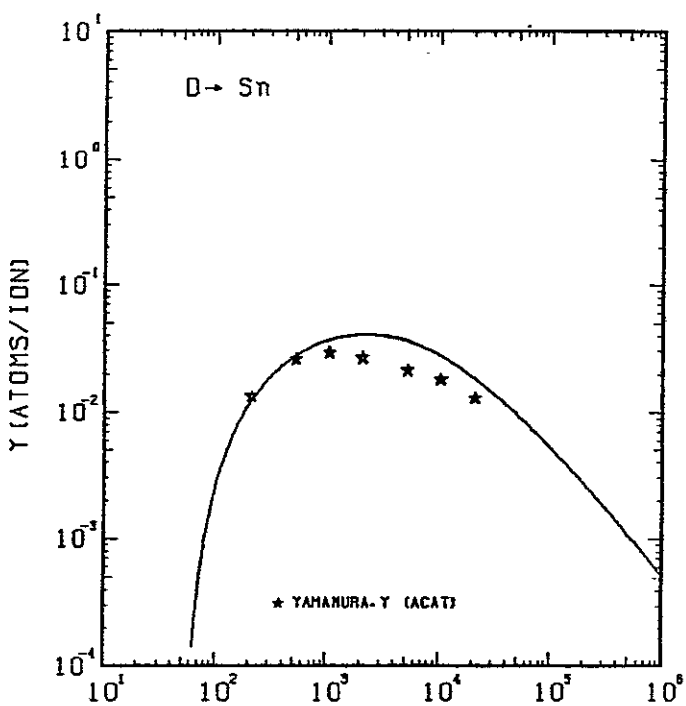


FIG. 223 ENERGY DEPENDENCE OF THE SPUTTERING YIELD OF SN WITH $O^+$.
A= 58.89, O= 0.47, Us= 3.14EV, S= 2.50,
W= 0.28Us.

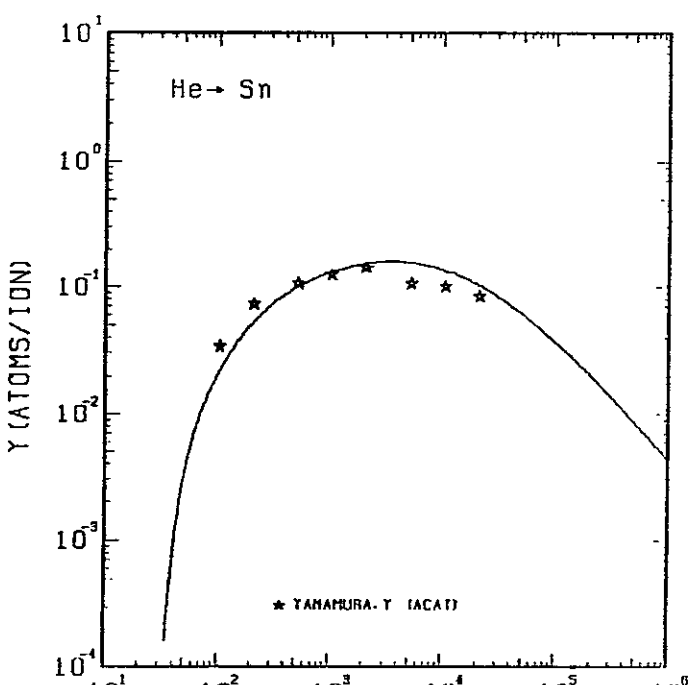


FIG. 224 ENERGY DEPENDENCE OF THE SPUTTERING YIELD OF SN WITH $HE^+$.
A= 29.63, O= 0.47, Us= 3.14EV, S= 2.50,
W= 0.28Us.

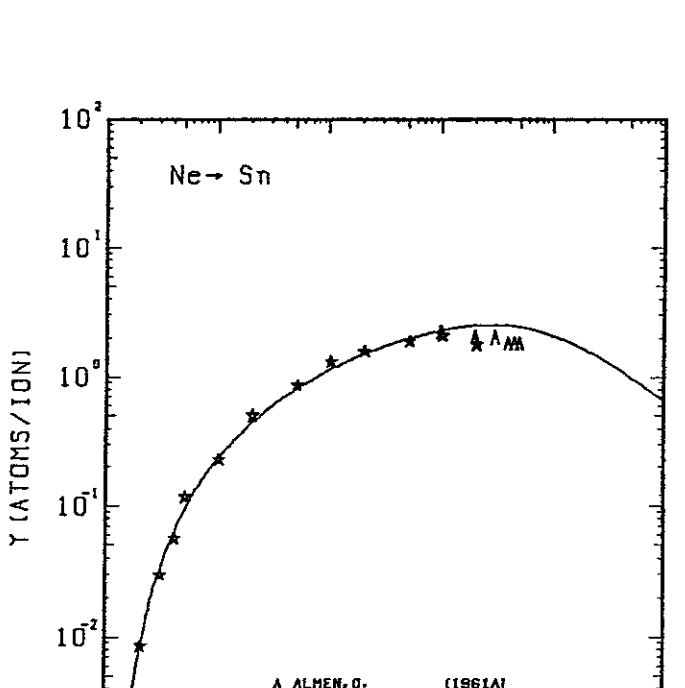


FIG. 225 ENERGY DEPENDENCE OF THE SPUTTERING YIELD OF SN WITH $NE^+$.
A= 5.88, O= 0.47, Us= 3.14EV, S= 2.50,
W= 0.28Us.

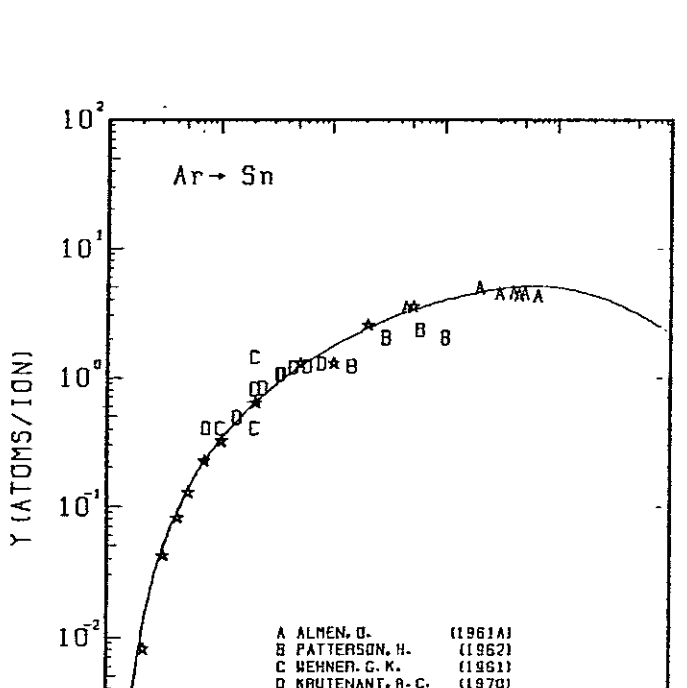


FIG. 226 ENERGY DEPENDENCE OF THE SPUTTERING YIELD OF SN WITH $AR^+$.
A= 2.97, O= 0.47, Us= 3.14EV, S= 2.50,
W= 0.28Us.

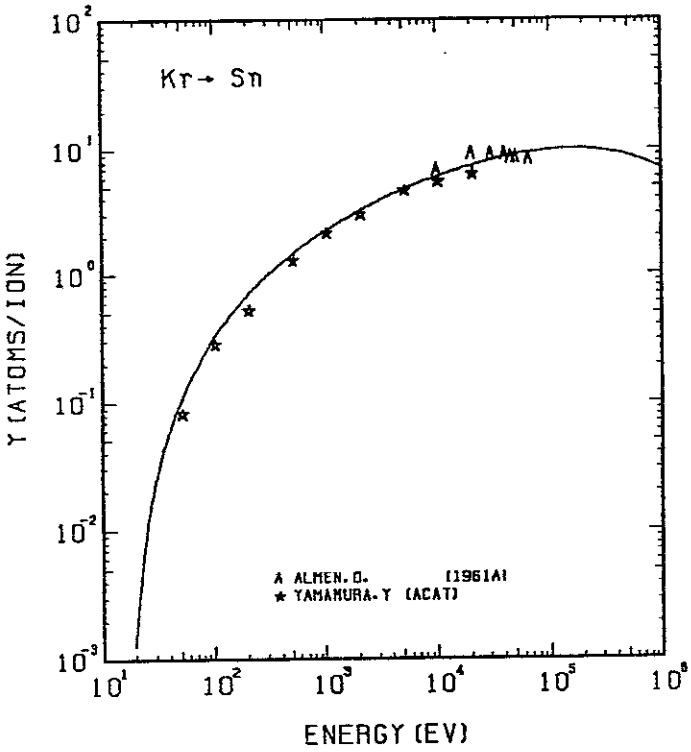


FIG. 227 ENERGY DEPENDENCE OF THE SPUTTERING YIELD OF SN WITH $KR^+$.
A= 1.42, D= 0.47, Us= 3.14EV, S= 2.50,
W= 0.28Us.

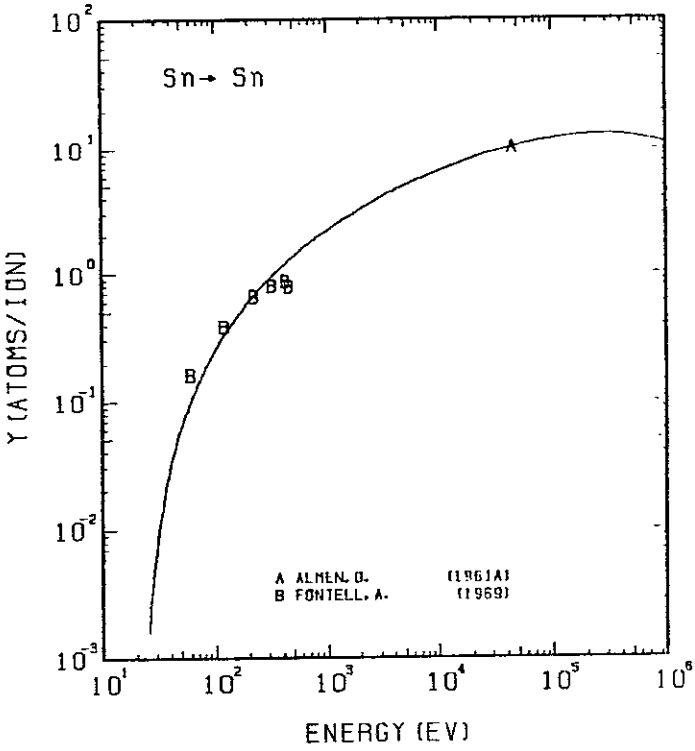


FIG. 228 ENERGY DEPENDENCE OF THE SPUTTERING YIELD OF SN WITH $SN^+$.
A= 1.00, D= 0.47, Us= 3.14EV, S= 2.50,
W= 0.28Us.

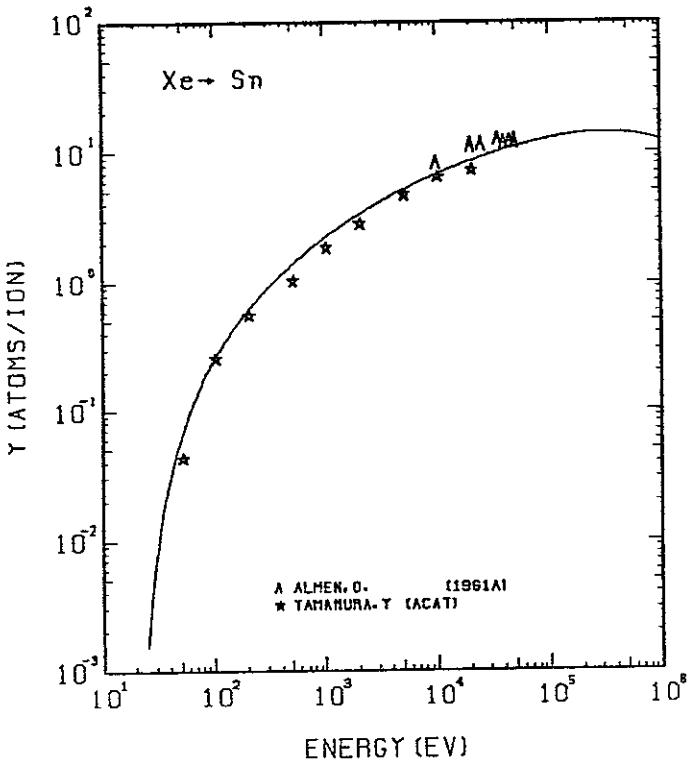


FIG. 229 ENERGY DEPENDENCE OF THE SPUTTERING YIELD OF SN WITH $XE^+$.
A= 0.90, D= 0.47, Us= 3.14EV, S= 2.50,
W= 0.28Us.

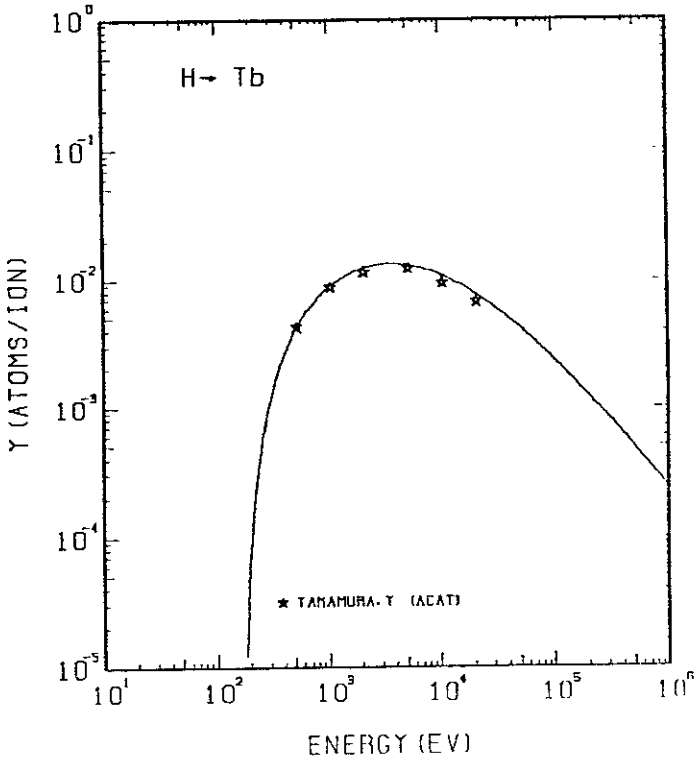


FIG. 230 ENERGY DEPENDENCE OF THE SPUTTERING YIELD OF TB WITH $H^+$.
A= 157.64, D= 0.90, Us= 4.05EV, S= 2.50,
W= 0.35Us.

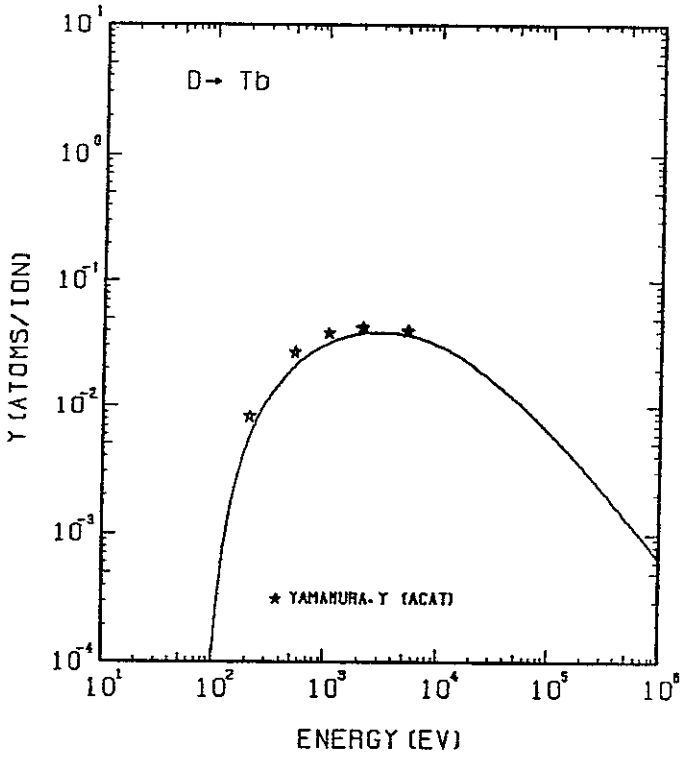


FIG. 231 ENERGY DEPENDENCE OF THE SPUTTERING YIELD OF TB WITH $D^+$.
A= 78.90, Q= 0.90, Us= 4.05EV, s= 2.50,
W= 0.35Us.

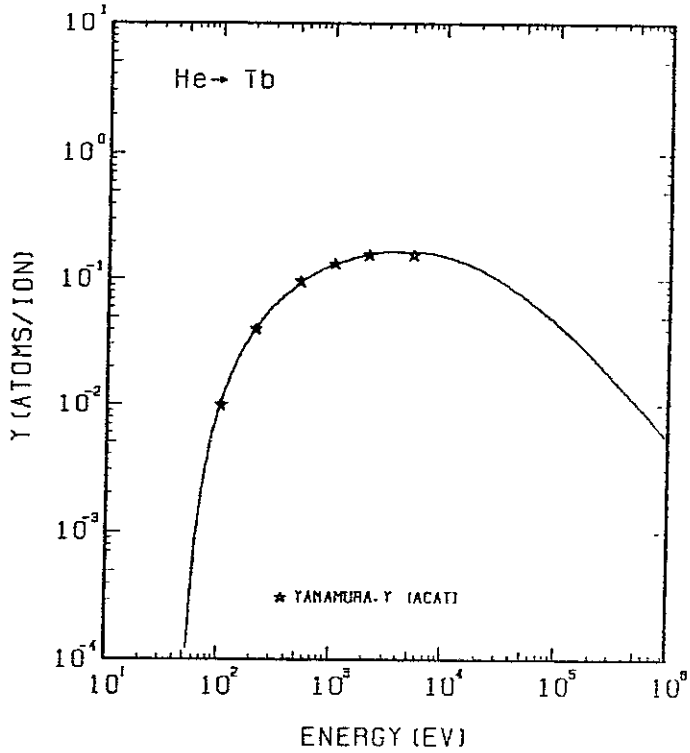


FIG. 232 ENERGY DEPENDENCE OF THE SPUTTERING YIELD OF TB WITH $HE^+$.
A= 39.70, Q= 0.90, Us= 4.05EV, s= 2.50,
W= 0.35Us.

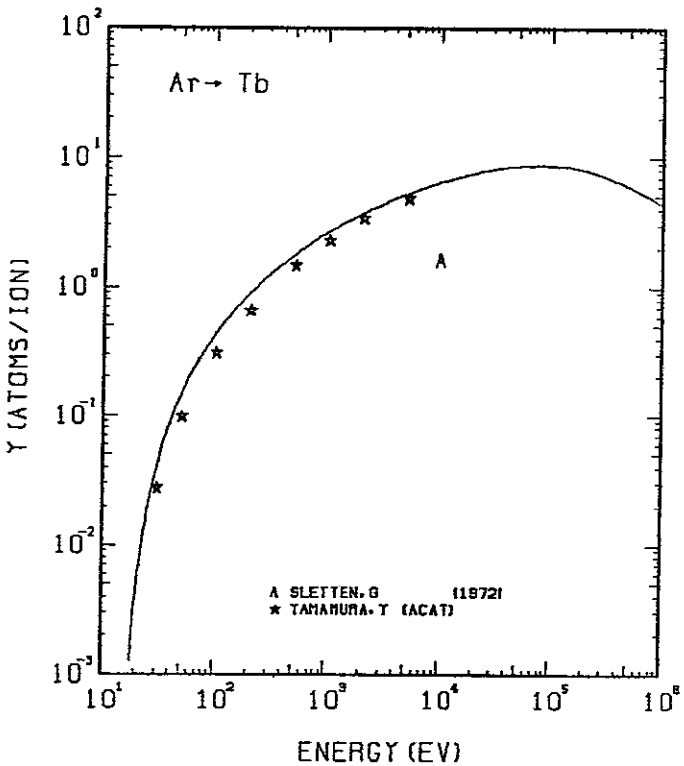


FIG. 233 ENERGY DEPENDENCE OF THE SPUTTERING YIELD OF TB WITH $AR^+$.
A= 3.98, Q= 0.90, Us= 4.05EV, s= 2.50,
W= 0.35Us.

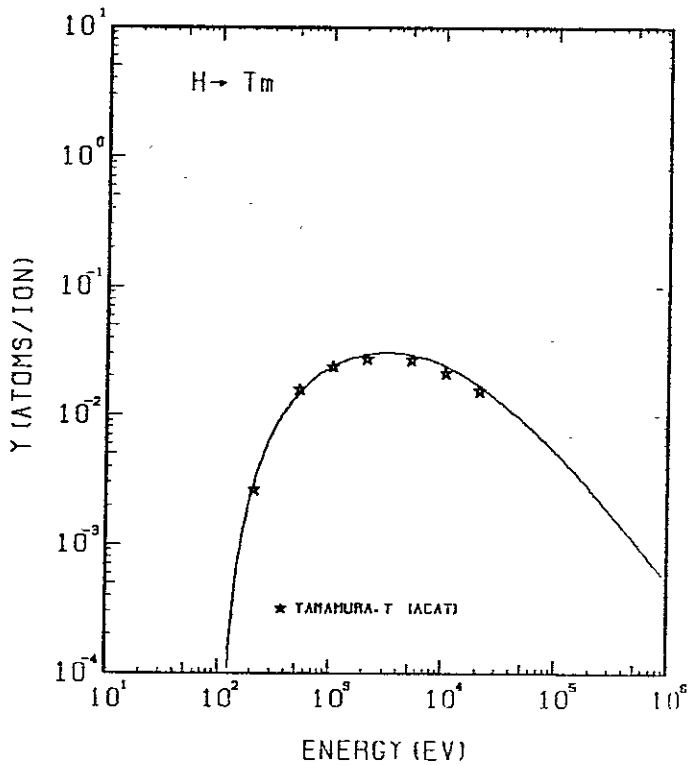


FIG. 234 ENERGY DEPENDENCE OF THE SPUTTERING YIELD OF TM WITH $H^+$.
A= 167.56, Q= 0.65, Us= 2.42EV, s= 2.50,
W= 0.35Us.

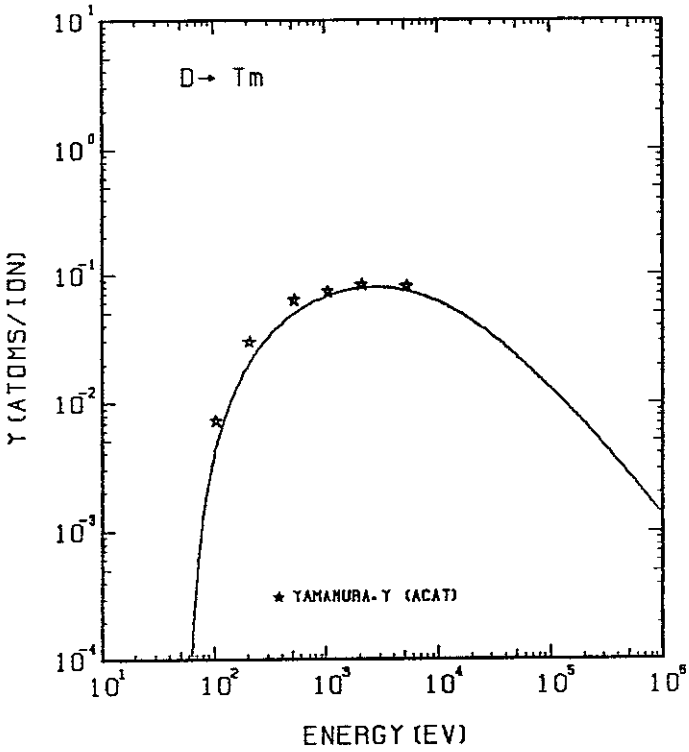


FIG. 235 ENERGY DEPENDENCE OF THE SPUTTERING YIELD OF TM WITH $D^+$.
A= 83.86, Q= 0.65, Us= 2.42EV, s= 2.50,
W= 0.35Us.

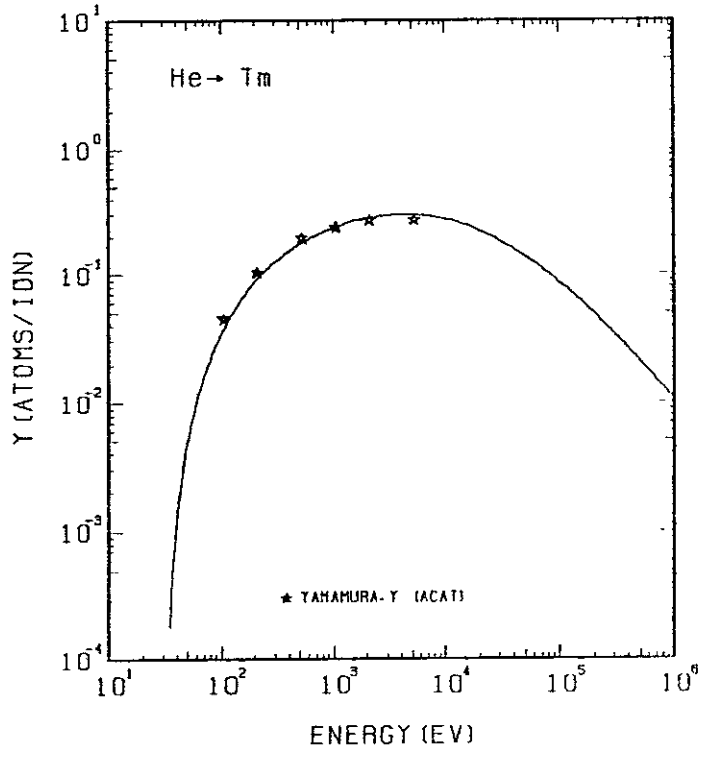


FIG. 236 ENERGY DEPENDENCE OF THE SPUTTERING YIELD OF TM WITH $HE^+$.
A= 42.19, Q= 0.65, Us= 2.42EV, s= 2.50,
W= 0.35Us.

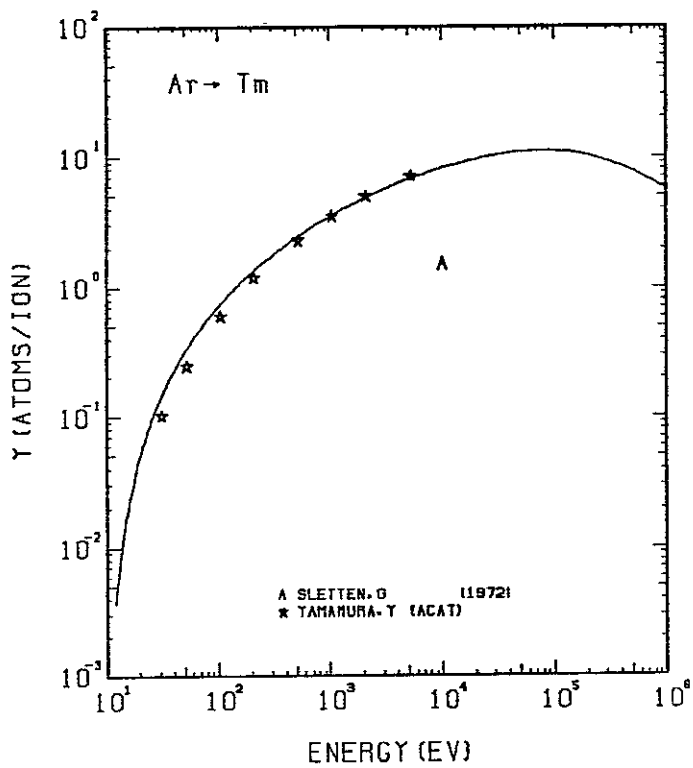


FIG. 237 ENERGY DEPENDENCE OF THE SPUTTERING YIELD OF TM WITH $AR^+$.
A= 4.23, Q= 0.65, Us= 2.42EV, s= 2.50,
W= 0.35Us.

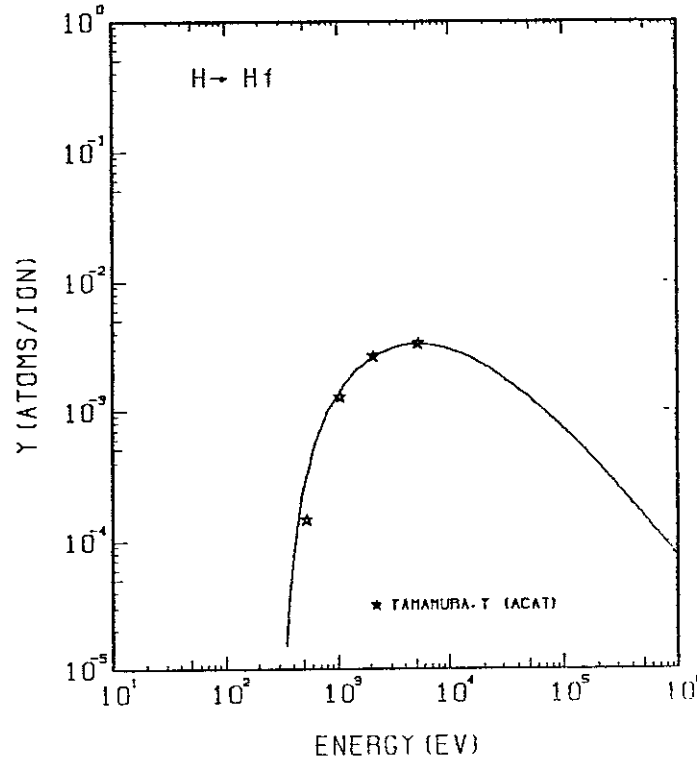


FIG. 238 ENERGY DEPENDENCE OF THE SPUTTERING YIELD OF HF WITH $H^+$.
A= 176.98, Q= 0.65, Us= 6.44EV, s= 2.50,
W= 0.35Us.

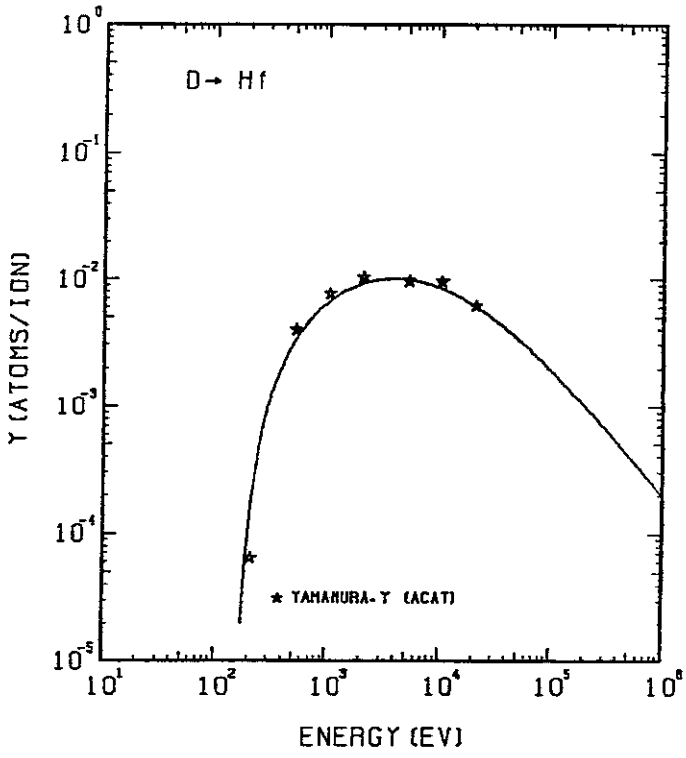


FIG. 239 ENERGY DEPENDENCE OF THE SPUTTERING YIELD OF HF WITH $D^+$.
A= 88.58, Q= 0.65, Us= 6.44EV, s= 2.50,
W= 0.35Us.

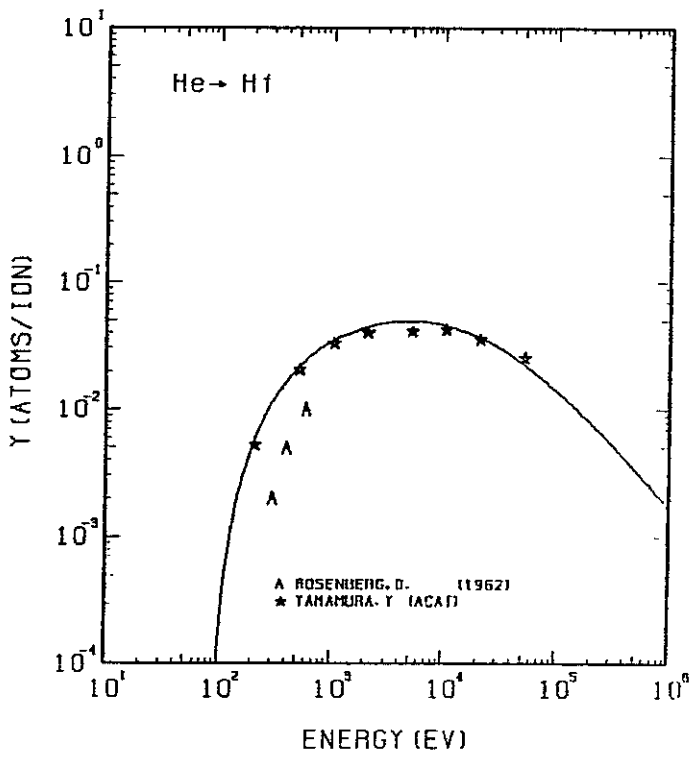


FIG. 240 ENERGY DEPENDENCE OF THE SPUTTERING YIELD OF HF WITH $HE^+$.
A= 44.57, Q= 0.65, Us= 6.44EV, s= 2.50,
W= 0.35Us.

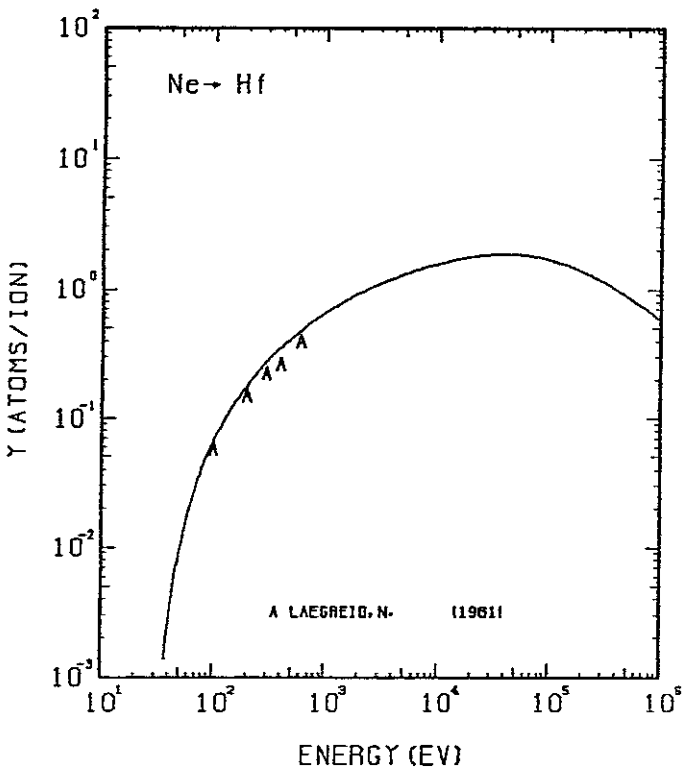


FIG. 241 ENERGY DEPENDENCE OF THE SPUTTERING YIELD OF HF WITH $NE^+$.
A= 8.84, Q= 0.65, Us= 6.44EV, s= 2.50,
W= 0.35Us.

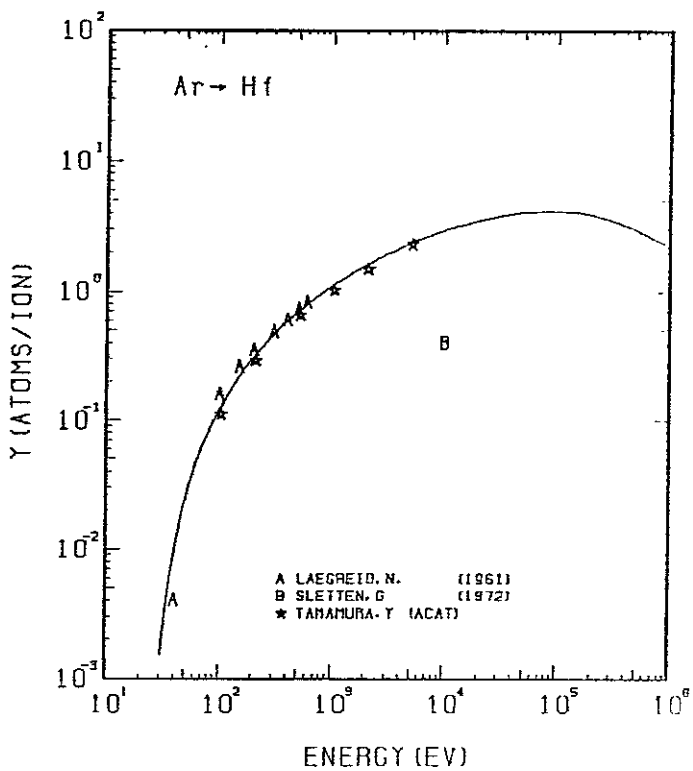


FIG. 242 ENERGY DEPENDENCE OF THE SPUTTERING YIELD OF HF WITH $AR^+$.
A= 4.47, Q= 0.65, Us= 6.44EV, s= 2.50,
W= 0.35Us.

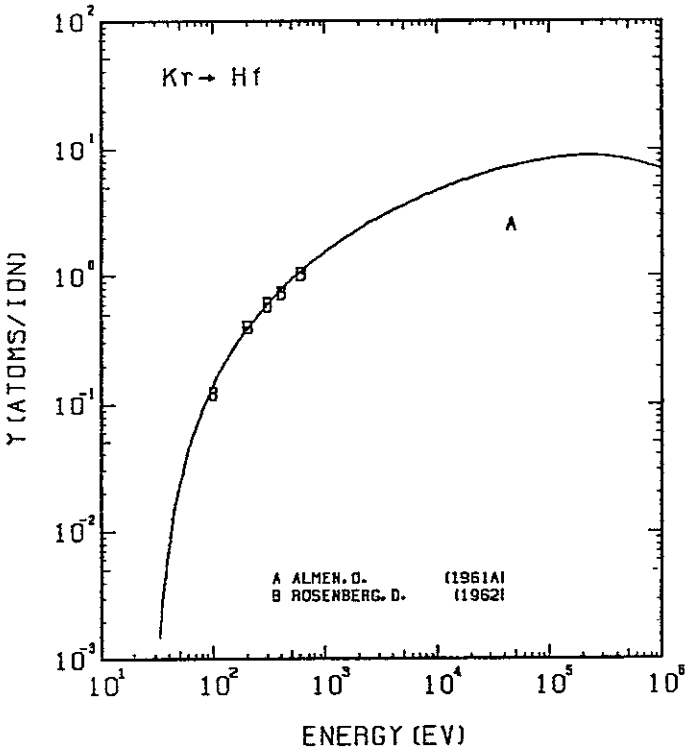


FIG. 243 ENERGY DEPENDENCE OF THE SPUTTERING YIELD OF HF WITH $KR^+$.
A= 2.13, Q= 0.65, Us= 6.44EV, S= 2.50,
W= 0.35Us.

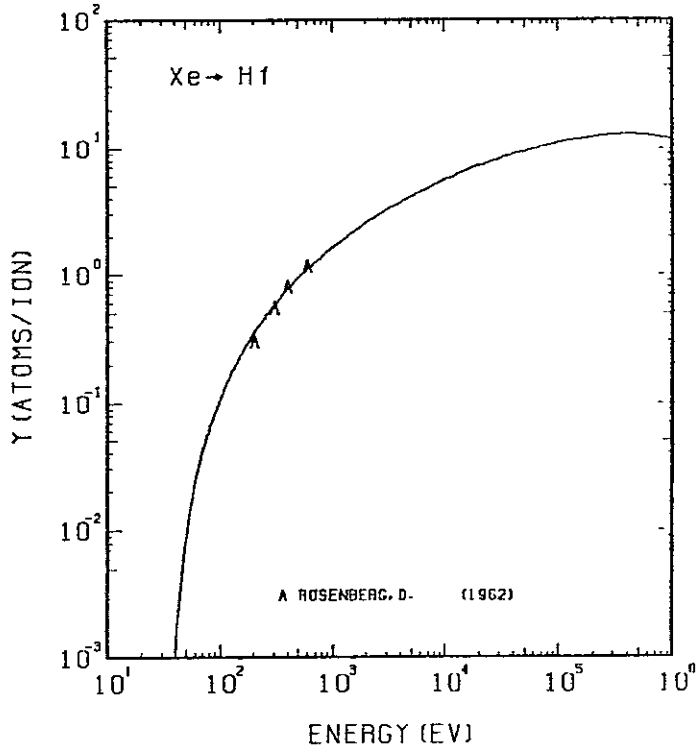


FIG. 244 ENERGY DEPENDENCE OF THE SPUTTERING YIELD OF HF WITH $XE^+$.
A= 1.36, Q= 0.65, Us= 6.44EV, S= 2.50,
W= 0.35Us.

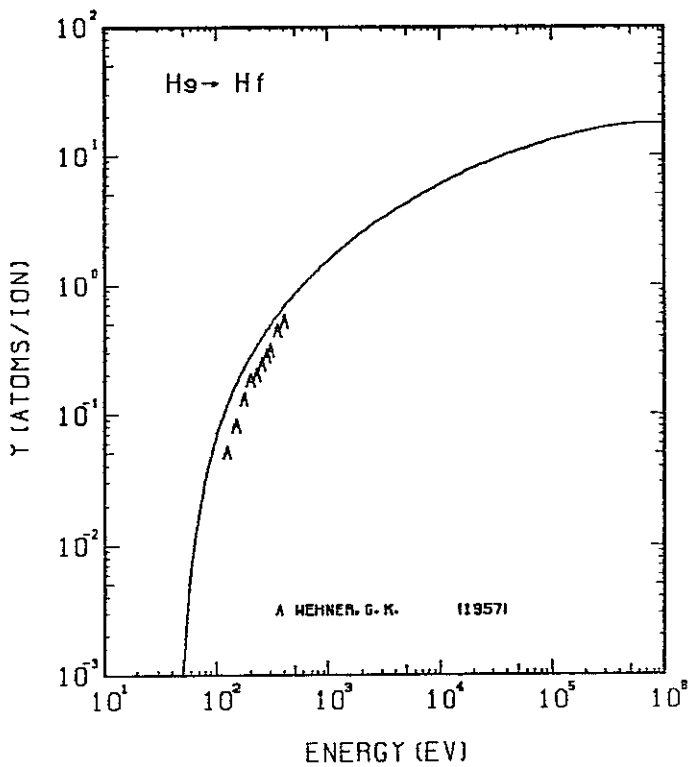


FIG. 245 ENERGY DEPENDENCE OF THE SPUTTERING YIELD OF HF WITH $HG^+$.
A= 0.89, Q= 0.65, Us= 6.44EV, S= 2.50,
W= 0.35Us.

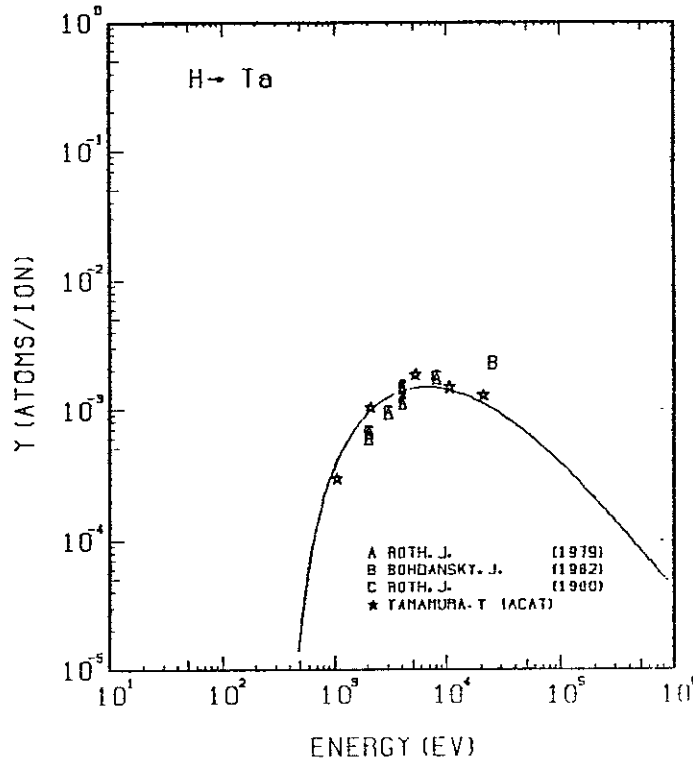


FIG. 246 ENERGY DEPENDENCE OF THE SPUTTERING YIELD OF TA WITH $H^+$.
A= 179.46, Q= 0.56, Us= 8.10EV, S= 2.80,
W= 0.35Us.

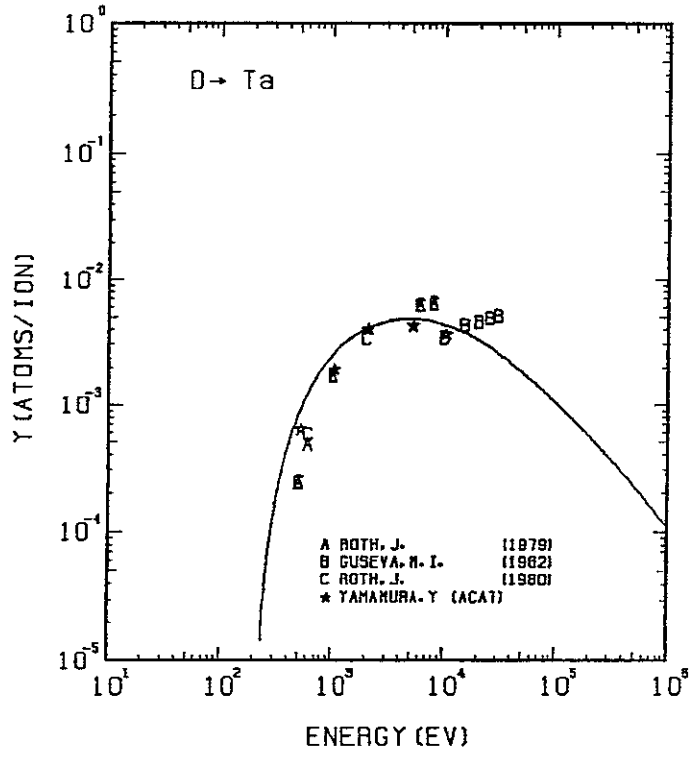


FIG. 247 ENERGY DEPENDENCE OF THE SPUTTERING YIELD OF TA WITH $D^+$.
A= 89.82, D= 0.56, Us= 8.10EV, s= 2.80, W= 0.35Us.

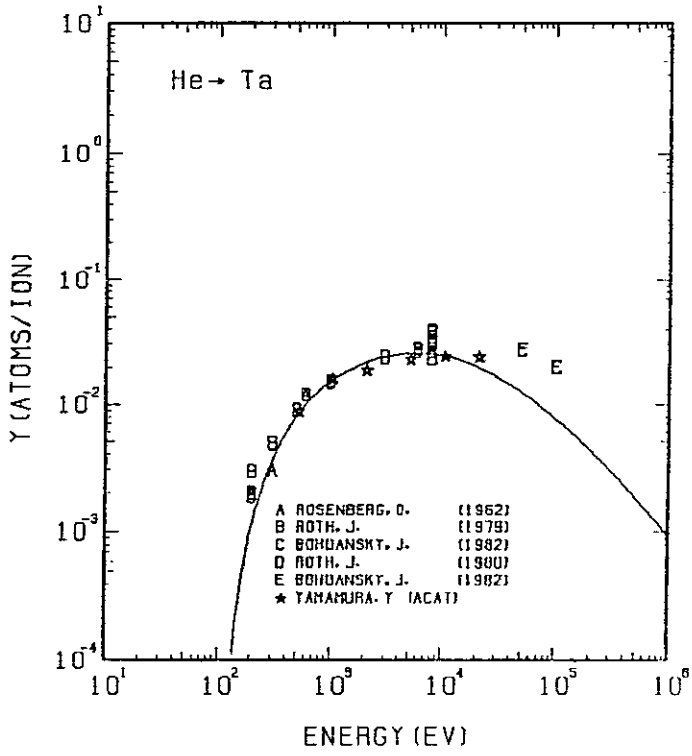


FIG. 248 ENERGY DEPENDENCE OF THE SPUTTERING YIELD OF TA WITH $HE^+$.
A= 45.19, D= 0.56, Us= 8.10EV, s= 2.80, W= 0.35Us.

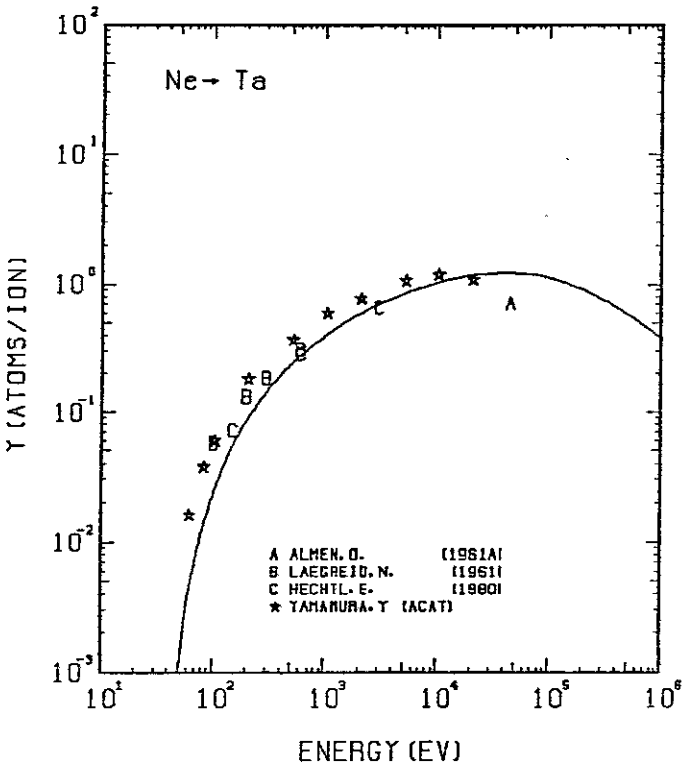


FIG. 249 ENERGY DEPENDENCE OF THE SPUTTERING YIELD OF TA WITH $NE^+$.
A= 8.96, D= 0.56, Us= 8.10EV, s= 2.80, W= 0.35Us.

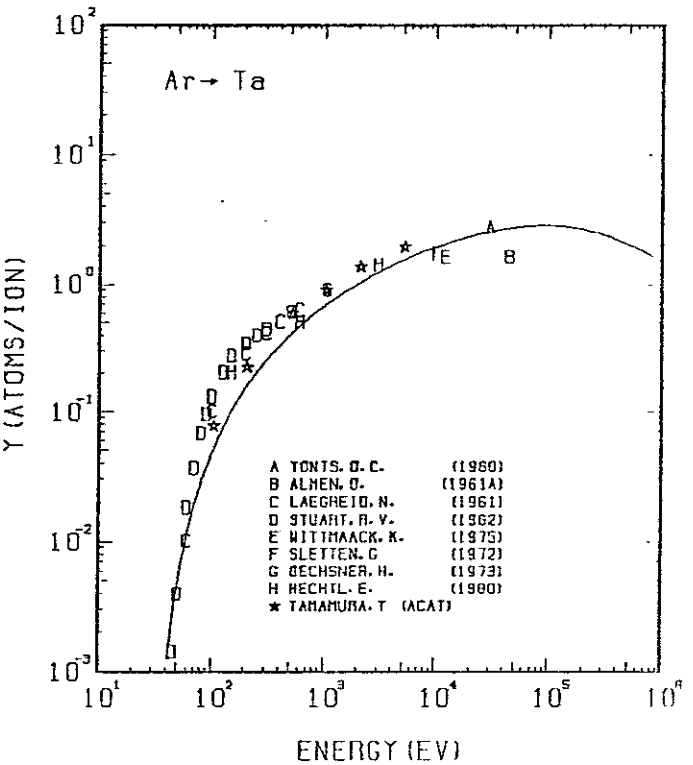


FIG. 250 ENERGY DEPENDENCE OF THE SPUTTERING YIELD OF TA WITH $AR^+$.
A= 4.53, D= 0.56, Us= 8.10EV, s= 2.80, W= 0.35Us.

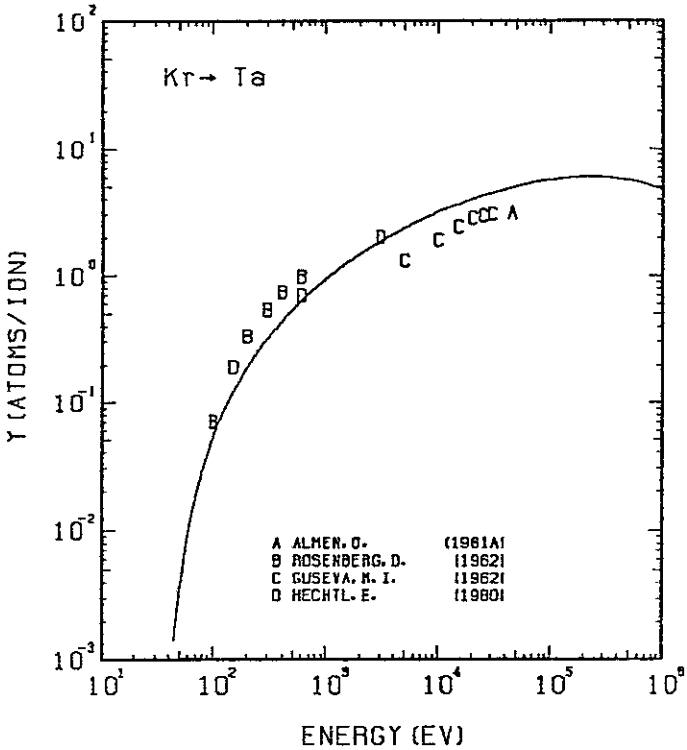


FIG. 251 ENERGY DEPENDENCE OF THE SPUTTERING YIELD OF TA WITH $KR^+$.
A= 2.16, D= 0.56, Us= 8.10EV, S= 2.80,
W= 0.35Us.

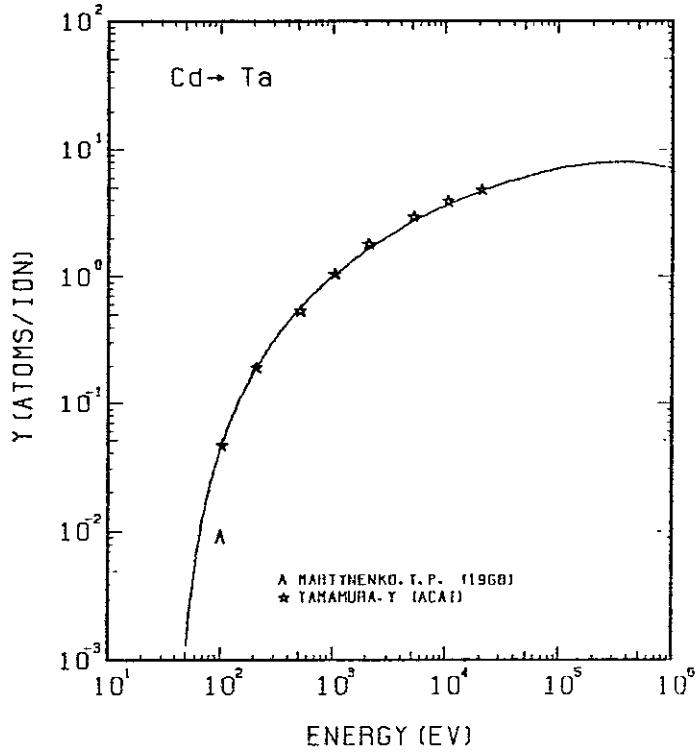


FIG. 252 ENERGY DEPENDENCE OF THE SPUTTERING YIELD OF TA WITH $CD^+$.
A= 1.61, D= 0.56, Us= 8.10EV, S= 2.80,
W= 0.35Us.

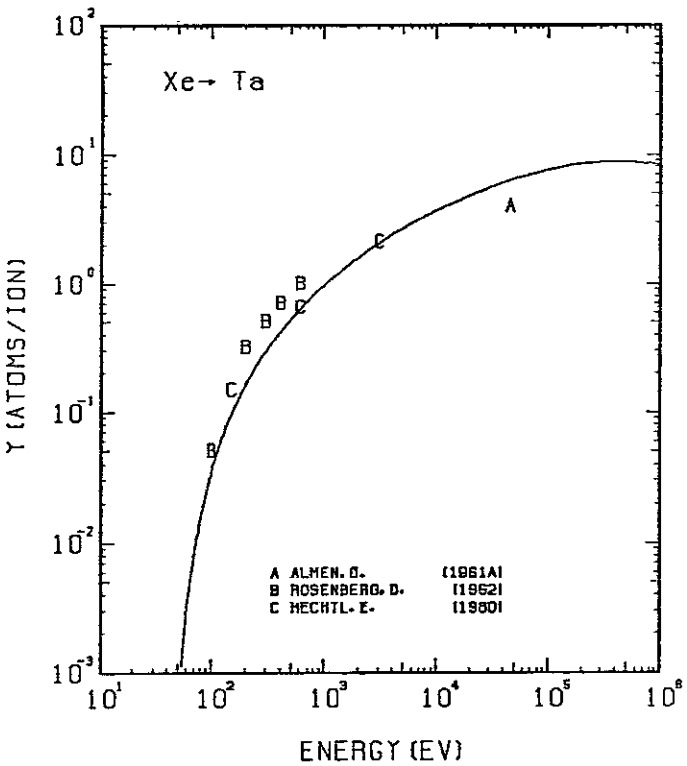


FIG. 253 ENERGY DEPENDENCE OF THE SPUTTERING YIELD OF TA WITH $XE^+$.
A= 1.38, D= 0.56, Us= 8.10EV, S= 2.80,
W= 0.35Us.

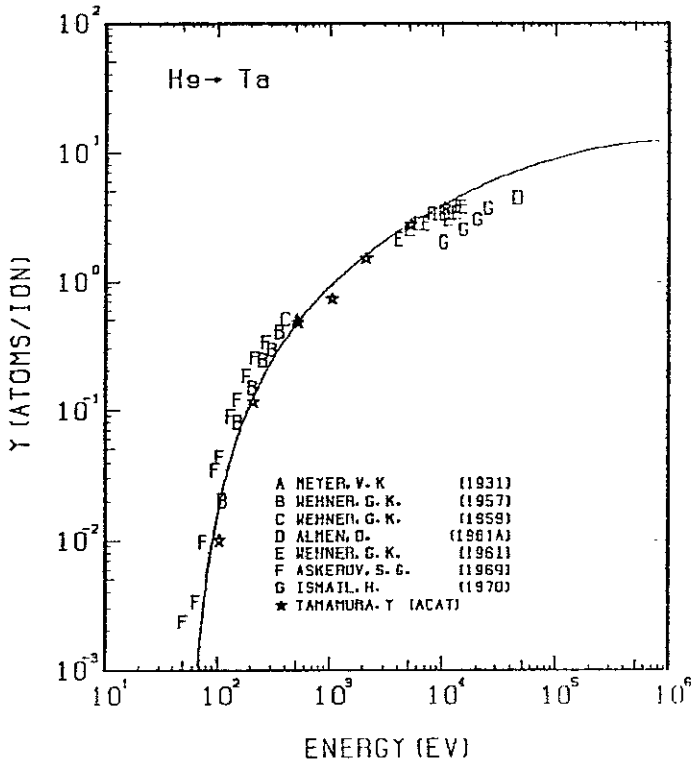


FIG. 254 ENERGY DEPENDENCE OF THE SPUTTERING YIELD OF TA WITH $HG^+$.
A= 0.90, D= 0.56, Us= 8.10EV, S= 2.80,
W= 0.35Us.

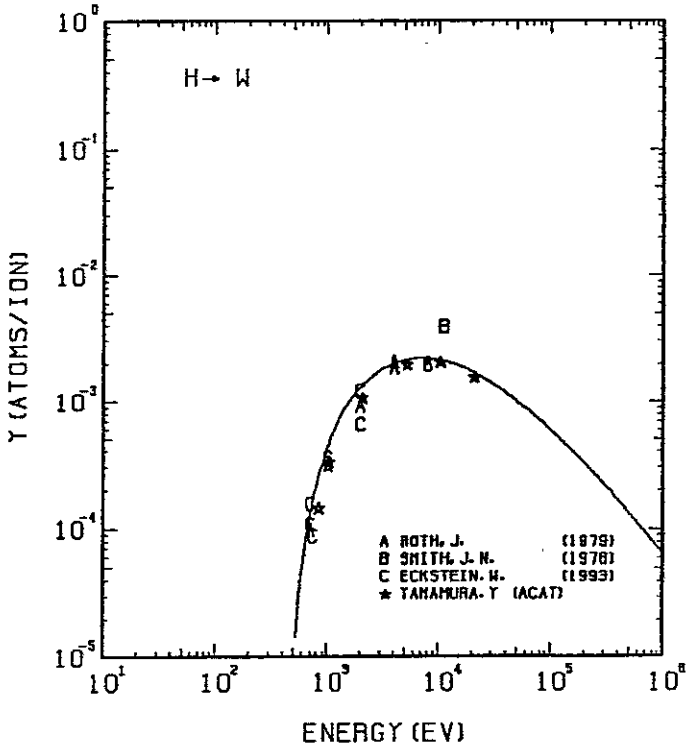


FIG. 255 ENERGY DEPENDENCE OF THE SPUTTERING YIELD OF W WITH $H^+$.
A= 182.34, Q= 0.72, Us= 8.90EV, s= 2.80,
W= 0.24Us.

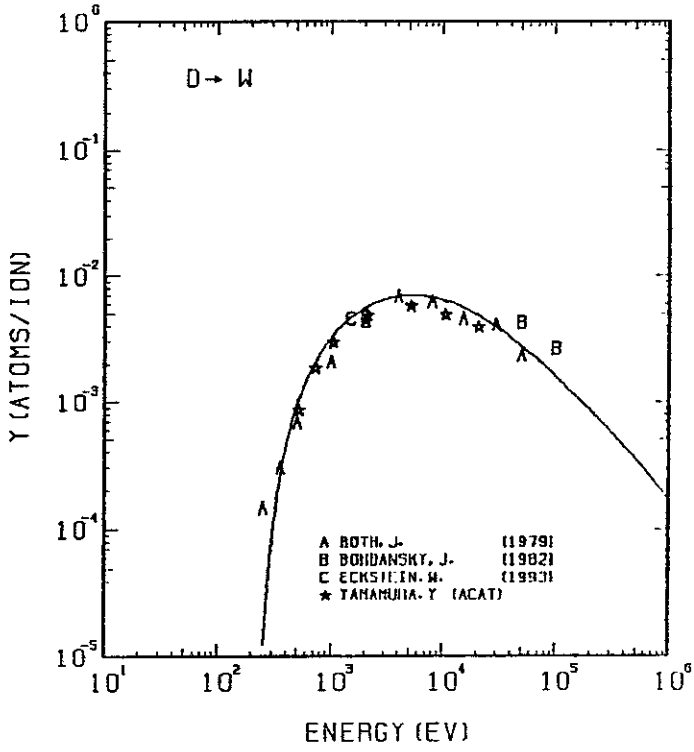


FIG. 256 ENERGY DEPENDENCE OF THE SPUTTERING YIELD OF W WITH $D^+$.
A= 91.26, Q= 0.72, Us= 8.90EV, s= 2.80,
W= 0.24Us.

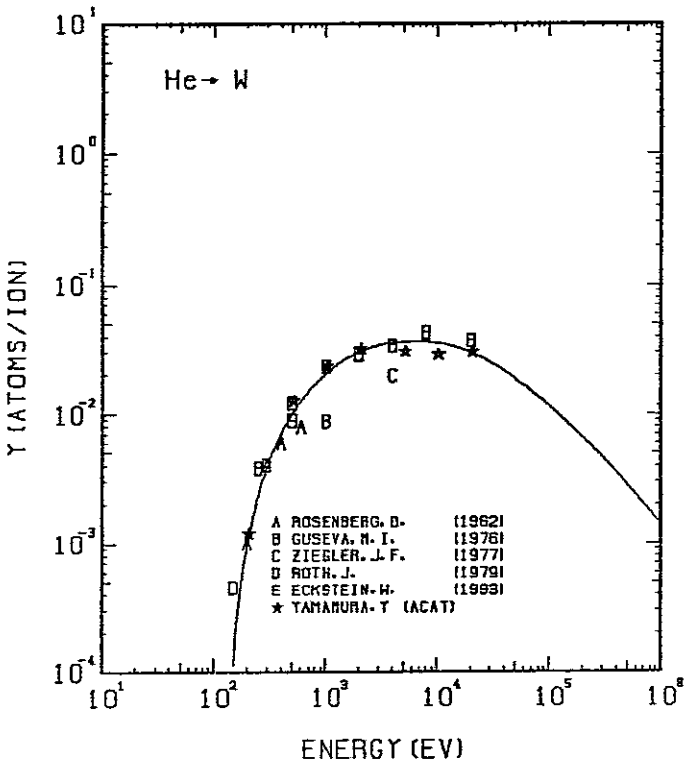


FIG. 257 ENERGY DEPENDENCE OF THE SPUTTERING YIELD OF W WITH $HE^+$.
A= 45.92, Q= 0.72, Us= 8.90EV, s= 2.80,
W= 0.24Us.

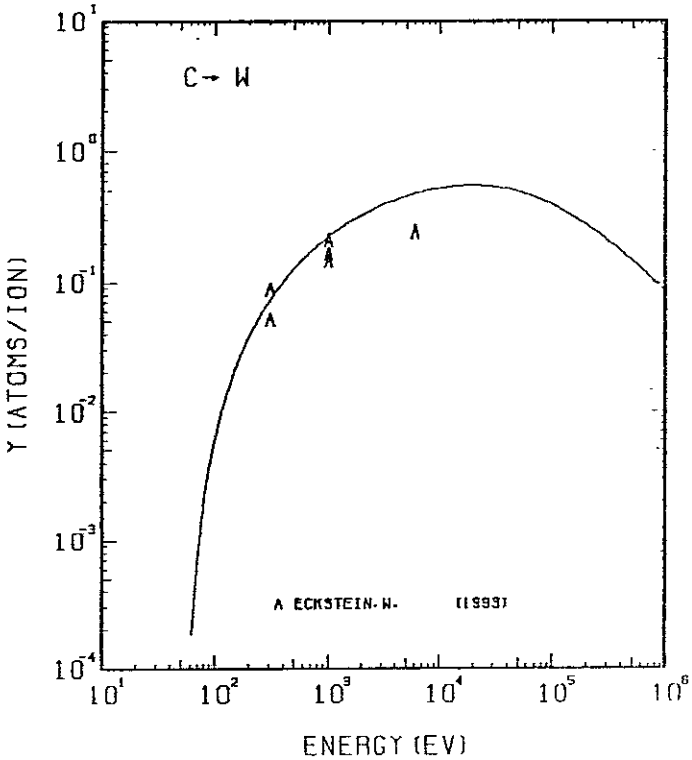


FIG. 258 ENERGY DEPENDENCE OF THE SPUTTERING YIELD OF W WITH $C^+$.
A= 15.30, Q= 0.72, Us= 8.90EV, s= 2.80,
W= 0.24Us.

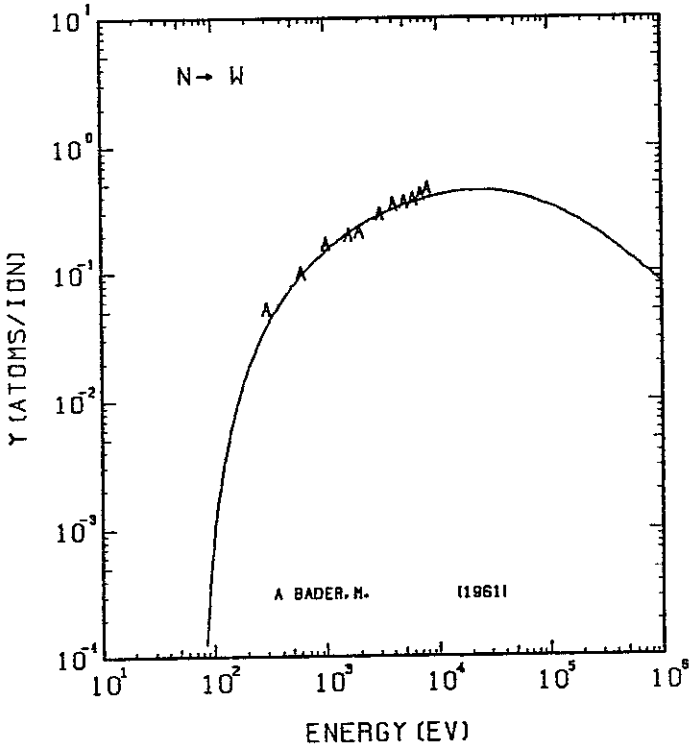


FIG. 259 ENERGY DEPENDENCE OF THE SPUTTERING YIELD OF W WITH $N^+$.
A= 13.12, D= 0.72, Us= 13.35EV, s= 2.80.
W= 0.24Us. THE BEST-FIT SURFACE BINDING ENERGY IS USED.

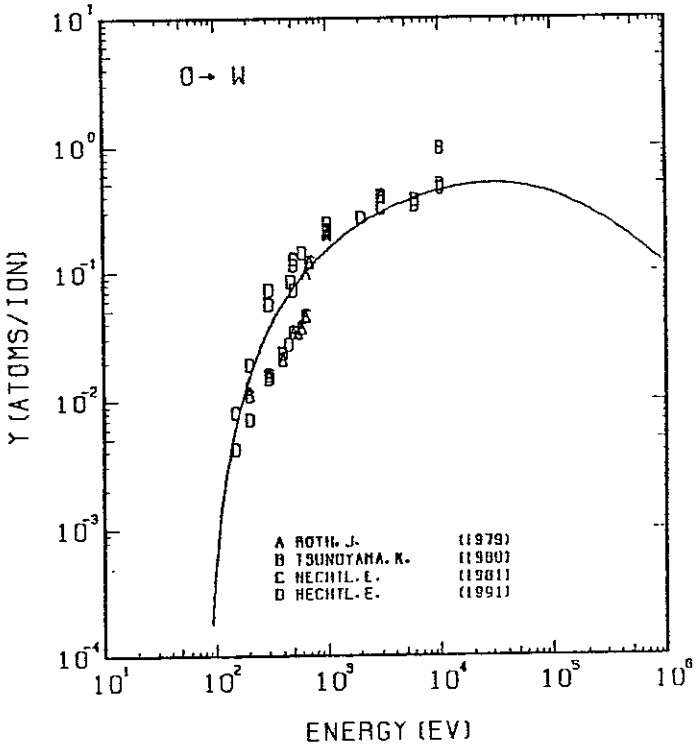


FIG. 260 ENERGY DEPENDENCE OF THE SPUTTERING YIELD OF W WITH $O^+$.
A= 11.49, D= 0.72, Us= 15.13EV, s= 2.80.
W= 0.24Us. THE BEST-FIT SURFACE BINDING ENERGY IS USED.

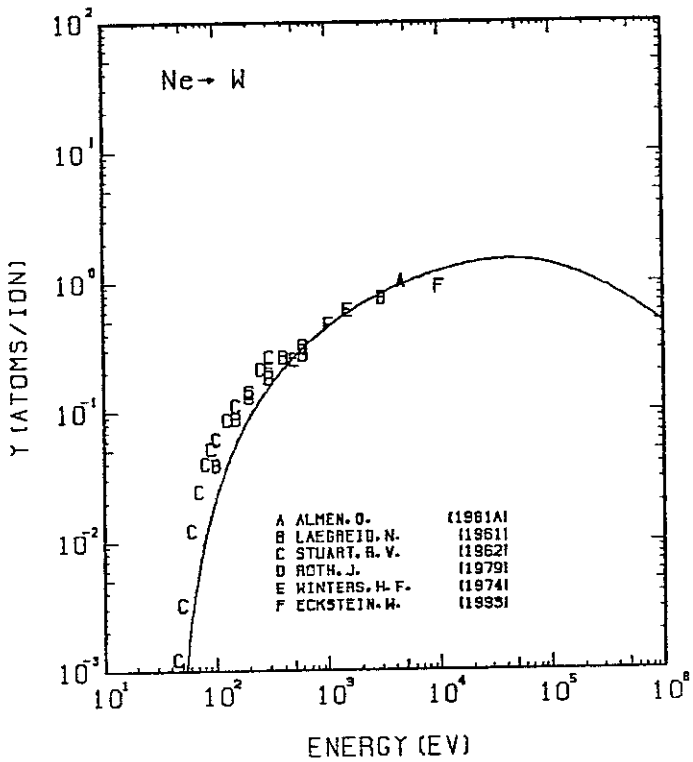


FIG. 261 ENERGY DEPENDENCE OF THE SPUTTERING YIELD OF W WITH $NE^+$.
A= 9.11, D= 0.72, Us= 8.90EV, s= 2.80.
W= 0.24Us.

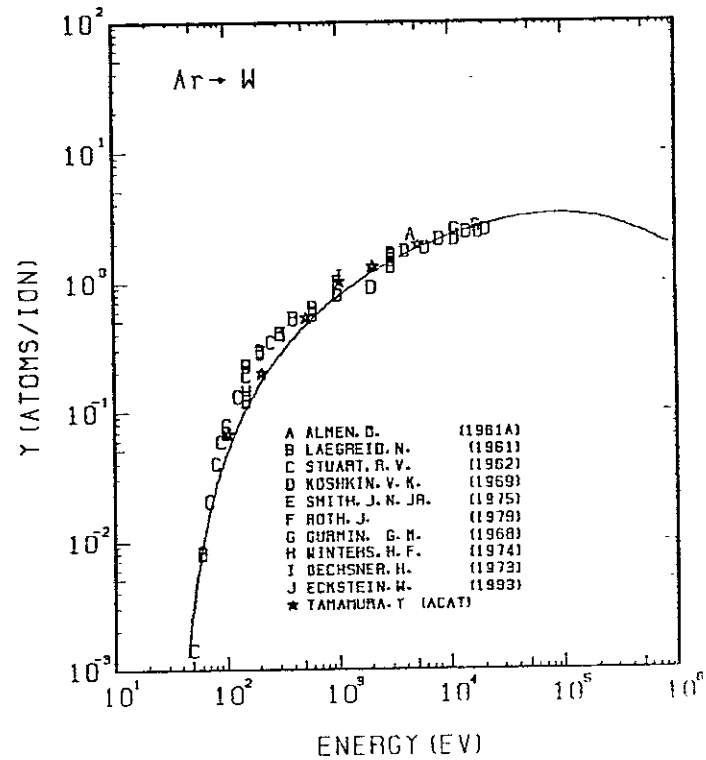


FIG. 262 ENERGY DEPENDENCE OF THE SPUTTERING YIELD OF W WITH $AR^+$.
A= 4.60, D= 0.72, Us= 8.90EV, s= 2.80.
W= 0.24Us.

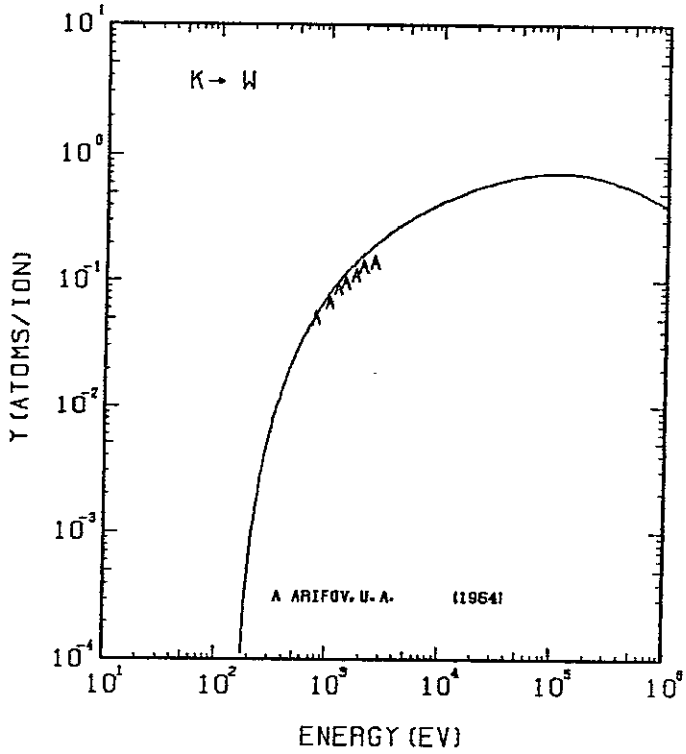


FIG. 263 ENERGY DEPENDENCE OF THE SPUTTERING YIELD OF W WITH $K^+$.
A= 4.70, D= 0.72, Us= 39.16EV, S= 2.80,
W= 0.24Us. THE BEST-FIT SURFACE BINDING ENERGY IS USED.

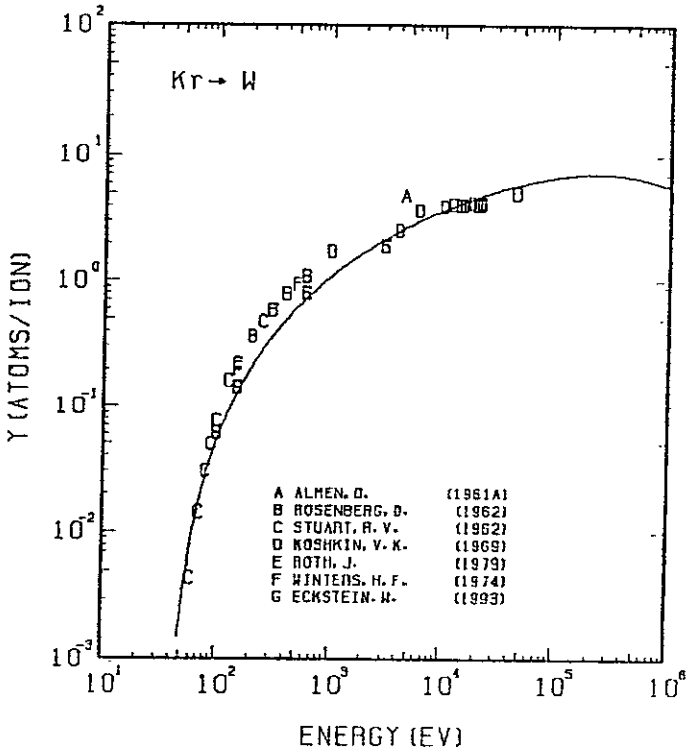


FIG. 264 ENERGY DEPENDENCE OF THE SPUTTERING YIELD OF W WITH $KR^+$.
A= 2.19, D= 0.72, Us= 8.90EV, S= 2.80,
W= 0.24Us.

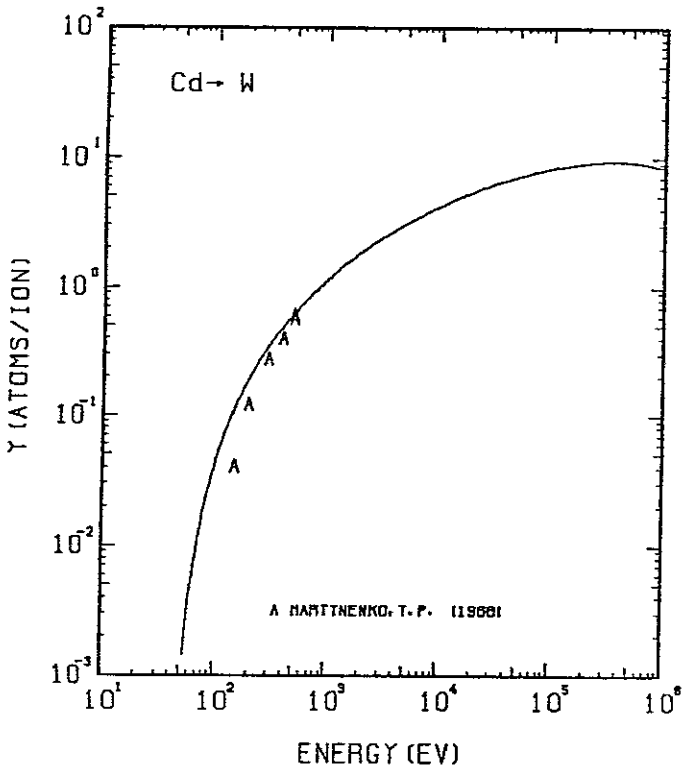


FIG. 265 ENERGY DEPENDENCE OF THE SPUTTERING YIELD OF W WITH $CD^+$.
A= 1.64, D= 0.72, Us= 8.90EV, S= 2.80,
W= 0.24Us.

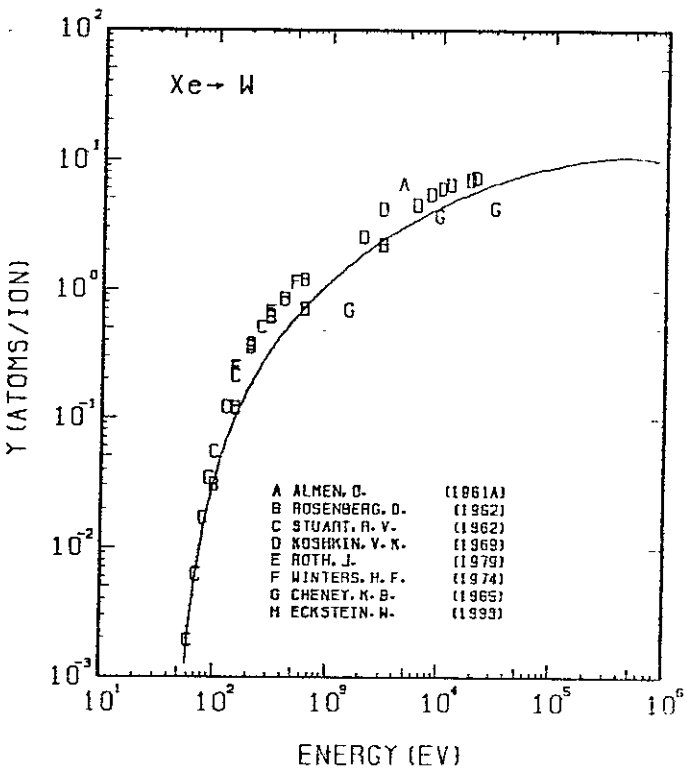


FIG. 266 ENERGY DEPENDENCE OF THE SPUTTERING YIELD OF W WITH $XE^+$.
A= 1.40, D= 0.72, Us= 8.90EV, S= 2.80,
W= 0.24Us.

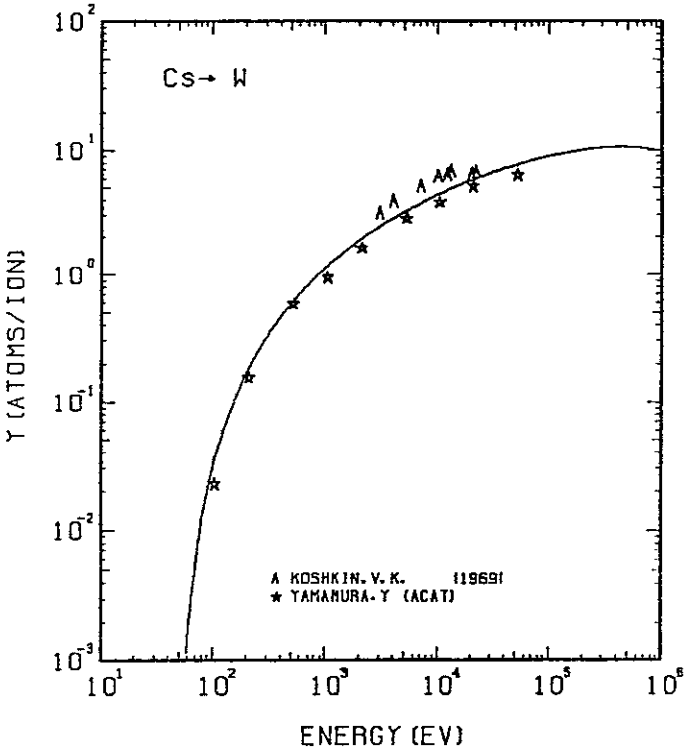


FIG. 267 ENERGY DEPENDENCE OF THE SPUTTERING YIELD OF W WITH $CS^+$.
A= 1.38, D= 0.72, Us= 8.90EV, S= 2.80,
W= 0.24Us.

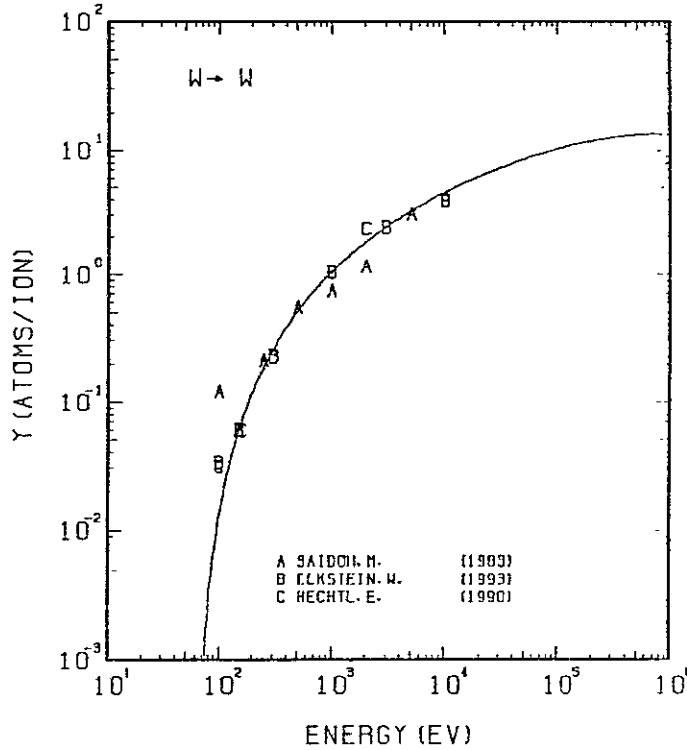


FIG. 268 ENERGY DEPENDENCE OF THE SPUTTERING YIELD OF W WITH $W^+$.
A= 1.00, D= 0.72, Us= 8.90EV, S= 2.80,
W= 0.24Us.

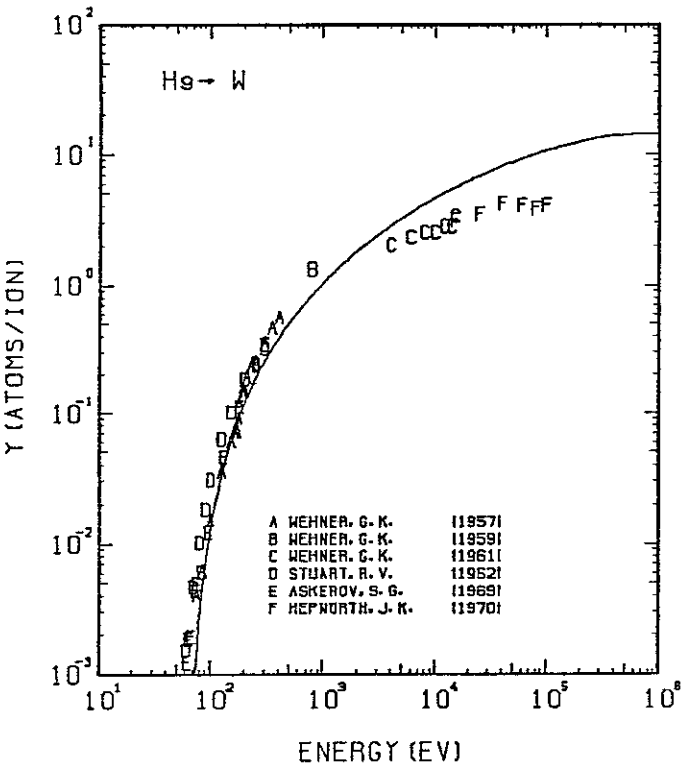


FIG. 269 ENERGY DEPENDENCE OF THE SPUTTERING YIELD OF W WITH $HG^+$.
A= 0.92, D= 0.72, Us= 8.90EV, S= 2.80,
W= 0.24Us.

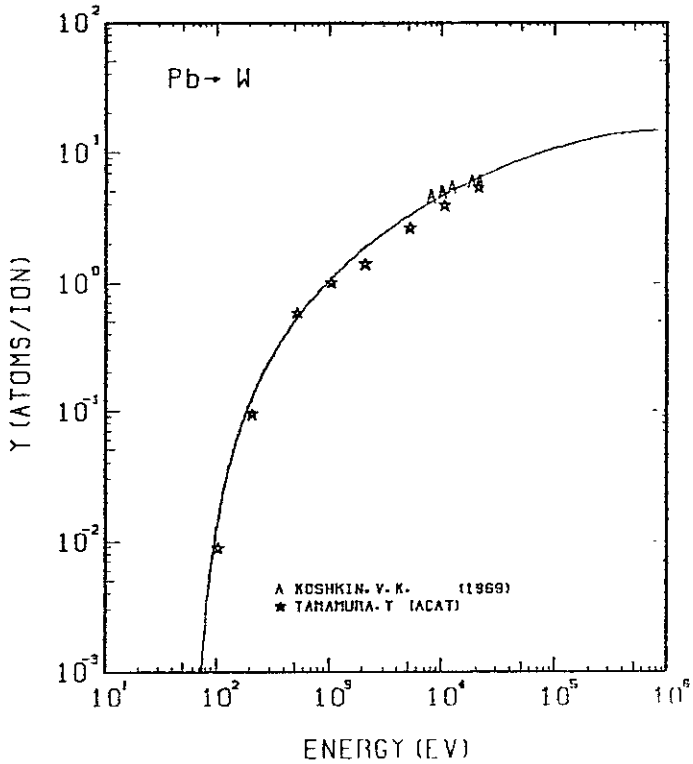


FIG. 270 ENERGY DEPENDENCE OF THE SPUTTERING YIELD OF W WITH $PB^+$.
A= 0.89, D= 0.72, Us= 8.90EV, S= 2.80,
W= 0.24Us.

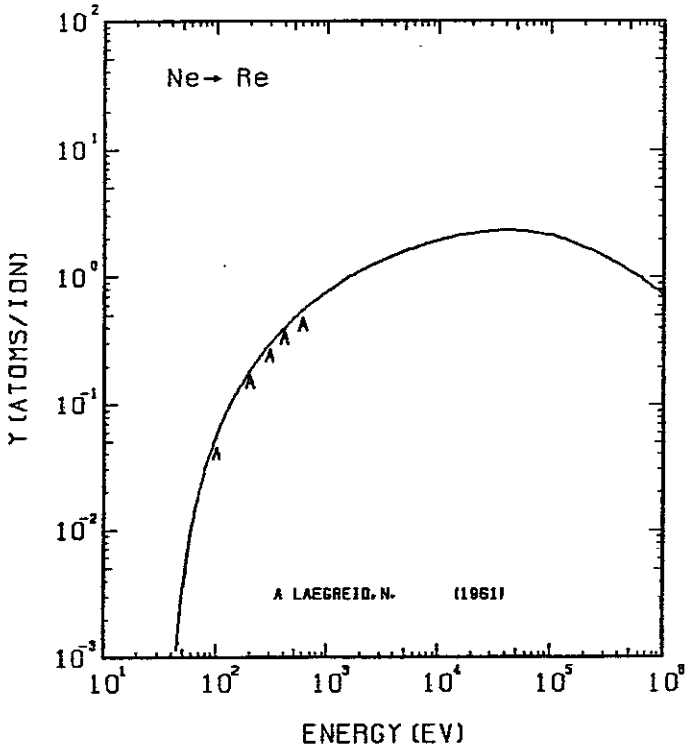


FIG. 271 ENERGY DEPENDENCE OF THE SPUTTERING YIELD OF RE WITH NE+.
A= 9.23, Q= 1.03, Us= 8.03EV, s= 2.50,
W= 0.35Us.

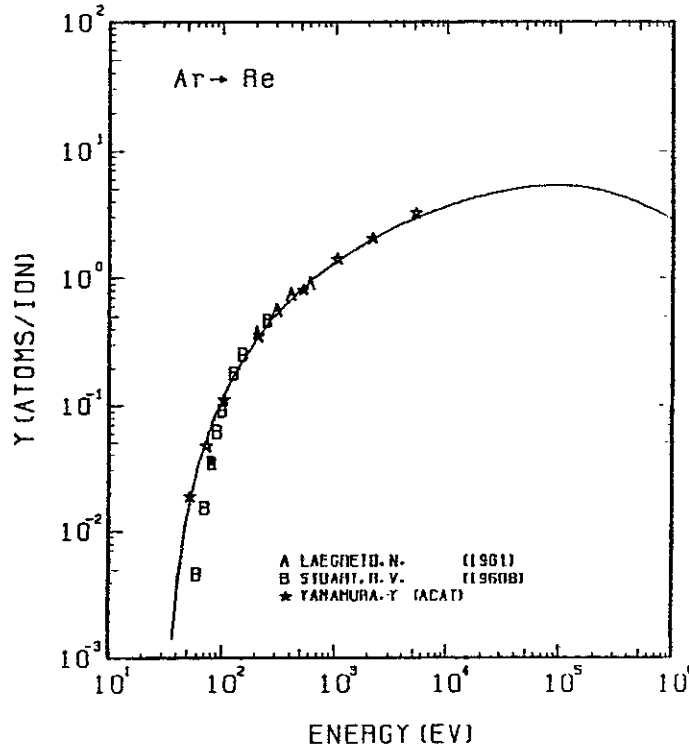


FIG. 272 ENERGY DEPENDENCE OF THE SPUTTERING YIELD OF RE WITH AR+.
A= 4.66, Q= 1.03, Us= 8.03EV, s= 2.50,
W= 0.35Us.

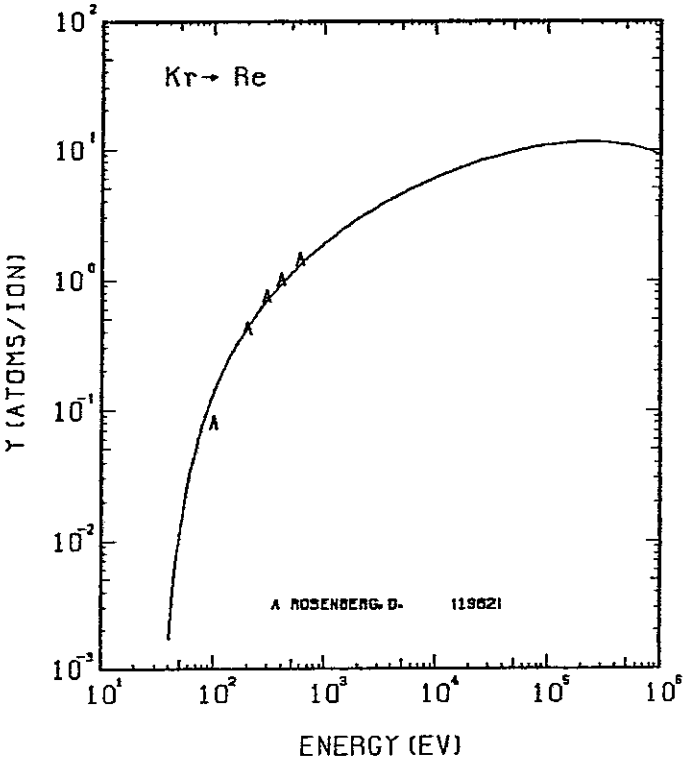


FIG. 273 ENERGY DEPENDENCE OF THE SPUTTERING YIELD OF RE WITH KR+.
A= 2.22, Q= 1.03, Us= 8.03EV, s= 2.50,
W= 0.35Us.

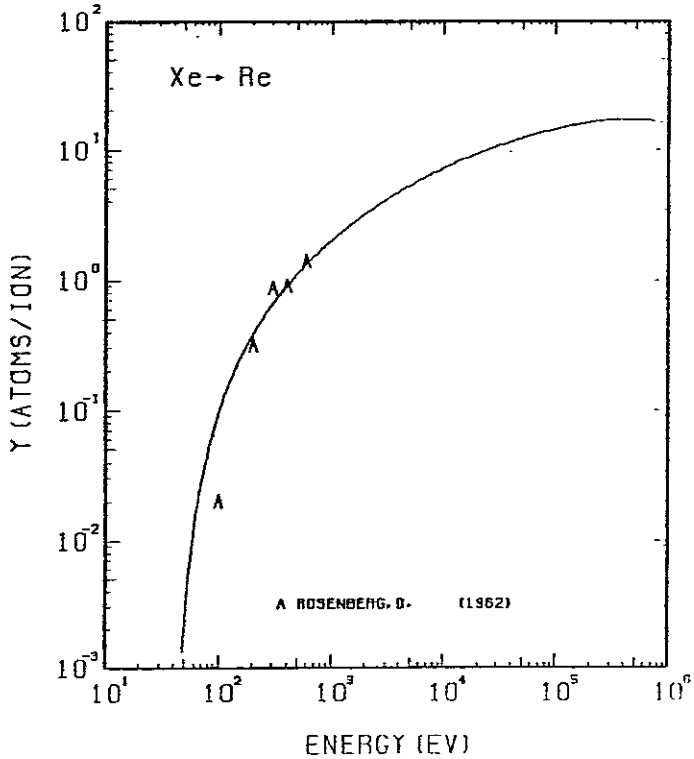


FIG. 274 ENERGY DEPENDENCE OF THE SPUTTERING YIELD OF RE WITH XE+.
A= 1.42, Q= 1.03, Us= 8.03EV, s= 2.50,
W= 0.35Us.

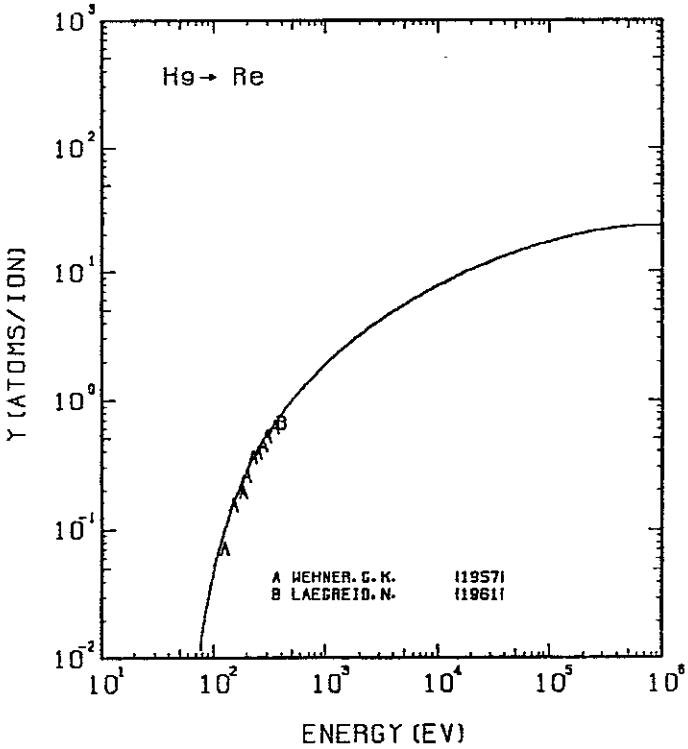


FIG. 275 ENERGY DEPENDENCE OF THE SPUTTERING YIELD OF RE WITH $HG^+$.
A= 0.93, 0= 1.03, Us= 8.03EV, s= 2.50.
W= 0.35Us.

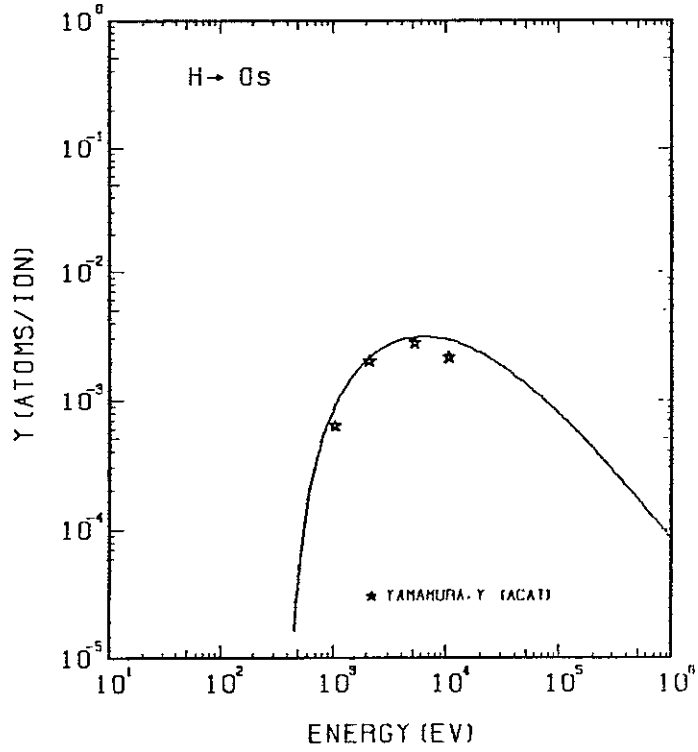


FIG. 276 ENERGY DEPENDENCE OF THE SPUTTERING YIELD OF OS WITH $H^+$.
A= 188.69, 0= 1.11, Us= 8.17EV, s= 2.50.
W= 0.35Us.

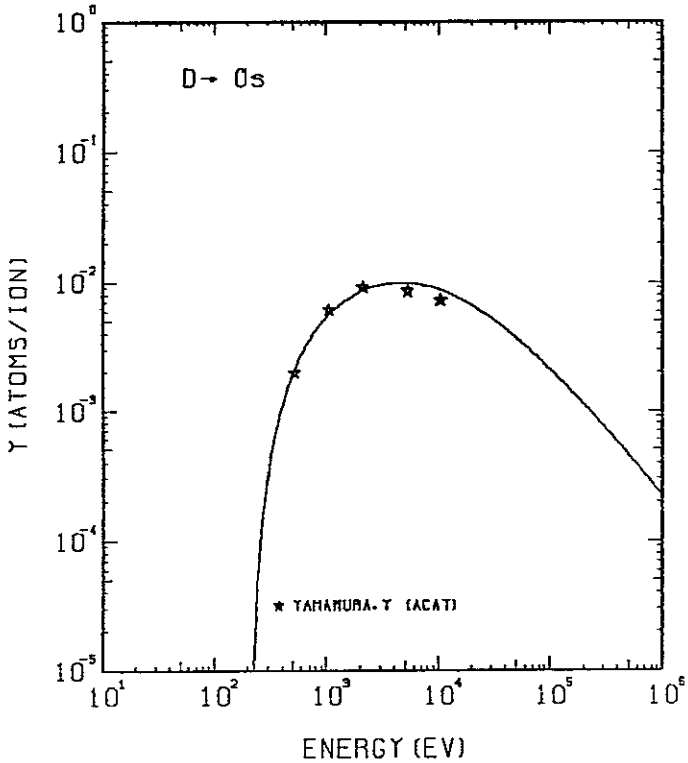


FIG. 277 ENERGY DEPENDENCE OF THE SPUTTERING YIELD OF OS WITH $D^+$.
A= 94.44, 0= 1.11, Us= 8.17EV, s= 2.50.
W= 0.35Us.

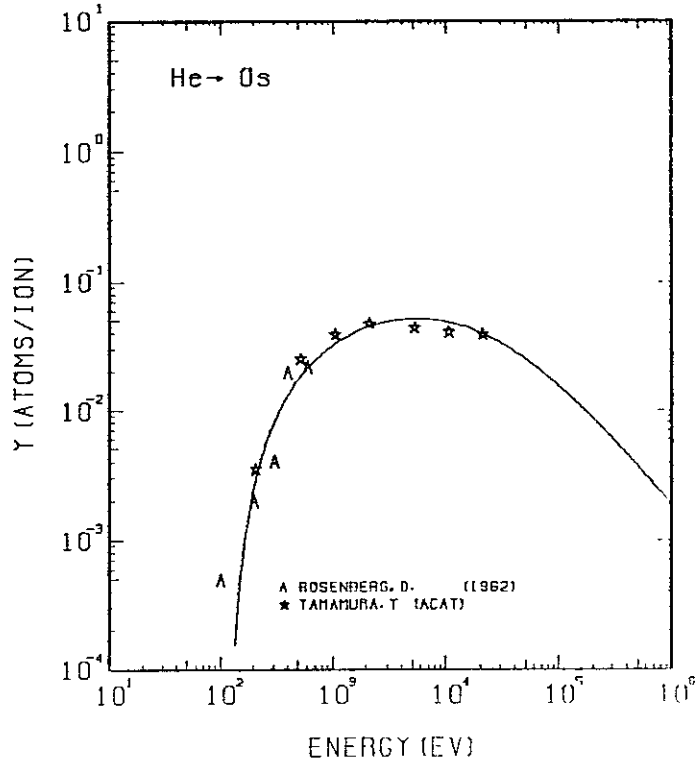


FIG. 278 ENERGY DEPENDENCE OF THE SPUTTERING YIELD OF OS WITH $HE^+$.
A= 47.51, 0= 1.11, Us= 8.17EV, s= 2.50.
W= 0.35Us.

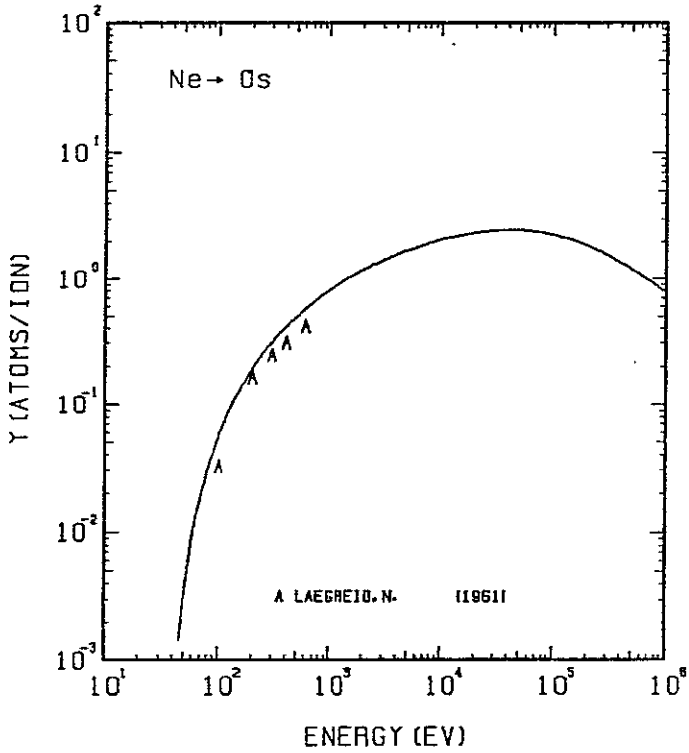


FIG. 279 ENERGY DEPENDENCE OF THE SPUTTERING YIELD OF OS WITH $NE^+$.
A= 9.43, Q= 1.11, Us= 8.17EV, s= 2.50.
W= 0.35Us.

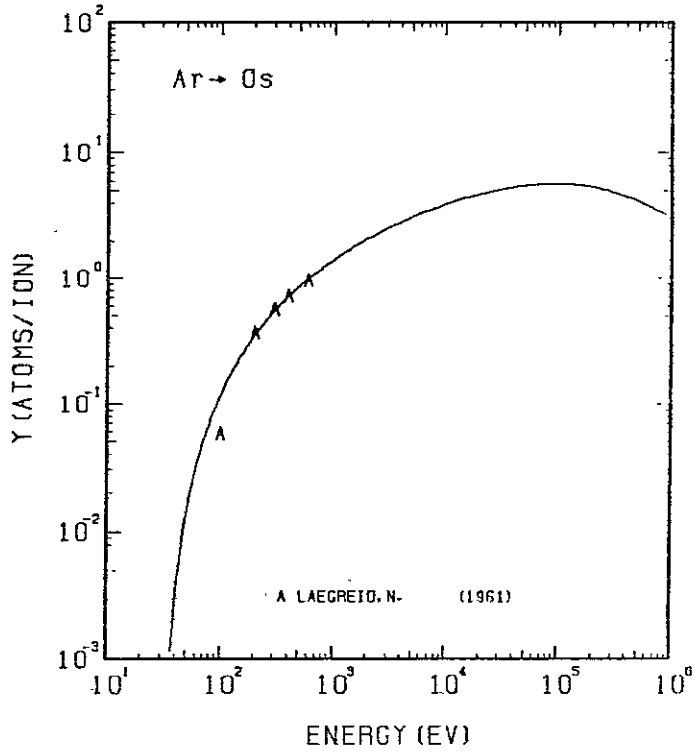


FIG. 280 ENERGY DEPENDENCE OF THE SPUTTERING YIELD OF OS WITH $AR^+$.
A= 4.76, Q= 1.11, Us= 8.17EV, s= 2.50.
W= 0.35Us.

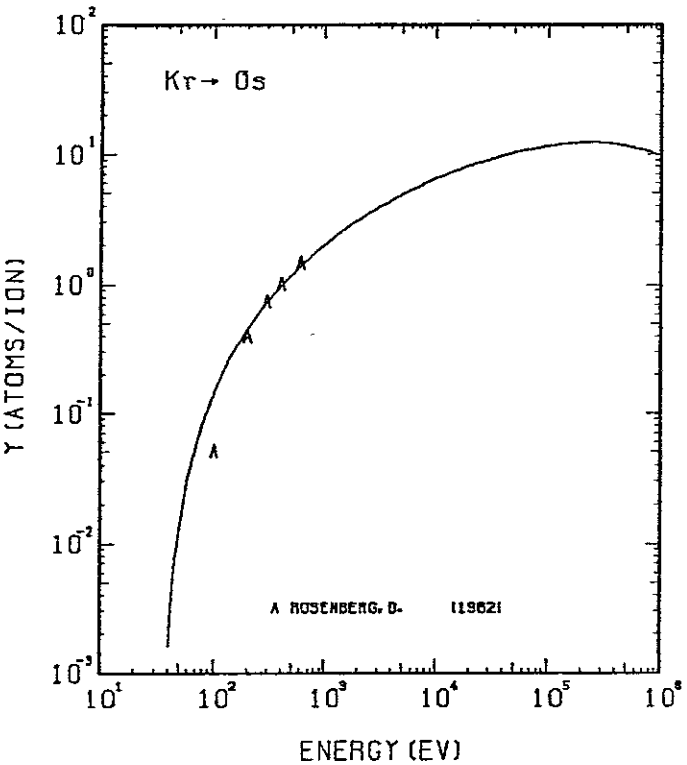


FIG. 281 ENERGY DEPENDENCE OF THE SPUTTERING YIELD OF OS WITH $KR^+$.
A= 2.27, Q= 1.11, Us= 8.17EV, s= 2.50,
W= 0.35Us.

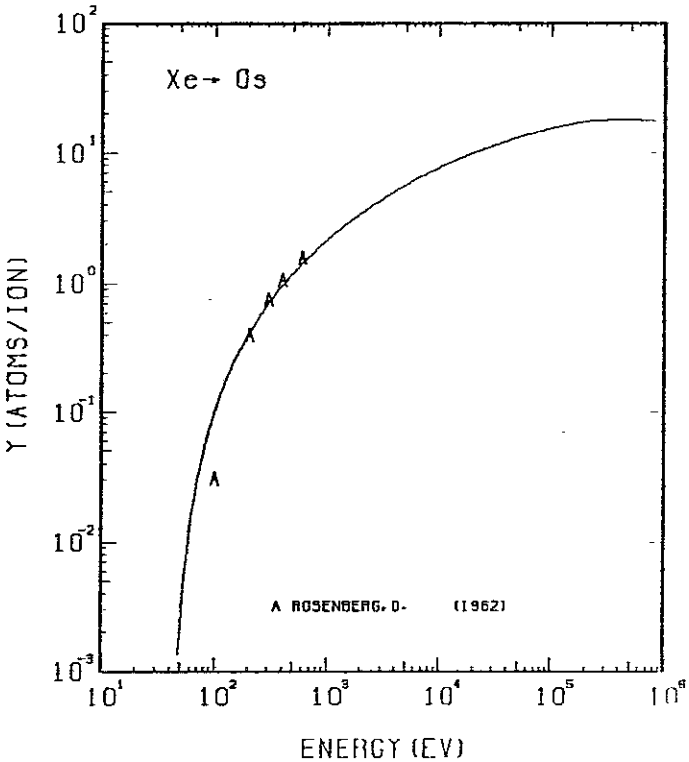


FIG. 282 ENERGY DEPENDENCE OF THE SPUTTERING YIELD OF OS WITH $XE^+$.
A= 1.45, Q= 1.11, Us= 8.17EV, s= 2.50,
W= 0.35Us.

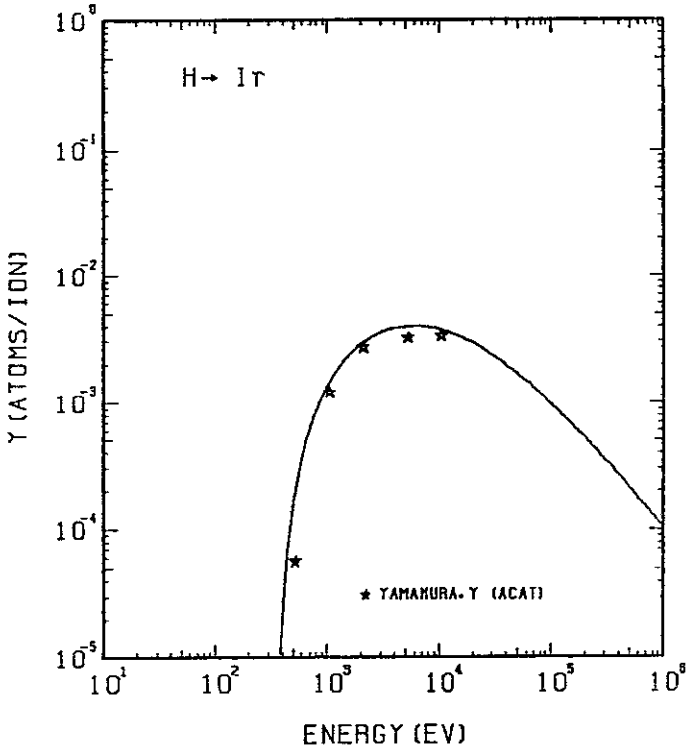


FIG. 283 ENERGY DEPENDENCE OF THE SPUTTERING YIELD OF IR WITH $H^+$.
A= 190.67, D= 0.96, Us= 6.94EV, s= 2.50,
W= 0.35Us.

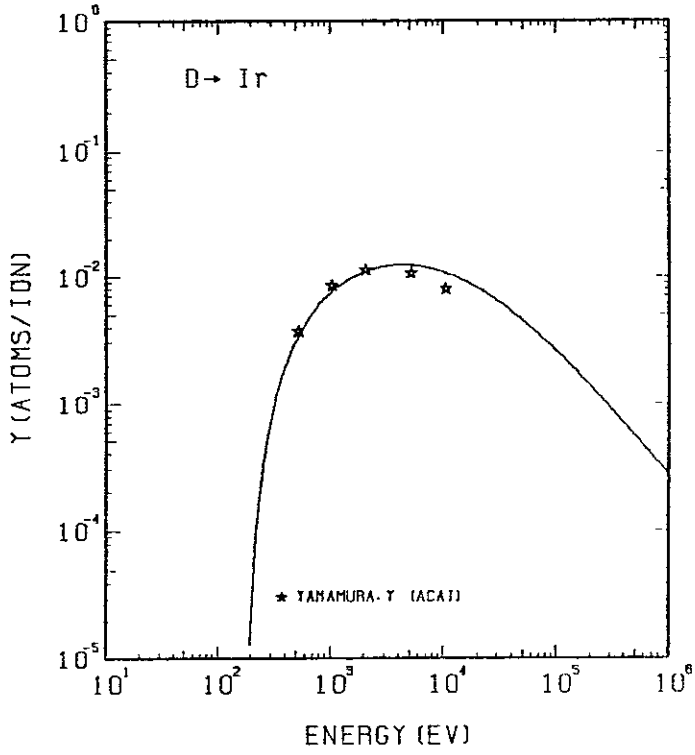


FIG. 284 ENERGY DEPENDENCE OF THE SPUTTERING YIELD OF IR WITH $D^+$.
A= 95.43, D= 0.96, Us= 6.94EV, s= 2.50,
W= 0.35Us.

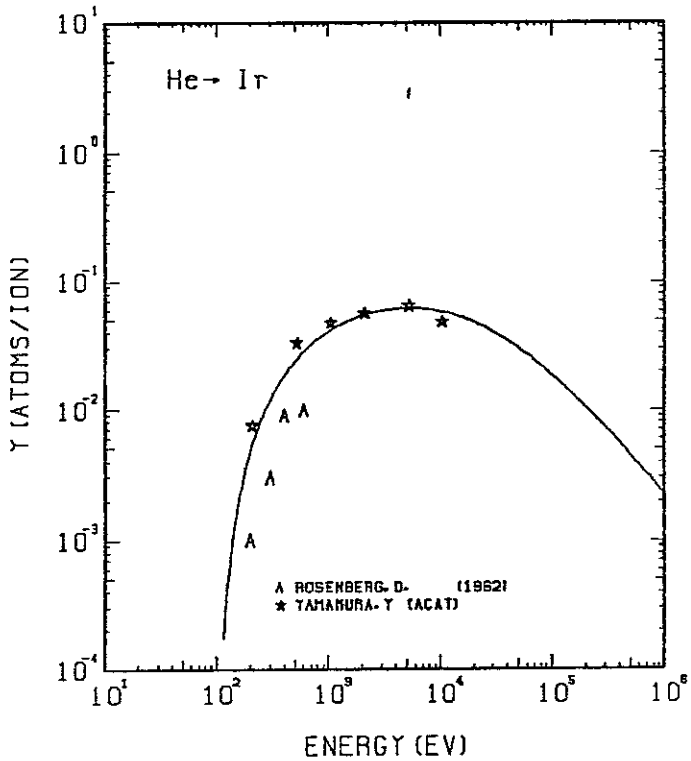


FIG. 285 ENERGY DEPENDENCE OF THE SPUTTERING YIELD OF IR WITH $HE^+$.
A= 48.01, D= 0.96, Us= 6.94EV, s= 2.50,
W= 0.35Us.

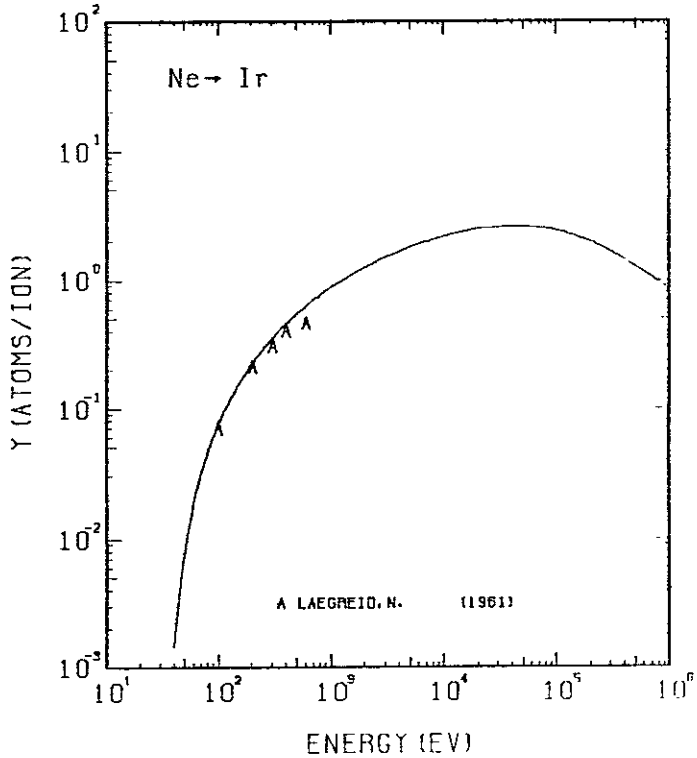


FIG. 286 ENERGY DEPENDENCE OF THE SPUTTERING YIELD OF IR WITH $NE^+$.
A= 9.52, D= 0.96, Us= 6.94EV, s= 2.50,
W= 0.35Us.

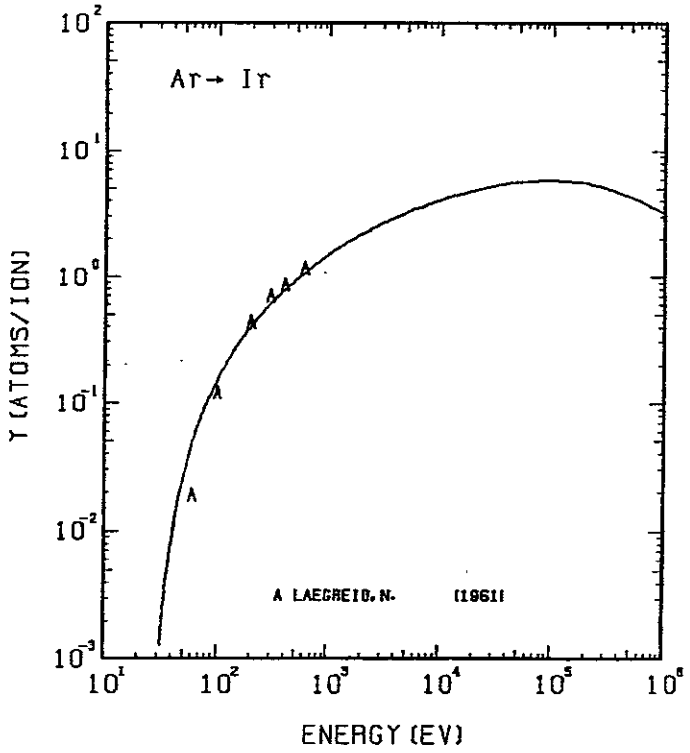


FIG. 287 ENERGY DEPENDENCE OF THE SPUTTERING YIELD OF IR WITH $AR^+$.
A= 4.81, D= 0.96, Us= 6.94EV, S= 2.50,
W= 0.35Us.

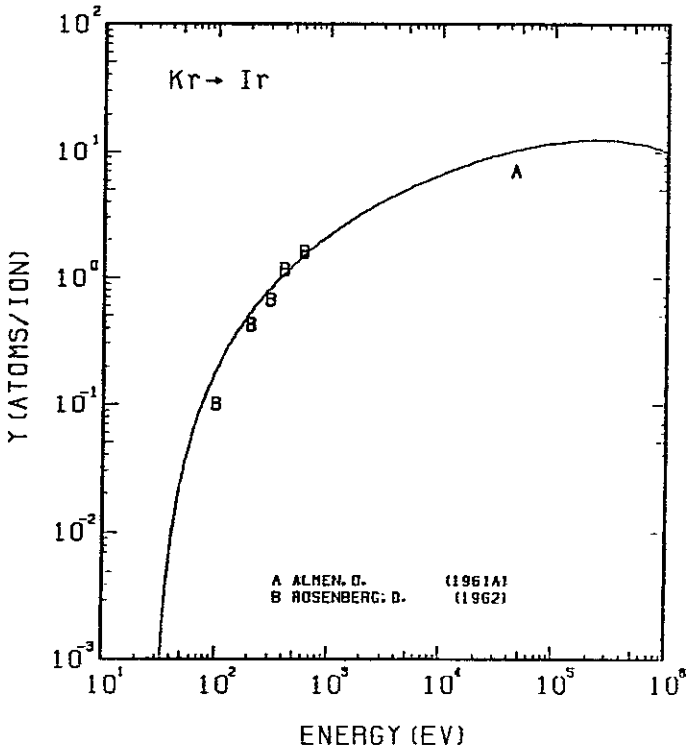


FIG. 288 ENERGY DEPENDENCE OF THE SPUTTERING YIELD OF IR WITH $KR^+$.
A= 2.29, D= 0.96, Us= 6.94EV, S= 2.50,
W= 0.35Us.

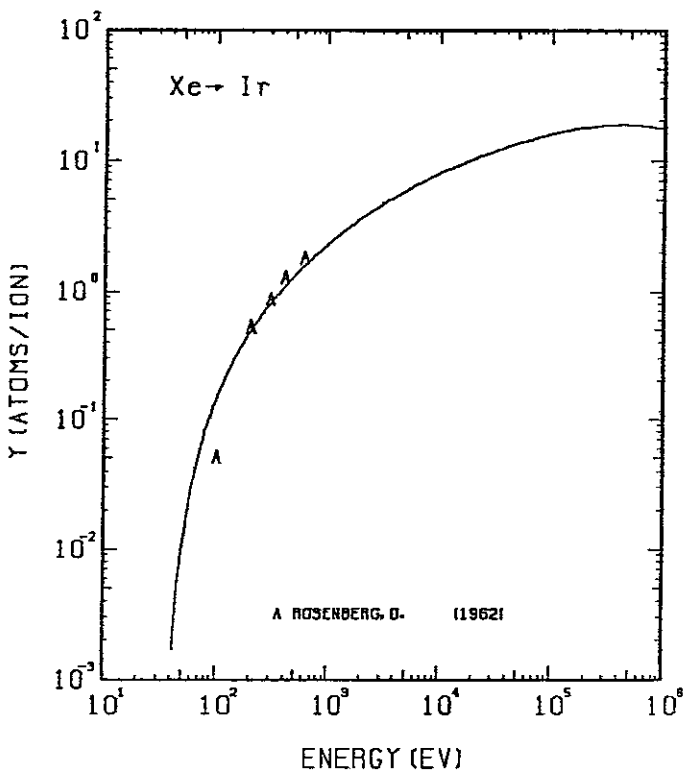


FIG. 289 ENERGY DEPENDENCE OF THE SPUTTERING YIELD OF IR WITH $XE^+$.
A= 1.46, D= 0.96, Us= 6.94EV, S= 2.50,
W= 0.35Us.

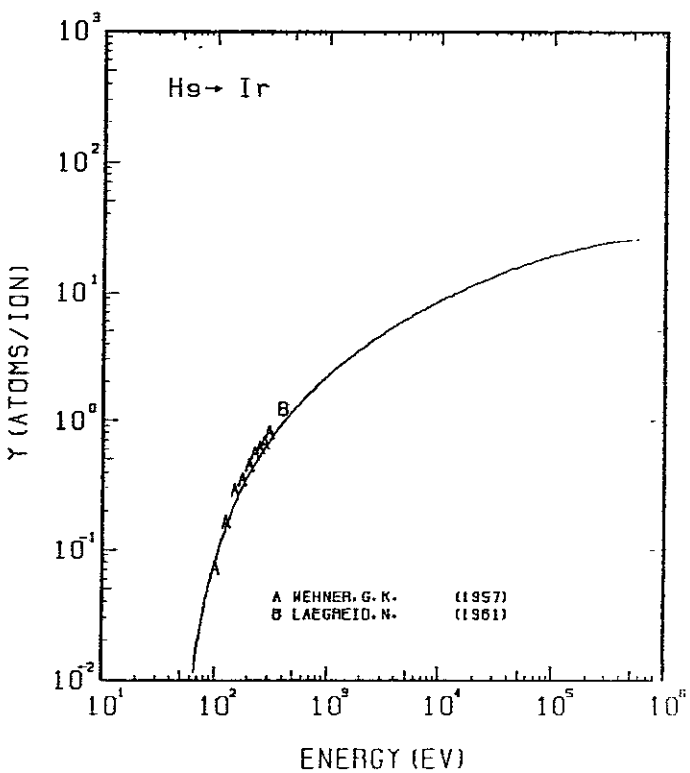


FIG. 290 ENERGY DEPENDENCE OF THE SPUTTERING YIELD OF IR WITH $HG^+$.
A= 0.96, D= 0.96, Us= 6.94EV, S= 2.50,
W= 0.35Us.

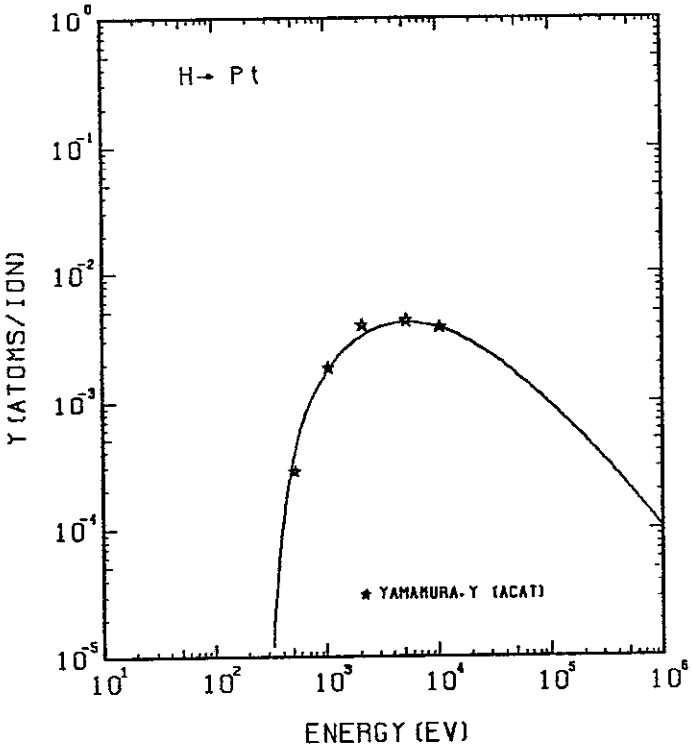


FIG. 291 ENERGY DEPENDENCE OF THE SPUTTERING YIELD OF PT WITH $H^+$.
A= 193.45, Q= 1.03, Us= 5.84EV, s= 2.50,
W= 0.55Us.

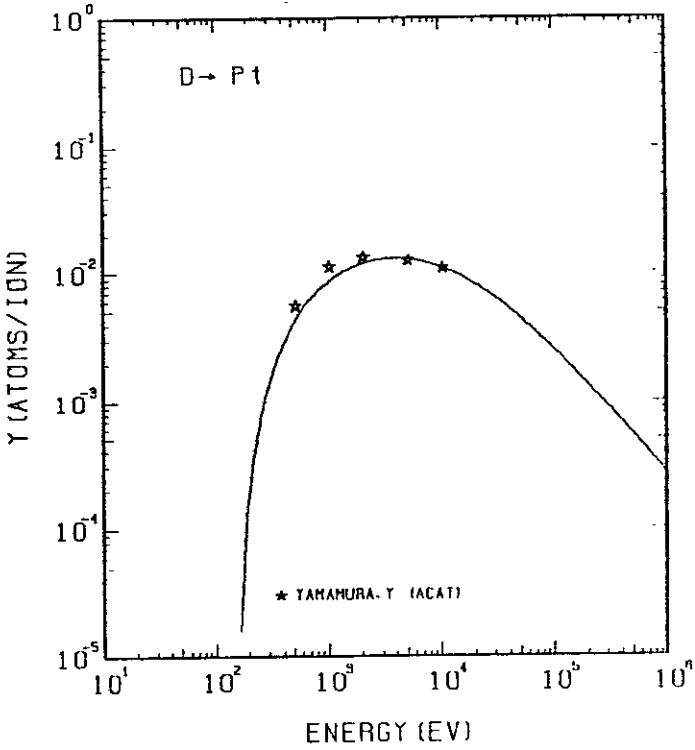


FIG. 292 ENERGY DEPENDENCE OF THE SPUTTERING YIELD OF PT WITH $D^+$.
A= 96.82, Q= 1.03, Us= 5.84EV, s= 2.50,
W= 0.55Us.

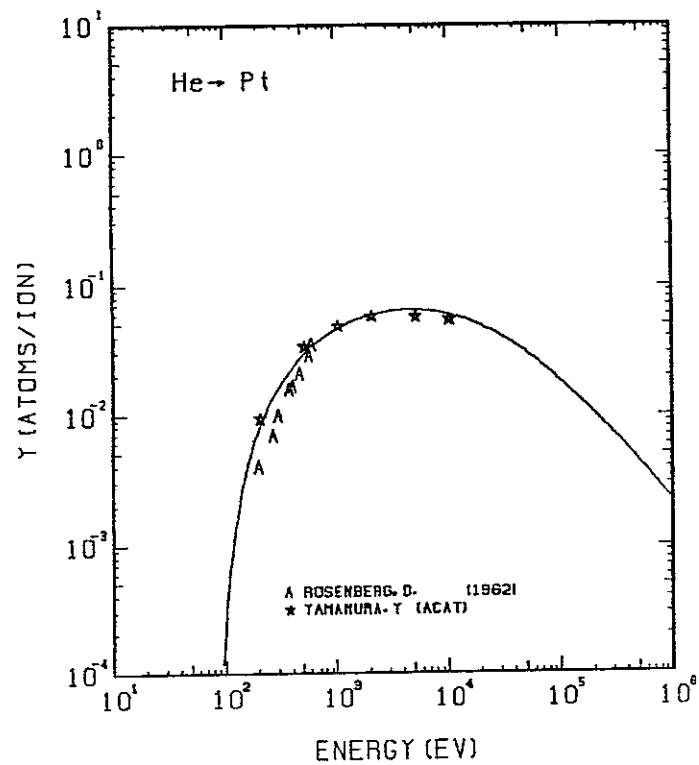


FIG. 293 ENERGY DEPENDENCE OF THE SPUTTERING YIELD OF PT WITH $HE^+$.
A= 48.71, Q= 1.03, Us= 5.84EV, s= 2.50,
W= 0.55Us.

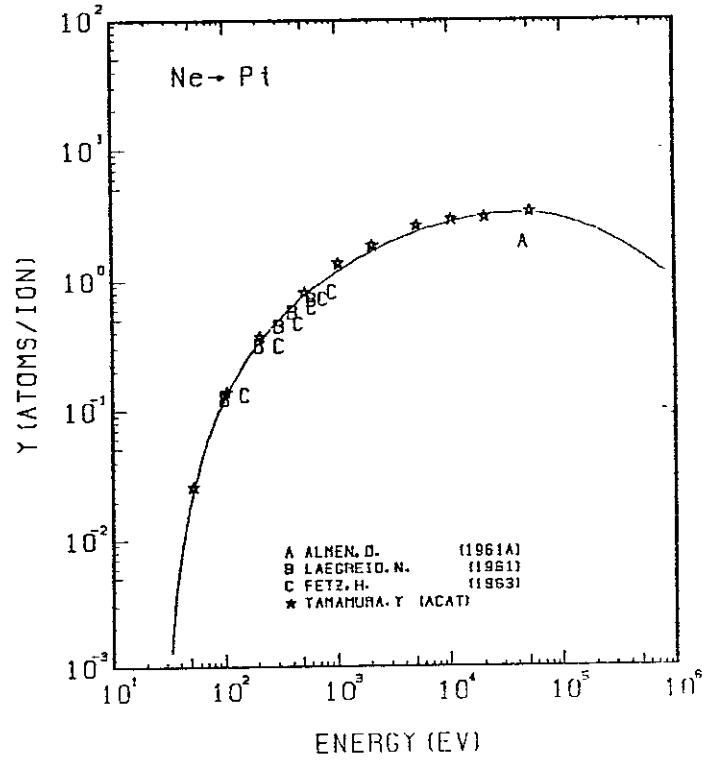


FIG. 294 ENERGY DEPENDENCE OF THE SPUTTERING YIELD OF PT WITH $NE^+$.
A= 9.66, Q= 1.03, Us= 5.84EV, s= 2.50,
W= 0.55Us.

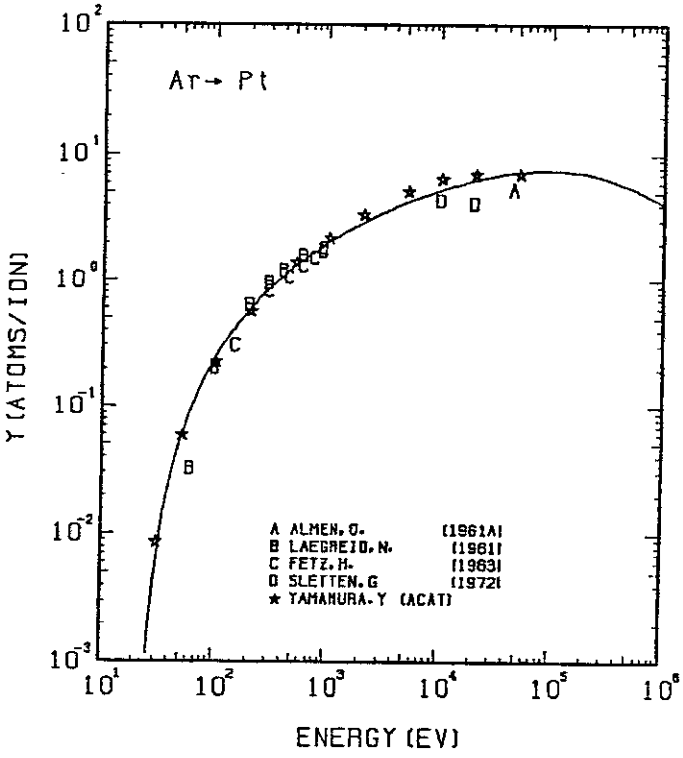


FIG. 295 ENERGY DEPENDENCE OF THE SPUTTERING YIELD OF PT WITH $AR^+$.
A= 4.88, D= 1.03, Us= 5.84EV, S= 2.50, W= 0.55Us.

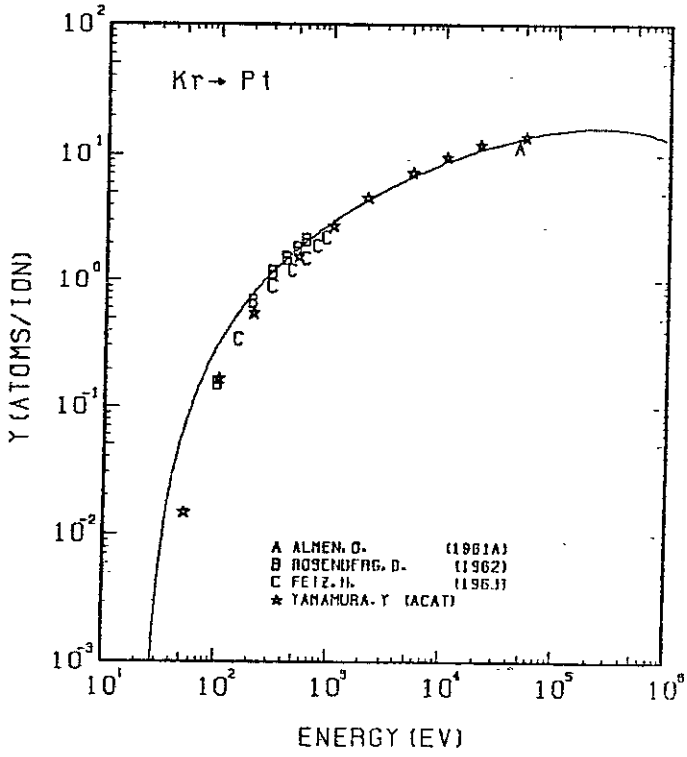


FIG. 296 ENERGY DEPENDENCE OF THE SPUTTERING YIELD OF PT WITH $KR^+$.
A= 2.33, D= 1.03, Us= 5.84EV, S= 2.50, W= 0.55Us.

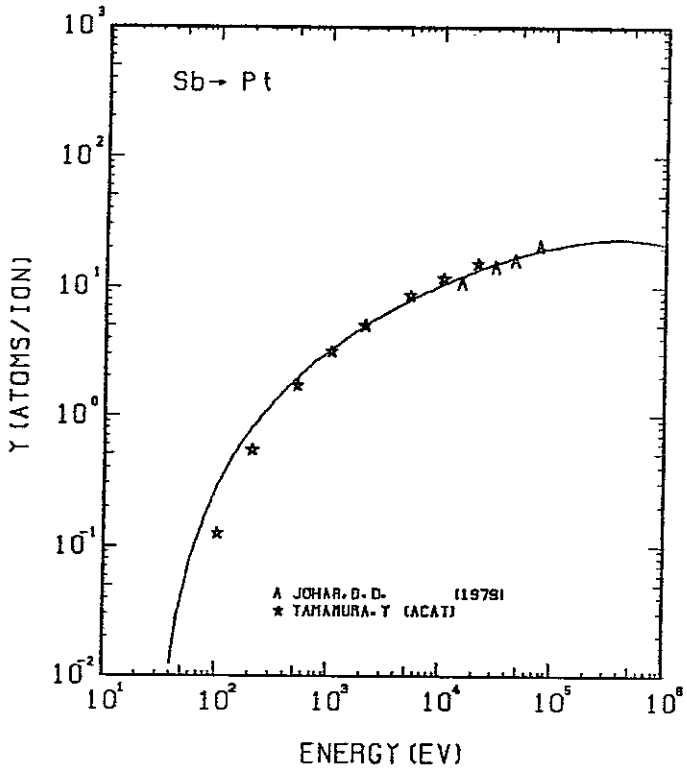


FIG. 297 ENERGY DEPENDENCE OF THE SPUTTERING YIELD OF PT WITH $SB^+$.
A= 1.60, D= 1.03, Us= 5.84EV, S= 2.50, W= 0.55Us.

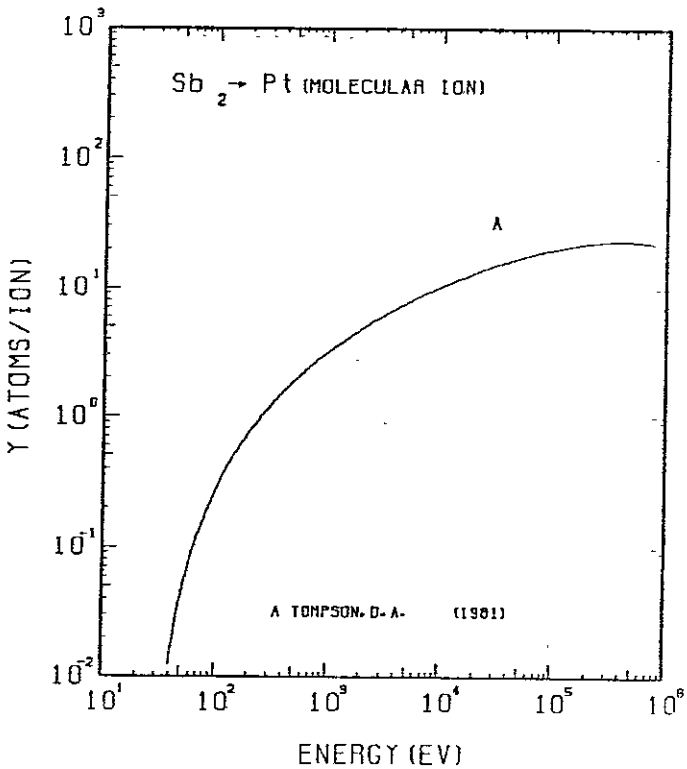


FIG. 298 ENERGY DEPENDENCE OF THE SPUTTERING YIELD OF PT WITH $SB_2^+$.
A= 1.60, D= 1.03, Us= 5.84EV, S= 2.50, W= 0.55Us. THE NON-LINEAR EFFECT IS OBSERVED DUE TO MOLECULAR IONS.

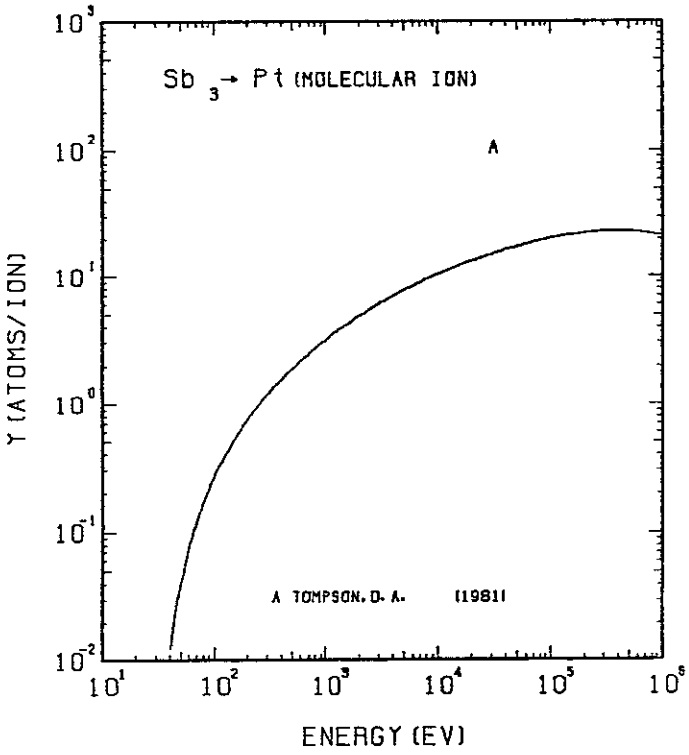


FIG. 299 ENERGY DEPENDENCE OF THE SPUTTERING YIELD OF PT WITH SB $_3^+$.
A= 1.60, D= 1.03, Us= 5.84EV, S= 2.50,
W= 0.55Us. THE NON-LINEAR EFFECT
IS OBSERVED DUE TO MOLECULAR IONS.

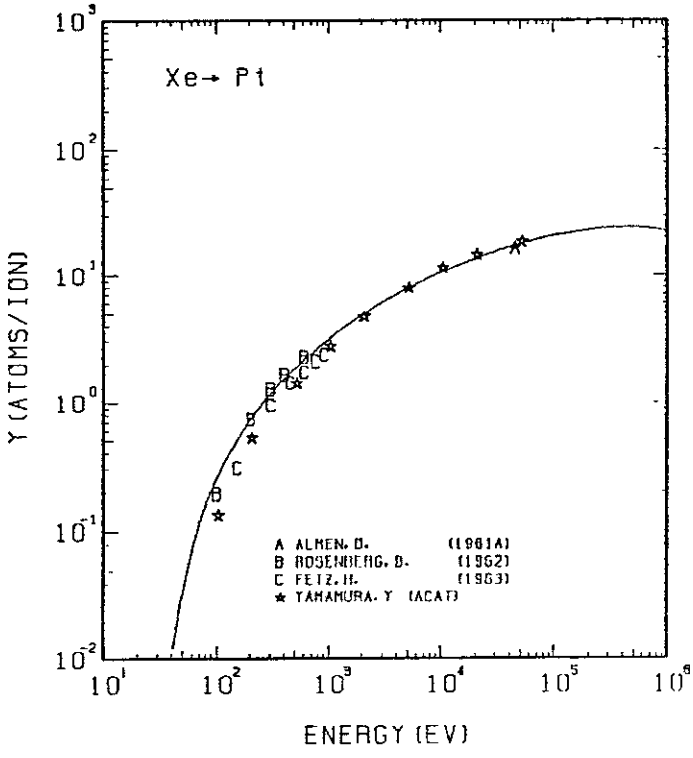


FIG. 300 ENERGY DEPENDENCE OF THE SPUTTERING YIELD OF PT WITH XE$^+$.
A= 1.49, D= 1.03, Us= 5.84EV, S= 2.50,
W= 0.55Us.

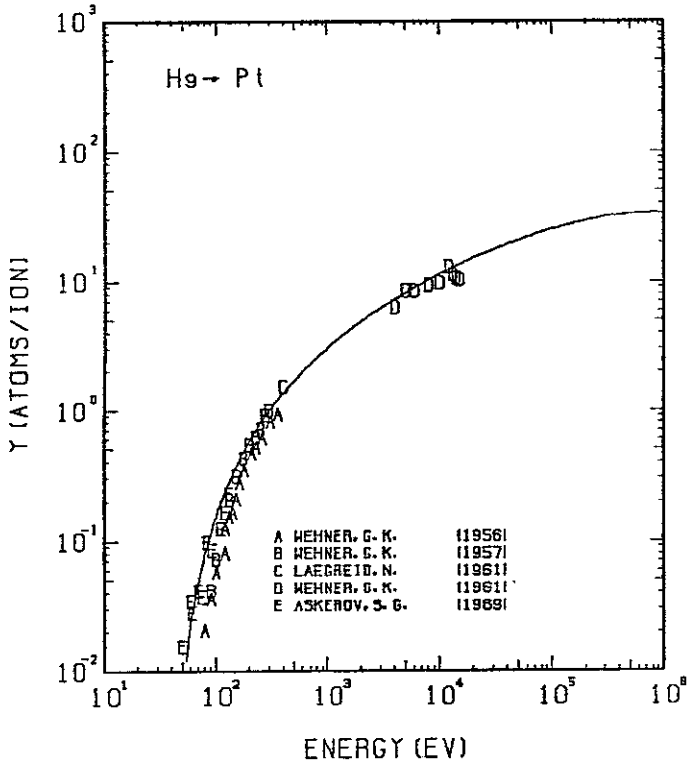


FIG. 301 ENERGY DEPENDENCE OF THE SPUTTERING YIELD OF PT WITH HG$^+$.
A= 0.97, D= 1.03, Us= 5.84EV, S= 2.50,
W= 0.55Us.

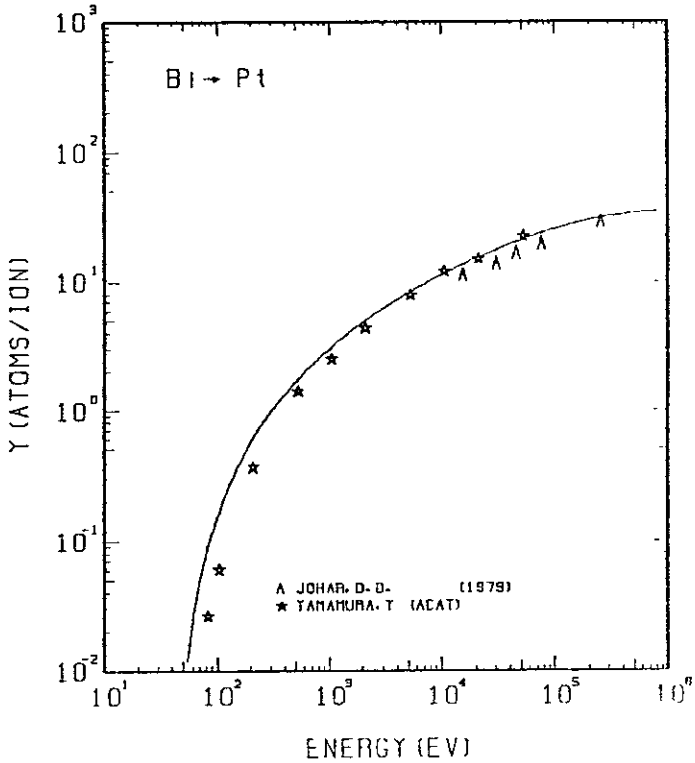


FIG. 302 ENERGY DEPENDENCE OF THE SPUTTERING YIELD OF PT WITH BI$^+$.
A= 0.93, D= 1.03, Us= 5.84EV, S= 2.50,
W= 0.55Us.

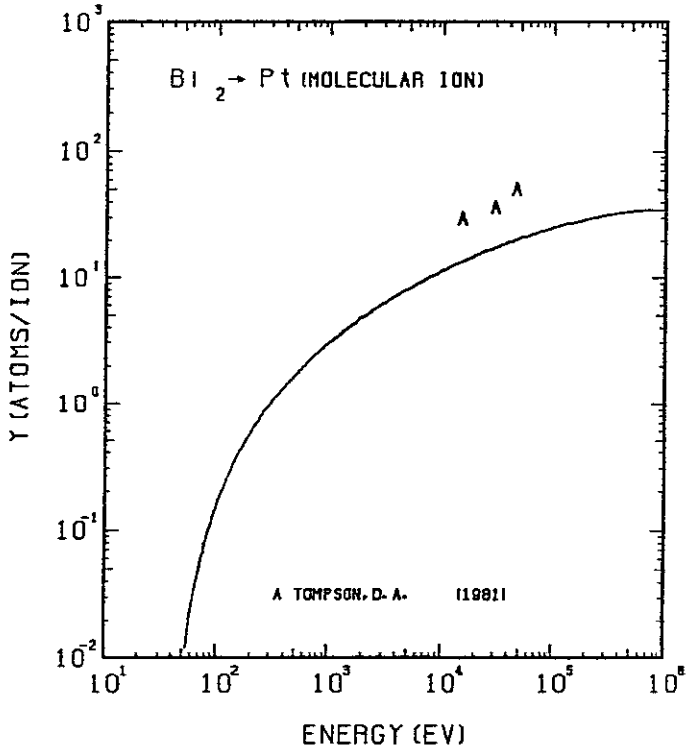


FIG. 303 ENERGY DEPENDENCE OF THE SPUTTERING YIELD OF PT WITH $Bi_2^+$. A= 0.93. 0= 1.03. Us= 5.84EV. s= 2.50. W= 0.55Us. THE NON-LINEAR EFFECT IS OBSERVED DUE TO MOLECULAR IONS.

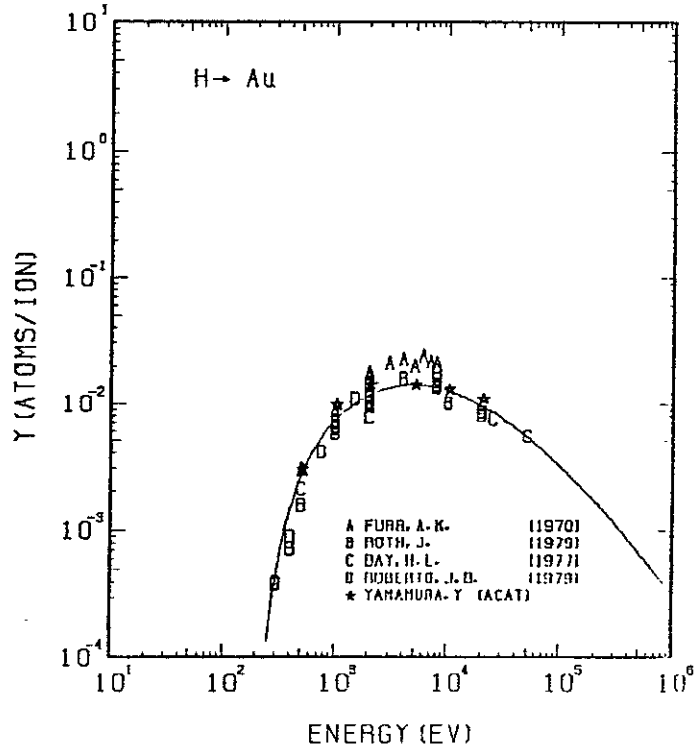


FIG. 304 ENERGY DEPENDENCE OF THE SPUTTERING YIELD OF AU WITH $H^+$. A= 195.34. 0= 1.08. Us= 3.81EV. s= 2.80. W= 0.43Us.

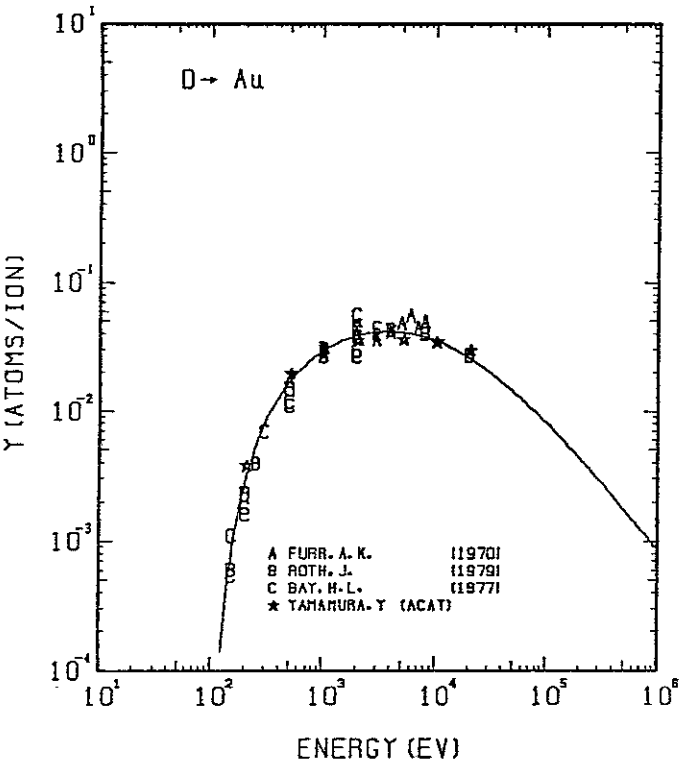


FIG. 305 ENERGY DEPENDENCE OF THE SPUTTERING YIELD OF AU WITH $O^+$. A= 97.77. 0= 1.08. Us= 3.81EV. s= 2.80. W= 0.43Us.

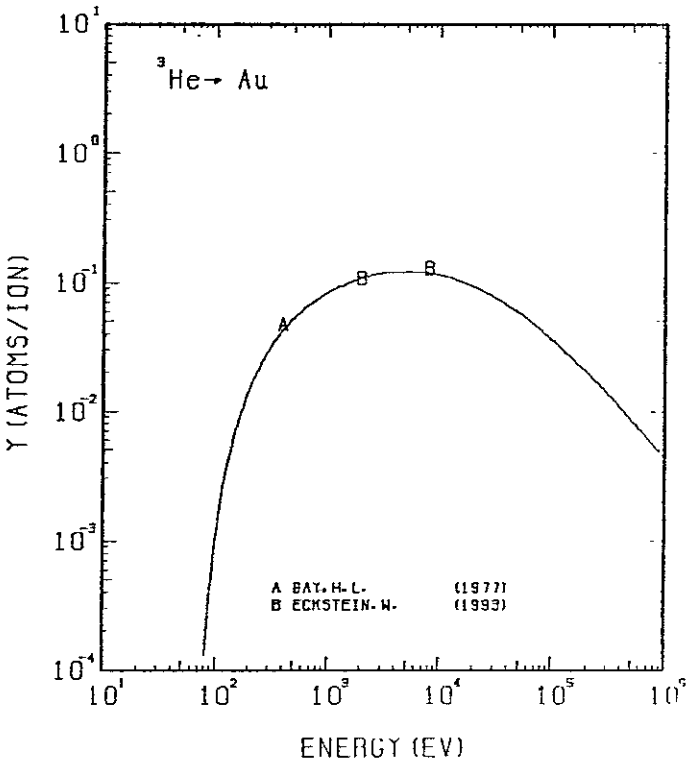


FIG. 306 ENERGY DEPENDENCE OF THE SPUTTERING YIELD OF AU WITH $^3HE^+$. A= 65.29. 0= 1.08. Us= 3.81EV. s= 2.80. W= 0.43Us.

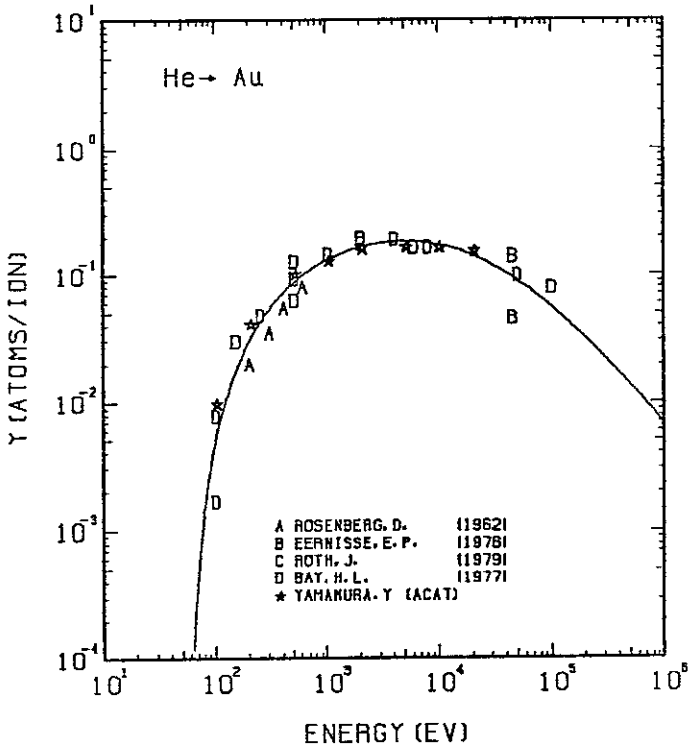


FIG. 307 ENERGY DEPENDENCE OF THE SPUTTERING YIELD OF AU WITH $HE^+$.
A= 49.19, D= 1.08, Us= 3.81EV, S= 2.80, W= 0.43Us.

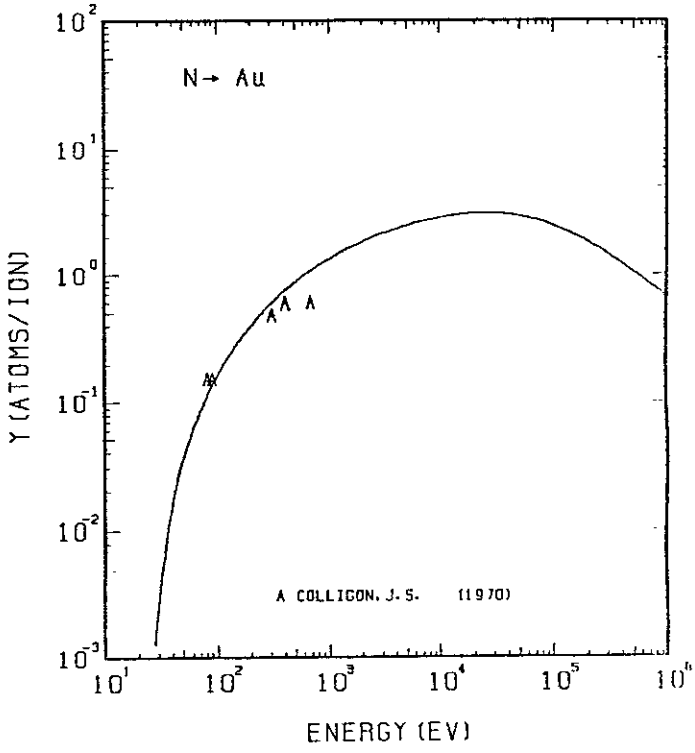


FIG. 308 ENERGY DEPENDENCE OF THE SPUTTERING YIELD OF AU WITH $N^+$.
A= 14.05, D= 1.08, Us= 3.81EV, S= 2.80, W= 0.43Us. THE BEST-FIT SURFACE BINDING ENERGY IS USED.

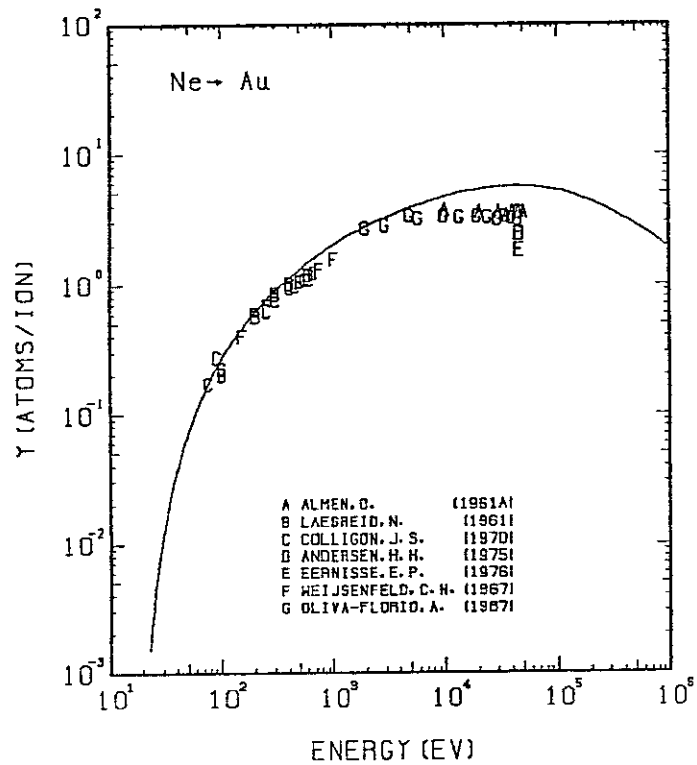


FIG. 309 ENERGY DEPENDENCE OF THE SPUTTERING YIELD OF AU WITH $NE^+$.
A= 9.76, D= 1.08, Us= 3.81EV, S= 2.80, W= 0.43Us.

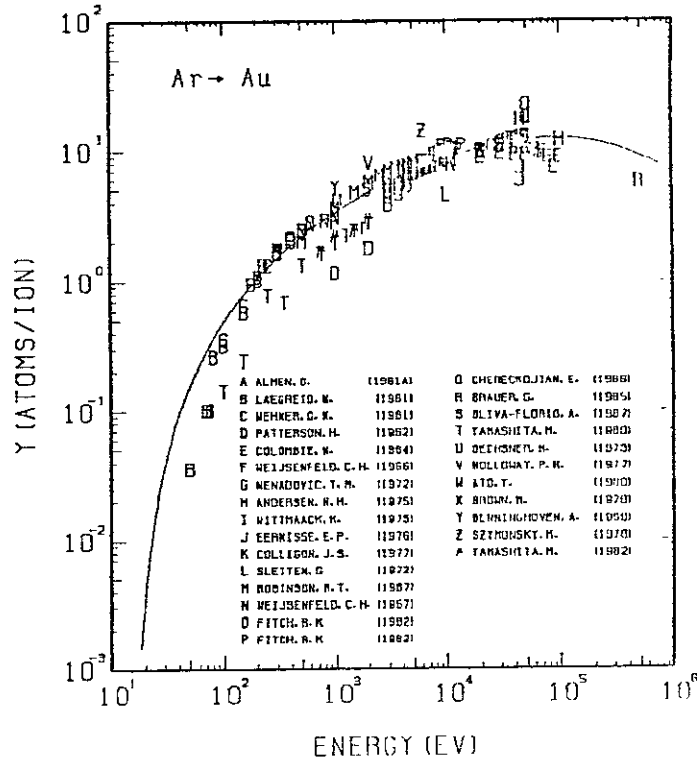


FIG. 310 ENERGY DEPENDENCE OF THE SPUTTERING YIELD OF AU WITH $AR^+$.
A= 4.93, D= 1.08, Us= 3.81EV, S= 2.80, W= 0.43Us.

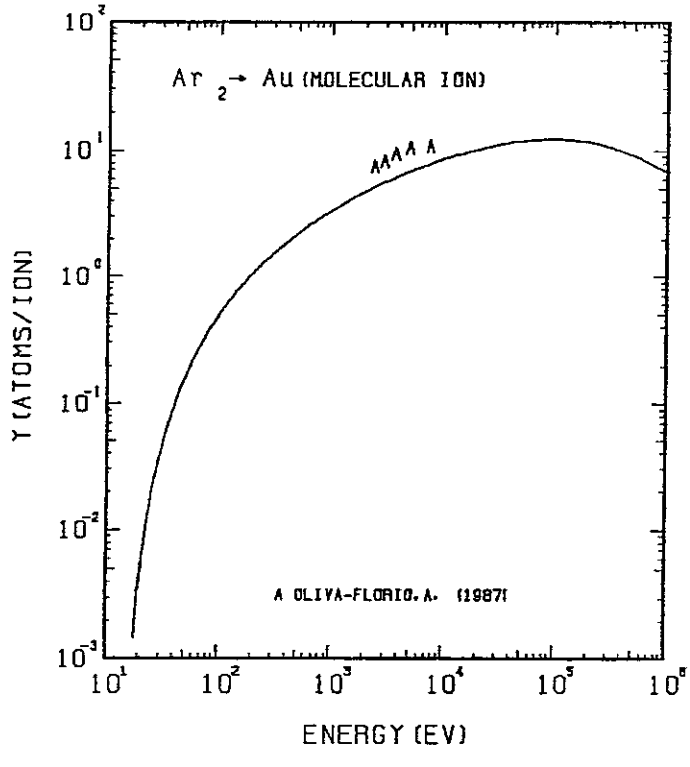


FIG. 311 ENERGY DEPENDENCE OF THE SPUTTERING YIELD OF AU WITH AR $_2^+$.
A= 4.93, D= 1.08, Us= 3.81EV, S= 2.80,
W= 0.43Us.

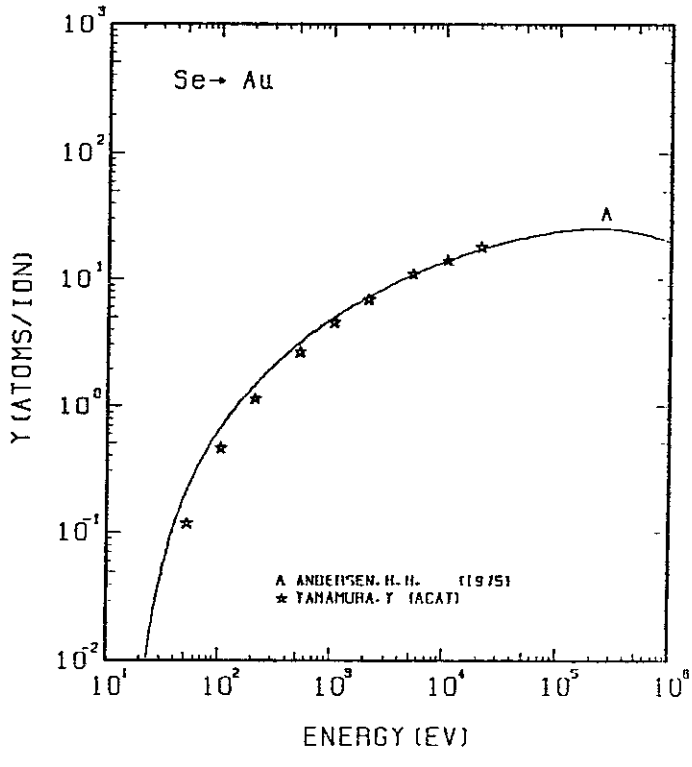


FIG. 312 ENERGY DEPENDENCE OF THE SPUTTERING YIELD OF AU WITH SE$^+$.
A= 2.49, D= 1.08, Us= 3.81EV, S= 2.80,
W= 0.43Us.

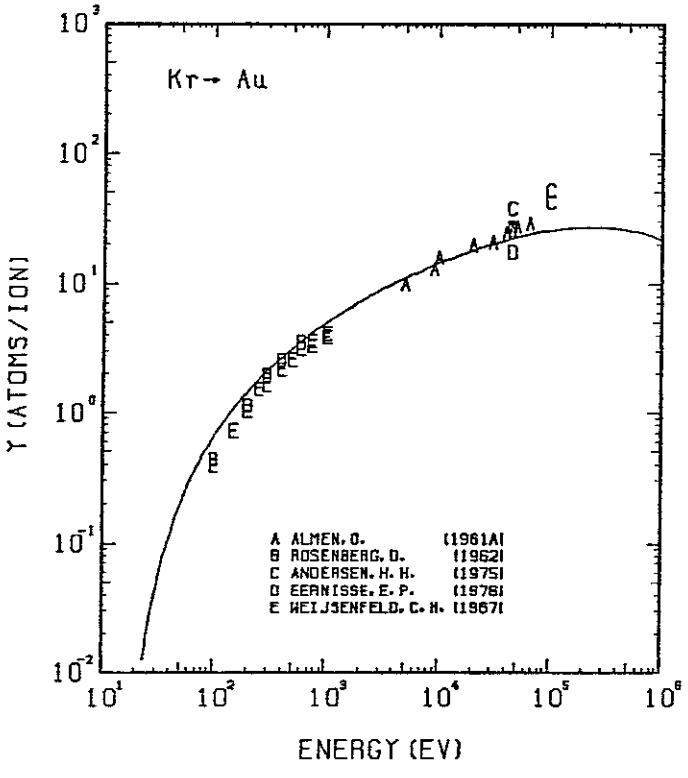


FIG. 313 ENERGY DEPENDENCE OF THE SPUTTERING YIELD OF AU WITH KR$^+$.
A= 2.35, D= 1.08, Us= 3.81EV, S= 2.80,
W= 0.43Us.

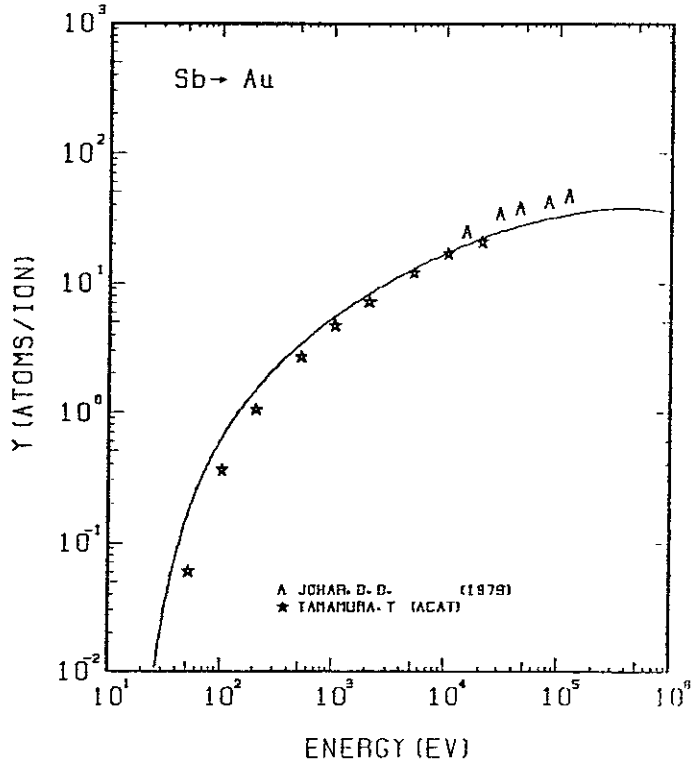


FIG. 314 ENERGY DEPENDENCE OF THE SPUTTERING YIELD OF AU WITH SB$^+$.
A= 1.62, D= 1.08, Us= 3.81EV, S= 2.80,
W= 0.43Us.

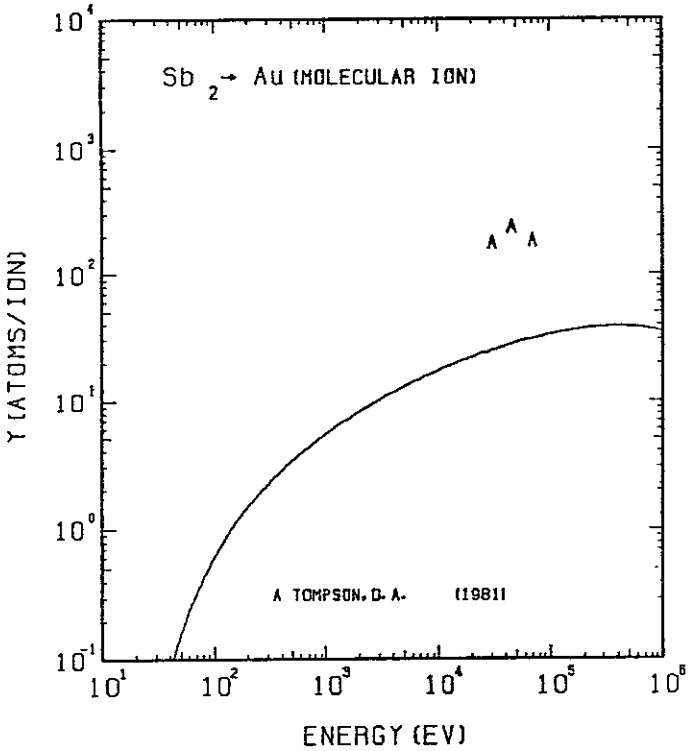


FIG. 315 ENERGY DEPENDENCE OF THE SPUTTERING YIELD OF AU WITH SB $_2^+$. A= 1.62, D= 1.08, Us= 3.81EV, S= 2.80, W= 0.43Us. THE NON-LINEAR EFFECT IS OBSERVED DUE TO MOLECULAR IONS.

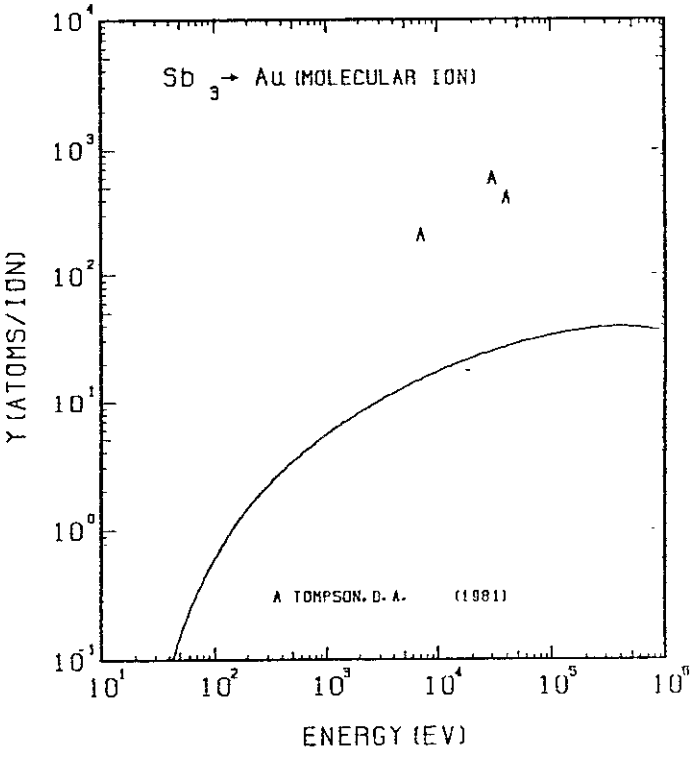


FIG. 316 ENERGY DEPENDENCE OF THE SPUTTERING YIELD OF AU WITH SB $_3^+$. A= 1.62, D= 1.08, Us= 3.81EV, S= 2.80, W= 0.43Us. THE NON-LINEAR EFFECT IS OBSERVED DUE TO MOLECULAR IONS.

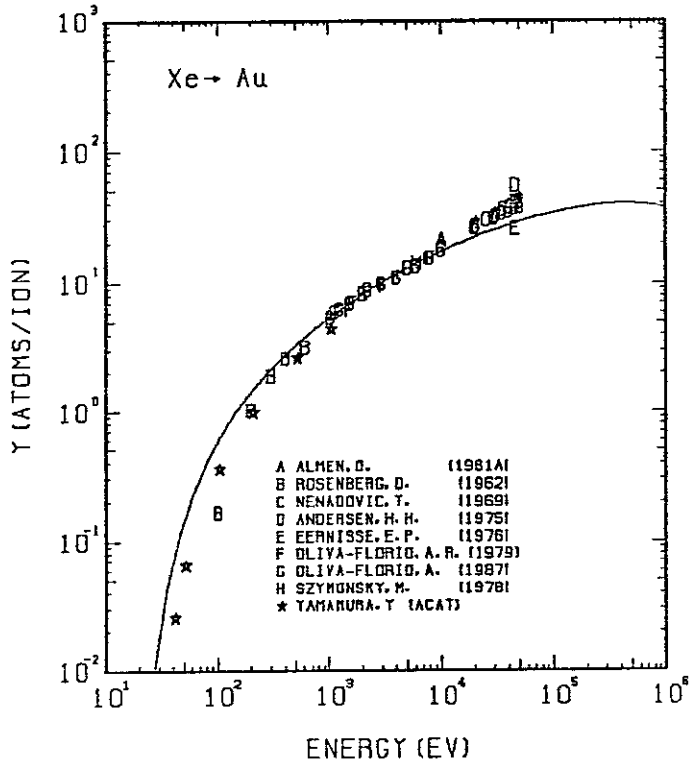


FIG. 317 ENERGY DEPENDENCE OF THE SPUTTERING YIELD OF AU WITH XE$^+$. A= 1.50, D= 1.08, Us= 3.81EV, S= 2.80, W= 0.43Us.

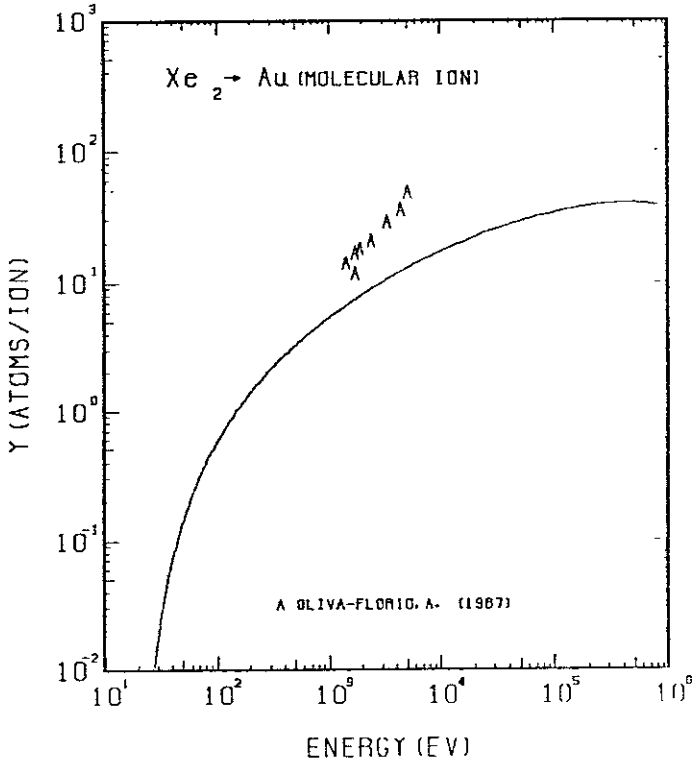


FIG. 318 ENERGY DEPENDENCE OF THE SPUTTERING YIELD OF AU WITH XE $_2^+$. A= 1.50, D= 1.08, Us= 3.81EV, S= 2.80, W= 0.43Us. THE NON-LINEAR EFFECT IS OBSERVED DUE TO MOLECULAR IONS.

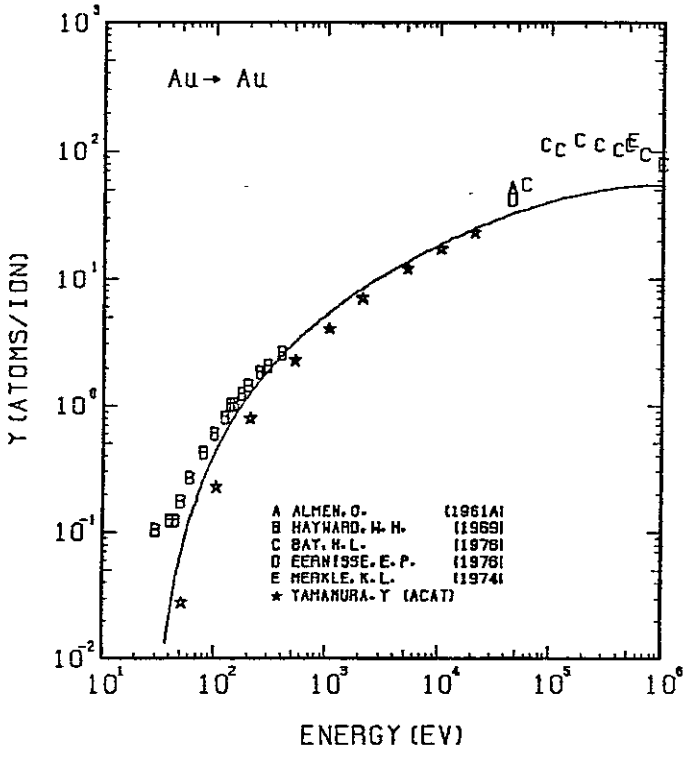


FIG. 319 ENERGY DEPENDENCE OF THE SPUTTERING YIELD OF AU WITH $AU^+$.
A= 1.00, D= 1.08, Us= 3.81EV, S= 2.80,
W= 0.43Us.

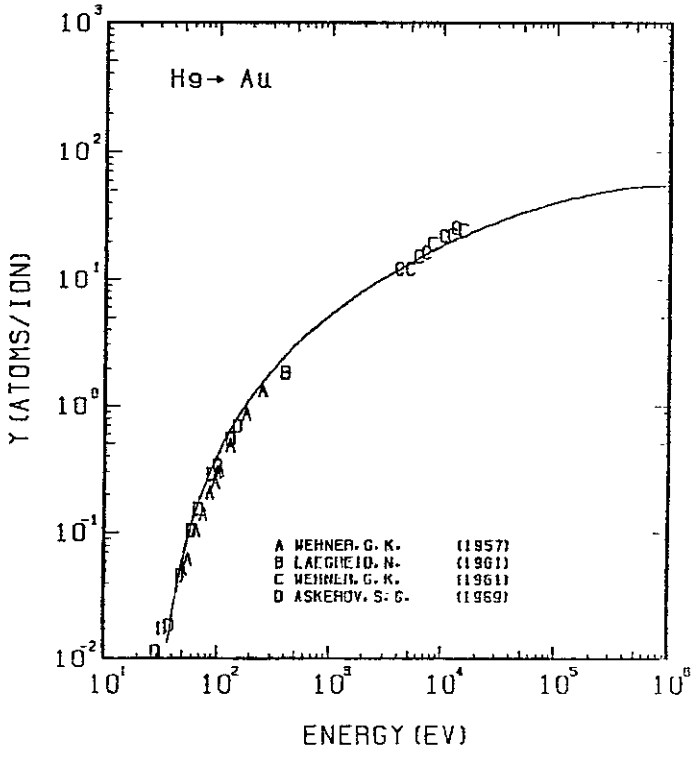


FIG. 320 ENERGY DEPENDENCE OF THE SPUTTERING YIELD OF AU WITH $HG^+$.
A= 0.98, D= 1.08, Us= 3.81EV, S= 2.80,
W= 0.43Us.

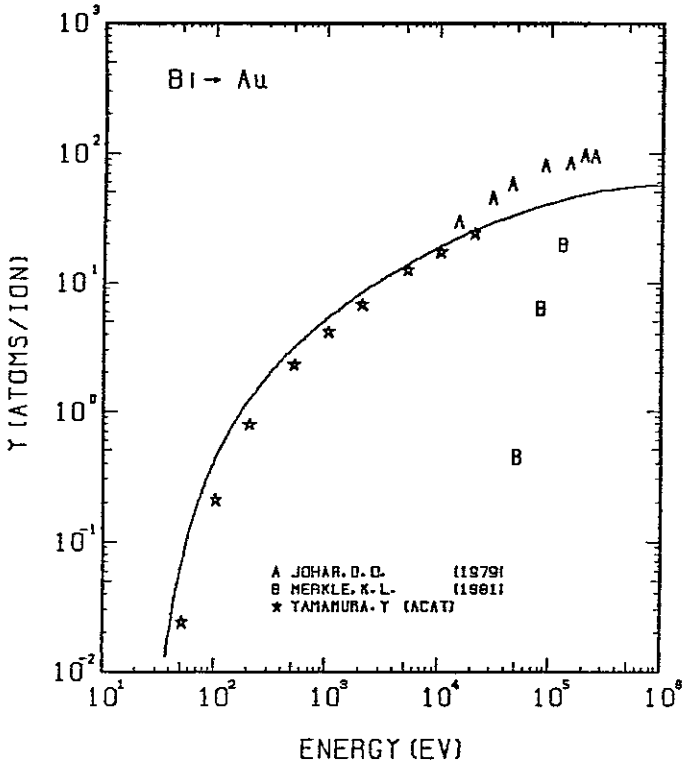


FIG. 321 ENERGY DEPENDENCE OF THE SPUTTERING YIELD OF AU WITH $BI^+$.
A= 0.94, D= 1.08, Us= 3.81EV, S= 2.80,
W= 0.43Us.

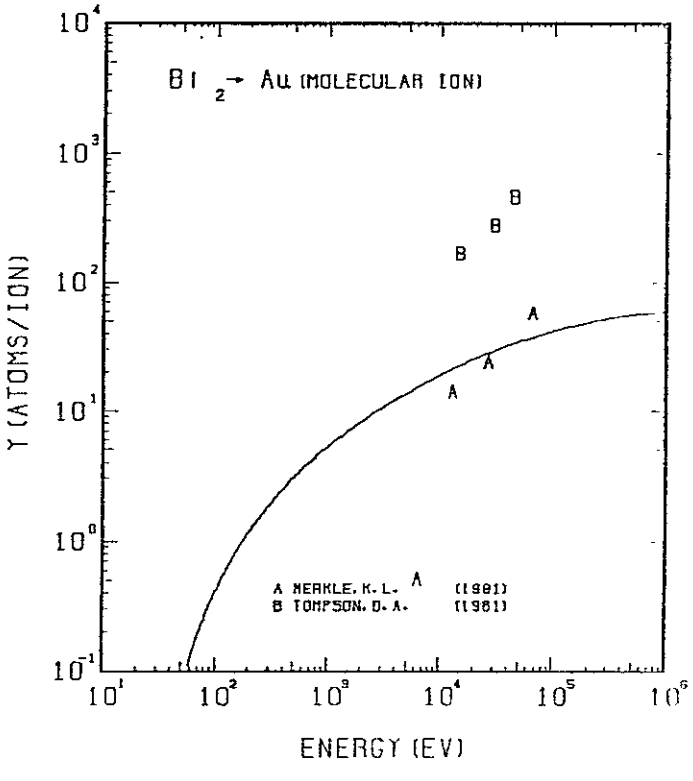


FIG. 322 ENERGY DEPENDENCE OF THE SPUTTERING YIELD OF AU WITH $BI_2^+$.
A= 0.94, D= 1.08, Us= 3.81EV, S= 2.80,
W= 0.43Us. THE NON-LINEAR EFFECT IS OBSERVED DUE TO MOLECULAR IONS.

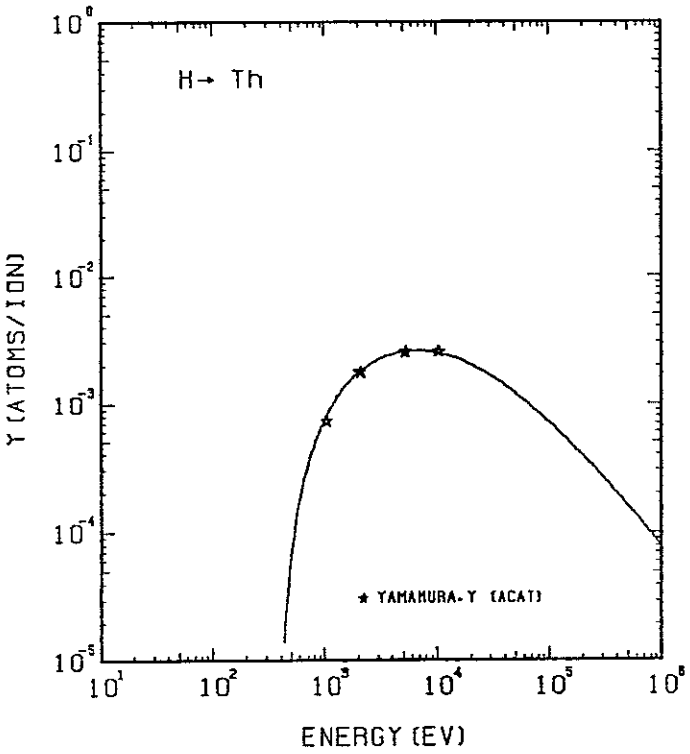


FIG. 323 ENERGY DEPENDENCE OF THE SPUTTERING YIELD OF TH WITH $H^+$.
A= 230.16, Q= 0.63, Us= 6.20EV, s= 2.50,
W= 0.45Us.

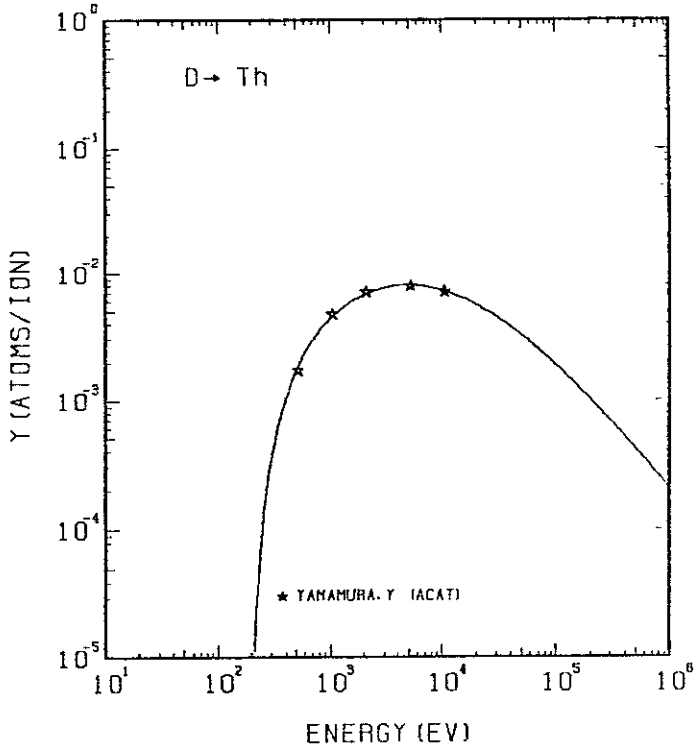


FIG. 324 ENERGY DEPENDENCE OF THE SPUTTERING YIELD OF TH WITH $D^+$.
A= 115.19, Q= 0.63, Us= 6.20EV, s= 2.50,
W= 0.45Us.

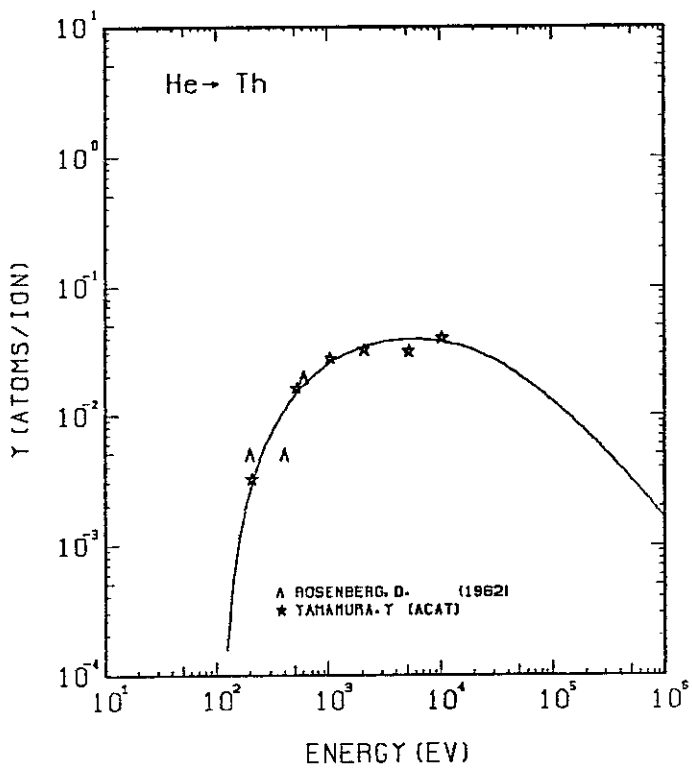


FIG. 325 ENERGY DEPENDENCE OF THE SPUTTERING YIELD OF TH WITH $HE^+$.
A= 57.96, Q= 0.63, Us= 6.20EV, s= 2.50,
W= 0.45Us.

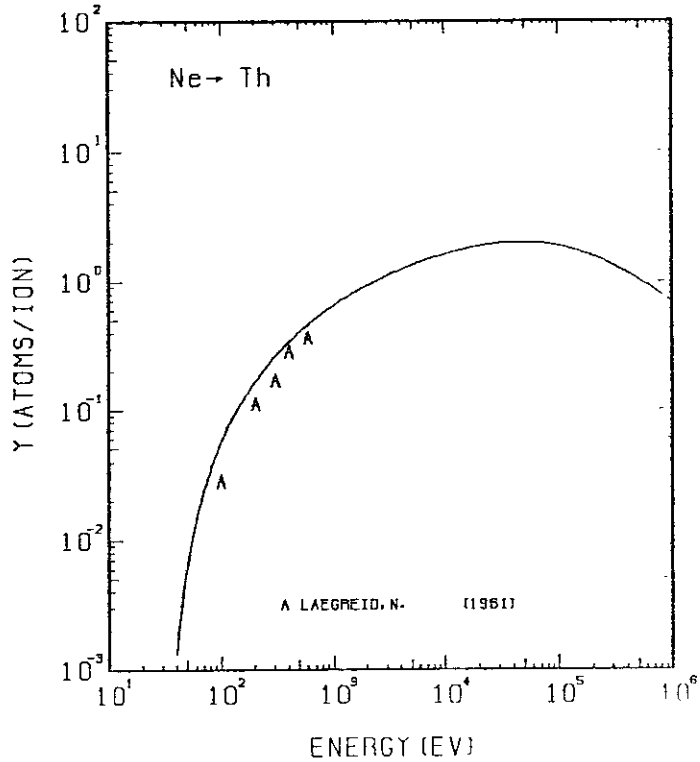


FIG. 326 ENERGY DEPENDENCE OF THE SPUTTERING YIELD OF TH WITH $NE^+$.
A= 11.50, Q= 0.63, Us= 6.20EV, s= 2.50,
W= 0.45Us.

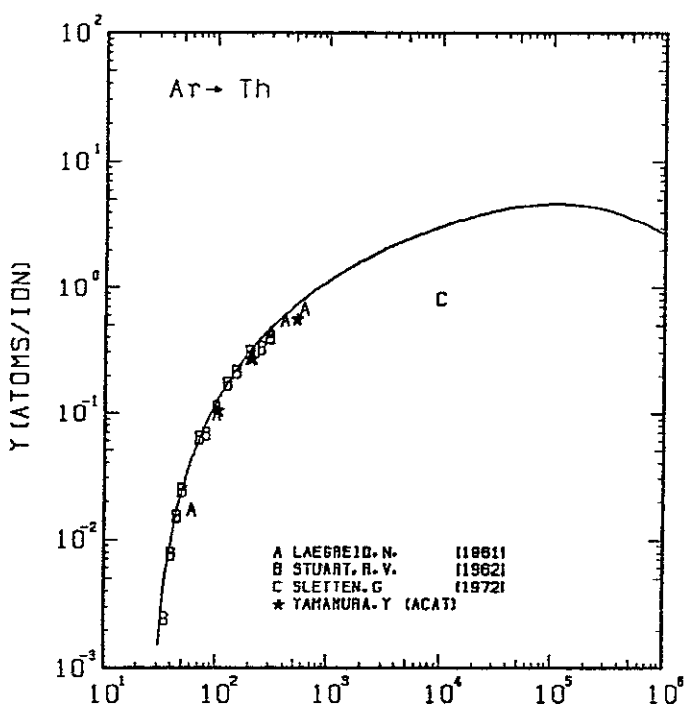


FIG. 327 ENERGY DEPENDENCE OF THE SPUTTERING YIELD OF TH WITH $AR^+$.
A= 5.81, D= 0.63, Us= 6.20EV, S= 2.50,
W= 0.45Us.

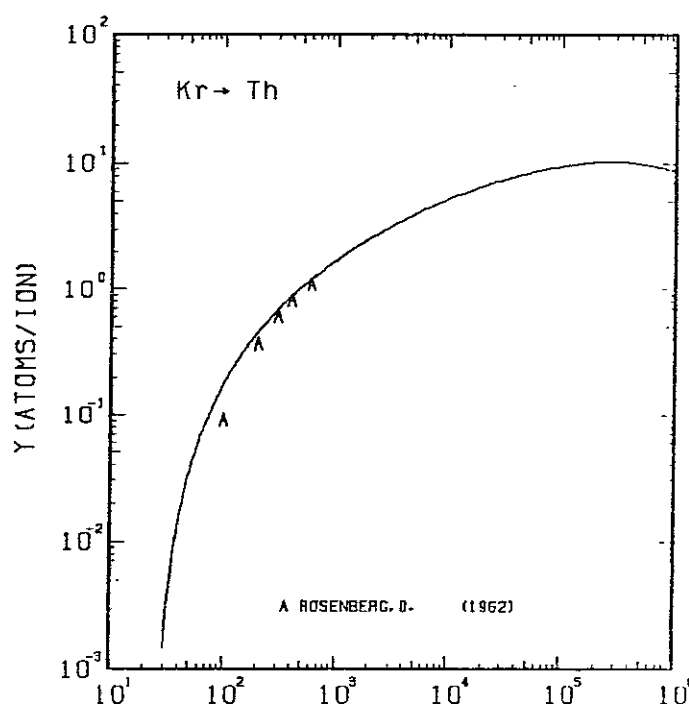


FIG. 328 ENERGY DEPENDENCE OF THE SPUTTERING YIELD OF TH WITH $KR^+$.
A= 2.77, D= 0.63, Us= 6.20EV, S= 2.50,
W= 0.45Us.

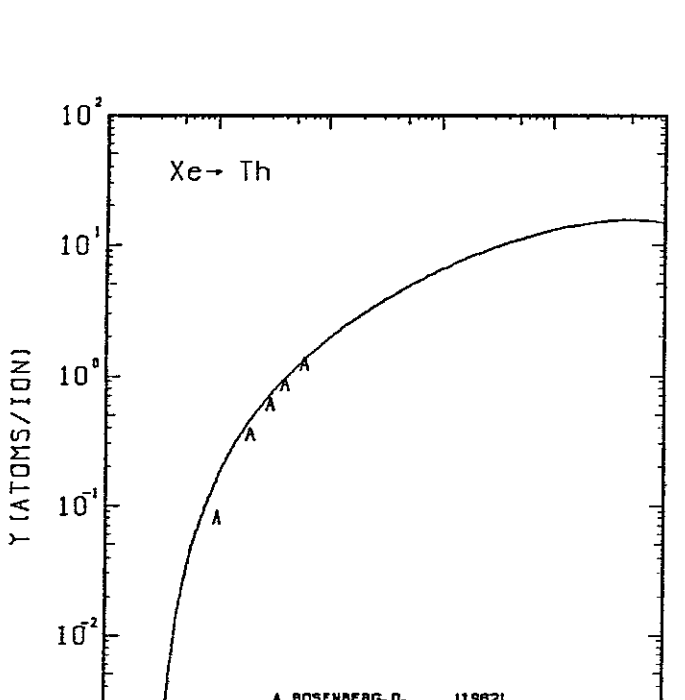


FIG. 329 ENERGY DEPENDENCE OF THE SPUTTERING YIELD OF TH WITH $XE^+$.
A= 1.77, D= 0.63, Us= 6.20EV, S= 2.50,
W= 0.45Us.

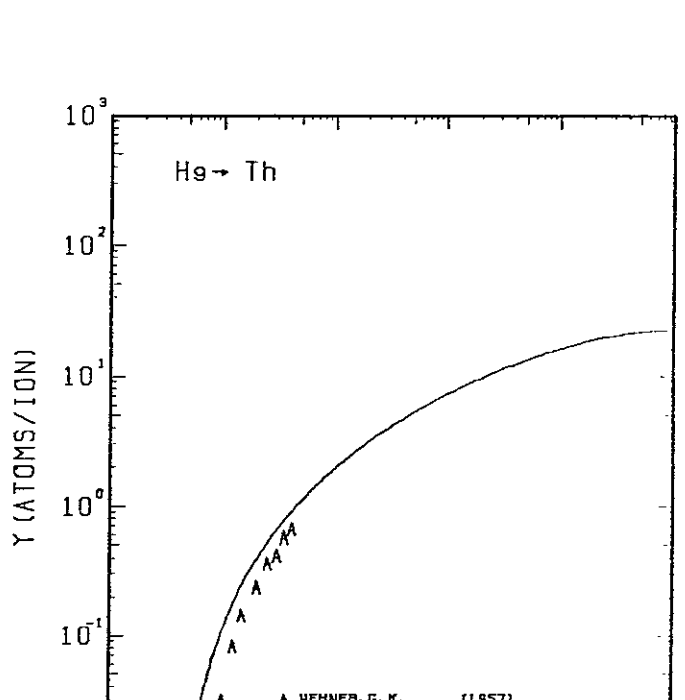


FIG. 330 ENERGY DEPENDENCE OF THE SPUTTERING YIELD OF TH WITH $HG^+$.
A= 1.15, D= 0.63, Us= 6.20EV, S= 2.50,
W= 0.45Us.

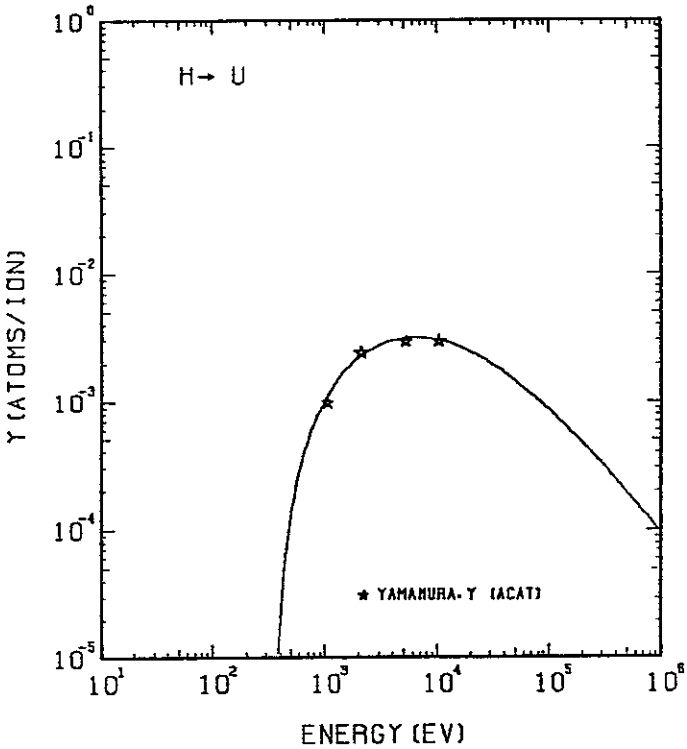


FIG. 331 ENERGY DEPENDENCE OF THE SPUTTERING YIELD OF U WITH $H^+$.
A= 236.11.0= 0.66.Us= 5.55EV.s= 2.50.
W= 0.50Us.

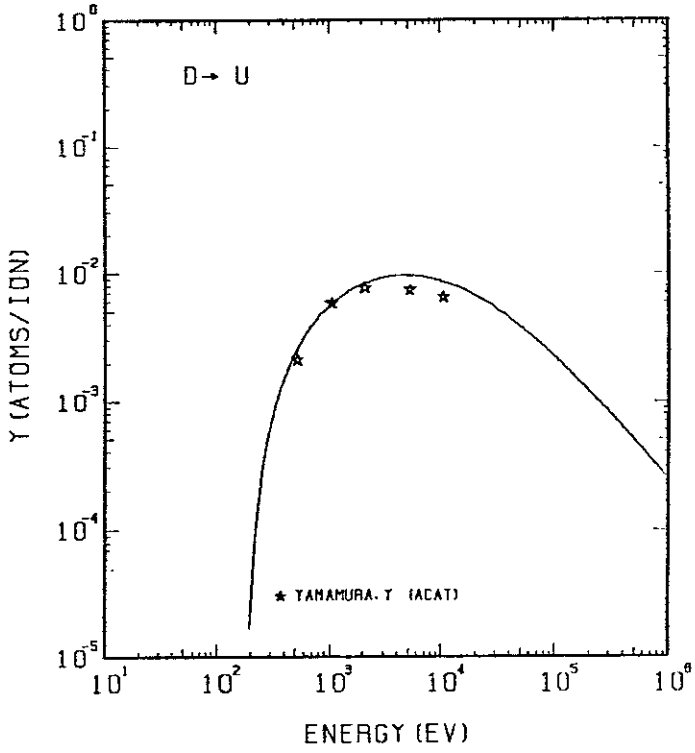


FIG. 332 ENERGY DEPENDENCE OF THE SPUTTERING YIELD OF U WITH $D^+$.
A= 118.17.0= 0.66.Us= 5.55EV.s= 2.50.
W= 0.50Us.

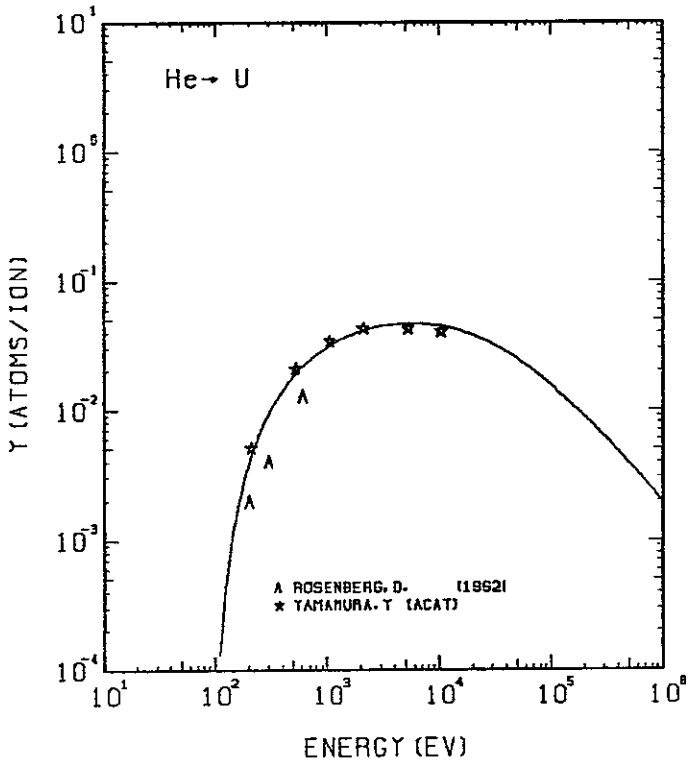


FIG. 333 ENERGY DEPENDENCE OF THE SPUTTERING YIELD OF U WITH $HE^+$.
A= 59.46.0= 0.66.Us= 5.55EV.s= 2.50.
W= 0.50Us.

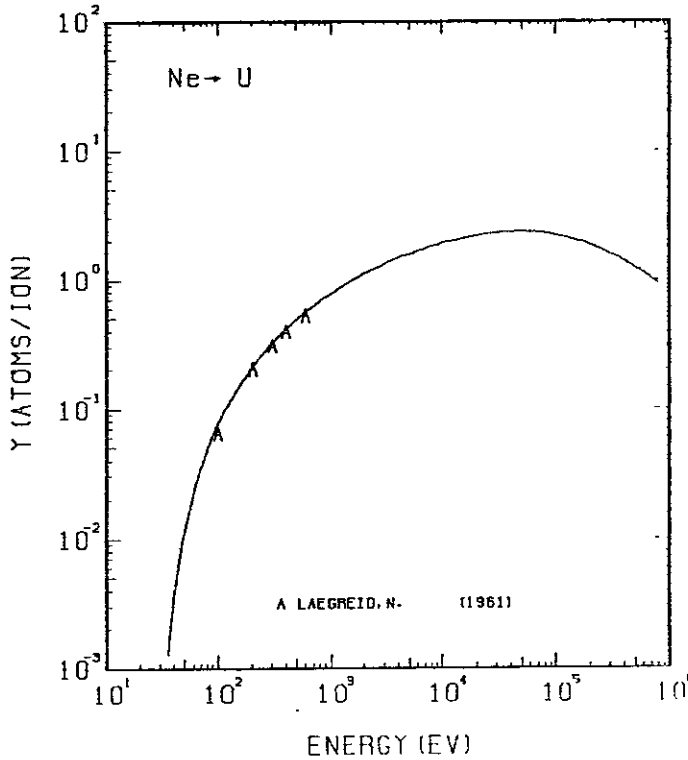


FIG. 334 ENERGY DEPENDENCE OF THE SPUTTERING YIELD OF U WITH $NE^+$.
A= 11.79.0= 0.66.Us= 5.55EV.s= 2.50.
W= 0.50Us.

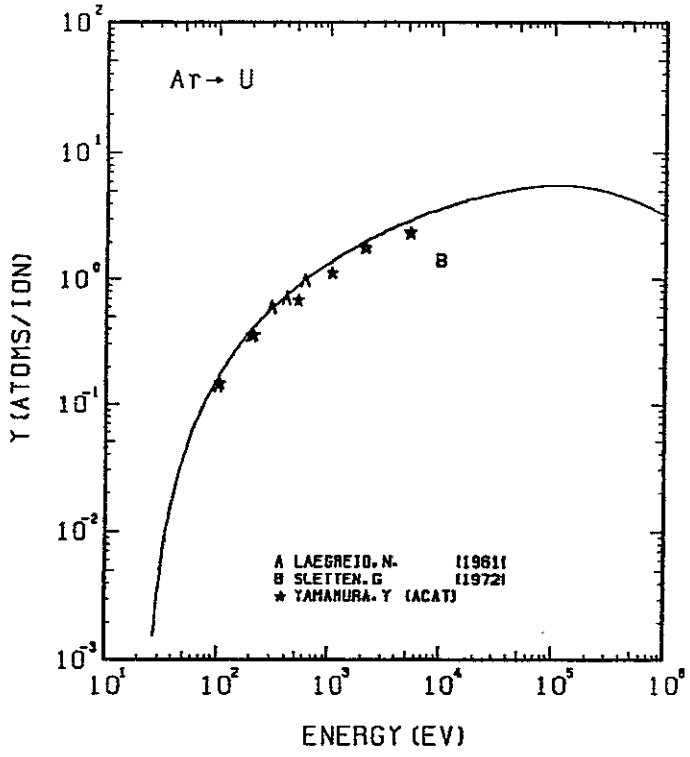


FIG. 335 ENERGY DEPENDENCE OF THE SPUTTERING YIELD OF U WITH AR+.
A= 5.96, D= 0.66, Us= 5.55EV, s= 2.50,
W= 0.50Us.

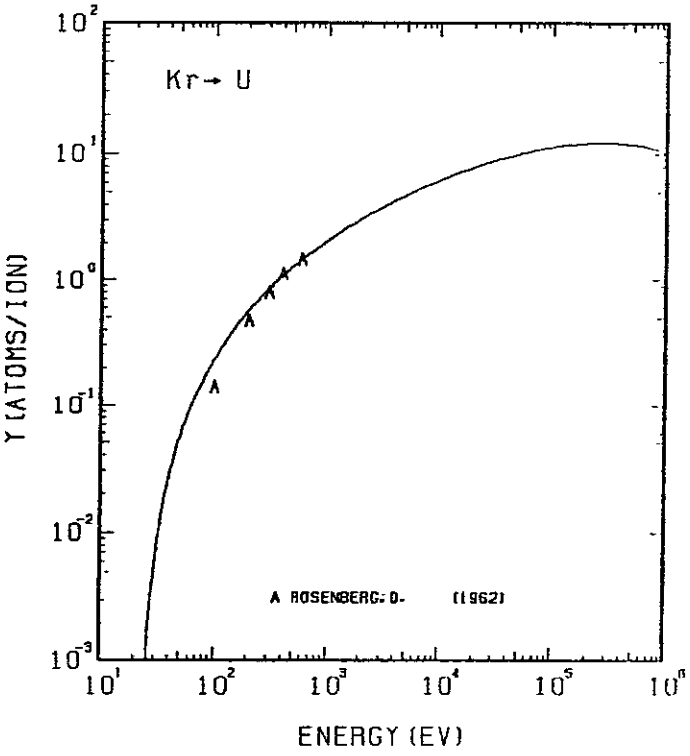


FIG. 336 ENERGY DEPENDENCE OF THE SPUTTERING YIELD OF U WITH KR+.
A= 2.84, D= 0.66, Us= 5.55EV, s= 2.50,
W= 0.50Us.

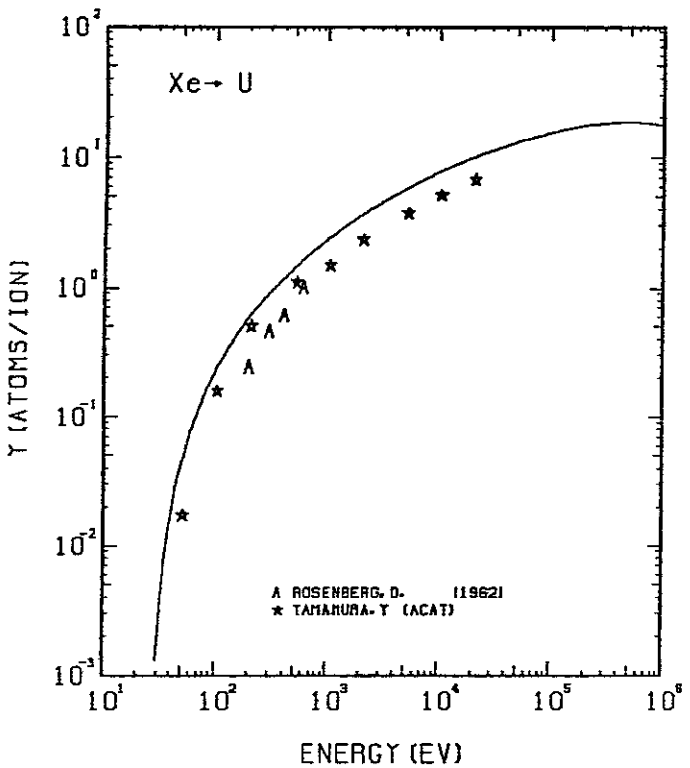


FIG. 337 ENERGY DEPENDENCE OF THE SPUTTERING YIELD OF U WITH XE+.
A= 1.81, D= 0.66, Us= 5.55EV, s= 2.50,
W= 0.50Us.

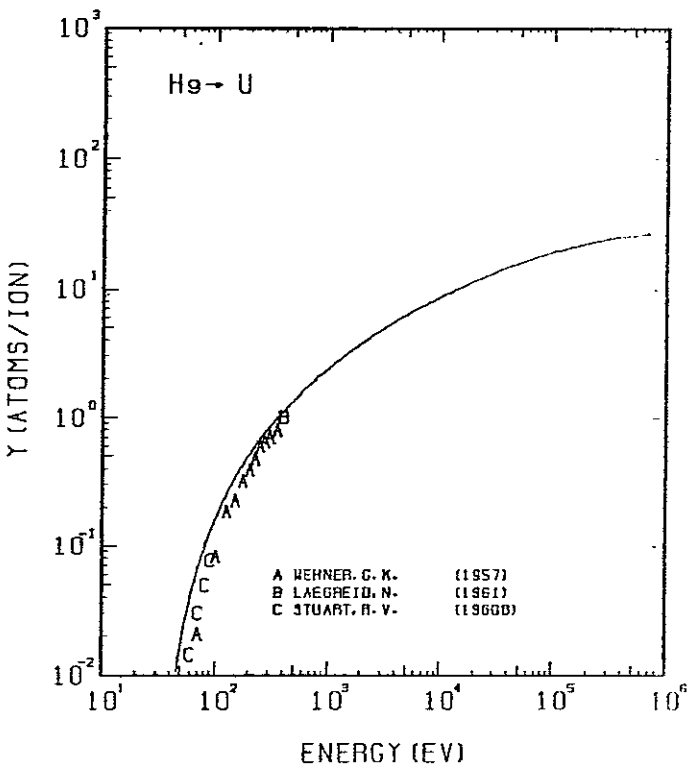


FIG. 338 ENERGY DEPENDENCE OF THE SPUTTERING YIELD OF U WITH HG+.
A= 1.19, D= 0.66, Us= 5.55EV, s= 2.50,
W= 0.50Us.

**References for graphs**


1. Mayer, V. K., and A.Guzentherschulze; Z. Physik ,**71**,19 (1931)

2. Keywell, F.; Phys. Rev., **97**, 1611 (1955).

3. Wehner, G.K.; Phys. Rev., **102**, 690 (1956).

4. Wehner, G.K.; Phys. Rev., **108**, 35 (1957).

5. O'Brian, C.D., A.Linder and W. J. Moore; J. Chem. Phys., **29**, 3 (1958)

6. Weiss., A., L. Heidt and W.J. Moore ; J. Chem. Phys., **29**, 7 (1958)

7. Wehner, G.K.; Phys. Rev. **112**, 1120 (1958)

8. Brown, W.F., Jr. ; Physica **24**, 692 (1958)

9. Wehner, G.K.; J. Appl. Phys. **30**, 1762 (1959)

10. Yonts, O.C., and D.E. Harrison, Jr.; ORNL-2802 (1959)

11. Yonts, O.C, C.E. Normann, and D.E. Harrison, Jr.; J. Appl. Phys. **31**, 447 (1960)

12. Yonts, O.C., C.E. Normann, and D.E. Harrison, Jr ; J. Appl. Phys. **31**, 1583 (1960)

13. Grolund, F., and W.J. Moore ; J. Chem. Phys. **32**, 1540 (1960)

14. Guseva, M.I.; Soviet Phys.-Solid State **1**, 1410 (1960)

15. Rol, P.K., J.M. Fluit and J. Kistemaker; Physica. **26**, 1000 (1960)

16. Stuart, R.V., and G. K.Wehner ; Phys. Rev. Lett. **4**, 409 (1960)

17. Bader, M., F.C. Witterbone and T.W. Snouse ; NASA Tech. Report R105 (1960)

18. Stuart, R.V., and G.K.Wehner ; Trans. 7th. National Vac. Symp. (1960) p290

19. Almen, O., and G. Bruce ; Nucl. Instr. Meth. **11**, 257 (1961)

20. Almen, O., and G. Bruce ; Nucl. Instr. Meth. **11**, 279 (1961)

21. Almen, O., and G. Bruce ; Trans. Vac. Symp., Washington D. C. (1961) p245

22. Fert, C., N. Colombie, B. Fagot and P.V. Chuong ;

    Ionic Bombardment., Bellevue (1961) p67.

23. Laegreid, N., and G.K.Wehner ; J. Appl. Phys. **32**, 365 (1961)

24. Perovic, B., and B. Cobic ;

    Proc. 5th Int. Conf. Ionization Phenomena in Gases, Munich (1961) p1165

25. Wehner, G. K. and D. Rosenburg; J. Appl. Phys. **32**, 887 (1961)

26. Wehner, G.K, R.V. Staurt and D. Rosenburg ; General Mills Report No. 2243 (1961)

27. Bader, M., F.C.Witteborn and T.W. Sonuse ; NASA Tech. Report, R105 (1961)

28. Patterson, H., and D.H.Tomlin ; Proc. Roy. Soc. London **A265**, 474 (1962)

29. Rosenburg, D., and G.K.Wehner ; J. Appl. Phys. **33**, 1842 (1962)

30. Stuart, R. V., and G.K.Wehner ; J. Appl. Phys. **33**, 2345 (1962)

31. Fetz, H. and H. Oechsner ;

Proc. 6th Int. Conf. Ionization Phenomena in Gases, Paris, Vol. II (1963) p39.

32. Magnuson, G.D., and C.E. Carlston; J. Appl. Phys. **34**, 3267 (1962)

33. Guseva, M.I.; Radio. Eng. Electron Phys. (USSR) **7**, 1563 (1962)

34. Sommerfeldt, H., E.S. Mashkova and V.A. Molchanov ;

Proc. 9th Int. Conf. Ionizion Phenomena in Gases, Bucharest (1963) p93.

35. Southern, A. L, W.R. Wills and M.T. Robinson ; J. Appl. Phys. **34**, 153 (1963)

36. Colombie, N. ; Thesis Of Univ. Toulouse (1964)

37. Kenknight, C.E., and G.K.Wehner ; J. Appl. Phys. **35**, 322 (1964)

38. Ramer, C.E., M.A. Narashimham, H.K. Reynolds and J.C. Allred ;

J. Appl. Phys. **36**, 1673 (1964)

39. Arifov, U.A., A.Kh. Ayukhanov, V.A. Shustrov, R.M. Khasanov and V.I. Polroratskii ;

Sov. Phys.-Doklady **9**, 214 (1964)

40. Cheney, K.B., and E.T. Pitkin ; J. Appl. Phys. **36**, 3542 (1965)

41. Dupp, G., and A. Scharmann ; Z. Physik. **192**, 284 (1966)

42. Weijsenfend, C.H. ; Thesis Of Univ. Utrecht (1966)

43. Finfgeld, C.R.; Saem Va-Report Oro-3557-15 (1967)

44. Robinson, M T, and A.L. Soutern ; J. Appl. Phys. **38**, 2969 (1967)

45 Weijsenfeld, C.H. ; Philip Research Report , Supplement No. 2 (1967)

46. Kurbatov, O.K. ; Sov. Phys.-Techn.Phys. **12**, 1328 (1968)

47. Gurmin, G.M., T.P. Martynenko and Tu.A. Ryzhov ; Sov. Phys.- Solid State **10**, 324 (1968)

48. Martynenko, T.P.; Sov. Phys.- Solid State **9**, 2232 (1968)

49. Askerov, S.G., and L.A. Sena ; Soviet Phys.-Solid State **11**, 1288 (1969)

50. Berisch, R., and R. Weissmann ; Phys. Lett. **30A**, 506 (1969)

51. Betz, G., R. Dobrozemaky, F.P.Veshbock and H.Wotke;

Proc. 9th Int. Conf. Phenomena Ionized Gases, Bucharest (1969) p91.

52. Fontell, A., and Arminen, E. ; Can. J. Phys. **47**, 2405 (1969)

53. Hayward, W.H., and A.R. Wolter ; J. Appl. Phys. **40**, 2911 (1969)

54. Holmen, G., and O. Almen ; Arkiv for Physik. **40**, 429 (1969)

55. Koshkin, V.K., J.A. Rysov, J.A. Rysov, I.I.Shkarban and B.M.Gourmin;

Proc. 9th Int. Conf. Phenomena Ionized Gases, Bucharest (1969) p92

56. Martynenko, T. P.; Soviet Phys.-Solid State **10**, 2274 (1969)

57. Nenadovic, T., and Z. Jurela ;

Proc. 9th Int. Conf. Phenomena Ionized Gases, Bucharest (1969) p90

58. Benninghoven, A.; Angew. Phys. **51**, 27 (1969)

59. Colligon, J.S., and R.W. Bramham ; Atomic Col. Solids, Brighton (1970) p258.

60. Dey, S. D., D. Basu and S.B.Karmohapatro ; Nucl. Instr. Meth. **77**, 242 (1970)

61. Furr, A.K. and C.R. Finfgeld ; J. Appl. Phys . **41**, 1739 (1970)

62. Hepworth, J.K.; J.Phys. D.; Appl. Phys. **3**, 1475 (1970)

63. Ismail, H.; Rev. Appl .Phys. **5**, 759 (1970)

64. Krutenant, R.C., and C. Panzera ; J. Appl. Phys. **41**, 4953 (1970)

65. Macdonald, R.J.; Advances in Physics **19**, 457 (1970)

66. Eernisse, E.P.; J. Appl. Phys.**42**, 480 (1971)

67. Summers, A.J., N.J. Freeman and N.R. Daly ; J. Appl. Phys. **42**, 4774 (1971)

68. Campbell, A.B. III, andC. B. Cooper ; J. Appl. Phys. **43**, 863 (1972)

69. Sommerfeldt, H., E.S. Mashkova and V.A. Molchanov ; Phys. Lett. **38A**, 237 (1972)

70. Nenadovic, T.M., Z.B.Fotiric and T.S. Dimitrijevic ; Surf. Sci. **33**, 607 (1972)

71. Dahlgren, S.D., and E.D. Macclanahan ; J. Appl. Phys. **43**, 1514 (1972)

72. Sletten, G and P. Krusen ; Nucl. Instr. Meth. **102**, 459 (1972)

73. Andersen, H.H., and H.L.Bay, ; Radiat. Eff. **67**, 13 (1972)

74. Smith, H.J.; Radiat. Eff. **18**, 55 (1973A)

75. Smith, H.J.; Radiat. Eff. **18**, 65 (1973B)

76. Smith, H.J ; Radiat. Eff. **18**, 73 (1973C)

77. Colligon, J.S., C.M. Hicks and A.P. Neokleous ; Radiat. Eff. **18**, 119 (1973)

78. Eckstin, W., B.M.U. Scherzer and H. Verbeek ; Radiat. Eff. **18**, 135 (1973)

79. Kelly, R. and N.Q. Lam ; Radiat. Eff. **19**, 39 (1973)

80. Weissman, R., and R.Behrisch ; Radiat. Eff. **19**, 69 (1973)

81. Andersen, H.H.; Radiat. Eff. **19**, 257 (1973)

82. Andersen, H.H. and H.L. Bay ; Radiat. Eff. **19**, 139 (1973)

83. Oechsner, H. ; Z. Phys. **37**, 261 (1973)

84. Andersen, H.H., and H.L. Bay ; J. Appl. Phys. **45**, 953 (1974)

85. Bach, H., I. Kitzman and H.Schroder ; Radiat. Eff. **21**, 31 (1974)

86. Winters, H.F., and D. Horne ; Phys. Rev. **B10**, 55 (1974)

87. Merkle, K.L, and P.P. Pronko ; J. Nucl. Mater. **231**, 53 (1974)

88. Andersen, H.H., and H.L. Bay ; J. Appl. Phys. **46**, 1919 (1975)

89. Andersen, H.H., and H.L. Bay ; J. Appl. Phys. **46**, 2416 (1975)

90. Gerhard, W and H.Oechsner ; Z. Phys. **B22**, **41** (1975)

91.McCraken, G.H.; Rep. Prog. Phys. **38**, 241 (1975)

92. Nizam, J., and N.B. Colombie ; Rev. Phys. Appl. **10**, 183 (1975)

93. Oechsner, H. ; Appl. Phys. **8**, 185 (1975)

94. Smith, J.N.Jr., C.H.Mayer and J.K. Layton ; Trans. Am. Nucl. Soc. **22**, 29 (1975)

95. Smith, J.N.Jr., C.H.Mayer and J.K. Layton ; J. Appl. Phys. **46**, 4291 (1975)

96. Wittmaack, K.; Surf. Sci. **53**, 626 (1975)

97. Holmen, G.; Radiat. Eff. **24**, 7 (1975)

98. Guzeva, M.I., and Y.V. Martynenko ; Fiz. Plaz. (USSR) Vol. **2**, No.4 593 (1976)

99. Bay, H.L., H.H. Andersen, W.O. Hofer and O.Nielson.; Nucl. Instr. Meth. **132**, 301 (1976)

100. Bohdansky, J., J. Roth and M.K. Sinha ;

Pro. 9th Symposium Fusion Technology, Pergaman (1976) p541.

101. Eernisse, E.P.; Appl. Phys. Lett. **29**, 14 (1976)

102. Hofer, W.O. and H. Lieble ; Ion Beam Surface Layer Analysis, Karlsruhe (1976) p659.

103. Poate, J. M., W.R. Brown, R. Homer, W.M. Augustyniak, J.W.Meyer, K.N.Tu and W.F. van der Weg ; Nucl. Instr. Meth. **132**, 345 (1976)

104. Krauss, A.R. and D.M.Gruen ; J. Nucl. Mater. **63**, 380 (1976)

105. Krautle, H.; Nucl. Instr. Meth. **137**, 553 (1976)

106. Ollerhead, R.W., F.M. Mann, D.W. Kneff, Z.E. Switkowskii and T.A. Tombrello ; Phys. Rev. Lett. **36**, 439 (1976)

107. Roth, J., J. Bohdansky, W. Poschrnrieder and M.K. Sinha; J. Nucl. Mater. **63**, 229 (1976)

108. Scherzer, B.M.U., R. Behrisch and J. Roth ; Plasma Wall Interaction. Julich (1976)

109. Switkowski, Z.E., F.M. Mann, K.W. Kneff, R.W.Ollerhead and T.A.Tombrello ; Radiat. Eff. **29**, 65 (1976)

110. Smith, J. N.Jr., C.H. Meyer and J.K.Layton ; Nucl. Technol. **29**, 318 (1976)

111. Brown, M., B. Emmoth and R. Buchta; Radiat. Eff. **77**, 28 (1976)

112. Akaishi, K., A. Miyahara, Z. Kabeya, S. Sukenobu, M. Komizo and T. Gotoh ; J.Vac. Soc. Japan **20**, 161 (1977)

113. Holloway, P.H.; Surf. Sci. **479**, 66 (1977)

114. Bay, H.L., J. Bohdansky and J. Roth ; J. Appl. Phys. **48**, 4722 (1977)

115. Behrisch, R., O.K. Harling, M.T. Thomas, R.L. Brodzinski, L.H. Jenkins, G.J. Smith, J.F. Wendelken, M.J.Saltmarsh, M. Kaminsky, S.K. Das, C.M. Longon, R. Meisenheimer, J.E. Robinson, M. Shimotomai and D.A.Thompson ; J. Appl. Phys. **48**, 3914 (1977)

116. Bay, H.L., J. Bohdansky and J. Roth ; Vacuum Congress and Solid Surface, Vienna (1977)

117. Colligon, J.S., and M.H. Patel ; Radiat. Eff. **32**, 193 (1977)

118. Coburn, J.W., H. F. Winters and T. J. Chuang ; J. Appl. Phys. **48**, 3532 (1977)

119. Martel, J.G., R.G. St-Jacques and B. Terreault ; J. Vac. Sci. and Tech. **14**, 543 (1977)

120. Smith, J.N., C.H.Mayer and J.K. Layton ; J. Nucl. Mater. **67**, 234 (1977)

121. Sone, K., H. Ohtsuka,T. Abe, R.Yamada, K.Obara, T.Narusawa, O. Tsukakoshi, T. Satake and S. Komizo; J. Vac. Soc. Japan **20**, 136 (1977)

122. Szymonski, M., and A.E.de Vries ; Phys. Lett. **63A**, 359 (1977)

123. Ziegler, J.F., J.J. Cuomo and J. Roth ; Appl. Phys. Lett. **30**, 268 (1977)

124. Bay, H.L., J. Bohdansky and W. Ottenberger ; J. Nucl. Mater. **76&77**, 163 (1978)

125. Borders, J.A., R.A. Langley and K.L. Wilson ; J. Nucl. Mater. **76&77**, 168 (1978)

126. Emmoth, B., T. Frird and M. Braun ; J. Nucl. Mater. **76&77**, 129 (1978)

127. Hofer, W.O., H.L. Bay, and P.J. Martin ; J. Nucl. Mater. **76&77**, 156 (1978)

128. Gregg, R. and T.A. Tombrello ; Radiat. Eff. **35**, 243 (1978)

129. Labunov, V.A. and Y. Borisenco ; Soviet Phys.-Solid State **20**, 712 (1978)

130. Miyagawa, S., Y.Ato and Y.Moriya ; J. Appl. Phys. **49**, 6194 (1978)

131. Ohtsuka, H., R. Yamada, K. Sone, M.Saidoh, and T. Abe ;
J. Nucl. Mater. **76&77**, 188 (1978)

132. Okajima, Y. and Y. Aizawa ; Mass Spectroscopy **26**, 83 (1978)

133. Smith J.N. and C.H. Meyer, Jr.; J. Nucl. Mater. **76&77**, 193 (1978)

134. Hechtl, E., H.L. Bay and J. Bohdansky .; Appl. Phys. **16**, 147 (1978)

135. Border, J.A., R.A. Langley and K.L.Wilson ; J. Nucl. Mater. **76&77**, 118 (1978)

136. Szymonsky, M., R.S. Bhattacsharya and A.E. de Vries. ; J. Phys. D. **11**, 751 (1978)

137. Bay, H.L., J. Bohdansky and E. Hechtl ; Radiat. Eff. **41**, 77 (1979)

138. Johar, D.D., and D.A. Thompson ; Surf. Sci. **90**, 319 (1979)

139. Kang, S.T., R. Shimizu and T. Okutani ; Jpn. J. Appl. Phys. **18**, 1717 (1979)

140. Oliva-Florio, A.R., E.V. Alomso, R.A. Baragiora and J. Ferron ;
Radiat. Eff. Lett. **50**, 3 (1979)

141. Roth, J., J. Bohdansky and W. Ottenberger ; IPP 9/26 Max-Plank-Institut (1979)

142. Roberto, J.B., R.A.Zuhr, J.L. Moore and G.D.Alton ;
J. Nucl. Mater. **85&86**, 1073 (1979)

143. Bohdansky, J. ; J. Nucl. Mater. **93&94**, 44 (1980)

144. Yamashita, M., S. Baba, and A.Kinbar ;
Poc. 4th Sym. Ion Source and Ion Application (1980) p311

145. Lam, S.K. and M. Kaminsky ; J. Nucl. Mater. **89**, 205 (1980)

146. Ato, Y. ; J. Vac. Soc. Jpn. **23**, 339 (1980).

147. Tsunoyama, K., T.Suzuki , Y. Ohashi and H. Kishidaka ;
Surface Interface Analysis **2**, 212 (1980)

148. Yung-Yi Tu, T.J. Chuang, and H.F. Winters ; Phys. Rev. **B23**, 823-5 (1981)

149. Saiki, K., H.Tanaka, S. Tanaka and A. Koma ; J. Nucl. Mater. **97**, 173-8 (1981)

150. Merkle, K.L.and W. Jäger, ; Phil. Mag. **A44**, 741 (1981) .

151. Tompson, D.A. ; J. Appl. Phys. **52**, 982 (1981)

152. S.Taichi, K. Miyake and T. Tokuma ; J. Appl. Phys. **20**, L411 (1981)

153. Morgan, A. E., H.A.M. de Grefte, N. Warmoltz, H.W. Werner and H.J. Tolle ;
Appl. Surf. Sci. **7**, 372 (1981)

154. Okajima, Y. ; Jpn. J. Appl. Phys. **20**, 2313 (1981)

155. Fink, D., and J.P. Biersack ; Radiat. Eff. **64**, 89 (1982)

156. Fitch, R.K., and E.A. Mahmoud ; Thin Solid Films, **87**, 379 (1982)

157. Allas, R.G., A.R. Knudson, J.M. Lambert, P.A. Treado and G.W. Reynolds ;
Nucl. Instr. Meth., **194**, 615 (1982)

158. Tompkins, H.G., R.A.Frank and D.L. Allara.; J. Van. Sci. Technol. **20** (3), 400 (1982)

159. Bohdansky, J., G.L. Chen, W. Eckstein, B.M.U. Scherzer and R. Behrisch ;
J. Nucl. Mater., **111&112**, 717 (1982)

160. Roth, J., J. Bohdansky and K.L.Wilson ; J. Nucl. Mater. **111&112**, 775 (1982)

161. Yamasita, M., S. Baba and A.Kinbara, ; J. Vac. Soc. Jpn. **25**, 93 (1982)

162. Zalm, P. C., L.J. Beckers and F.H.M. Sanders ; Nucl. Instr. Meth. **209&210**, 561 (1983)

163. Kaminsky, M. ; private cmmunication (1983)

164. Saidoh, M. and K. Sone ; JAERI-Memo 58-144 (1983)

165. Ghoes, D., Basu, D., and S.B. Karmohapatro ; Phys. Stat. Sol. (A)**77**,121 (1983)

166. Doris V. Stevanovic, D.A. Thompson and J.A. Davies ;
Nucl. Instr. Meth. **B1**, 315 (1984).

167. Trbojevic, D., P.A.Treado and GS. Danel ; Nucl. Instr. Meth. **B10&11**, 743- (1985)

168. Brauer, G., D. Hasselkamp, W. Krüger and A. Scharmann;
Nucl. Instr. Meth. **B12**, 458 (1985)

169. O`Shaughnessy, D.J., J.W. Boring, J.A. Phipps and R.E. Tohnson ;
Nucl. Instr. Meth. **B13**, 304 (1986)

170. Tomita, M.,T. Nate, S.Miyagi and M.Sakisaka; J. Nucl. Mater. **138**, 248 (1986)

171. Ellegaard, O., J. Schou and H. Sorensen ; Nucl. Instr. Meth. **B13**, 568 (1986)

172. Hechtel, E., and J. Bohdansky ; J. Nucl. Mater. **141-143**, 139 (1986)

173. Cherckdjian, S. and I.H. Wilson ; Nucl. Instr. Meth. **B13**, 426 (1986)

174. Saidoh, M., H. Gnaser and W.O. Hofer; Appl. Phys. **A.40**, 197 (1986)

175. O`Connor, J.P., L.M. Baumel, P.G. Blauner, K.M. Hubbard, M.R. Weller and R.A. Weller; Nucl. Instr. Meth. **B13**, 365 (1986)

176. Oostra, D. J., R.P.van Ingen, A. Haring, A.E. de Vries and G.N. van Veen; Appl. Phys. Lett. **50**, 1506 (1987)

177. Oliva-Florio, A., R. A. Baragiola, M.M. Jakas, E.V. Alonso and J. Ferron; Phys. Rev. **35**, 2198 (1987)

178. Bohdansky, J. and J.Roth, ; J. Nucl. Mater. **145**, 387 (1987)

179. Schou, J., Ole Ellegaard, H. Sorensen and R. Fedrys ; Nucl. Instr. Meth. **B33**, 808-814 (1988)

180. Ray, P., A. Mukherjee, and A. Handoo ; Nucl. Instr. Meth. **B40&41**, 299-301 (1989)

181. Roth, J., J. Bohdansky and W. Ottenberger, ; J. Nucl. Mater. **165**, 193 (1989)

182. Haasz, A.A., and J.W. Davis ; J. Nucl. Mater. **162-164**, 915(1989)

183. Santaniello, A., J. Appelt, J. Bohdansky and J. Roth ; J. Nucl. Mater. **162-164**, 951 (1989)

184. Vincenz, A.M., P.A. Treado, J.M. Lambert and O.F. Goktepe; Nucl. Instr. Meth.**B40/41**, 296 (1989).

185. Gauthier, E., W. Eckstein, J. László and J. Roth, J. Nucl. Mater. **176&177**, 438 (1991).

186. Roth, J., E.Vietzke, and A.A. Hass; *Atomic and Plasma-Material Interaction Data for Fusion, Suppl*, to Nuclear Fusion **1**, 63 (1991).

187. Hechtel, E., W. Eckstein, J. Roth and J. László ; J. Nucl. Mater. **179-181**, 290 (1991).

188. Hechtel, E., A. Mazone W. Eckstein and J. Roth ; J. Nucl. Mater. **196-198**, 713 (1992).

189. Eckstein, W. C. Garcia-Rosales, J. Roth and W. Ottenberger, IPP 9/82 (1993).

# Publication List of NIFS-DATA Series

NIFS-DATA-1 Y. Yamamura, T. Takiguchi and H. Tawara, *Data Compilation of Angular Distributions of Sputtered Atoms ;* Jan. 1990

NIFS-DATA-2 T. Kato, J. Lang and K. E. Berrington, *Intensity Ratios of Emission Lines from OV Ions for Temperature and Density Diagnostics* ; Mar. 1990 [ At Data and Nucl Data Tables 44(1990)133]

NIFS-DATA-3 T. Kaneko, *Partial Electronic Straggling Cross Sections of Atoms for Protons* ; Mar. 1990

NIFS-DATA-4 T. Fujimoto, K. Sawada and K. Takahata, *Cross Section for Production of Excited Hydrogen Atoms Following Dissociative Excitation of Molecular Hydrogen by Electron Impact* ; Mar. 1990

NIFS-DATA-5 H. Tawara, *Some Electron Detachment Data for $H^-$ Ions in Collisions with Electrons, Ions, Atoms and Molecules –an Alternative Approach to High Energy Neutral Beam Production for Plasma Heating–*; Apr. 1990

NIFS-DATA-6 H. Tawara, Y. Itikawa, H. Nishimura, H. Tanaka and Y. Nakamura, *Collision Data Involving Hydro-Carbon Molecules* ; July 1990 [Supplement to Nucl. Fusion 2(1992)25]

NIFS-DATA-7 H.Tawara, *Bibliography on Electron Transfer Processes in Ion-Ion/Atom/Molecule Collisions –Updated 1990–*; Aug. 1990

NIFS-DATA-8 U.I.Safronova, T.Kato, K.Masai, L.A.Vainshtein and A.S.Shlyapzeva, *Excitation Collision Strengths, Cross Sections and Rate Coefficients for OV, SiXI, FeXXIII, MoXXXIX by Electron Impact($1s^22s^2$ -$1s^22s2p$-$1s^22p^2$ Transitions)* Dec.1990

NIFS-DATA-9 T.Kaneko, *Partial and Total Electronic Stopping Cross Sections of Atoms and Solids for Protons;* Dec. 1990

NIFS-DATA-10 K.Shima, N.Kuno, M.Yamanouchi and H.Tawara, *Equilibrium Charge Fraction of Ions of Z=4-92 (0.02-6 MeV/u) and Z=4-20 (Up to 40 MeV/u) Emerging from a Carbon Foil;* Jan.1991 [AT.Data and Nucl. Data Tables 51(1992)173]

NIFS-DATA-11 T. Kaneko, T. Nishihara, T. Taguchi, K. Nakagawa, M. Murakami, M. Hosono, S. Matsushita, K. Hayase, M.Moriya, Y.Matsukuma, K.Miura and Hiro Tawara,

*Partial and Total Electronic StoppingCross Sections of Atoms for a Singly Charged Helium Ion: Part 1*;Mar. 1991

NIFS-DATA-12 Hiro Tawara, *Total and Partial Cross Sections of Electron Transfer Processes for $Be^{q+}$ and $B^{q+}$ Ions in Collisions with H, $H_2$ and He Gas Targets -Status in 1991-;* June 1991

NIFS-DATA-13 T. Kaneko, M. Nishikori, N. Yamato, T. Fukushima, T. Fujikawa, S. Fujita, K. Miki, Y. Mitsunobu, K. Yasuhara, H. Yoshida and Hiro Tawara,
*Partial and Total Electronic Stopping Cross Sections of Atoms for a Singly Charged Helium Ion : Part II;* Aug. 1991

NIFS-DATA-14 T. Kato, K. Masai and M. Arnaud, *Comparison of Ionization Rate Coefficients of Ions from Hydrogen through Nickel ;* Sep. 1991

NIFS-DATA-15 T. Kato, Y. Itikawa and K. Sakimoto, *Compilation of Excitation Cross Sections for He Atoms by Electron Impact*; Mar. 1992

NIFS-DATA-16 T. Fujimoto, F. Koike, K. Sakimoto, R. Okasaka, K. Kawasaki, K. Takiyama, T. Oda and T. Kato, *Atomic Processes Relevant to Polarization Plasma Spectroscopy* ; Apr. 1992

NIFS-DATA-17 H. Tawara, *Electron Stripping Cross Sections for Light Impurity Ions in Colliding with Atomic Hydrogens Relevant to Fusion Research;* Apr. 1992

NIFS-DATA-18 T. Kato, *Electron Impact Excitation Cross Sections and Effective Collision Strengths of N Atom and N-Like Ions -A Review of Available Data and Recommendations-* ; Sep. 1992

NIFS-DATA-19 Hiro Tawara, *Atomic and Molecular Data for $H_2O$, $CO$ & $CO_2$ Relevant to Edge Plasma Impurities*, Oct. 1992

NIFS-DATA-20 Hiro. Tawara, *Bibliography on Electron Transfer Processes in Ion-Ion/Atom/Molecule Collisions -Updated 1993-;*
Apr. 1993

NIFS-DATA-21 J. Dubau and T. Kato,
*Dielectronic Recombination Rate Coefficients to the Excited States of C I from C II;*
Aug. 1994

NIFS-DATA-22 T. Kawamura, T. Ono, Y. Yamamura,
*Simulation Calculations of Physical Sputtering and Reflection Coefficient of Plasma-Irradiated Carbon Surface;*

Aug. 1994

NIFS-DATA-23 Y. Yamamura and H. Tawara,
*Energy Dependence of Ion-Induced Sputtering Yields from Monoatomic Solids at Normal Incidence;* Mar. 1995